Springer Series in Wood Science

Roza Aseeva
Boris Serkov
Andrey Sivenkov

Fire Behavior and Fire Protection in Timber Buildings

Springer

Springer Series in Wood Science

Series Editor

Rupert Wimmer, *Universität für Bodenkultur Wien Botanisches Institut, Wien, Austria*

For further volumes:
http://www.springer.com/series/760

Roza Aseeva • Boris Serkov • Andrey Sivenkov

Fire Behavior and Fire Protection in Timber Buildings

Springer

Roza Aseeva
Fire Safety in Buildings
State Fire Academy Ministry
of Civil Protection and Emergency
Moscow, Russia

Boris Serkov
Fire Safety in Buildings
State Fire Academy Ministry
of Civil Protection and Emergency
Moscow, Russia

Andrey Sivenkov
Fire Safety in Buildings
State Fire Academy Ministry
of Civil Protection and Emergency
Moscow, Russia

Series Editor
Rupert Wimmer
Universität für Bodenkultur Wien
Botanisches Institut
Wien, Austria

ISSN 1431-8563
ISBN 978-94-007-7459-9 ISBN 978-94-007-7460-5 (eBook)
DOI 10.1007/978-94-007-7460-5
Springer Dordrecht Heidelberg New York London

Library of Congress Control Number: 2013954995

Preface

Fire safety for timber buildings and structures is the issue of the day in view of the new momentum this construction industry sector is gaining and the boom in novel technologies and timber materials.

The engineering idea behind this book is based on the concept we have embraced: Timber is a natural composite, and its behavior in fire conditions and fire resistance depend both on its physical structure (morphology) and features of its chemical structure as well as material chemical composition.

This has determined the principle of the book's arrangement and its division in three parts.

The first part (Chaps. 2, 3, 4, 5, 6, and 7) contains data on the structure and properties of various timber species and examines their behavior under high-temperature heating and response to fire. We show the effect of temperature and moisture on the thermal, physical, and mechanical properties of timber. We present the results of experimental and theoretical studies of pyrolysis, ignition, heat release, flame spread, and generation of smoke and toxic combustion products of various timber species. We offer the original form of presenting lower complete combustion heat of timber as a function of its chemical composition. This allows us to determine the lower complete combustion heat values for extractives and hemicelluloses into individual timber species.

The second part of the book (Chaps. 8 and 9) addresses the issues of fire safety, fire resistance, and fire protection of construction members of timber buildings and structures. We present an approach to the fire safety system in buildings and assessing the temperature regime during a fire. We show an engineering way to predict the time of the achievement of critical values of fire hazards factors (temperature, smoke, toxic gases, oxygen deficit) at the initial stage of fire development in a compartment with timber linings. We present data on the charring rate in timber structural members and properties of the char surface layer. We also describe modern trends in enhancing fire safety and fire resistance of timber structures. This part presents a detailed analysis of the fire-protection efficiency of two types of systems: impregnation compositions and intumescent coatings, where the latter is produced from plant raw material and is free of additional fire retardants.

We show the effect of fire-retardant impregnation on the charring parameters of timber structural elements in standard fire regime.

The third part of the book (Chaps. 10 and 11) presents our original data concerning the effect of long-term natural (up to 700 years) and artificial aging of deciduous and coniferous timber species on fire safety characteristics. We address to transformations in physical structure, chemical composition, and properties of timber during natural aging of timber buildings and structures. We provide analysis of the effect of aging on timber charring parameters and properties of the charred layers formed during a fire. The process of biodegradation of timber constructions and the efficiency of a new bio-moisture fire-protective composition is also examined.

This part describes an artificial aging method producing the equivalent to timber buildings that have been in service for up to 500 years. It is accompanied by experimental results of thermal and chemical analysis of timber specimens artificially aged to 150 years showing the change in the fire safety indices.

We would like to express our gratitude to Professor, Dr. Fyodor Shutov for his interest in our work, assistance, fruitful discussions, and valuable remarks.

Moscow, Russia

Roza Aseeva
Boris Serkov
Andrey Sivenkov

Contents

Chapter 1
Introduction

Abstract This chapter presents the detailed description of the main timber species applicable in construction industry. Numerous statistical data related to the fire cases in the twenty-first century are discussed (basically in Russia). These data emphasize that the timber and timber products are the main reason for most of the fire cases in timber buildings and structures. The original approach for understanding the fire behavior of timber of different species has been developed: the intensity of fire is a complex function of several interrelated parameters such as chemical structure, physical morphology, technical properties, age of timber constructions, and intensity of external heat flow.

Forests are the primary source of timber. Russia is one of the most forested countries in the world. Almost a quarter of our planet's forests grow on its territory. With a relatively small number of main tree species, we observe great intraspecific variety. The main species usually include those occupying more than 0.1 % of the forested area. They include six coniferous and 13 domestic leaf species (Ugolev 2001). However, a large number of subspecies, varieties, climatic populations, clones, spontaneous crossbreeds, and other biological forms of these main species have been distinguished and described (Ugolev 2001; Kalutskiy 1982).

The formation of rich intraspecific tree polymorphism was facilitated by our country's enormous area; vast forest range; different combinations of soil, hydrologic, and climatic conditions; and many other factors (Shirnin 2004).

It should be borne in mind that the forest ecosystem plays the key role in generating oxygen for the Earth's atmosphere. By also having other environmental (water and climate regulating) functions, it actually determines the condition and survival resources of modern civilization (Kuznetsov and Baranovskiy 2009).

The species composition of Russian forests varies considerably from north to south and from west to east in our country. On the whole, coniferous forests prevail. However, their percentage changes from north to south with consideration of the amount of woodland in different regions. Thus, the percentage of coniferous in the

R. Aseeva et al., *Fire Behavior and Fire Protection in Timber Buildings*,
Springer Series in Wood Science, DOI 10.1007/978-94-007-7460-5_1,

boreal forest is almost 80 %. They occupy about half of the forest stands in the mixed forest area. In the forest-steppe zone, coniferous forests cover a 25 % of woodlands, while in the steppe regions, they occupy only 12 % of forest lands.

Soft deciduous species like birch, aspen, and lime prevail among in the mixed forest area. In the forest-steppe area, mainly hard deciduous species prevail, with oak being predominant (Kalutskiy 1982).

The main forest-forming coniferous in Russia are larch, pine, and fir trees. Larch forests occupy 2/5 of the country's forest land and account for a third of the timber resources. Up to 14 different larch species grow in Russia. Their areas are geographically separated. In the northern limit of the forest ecosystem (subarctic area), Dahurian larch (Gmelin) and Cajander larch are absolutely dominant. It is assumed that during evolution these larch varieties acquired the features allowing them to adapt to extreme frozen ground conditions as well as to fires (Benkova and Benkov 2004).

Tree species such as the Dahurian larch (it occupies 56 % of the area of larch forests), Siberian larch (13.9 %, respectively), and Sukachev larch (total of 0.1 % of woodlands) have the greatest national economic value (Ugolev 2001; Chakhov and Lavrov 2004). Larch-based materials are widely used in civil and industrial construction. Due to their increased decay resistance, they are used in hydrotechnical structures. Like other species, they are also used in the most varied areas of the national economy.

Pine forests rank second among coniferous in abundance, occupying 1/6 of the country's forests, while fir forests rank third (about 1/8 of the area, respectively). Other main coniferous species, in addition to the above-mentioned, include cedar (as well as the Pinus pine), silver fir (Abies genus), and yew (Taxus genus).

Although deciduous forests occupy only 1/5 of our country's forests, they are characterized by greater variety than coniferous ones. Oak (Quercus genus), beech (Fagus genus), ash (Fraxinus genus), lime (Tilia genus), maple (Acer genus), birch (Betula genus), aspen and poplar (Populus genus), elm (Ulmus genus), alder (Alnus genus), walnut (Junglas genus), and others have commercial value for manufacturing various products (Ugolev 2001).

Studies of the variety of morphologic tree species forms in natural forest populations based on the nature of the plants' genetic constitution and genetic conditionality increased rapidly in the second half of the past century. These studies are the scientific basis for the development of applied areas of forestry, have great practical importance for solving problems of breeding timber plants, and for improving timber productivity and quality. The interaction of a certain plant genotype with the growth habitat conditions and the impact of genetic and environmental factors on timber structure, chemistry, and properties (distinctive features) are of special interest here (Rone 1980).

Tree genotypes have individual responses to environmental influence. Tree biometric parameters are most often used as external plant features dependent on hereditary factors. Tree growth parameters are used (in particular, the beginning and end of growth and the ratio of spring and autumn wood in annual rings) to analyze the biological effects of interaction in the genotype–environment system.

Wood strength properties are used as an indication of wood quality. The amount of data on physical and mechanical properties of many tree species from different regions of world countries has increased recently. It is shown that wood's physical and mechanical properties are under strict genetic control. The share of genotype influence on various physical and mechanical properties of timber, e.g., of poplars from the Lower Volga floodplain, reaches 47–77 % (Shirnin 2004).

It is notable that quantitative analysis of purely genetic effects of the development of tree populations considers some biochemical features as well. In particular, data on the number of isoperoxidases in fir needles, as well as on monoterpene content in pine needles, have been successfully used for this purpose (Rone 1980; Baumanis et al. 1978).

Forest woody populations, like other higher green plants, are remarkable living forms having immense biosynthetic capabilities. By consuming water and carbon dioxide, microelements and simple inorganic nutrients providing the plant with only six elements, namely, carbon, hydrogen, oxygen, nitrogen, sulfur, and phosphorus, they are able to synthesize all of the complex organic substances required to make the components of plant tissues, for tree growth and reproduction. Sunlight is the primary source of energy for biochemical synthesis processes.

At present, extensive data have been accumulated on the anatomical organization and microstructure of various tree species and kinds as well as plant tissue chemistry.

Biochemical genetics of woody plants on the molecular level is the least studied wood science. However, on the basis of available data, the scientific community is already coming to the conclusion today that evolutionary development of woody plants and their natural selection and adaptation are primarily controlled by molecular mechanisms, and only then are determined by ambient conditions. Environmental stresses to a greater or lesser extent affect biosynthesis of the main chemical compounds and so-called metabolites and change the percentage of chemical components in timber.

Timber is a combustible material, like any other organic substance. Timber combustion is primarily a chemical oxidation-reduction process characterized by material degradation, heat liberation, and the formation of various reaction products. But the process of combustion onset, spread, and damping is very complex. It is a combination of both chemical reactions and many purely physical processes (phase transitions, diffusion, heat exchange, mass transfer processes, etc.). For this reason, in order to understand the mechanisms of timber ignition and combustion, and its fire-hazardous characteristics, in addition to knowledge of the chemistry and quantitative content of the main chemical components, one also needs data on the specific features of the timber's texture and its thermophysical and other properties. The nature of thermal impacts on timber-based materials, as well as its operating environment, is very important.

Timber was in fact the first object of an organic polymeric nature used to study the patterns of combustion in solid condensed systems as well as the factors affecting this process. At first, these studies were of a purely empirical nature. They were prompted by the wish to make the most effective use of wood as fuel.

Table 1.1 Effect of fire-resistance rating and building footprint (S, m^2) on the number of fires and human deaths in 2000

Building fire-resistance rating	Building footprint, S, m^2							
	Up to 25		25–100		101–500		More than 500	
	Fires	Deaths	Fires	Deaths	Fires	Deaths	Fires	Deaths
I–II	302	18	97	9	47	2	7	0
III	898	14	448	11	397	6	113	55
IV–V	2,907	67	2,848	60	2,582	95	448	82

Even in the first half of the twentieth century, timber provided most of the total thermal energy consumed in many industrially developed countries (Dunkerely 1980). Timber was attractive because it was a cheap and renewable thermal energy source. At present, timber is a raw material for making many valuable substances and materials, and active efforts are underway to create new technologies for producing gaseous and liquid biofuels from wood. However, the issue of timber's fire safety and the creation of the essential principles of its combustion process and fire protection have come to the forefront.

Global fire statistics shows that fires related to burning forests and timber-based and other organic materials in various kinds of structures pose a real hazard to modern civilization, adding to destabilization of life on our planet (Brushlinskiy et al. 2007). About 6.5–7.5 million fires are registered annually throughout the world, causing the death of 70,000–75,000 people and injuring about one million people. It has been determined that 35 % of all fires occur in buildings, in the majority of cases in residential buildings. Furthermore, the most destructive character of fires with a large number of dead and injured persons, as well as significant material damage, occurs in buildings with timber structures (buildings with fire-resistance rating IV–V). This is obvious from statistical data on fires in Russia for 2000 (Table 1.1) (Data on fires and their consequences for constituent entities of the Russian federation 2000).

Many Russian regions are still characterized by a large area occupied by buildings and structures with fire-resistance rating IV–V (Karelia, Republic of Komi, Arkhangelsk, Vologda, and other regions where timber is a traditional building material).

The observed situation with fires involving timber is not surprising. Chronicles of peoples from various countries include multiple examples of not only huge forest areas destroyed by fires but also of whole cities, which required years of painstaking restoration work. Thus, Moscow's timber buildings were completely burned in 1176. The fires of 1331 and 1337 destroyed the wooden Moscow Kremlin. Even today, forest fires cause enormous damage and destroy the living ecological environment. According to (Fires and fire safety in Russian Federation for 2007–2011 years 2012), as of November 1, 2011, forest fires in the Russian Federation affected millions of hectares of land, destroyed millions of cubic meters of standing forests, and eliminated significant areas of young forests (Table 1.2).

Table 1.2 General data on forest fires in Russia

Years	2007	2008	2009	2010	2011
Number of forest fires	17,812	26,285	23,245	34,812	21,074
Area of lands affected by forest fires, thousand hectares	1,620.3	2,534.8	2,592.6	2,475.3	1,673.8
Burned standing timber, million m^3	16.5	30.1	25.4	93.1	28.7
Dead young forests, thousand hectares	86.2	294.4	119.7	126.6	102.7

Lightning discharges are an important cause of forest fires. However, forest fires are caused to a large extent by human impact (over 60 % of the total number of fires on average). Careless handling of fire is the main cause of 80–90 % of man-induced fires. Factors such as moisture content of timber-based combustible materials, as well as meteorological parameters of atmospheric environment (temperature, humidity, wind speed), have great influence on the character of forest fires. The closeness of populated area and their increased population contribute to an increase in the number of seasonal forest fires. However, a reverse relation is also noted: the impact of forest fires on the occurrence of fires spreading to nearby timber structures of populated areas.

In 2010, forest fires in Moscow Region completely destroyed some villages with timber buildings and structures located close to a forest.

Wood makes up most of the forest ecosystem phytomass. There is a lot in common between the patterns of the onset and spread of combustion during fires in forests and buildings and structures of fire-resistance rating IV–V using timber constructions and building materials. This similarity is due to the organic nature of timber-based combustible materials and constructional timber, which is the main structural component of woody plants.

Consideration of forest fires as a more complex macrosystem, which involves combustion not only of living trees but also of biomass on their tops, undergrowth, and ground cover in the form of tree cutting, fallen needles and leaves, branches, and grass depending on the state of the atmospheric environment, is outside the scope of this book.

Here we confine ourselves only to consideration of the fire safety of most timber products as a material widely used in construction.

It should be noted that partial or full replacement of timber building materials with other inorganic structural materials has increased fire safety of buildings and structures. However, at present they are being increasingly equipped with articles made not only of natural but also of man-made and/or synthetic organic polymeric materials. Therefore, we must agree with the conclusion made by the authors of outline (Brushlinskiy et al. 2007), "that, unfortunately, human life without fires in the foreseeable future is still not guaranteed."

The reason for the majority of fires in buildings and structures according to statistical data for the Russian Federation is careless handling of fire and violation

Table 1.3 Statistical data for fires in RF cities

Main indices	2007	2008	2009	2010	2011
Number of fires, thousand	138.3	130.0	116.5	109.8	103.6
Loss of life, persons	8,643	8,432	7,363	6,809	6,129
Injured persons	9,608	8,887	9,151	8,965	8,565
Direct material damage, billion roubles	5.172	8.221	7.252	7.101	12.660

Table 1.4 Statistical data for fires in RF rural areas

Main indices	2007	2008	2009	2010	2011
Number of fires, thousand	74.3	72.0	71.0	69.8	65.0
Loss of life, persons	7,423	6,869	6,583	6,261	5,889
Injured persons	4,080	4,000	4,118	4,182	3,951
Direct material damage, billion roubles	3.524	4.007	3.941	7.454	5.382

of electrical equipment installation and operation rules. Thus, in 2005, nearly every second fire was caused by careless handling of fire and every fifth one by violation of electrical equipment operation rules. In 80 % of cases, loss of life in fires is caused by poisoning by toxic combustion products.

Tables 1.3 and 1.4 give the main statistical data for fires in RF cities and rural areas from 2007 to November 2011 (Fires and fire safety in Russian Federation for 2007–2011 years 2012).

A comparison of statistical data shows that the number of fires in cities is about twice as high as in rural areas. However, a higher number of victims in relation to the number of fires is characteristic of rural areas. This is related to the wide use of timber and timber-based materials in rural areas for constructing various buildings and structures.

The wide use of timber as a structural building material and its higher combustibility promoting the development and spread of fires are prompting focused efforts to protect timber structures and materials against fire and high temperatures. A successful solution to the issue of fire safety and finding the most reasonable and efficient measures for protecting timber against fire are impossible without knowledge of the fundamental scientific basis of timber combustion and factors affecting the mechanisms of this process.

The phenomenological pattern and physical and chemical basis of the wood combustion process are shown in the following diagram (Fig. 1.1).

A combustible material is heated when it is subjected to an external heat flow (radiant, convective, or combination thereof). If heat flow is relatively high, the material's surface temperature reaches the level at which its pyrolysis begins. Timber pyrolysis is the unreversible reaction of thermal decomposition of material forming volatile and nonvolatile products in the condensed state. The gases or vapors of combustible products that are formed are mixed with air in the layer boundary. Under certain conditions, this mixture exceeds the lower flammability limit of combustible substances and ignites. The timber ignition process may be spontaneous or initiated by a small ignition source localized in the boundary layer.

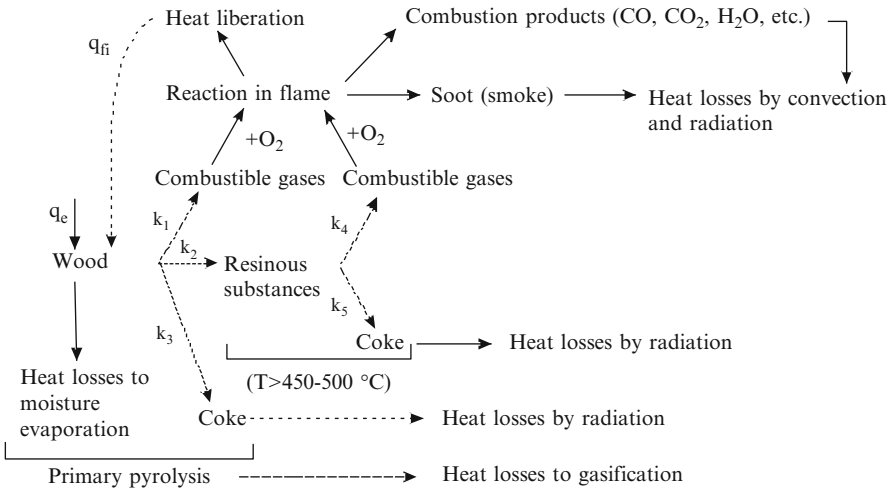

Fig. 1.1 Diagram of the chemical and physical processes during flame combustion of timber

This source may be a small flame of a gas burner, electric spark, or red-hot wire. In scientific literature, this process of ignition of flammable condensed systems is called piloted ignition. After ignition, heat flow to the timber surface is a combination of the external flow and reverse heat flow from the initiated flame.

Chemical and physical processes during combustion of polymeric materials occurring in the gas phase (ignition, flame spread, extinguishing, exothermal reactions in flame, etc.) determine many of the fire safety characteristics of materials.

Heating and decomposition of organic material are important stages of the timber combustion process. The speed of heating to the decomposition temperature depends not only on the intensity of the external heat source but also on the timber's thermophysical properties, which are closely related to its structure. Timber decomposition rate under the given heating conditions is to a large extent determined by the chemistry of this natural composite.

Timber is a striking representative of polymeric carbonaceous materials (Aseeva and Zaikov 1981). As the pyrolysis front moves inside the material, a char layer forms and grows on its surface. This reduces the amount of combustible volatile products, since a portion of the carbon and hydrogen (the main combustible elements in the chemical composition of timber) remains in the condensed phase. The char layer with low thermal conductivity acts as heat insulation, reducing the heat flow to the underlayers of the original wood. At the same time, it may act as a physical barrier hindering the escape of decomposition products to the gaseous phase or oxygen access to the timber surface. In addition to these effects, the temperature increase on the char layer surface during combustion development causes increased heat loss due to radiation from the char surface. The above-mentioned factors taken together have a great impact on the mechanisms of the timber combustion process.

We should expect that variations in timber chemistry and structural properties depending on the species and variety will affect the direction of chemical reactions, the macrokinetic features of timber pyrolysis and carbonization, and the amount (thickness), structure, and properties of the char that is formed. All other conditions being equal, it should affect the speed of burnout, ignition, and flame spread along the timber surface, the formation of smoke, and toxic combustion products, and in the long run, the main fire safety indices for timber-based materials. This is the reason for the recent interest in comparative studies of pyrolysis and thermo-oxidative decomposition of various timber species and the separate chemical components of wood in a wide temperature range. The speed and degree of timber pyrolysis determine the speed of timber burnout, carbonization and integrity, as well as the mechanical strength of timber structures during fires.

The detailed mechanism and kinetics of chemical reactions of wood pyrolysis and carbonization have still not been conclusively established. Earlier works in this area focused almost exclusively on materials based on cellulose or its derivatives (Shafizadeh 1984; Roberts 1970).

Until the 1970s, there were heated discussions about whether the results of pyrolysis kinetic studies conducted on small samples of substances and materials by thermal analysis methods (TG, DTG, DTA, DSC) under isothermal or dynamic heating conditions could be used for modeling pyrolysis and burnout of large bulk samples. This was because pyrolysis first of all has a volumetric character and occurs in the entire volume of a sample heated to a certain temperature. Second, it starts on the surface and moves inside the sample and has properties of linear pyrolysis. Higher temperatures and large temperature gradients are observed near the material surface. The decomposition process, in fact, takes place in a narrow area, the width of which depends on the thermal and physical characteristics of the polymeric material and heating conditions. Detailed studies have shown that pyrolysis occurs throughout the volume of this narrow reaction zone. The effective macrokinetic parameters of pyrolysis of many polymeric materials, including wood, obtained from data of thermogravimetric measurements at lower heating rates and temperatures than during combustion, are quite in keeping with the parameters of linear pyrolysis of large samples (Aseeva and Zaikov 1981; Roberts 1970).

Modern instrumental equipment and computer software for thermal analysis make it possible to study pyrolysis of substances on very small samples (weighing 1 mg or less). It prevents the dynamics of pyrolytic reactions from being affected by adverse diffusion effects and nonuniform temperature distribution in the sample, and allows the macrokinetic parameters at certain stages of the substance decomposition process, as well as thermal effects of reactions in a wide temperature range, to be determined with high accuracy and reliability. Moreover, the procedure developed for processing experimental thermal analysis results allows an assessment of the type of mechanism of solid-phase reactions of substance decomposition (Shestak 1987; Rogers and Ohlemiller 1981).

Timber pyrolysis under the impact of high-temperature heat flows causes the formation of various products that enter the gaseous phase and support the flaming process. Several main spatial areas differing in their temperature characteristics,

type, and speed of chemical reactions can be distinguished in the diffusion flame during timber combustion, the same as in the condensed phase. The gas-vapor flame portion adjacent to the surface is considered the pre-flame area, visually observed in the form of a dark region in the lower flame portion. It is sometimes called the cold flame zone. The active exothermal reaction of oxidation of combustible volatile products of wood substance decomposition occurs in a narrow area of the flame front. Very high temperatures and a higher temperature gradient are observed here in the bright reaction layer on the flame surface. It is thought that oxygen diffusing from the ambient air to the flame reacts with gaseous fuel in the flame front in a stoichiometric ratio. Finally, the intensely luminous area inside the flame is an area of combustion products from which condensed particles are emitted as smoke through the flame peak.

There are no experimental data on stable compounds and active particles that should be characteristic of different areas of a timber diffusion flame. This is due not only by issues related to flame probing and analysis and the labor intensity of these procedures but also to the complexity of the multicomponent carbonaceous system being analyzed. It is known that carbonization affects flame structure stability (Aseeva and Zaikov 1981).

Timber pyrolysis during heating without air access up to 500 °C is well known in wood science as the dry distillation process for obtaining many valuable substances (Fengel and Vegener 1988).

Beginning in the twelfth century, this was one of the first processes of the chemical technology of organic substance production widely used in Russia to make resin, and later charcoal.

Modern analysis methods have revealed that products of timber pyrolysis in an inert medium contain more than a hundred compounds belonging to different chemical classes (Fengel and Vegener 1988). They vary in volatility at the temperature reached on a timber surface during an external thermal action. Ignition and combustion of each compound have their own features and patterns. The situation becomes even more complicated when mixtures of these compounds react. Various chemical reactions involving gaseous compound transformation occur in each flame zone. Polymeric materials less complex than wood were used to obtain experimental evidence that active processes related to cracking of organic compounds. That is, volatile products of polymer pyrolysis already occur in the pre-flame area (Aseeva and Zaikov 1981). The formation of smoke aerosol during timber combustion is an evidence of incomplete oxidation of pyrolysis products in the flame.

Mathematical modeling of these processes, followed by comparing the numerical results obtained with the experimental data, is an important tool for analyzing various factors affecting timber ignition and combustion.

The first attempts at a theoretical study of gas-phase ignition of solid fuels under the impact of external heat flow were based on thermal models focusing on chemical processes in the gaseous phase. The ignition criterion was a fast exothermal chemical reaction in the gaseous phase (Aseeva and Zaikov 1981; Kashiwagi 1974). The main problem with practical use of these models is related to the need to know many important characteristics of processes occurring in the

gaseous phase. However, it is very difficult to determine these parameters as the specific reaction rates of gaseous compounds or their mass transfer coefficients at high temperatures.

Some researchers suggested an alternative, less complex approach to modeling wood ignition and combustion. This approach is based on the use of indirect ignition criteria reflecting the required inflow of combustible products into the gaseous phase due to solid fuel pyrolysis. Until then, it was considered an inert material (Aseeva and Zaikov 1981; Janssens 1991).

In turn, modeling of the process of flame spread along the surface of solid materials is based on the concept of continuous gas-phase ignition of material decomposition products. In this case, the initiated flame acts not only as a source of material heating and pyrolysis but also as a piloted source of ignition of the volatile flammable compounds produced. Considering the features of pyrolysis of carbonaceous materials, such as timber, allows an assessment of the critical conditions for flame spread along the surface of these materials.

Mathematical models of varying complexity were developed to describe timber pyrolysis and carbonization, and burnout in flaming and smoldering modes. These topics will be considered in greater detail in subsequent chapters of the book.

Analysis of the results of experimental and theoretical research on timber pyrolysis, ignition, and combustion makes it possible to distinguish a number of factors as the key variables affecting the fire safety of timber-based materials. Some of them depend on the timber variety and thus on its chemistry and structure (e.g., density, thermophysical, and thermochemical properties). Other factors are determined by the conditions under which the above-mentioned processes can take place (intensity and type of external thermal effect, environmental properties, sample orientation and size).

Timber remains one of the most attractive materials for the construction industry. It is used as load-bearing and enclosing structures of buildings, finishing, and facing materials. The development of modern house-building was largely facilitated by the creation of advanced industrial processes for manufacturing new structural materials from timber. In the first place, there is glued laminated timber (glulam), CLT (cross-laminated timber) panels, slabs, LVL (laminated veneer lumber) beams, and OSB (oriented strand boards) made of large wood particles. The specific geometry and orientation of wood particles in the OSB board structure increase the strength of this material and expand the opportunities for using it in building structures.

In the USA, Canada, and Europe, the low- and medium-rise frame timber house-building sector is developing very rapidly. The appropriate space planning and engineering solutions have been developed using passive and active fire protection means to ensure fire safety in timber buildings.

Modern timber house-building technologies are implemented less actively in Russia than in European countries. Thus, the relative volume of timber used in domestic house-building is 20 times less than in Finland or Sweden (Kobeleva 2012). To a large extent, this is due to insufficient development of domestic fire protection standards for timber house-building as well as the absence of a unified system program for building timber houses and structures in the Russian Federation.

In spite of the existing materials science, technological and regulatory barriers, real estate market experts anticipate that Russia will have an average annual growth rate in demand for timber buildings of 10 % until 2015 and 20–25 % by 2020 (Kobeleva 2012).

At present, glued load-bearing timber structures (columns, beams, arcs, frames) are being used to construct several unique large span structures. It suffices to name the sports complex in Arkhangelsk with a span of 63 m, an indoor ice rink in Tver with a span of 58 m, a mineral fertilizer warehouse in the port of St. Petersburg with a span of 63 m, and arc comb height of 45 m (Aseeva et al. 2010). Designs for public timber frame buildings and structures more than 9 m high have been developed, which, however, require specific engineering solutions for fire protection of timber structures and fire safety of facilities (Architectural and educational resource).

The stability of buildings and structures in case of fire depends on the fire-resistance rating of its load-bearing constructions. It is known that timber constructions lose their bearing capacity due to timber charring and the resistance of the material and joint connections to mechanical and thermal loads is significantly reduced. The fire-resistance rating of load-bearing constructions is determined according to the time of reaching the limit state according to a specified feature (R) when the structures are tested in standard temperature conditions of fire. It is very important to know the speed of timber charring, how its mechanical properties change during fire, and to what extent the given characteristics depend on the nature and variety of the timber, its humidity, a change in fire conditions, and construction heating.

Unlike load-bearing structures, the functions of enclosures and enclosing parts of buildings and structures amount to preventing fire from spreading to rooms adjacent to the fire seat and limiting the impact of hazardous fire factors on humans (smoke, toxic products, temperature increase, etc.). Therefore, fire resistance of an enclosure is assessed according to time (a) of structure integrity damage with the formation of cracks and through holes through which combustion products and flame penetrate (feature E), (b) of loss of thermal insulating capacity and a critical increase in the construction's surface temperature on the other side not exposed to fire (feature I), and (c) of reaching the permissible heat flux density (3.5 kW/m^2 $\pm$ 5 %) at a standardized distance (0.5 m) from the structure's unheated surface (feature W).

Criterion I is fulfilled if the average temperature on the unheated surface of the entire timber structure does not exceed 140 °C, while the maximum temperature rise at any point on the surface does not exceed 180 °C.

Various methods have been suggested to protect timber structures against fire, including both structural fire protection and surface treatment with flame retardants. New effective fire protection means for timber structures that retain the natural material's appearance, beauty, and texture under normal operating conditions are of great interest. This is particularly important with respect to preserving and protecting ancient architectural monuments. However, the question of the influence of timber variety and its structural features on the effectiveness of fire-protection treatment remains open.

Timber structures are a priori considered less durable than stone, brick, or reinforced concrete ones. However, the unique timber architectural monuments surviving to our time show that timber as a structural material has relatively high durability (over 300 years). Remnants of ancient archaeological timber several thousand years old have been found (Fengel and Vegener 1988).

Material durability usually means its duration of service under various conditions without significant loss of performance. Under natural conditions of timber members operation, complex interrelated physical and chemical processes of timber aging occur under the impact of light, heat, moisture, wind, biological destroyers, and other factors. Destructive reactions change the structure and chemistry of timber and many of its properties. Scientific literature has not given due consideration to the impact of natural and artificial wood aging on the change on fire safety and fire resistance of timber structures.

We have adopted a concept according to which wood is considered as a natural composite carbonaceous material. Its behavior during fire, as well as the fire safety and fire resistance of timber structures, should simultaneously depend both on the physical (morphological) structure and the material chemical composition, including the chemical nature of the components in this composite and thermal action conditions. This approach provides an understanding of the behavior of different kinds of timber in case of fire, impact of the duration of aging on the change in fire safety characteristics, charring speed, and properties of the char layer forming on a timber surface.

This is why we believed that first of all, it was necessary to briefly present the known data on the structural features, chemistry, and some properties of timber. It also seemed reasonable to consider biogenetic and biochemical aspects of timber polymorphism. This information helps us to understand the difference in the behavior of timber-based materials in their reaction to fire and high-temperature effects as well as how great or small the differences in fire safety characteristics of various species and kinds of timber may be.

References

Architectural and educational resource. Project contest “House on Roof”, http://architime.ru/competition/compexibition270511.htm. Item – 30.09.2011 Named winners of the “House on Roof” contest. ARTPLAY CENTRE

Aseeva RM, Zaikov GE (1981) Combustion of polymeric materials. Nauka, Moscow, 280 p

Aseeva RM, Serkov BB, Sivenkov AB (2010) Wood combustion and fire-hazardous properties. SFS Academy, Moscow, 262 p

Baumanis II, Rone VM, Birgelis YaYa (1978) Genetic characteristics of needle monoterpenes in common fir populations. Selection of forest wood materials, Riga, Zinatne, pp 83–94

Benkova VE, Benkov AV (2004) Adaptive features of the structure of xylem of Siberian Larch species from the permafrost zone. In: Proceedings of IV international symposium on “wood structure, properties and quality”, vol 1. SPbGLTA, St. Petersburg, pp 41–44

Brushlinskiy NN, Sokolov SV, Vagner P (2007) Humanity and fires (outline). SFS Academy, Moscow, 121 p

Chakhov DK, Lavrov MF (2004) Study of the wood properties of larch growing in Yakutia. In: Proceedings of IV international symposium on "wood structure, properties and quality – 2004", vol 1. SPbGLTA, St. Petersburg, pp 377–379

Data on fires and their consequences for constituent entities of the Russian Federation. Russian insurance bulletin. Ekonomicheskaya Gazeta Publishing House, Moscow, 2000, No. 6, pp 22–34

Dunkerely J (1980) International energy strategies. Oelgeschlager, Gunn and Hain, Publishers, Inc., Cambridge, MA, p 60

Fengel D, Vegener G (1988) Wood: chemistry, ultrastructure, reactions. Lesnaya promyshlennost, Moscow, 512 p

Fires and fire safety in Russian Federation for 2007–2011 years (2012). Statistical collection by Ed. V.I. Klimin, VNIIPO, Moscow, 137 p

Janssens M (1991) Piloted ignition of wood: a review. Fire Mater 15:151–167

Kalutskiy KK (ed) (1982) The world's wood species, vol 3: The USSR's wood species. Lesnaya Promyslennost, Moscow, 264 p

Kashiwagi TA (1974) Radiative ignition model of a solid fuel. Combust Sci Technol 8:225–236

Kobeleva SA (2012) Prospects of timber house-building. Collection of scientific papers "Topical issues of the forest complex", issue 32. Publishing House of Bryansk State Engineering and Technology Academy, Bryansk, pp 83–86

Kuznetsov GV, Baranovskiy NV (2009) Forecast of forest fire development and environmental impact. SO RAN Publishing House, Novosibirsk, 301 p

Roberts AF (1970) A review of kinetics data for the pyrolysis of wood and related substances. Combust Flame 14:261–272

Rogers FE, Ohlemiller TJ (1981) Pyrolysis kinetics of a polyurethane foam by thermogravimetry: a general kinetic method. J Macromol Sci Chem A15(1):169–185

Rone VM (1980) Genetic analysis of forest populations. Nauka, Moscow, 160 p

Shafizadeh F (1984) Chapter 13: The chemistry of pyrolysis and combustion. In: Rowell R (ed) The chemistry of solid wood, Advances in chemistry series 207. American Chemical Society, Washington, DC

Shestak Y (1987) Thermal analysis theory. Mir, Moscow, 456 p

Shirnin VK (2004) Development and prospects of cross-breeding for wood quality. In: Papers of the IV international symposium "wood structure, properties and quality – 2004", vol 1. SPbGLTA, St. Petersburg, pp 145–149

Ugolev BN (2001) Wood science with fundamentals of forest merchandizing. MGUL Publishing House, Moscow, 340 p

Part I
Behavior of Constructional Timber at High Temperature Heating and Fire

Chapter 2
Specificity of Structure and Properties of Timber Species

Abstract This chapter describes the data related to micro- and macro-structure of deciduous and coniferous species, dry and wet density, and basic relationship between thermal conductivity, specific heat capacity, thermal diffusivity, thermal inertia and humidity, and density and anisotropy of various types of timber, and some genetic aspects of timber diversity are considered. The basic relationship between mechanical properties and ambient temperature is presented.

2.1 Macro- and Microstructure of Deciduous and Coniferous Timber Species

In a visual inspection of the anatomy of coniferous and deciduous timber trunks in cross section, the macrostructural features they have in common are easily seen. In the first place, these are more or less well-defined spatial zones (layers).

The outer zone is the bark consisting of a cork layer of dead plant cells, which provide the tree with basic protection from external damage and a thin inner live bast layer. In many timber species, the light sapwood zone stands out from the darker central heartwood zone, where the latter formed as a result of gradual changes and dying-off of living cells in sapwood. Sapwood width depends on the time the heartwood formed. The later this phase starts, the wider it is. But in certain species (spruce, fir, beech, aspen), the borderline between sapwood and heartwood is poorly discerned visually, but the heartwood zone has lower moisture. The trunk pith is a dark-colored zone formed during initial trunk and branch elongation. Certain timber species have clearly visible 0.05–1 mm wide pith rays in cross section, which connect different layers from pith to bark and serve to store and transport nutrients.

Between bark and wood, there is a cambial layer of living cells, which can only be seen through a microscope. Wood and bark elongation and diameter growth occur through plant cell division and growth in this layer. Annual growth of wood is called the growth layer. Every growth layer consists of earlywood and latewood zones. The

R. Aseeva et al., *Fire Behavior and Fire Protection in Timber Buildings*,
Springer Series in Wood Science, DOI 10.1007/978-94-007-7460-5_2,

earlywood zone located closer to the pith is usually less solid and outwardly clear. Earlywood is formed during the first period of vegetation and contains a certain number of living cells. Latewood is formed at the end of the vegetation period and is more solid and darker. The earlywood layer carries water and nutrients upward. Latewood mainly performs mechanical functions. Its content often serves as the basis for assessing the robustness of timber material (Ugolev 2001).

In certain tropical areas, the vegetation period may last whole year. In such cases, there is no clearly outlined borderline either between early and latewood layers or between growth layers.

For all natural zone characteristics uniformity, every species and variety of timber has its specificity. They show up particularly in the quantitative relationship between macrostructure elements, in their dimensions, colors, and properties (Ugolev 2001).

It should be noted that certain elements of timber structure are inherent only in deciduous species or only in particular varieties of coniferous species. Thus, resin channels are a feature only of coniferous species. In cross sections of pine, cedar, larch, and spruce, they can be seen as 0.08–0.14 mm white spots. These spots are the cuts of vertical resin channels that thread the timber. Only deciduous species have pores (vessels) conspicuous in cross sections in the form of round holes.

Deciduous species are subdivided by pore location into species with diffuse-porous structure, where the pores are uniformly distributed in the growth layer, and species with ring-porous structure. In the latter case, large pores 0.2–0.4 mm in diameter are usually concentrated in the early zone of the growth layer forming a continuous ring, whereas small pores (diameter 0.016–0.1 mm) are concentrated in the late zone. Species with the ring-porous structure are differentiated by distribution of small pore groups in the latewood into radial, tangential, and disordered arrangement of these groups. In timber structures with the radial group arrangement (oak, chestnut), they have the shape of a tongue of flame. In the tangential arrangement, they form solid or dashed wavy lines (elm species) drawn along the growth layers. In the disordered arrangement (ash), small pores are seen in cross section as clear bars or dots (Fig. 2.1) (Ugolev 2001).

More in-depth information on the composition and microstructure of coniferous and deciduous timber species is obtained through modern chemical, physicochemical, and physical methods of analysis, including various electronic microscopy techniques that are able to identify structural elements with dimensions down to 0.1–2 nm.

The basic elements of wood structure are plant cells, which form tissues of various structures and functions. Every living cell of woody plants consists of metabolically active protoplast encased in a membrane. A membrane is a cell wall consisting of a fairly robust multilayer formation. The cell wall is a specific attribute that distinguishes a plant cell from an animal cell.

Plant cells are subdivided by shape into two groups: multifaceted or round parenchymal cells 0.01–0.1 mm in diameter and prosenchymatous cells with an oblong shape. The diameter of prosenchymatous cells ranges between 0.01 and 0.05 mm, and their length from 0.5 to 3–8 mm. Their walls are usually thicker than parenchymal cell walls. In the wood of a growing tree, only 5–10 % of early zone

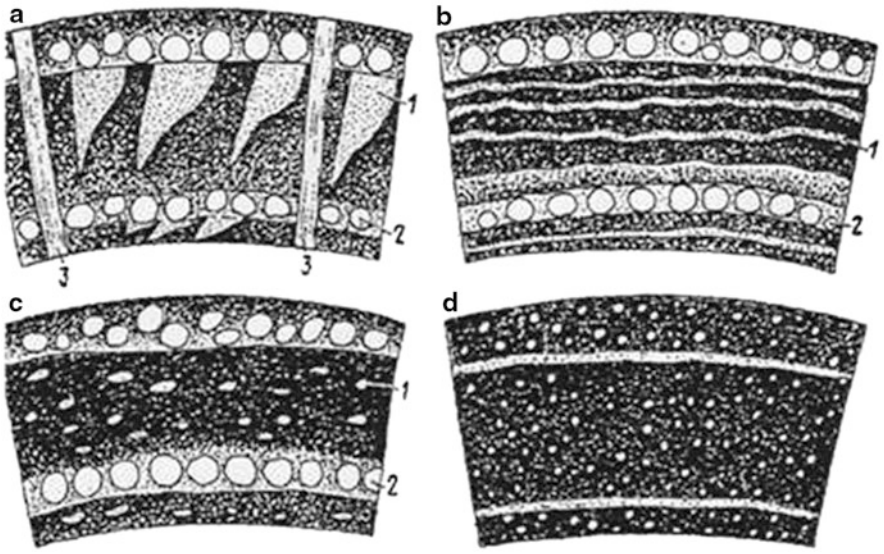

Fig. 2.1 Pore arrangement in deciduous timber species: (**a–c**) ring-porous structure species with radial, tangential, and disordered arrangement of small pores in the late zone; (**d**) diffuse-porous structure: *1* small pores in the late zone, *2* large pores in the early zone, *3* wide pith rays

parenchymal cells maintain metabolically active protoplast. The other cells die off after the maturation process is completed and are filled with water or air instead of protoplast.

Therefore, the timber framework is made of cell membranes that mainly perform mechanical functions. The basic substance is cellulose, which renders the cell membrane stable and robust.

Cell wall structure, formation and development are addressed in a large number of scientific works. We are particularly interested not only in studies of the physical microstructure of timber but also of the chemical composition and structure of its individual elements during woody plant growth and their common and distinguishing features for various species (Ugolev 2001; Antonova 1999).

The cell wall is formed in the process of living cambium cell division. Division starts with the formation of a cell plate that splits the protoplast of the primary plant cell into two parts and later turns into middle lamella between daughter cells. It has a high pectin content. The daughter cells initially acquire primary membranes formed from cellulose macromolecules. Cellulose macromolecules in the primary membranes have a relatively low degree of polymerization (they contain from 2,000 to 4,000 repetitive glycosidic linkages in the main chain) and are polydisperse. Due to hydrogen bonds between molecules, they group into microfibers. In primary membranes, cellulose microfibers are arranged haphazardly about one another. Between them lie the substances of the so-called matrix (pectins and hemicelluloses) as well as water molecules. Matrix plasticity facilitates the expansion of daughter cells and an increase in their longitudinal and lateral dimensions. When cell growth

by expansion is completed, the secondary membrane is formed. Cellulose in the secondary membranes has a higher average degree of polymerization (up to 10^4) and is practically monodisperse. A secondary membrane, which is often called a secondary cell wall, consists of three layers, where cellulose microfibers are arranged in each of them in the form of spirals at different angles to the cell's longitudinal axis. In the outer layer S_1 of a secondary membrane, the microfiber spirals are oriented at an angle of 60°–80° in coniferous species and at about 45° in deciduous species. The S_1 layer is 0.2–0.5 μm wide in earlywood cells but may be up to 1.0 μm in latewood. The dominating layer of the cell wall secondary membrane is the middle layer S_2. Cellulose microfibers in this layer are inclined at 5°–15° in earlywood cells and up to 30° in latewood. This S_2 layer is 1–2 and 3–8 μm thick in plant cells of earlywood and latewood, respectively, depending on timber species and variety. The inner layer S_3 of the cell wall secondary membrane is 0.1–0.2 μm thick, regardless of early or late plant vegetation period, and has gently sloping cellulose microfibers with a spiral inclination angle of 90°.

As the active growth of cells comes to an end, the nature of polysaccharides of cell wall matrix changes. A predominant content of pectins turns into a predominant content of hemicelluloses. In addition, the set of different types of hemicelluloses also changes. One more cell wall layer adjacent to the S_3 layer and covering the cell's interior occurs in the structure of cell walls of certain timber species. This is the so-called warty layer W. It consists of a membrane and lumpy formations, i.e., warts, has an amorphous structure, and contains hemicelluloses, a small amount of lignin and simple proteins.

Lignin serves as an additional substance strengthening cell walls. Study of the lignification process of cell walls in coniferous and deciduous timber species at individual phases of their vegetative growth is of great interest from various points of view, including the structure of lignin itself (Antonova 2000). The example of larch shows that the onset of lignification corresponds to the start of secondary membrane formation in cell walls. Lignin is formed, first of all, around the corners of middle lamella in the intercellular space of adjacent plant cells. During the formation of earlywood, this phase corresponds to deposition of 22–26 % of the wall mass in the secondary membranes. In latewood formation, only 6–10 % of the wall mass, mainly represented by cellulose, is deposited prior to the onset of lignification. At the time lignification of plant cell walls starts, the product of lignin biosynthesis is most likely its precursor substance, because although it contains the building blocks of lignin molecules, it has low molecular mass (Antonova 2000). The progress of the cell wall lignification process is not the same in earlywood and latewood. In earlywood formation, lignification proceeds gradually and achieves its maximum intensity at the last phase of plant tissue maturation. In latewood formation, the maximum intensity of lignification is seen right from the start and decreases toward the end of the vegetation period. Lignin distribution in the cell wall is uneven. The layers that were deposited first usually contain more lignin. For this reason, lignin content around the corners of middle lamellas, in the middle lamellas themselves, and in primary membranes of plant cells is higher toward the end of the vegetation period compared to secondary membranes.

It must be emphasized that lamellar morphology of cell walls is a common feature of all principal structural elements of plant tissues in various timber species (tracheids, libriform fibers, pores, pith rays). There is a difference in the details of structural organization at the quantitative level and in the specific character of biosynthetic processes in the chemical components of structural elements (Goodwin and Mercer 1986). A good illustration of this is the difference in formation and composition of lignin in the plant cells of coniferous and deciduous timber species (Antonova 2000; Antonova et al. 2002).

Lignin of coniferous timber species has a predominantly guaiacyl type of three-dimensional polymer buildup with phenylpropanoid repeating units, which contain one phenolic hydroxy group and one methoxy group in an aromatic ring. The source of these units is coniferyl alcohol. Syringyl type (most conspicuous in the lignin of earlywood) and *n*-coumaric phenylpropane units have also been discovered. Their sources are sinapic and *n*-coumaric alcohols, respectively. Phenol-containing aromatic structures (coniferyl alcohol – 4, sinapic alcohol – 5, *n*-coumaric alcohol – 6) are shown below.

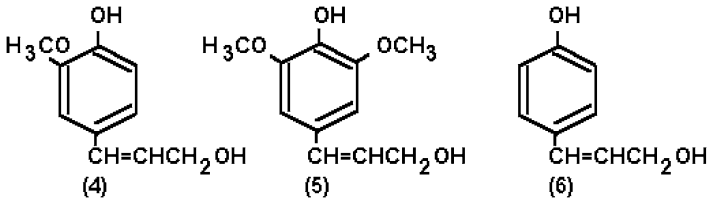

Lignin macromolecules of deciduous timber species include both guaiacyl and syringyl repeating units with two methoxy groups in a phenolic ring. That is why lignin of deciduous species is often considered a copolymer of coniferyl and sinapic alcohols in various ratios between them depending on timber variety. The author of work (Antonova et al. 2002) states that lignin with guaiacyl repeating units is mainly located in middle lamellas, which surround all basic structural elements of oak wood. Syringyl lignin is concentrated in the walls of libriform and tracheid fibers, mainly latewood.

The microstructure of coniferous timber species consists of a system of fibers (tracheids) arranged along and across the trunk, pith rays, and vertical and horizontal resin channels located in the intercellular space (Ugolev 2001). Figure 2.2 shows the arrangement of microstructure elements of pinewood (typical coniferous species) in cross-sectional, radial, and tangential views of a trunk cut (Ugolev 2001).

On the radial walls of longitudinal tracheids of the earlywood zone in the growth layer, there are many large bordered pores (from 50 to 300 per tracheid). The walls of late tracheids have fewer pores. They are smaller, often have the form of slits, and may be found not only on radial but also on tangential walls. The pores of adjacent vertical tracheids located opposite each other transport nutrients and water in the horizontal direction. In the vegetation period, the flow

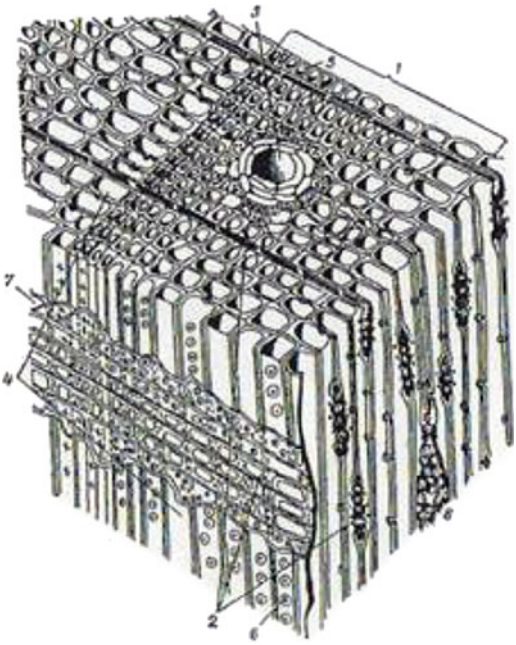

Fig. 2.2 Microstructure of pinewood in cross-sectional, tangential, and radial views

of liquid matter also goes in the same direction through pith rays, which in the dormant period function as storehouses of reserve nutrients. Separate elements in the microstructure of pinewood have the following volumes in approximate percentage:

Longitudinal tracheids	93 %
Pith rays and ray tracheids	6 %
Resin channels	1 %

According to certain other data, the proportion of ray elements in wood microstructure of various coniferous species ranges from 3.4 to 11.7 %, with 7 % as the average (Siau 1984).

The microstructure of deciduous timber species is more varied and complex compared to coniferous species. Figures 2.3 and 2.4 show the microstructure of deciduous timber with ring-porous and diffuse-porous structure, respectively.

In the typical ring-porous structure of oak (Fig. 2.3), a significant volume (up to 25 %) is occupied by large porous elements in the earlywood zone (200–400 μm in diameter) and smaller pores of latewood (30–40 μm in diameter). The pores are long vertical tubes built of short plant cells (segments) with wide cavities and thin walls. Pore cavities, as well as simple and scalariform (slit-shaped) perforations and bordered pores in the walls of pore cells, participate in the general aquiferous system of deciduous timber species. As a rule, a small number of porous tracheids are located next to pores, and they are a transitional form between typical tracheids and pores. In their structural organization, they resemble the segments of small pores.

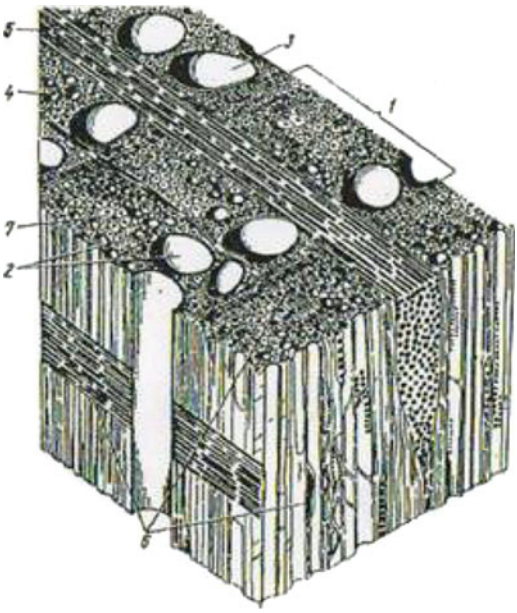

Fig. 2.3 Ring-porous microstructure of oak wood

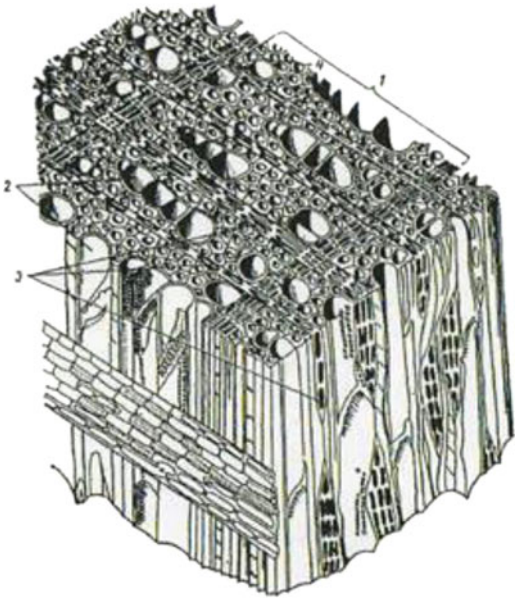

Fig. 2.4 Diffuse-porous microstructure of birch wood

The main mechanical function in deciduous timber species is performed by fibers, which fill from 20 to 75 % of the volume of wood pulp depending on the timber variety. These fibers consist of fiber tracheids and libriform fibers, which derive their names from the Latin words “libri” meaning bast and “forma” meaning

form. Libriform fibers are relatively short, very thin, and have narrow cavities and thick walls with slit-shaped pores. Fiber tracheids in deciduous species are shorter and narrower than tracheids of coniferous timber species and have thick walls with bordered pores.

Parenchymal cells of mainly horizontally arranged pith rays occupy a very significant volume (up to 40 %) in the microstructure of deciduous timber species. Parenchymal cells may be located within the ray width in one or several rows depending on the timber variety. Pith rays also show great diversity in height and may contain from several (in willow wood) to more than a hundred cell rows (e.g., beech wood) (Ugolev 2001). Vertical parenchymal cells (the so-called wood parenchyma) occupy less volume, partially performing the function of storehouses for reserve nutrients.

Timber with diffuse-porous structure (Fig. 2.4) differs from that with ring-porous structure in a higher volume content of pores (ranging from 20 to 60 %), their relatively even distribution in the growth layer, and uniform dimensions.

Pore diameter in the wood structure of most diffuse-porous timber growing in temperate climates ranges from 20 to 100 μm.

Volume distribution of structural elements characteristic of typical diffuse-porous timber may be represented as follows (Siau 1984):

Pores	55 %
Libriform fibers and tracheids	26 %
Wood parenchyma	1 %
Pith rays	18 %

Variations in the composition and ratio of structural elements in the timber of different species and varieties affect various timber properties, particularly important properties affecting wood combustion regularities such as density, moisture, heat transfer, thermochemical, diffusion, and some other properties.

According to contemporary notions about wood structure, the specific features of the conducting and transport systems play an enormous role in realization of individual genetic program of woody plant development (Siau 1984; Gamaley Yu 2004).

Without going into all the details of the complicated organization of the transport system in woody plants, let us mention its principal features. Today, the persistent idea is that there are two independent transport channels carrying counter flows: an upward flow of aqueous solutions of nutrients from the roots to needles or leaves of the crown and a downward flow of photoassimilates and metabolites from leaves (needles) to the roots. Thus, there are two poles for generating these flows or two opposite centers for controlling plant development and two zones for loading and unloading transportation lanes (Gamaley Yu 2004). Transportation lanes serve to distribute assimilates and metabolites among the cells and tissues of a plant. Cells of the living layer of cambium are involved in the formation of these transport lanes. After their division, the cells and tissues of the bast (called “phloem” in the

scientific literature) are deposited on one side, while wood cells (its conducting tissues have the common name "xylem") are deposited on the other side. The upward flow of nutrients and water goes through xylem. The structural elements of wood performing conducting functions have already been addressed. The downward flow of assimilates and secondary metabolites derived from them occurs through the sieve cells and sieve tubes of the phloem (bast tissue). The structural organization of phloem is still poorly understood (Gamaley Yu 2004).

The transport system of woody plants, along with the on-range echelon of movement of various substances toward the trunk, includes a midrange echelon, i.e., radial intercellular flows in parenchymal tissues, as well as short-range transport inside the cells. The intercellular exchange process is the initial phase of all transport processes. One of the leading intercellular mechanisms is believed to be molecular transmembrane transfer of substances with the participation of carrier proteins as receptors and transporters. Special genes in a plant genome are responsible for carrier protein biosynthesis (Gamaley Yu 2004). The transport system of woody plants generally performs a regulatory function in the delivery and distribution of various assimilates and their derivatives among the cells and tissues, thus influencing all processes of plant development.

2.2 Biological and Genetic Aspects of Timber Species Diversity

The first, most ancient forests came into being in the Paleozoic era of the Earth's evolution more than 300 million years ago and consisted of a cluster of evergreen coniferous (gymnospermous) plants. Deciduous (angiospermous) woody plants appeared later, in the Jurassic period of the Mesozoic era 165 million years ago. They are believed to originate from Mesozoic gymnospermous plants, were at first evergreen, and only later turned into plants with seasonal leaf appearance and shedding. They became widespread in the Cenozoic era 75 million years ago, and they continue to spread to the present day. Further evolution of the ancient plant forms follows the sequence from big trees to arboreal forms of shrubs, then to perennial grasses, and finally to annual grasses. Flowering angiospermous plants further evolved into dicotyledonous and monocotyledonous plants. The best-known contemporary monocotyledonous plants are palms. However, palms are not considered genuine trees, because they originate from ancient herbaceous plants (Zhdanov 1990). According to the theory of evolution, the division of the plant kingdom into arboreal forms and grasses must be traced back to the Cretaceous period of the Mesozoic era (135–110 million years ago) (Zhdanov 1990).

Contemporary deciduous timber species differ from coniferous species by a greater number of varieties. For example, in the European part of Russia alone, there are 70 varieties of birch and 50 varieties of the poplar genus Populus, while 150 varieties of eucalyptus grow on the Black Sea Coast of the Caucasus (Ugolev 2001).

Understanding of the evolution and polymorphism of arboreal populations is based on the understanding of the inherited, genetic principles of their diversity and adaptation to the environment. One of the fundamentals of genetics is the chromosome theory of heredity, according to which all hereditary information on an organism's development and properties is accumulated mainly in molecular chromosome structures. They are contained in the nuclei of all the organism's cells. The material carrier of information is the genome – polymer deoxyribonucleic acid (DNA) is the physical information medium.

In order to envision the mechanism of hereditary transfer of features from parent organism to daughter organism, let us start by briefly analyzing the intercellular organization of a protoplast – the metabolically active component of a plant cell.

A protoplast consists of two parts: cytoplasm and vacuole. They are separated from the cell wall and from each other by membranes (so-called plasmalemma and tonoplast, respectively). Cytoplasm is a liquid material with varying density. It contains multiple corpuscular inclusions, each of which is surrounded by its own membrane with specific porosity and permeability.

The largest inclusion is the nucleus. Its nucleoplasm is where nuclear chromosomes are contained. It also contains a karyonucleus, where nuclear ribosomes originate. Ribosomes, which contain macromolecules of ribonucleic acids (RNA), are the most numerous corpuscular inclusions in cytoplasm. They may be both in the unbound state and bound state with the membranes of other inclusions and may be part of intracellular organelles such as chloroplasts and mitochondria. The group of small corpuscular inclusions consists of spherosomes, peroxisomes, and glyoxisomes with various functions. Some of them are present in photosynthetic cells of leaves, and others in the cells of seeds. The major membrane inclusion in the protoplasm is endoplasmic reticulum, which consists of interlocking membrane tubules and bubbles. The membrane of endoplasmic reticulum is connected to the nuclear membrane. Dictyosomes (which have the appearance of stacked flat bubbles) of the Golgi apparatus, which combines a corpuscular and membrane structure, are also closely linked with these same membranes. Intracellular transport exchange takes place due to this network of links. It is assumed that the synthesis of many compounds, including polysaccharides of the wall cell matrix, occurs in the dictyosomes of the Golgi apparatus (Goodwin and Mercer 1986). Part of these substances goes into a vacuole through the tonoplast. Vacuoles serve as a sort of storage for the nutrients that a plant accumulates. Although chloroplasts and mitochondria possess a certain genetic autonomy because they contain their own DNA and ribosomes, the decisive role in transferring hereditary features belongs to the nucleus.

Mitochondria are the centers of intracellular respiration owing to the oxidation of substances into CO_2 and H_2O with energy emission and oxidative phosphorylation with the formation of adenosine triphosphate (ATP), an essential compound for biosynthesis, and they also contain the ferments for many important metabolic reactions (Goodwin and Mercer 1986). Depending on the type and dimensions of a cell, one plant cell may have 100 or even 1,000 mitochondria.

Chloroplasts are detected in the cells of leaves and all green tissues of woody plants. They are not present in the living cells of sprouts and roots. One cell usually holds from 2 to 400 of these corpuscular inclusions. The processes that occur in chloroplasts are formation of chlorophyll, biosynthesis of carotenoids and fatty acids, and photosynthesis of monosaccharides – precursors of oligosaccharides, the most important of which is saccharose.

Genomes of mitochondria and chloroplasts are not only smaller than nuclear DNA but also differ in nucleotide composition. Furthermore, mitochondria and chloroplasts have many copies of DNA molecules in contrast to DNA of nuclear chromosomes. Ribosomes located in chloroplasts and mitochondria also have smaller dimensions than ribosomes in cytoplasm.

As previously stated, DNA functions as the carrier and depositary of hereditary information. This information is coded in the genes, which are specific linear sections (blocks) of DNA macromolecules.

Each chromosome is a sort of nucleoprotein DNA complex with a large number of histone proteins of relatively low molecular weight. Two gigantic chains of DNA molecules, whose length in expanded form may amount to 1–2 m, form a double spiral. After further curling, this spiral provides a still better level of compact packing of DNA, so that DNA may occupy only 40–50 μm^3 within the nucleus volume. Therefore, a plant cell may hold not one but many chromosomes. Access to DNA information coded in the genes is only possible after dismantling all levels of packing and disengagement of the double DNA spiral. A major role in this DNA gene deactivation procedure is played by histones, the proteins mentioned above.

Information contained in the DNA molecule is not actualized immediately but is first decoded onto a matrix, messenger macromolecule of ribonucleic acid (mRNA) and then transported by transfer RNA molecules (tRNA) into the cell cytoplasm for protein biosynthesis. Protein synthesis is carried out with the participation of cytoplasm ribosomes and ferments. Cytoplasm ribosomes based on information transferred from the genes by mRNA molecules with the aid of tRNA combine various amino acids in sequential order and synthesize the protein of the coded composition.

From the chemical point of view, DNA is a sequence of deoxyribonucleotide structural units interconnected by phosphodiester linkages through $3' \rightarrow 5'$ carbon bonds of the ribose carbohydrate cycle. Deoxyribonucleotide units contain purine bases, adenine and guanine, as well as pyrimidine bases, thymine and cytosine. The DNA structural link is shown in simplified form in Fig. 2.5.

A DNA macromolecule may contain various combinations and sequences of nucleotides with the bases indicated above. Every three sequences of nucleotides capable of coding the synthesis of one amino acid in a protein molecule are called a codogene, whereas each such triplet in the corresponding macromolecule of messenger RNA is called a codon and anticodon – in transfer RNA.

RNA macromolecules are similar in chemical composition to DNA, because they consist of a row of ribonucleotides linked by phosphodiester linkages in $3' \rightarrow 5'$ position of the ribose cycle. But in contrast to DNA, one of the nucleotides of RNA structural units contains a uridine base instead of thymine.

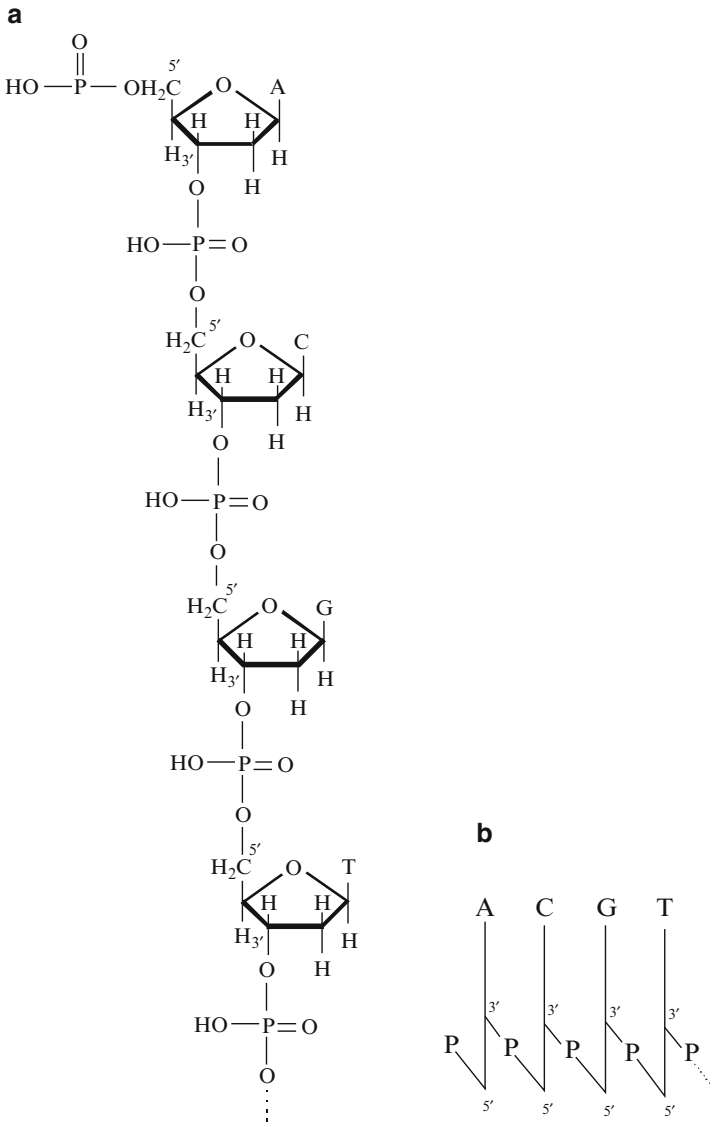

Fig. 2.5 Primary structure of the polydeoxyribonucleotide chain (**a**) and its contracted representation (**b**). A adenine, C cytosine, G guanine, T thymine

Intra- and interspecies polymorphism by chromosome number in plant cells was discovered in the first half of the twentieth century. Every plant species has an inherent set of a strictly determined number and type of chromosomes in the cell nuclei. This set is connected to the nature of the cell division process and to the evolution of plant cell structure.

The process of plant cell division occurs simultaneously with the cycle of doubling and division of chromosomes and other cell components. The newly formed cells maintain a strictly constant number and set of chromosomes intrinsic to the given species of woody plant.

According to the chromosome theory of heredity, the basis of biological diversity of woody plants is the difference in chromosome set types in the cells. The baseline is a single, so-called haploid set with one molecular DNA chain in the chromosome (haplotype is denoted by the letter "*n*," where n is the chromosome number). A haploid chromosome set is found in germinal cells of an organism and in the nuclei of plant fragments. Thus, in deciduous species, the pistillate haploid generation is enclosed in the embryo sac located in the seed-bud, whereas staminate generation is located inside the pollen grain.

A double, or diploid set ($2n$), consists of 2 haploid sets. It is formed during fertilization as a result of the combination of maternal and paternal haploid sets. One more type is the polyploid set, where the cell nuclei contain more than two chromosome sets. Plants with multiple haploid chromosome sets are correspondingly triploid ($3n$), tetraploid ($4n$), and so on. Diploid chromosomes undergoing the cycle of duplication and division inside the cell nucleus without breaking its membrane may form tetraploid ($4n$) and then multiploid nuclei, e.g., hexaploid ($6n$) or octaploid ($8n$).

The chromosome composition of many widespread woody plants has now become known. Polymorphism of coniferous species has been studied more in this respect. Thus, the number of chromosomes in plant cells has been determined in about 80 % out of 800 studied coniferous species (Grif 2007). Coniferous plants most commonly have a diploid set with large chromosomes $2n = 16$–24. Exceptions are the natural hybrid – polyploid of Sierra redwood with $6n = 66$ chromosomes and golden larch with chromosome set $4n = 44$ (Grif 2007; Tsarev et al. 2000). A triploid hybrid of larch was artificially obtained, and it is distinguished by rapid tree growth and resistance to low temperatures (Tsarev et al. 2000).

Deciduous timber species show more diversity compared to coniferous species. Along with diploid type, widespread occurrence of intraspecific and interspecific polyploidy has also been observed in them (Grif 2007). The chromosome number in the nuclei of deciduous species cells may vary over a wide range (from 4 to 200). As a rule, as the chromosome number increases, their dimensions are reduced. Interestingly, polyploidy enhances the intensity of synthesis of various useful chemical compounds. The optimum polyploidy level in deciduous species is a triploid set of chromosomes. It may be the result of environmental stress or obtained through dedicated hybridization. For example, the triploid versions of poplar, birch, and alder, which feature not only rapid growth but also high-quality wood, were obtained by hybridization of diploid and tetraploid forms of woody plants. Polyploids are especially numerous among the willow and birch families. For example, within the Salix genus of willows, whole polyploid rows were discovered with chromosome numbers 38, 44, 57, 76, 88, 114, 152, and 190. They are represented by two polyploid series with main haplotypes $n = 19$ and $n = 22$. The specified row numbers include haploid chromosome set $2n = 38$ and a set of

higher forms up to decaploid with chromosome number $10n = 190$. Chromosome numbers 44 and 88 in this row are attributed to the diploid and tetraploid versions and in the second series of haploid set $n = 22$ (Afonin).

Certain woody plants typically have an aneuploid chromosome set in plant cells. Aneuploidy along with polyploidy is one more type of mutation resulting from dilation or addition of haploid chromosomes to the already existing set in the cell. Thus, along with the tetraploid version of the Siberian pea shrub with 32 chromosomes in its nuclei, aneuploid versions have been discovered with 27 and 29 chromosomes (Borodina 1982).

At present, it has become evident that polymorphism of woody plants is based on specificity of molecular structure and great variety of genome (DNA) states.

Possible molecular mechanisms that change the state of genomes, namely, of their active part, are addressed in work (Romanovsky 1994). These mechanisms may be changes in the conformational state of DNA sections and in the activity of genes linked to these sections; activation or repression of genes as a result of proteins bonding with certain DNA sections or disruption of these bonds; a change in gene order through rearrangement made by ring structures; reaggregation of genetic information through crossing over. The phenomenon of crossing over consists in modification of the qualitative composition chromosomes without altering their number. This happens as a result of interchange of certain sections between closely adjacent chromosomes, passage of part of the genes from paternal chromosomes to maternal chromosomes, and vice versa.

Regarding polymorphism as a consequence of various mutations in a plant organism resulted in subdivision of mutations into a series of classes or types (Grif 2007). The following types are the most common among timber populations:

1. Gene (point) mutations – when one or several pairs of nucleotides in DNA are substituted for others not involved in prominent chromosome alterations.
2. Chromosome mutations like crossing over and aneuploidy.
3. Genome mutations involving alterations in the number of chromosome sets. Polyploidy is the most common type of genome mutagenesis. It predominates due to the possibility of increasing the number of genes and maintaining the integrity of the original genome and its functions.

In the opinion of several authors (Grif 2007; Golubovsky 2000), there is one more type of mutation, which affects hereditary features and polymorphism of plant organisms. These are cytoplasmic mutations. This opinion is based on the data of possible independent (outside of chromosomes) existence of gene loci (blocks of genes) responsible for certain chereditary features in cytoplasm.

More in-depth modern studies of the biogenetic aspects of mutability and of evolution of woody plants and their adaptation to the environment involve newly developed methods and approaches to solving the problem at the genome level (Krutovsky 2006).

In the past decade, it has become possible to employ new types of molecular genetic markers with a known sequence of nucleotide buildup and known functions. Various molecular markers of expressed (i.e., capable of activation) genes were

obtained from those of dinucleotide nature to the full nucleotide sequence of genes – blocks of various genomes. Hundreds of thousands of such nucleotide sequences for many forest trees, including pine, spruce, poplar, and eucalyptus, have been discovered.

The full gene structure of the nuclear genome of the poplar Populus trichocarpa was determined in 2006 (Tuskan et al. 2006). The nuclear genome of this poplar with haploid number of chromosomes $n = 19$ has relatively small dimensions: about 500 Mb (1 Mb is the unit of measurement of genome length equal to one million nucleotides). The nuclear genome of the poplar has been found to hold more than 45,000 genes that code protein synthesis. However, a significant part of DNA molecule consists of "dormant" genes, which do not participate in protein synthesis. Scientists (Tuskan et al. 2006) believe that full DNA sequencing will help to identify the genes associated with biosynthesis of a lignocellulosic cell wall, with development of plant tissues, transport of metabolites, and with other important processes.

Biochemical reactions of synthesis of many compounds that proceed in a living woody organism involving various catalytic ferment systems are very complicated. Even a brief description of biosynthesis of basic wood components of interest to us would take up too much space and would be difficult for an unprepared reader to understand. We do not consider it advisable, because this subject goes beyond the issues addressed in this book.

2.3 Density and Moisture of Timber Species

Density is an essential characteristic of timber quality closely associated with its anatomy.

Structural features of timber directly affect not only its density but also capacity to interact with water molecules. And this in turn affects the thermophysical and mechanical properties of timber.

Timber density and moisture, as will be shown in later sections of the book, greatly affect the flammability and fire behavior of this material. It is known, however, that timber density and moisture are to some extent interrelated characteristics.

In the bone-dry state, the timber density, ρ_0, may be taken as the ratio of dry sample mass, m_0, to its volume, V_0:

$$\rho_0 = m_0 / V_0, \ \mathrm{g/cm^3} \left(\text{or } \mathrm{kg/m^3}\right)$$

Moistening bone-dry timber not only increases sample mass but also increases its volume due to swelling. It was noted that when timber is left in water or air with enhanced humidity, the sample volume increases only to a definite limit. This limit corresponds to full water saturation of the timber cell walls in the form of so-called imbibed water. A further increase in water content in timber due to the filling of

pores, capillaries, and other void spaces in the timber structure by so-called free water leads only to an increase in total sample mass without increasing moist timber volume.

As a result, moist timber density, expressed as the ratio of sample mass at a given moisture to its volume at the same moisture, increases significantly compared to the density of bone-dry timber.

In order to provide an accurate comparison of various timber species by density, the notions of density of timber with normalized moisture, as well as basic density (previously called conventional density), were introduced. Normalized timber density is the density of timber at 12 % moisture:

$$\rho_{12} = \frac{m_{12}}{V_{12}}$$

Basic density is expressed as the ratio of bone-dry sample mass to its volume at a moisture equal to or greater than the saturation limit of cell walls, $V_{\max}$:

$$\rho_{\mathrm{b}} = \frac{m_0}{V_{\max}}$$

In effect, this parameter reflects the content of wood matter in the unit of volume of timber maximally swollen in water (including freshwood basic density estimation).

Along with the saturation limit of cell walls, W_{SL}, which is understood as the maximum moisture of cell walls when timber is moistened in water, the notion of wood hygroscopicity limit W_{HL} is also used. This parameter corresponds to the maximum moisture of cell walls achieved during sorption of water vapor from the air.

The hygroscopicity limit depends on the temperature, whereas the saturation limit of cell walls is not influenced by it. At zero temperature, these parameters nearly coincide: $W_{\mathrm{SL}} = W_{\mathrm{HL}}$, because at 0 °C W_{HL} reaches its maximum value. At temperatures above 0 °C, the condition $W_{\mathrm{HL}} < W_{\mathrm{SL}}$ is always observed for a specific timber variety.

Although the saturation limit of cell walls may vary from 22 to 53 % in different timber species depending on timber density, the figure often used in calculations is the average value $W_{\mathrm{SL}} = 30$ % (Ugolev 2001). In the opinion of many authors (Chudinov 1984), the structure and chemical composition of timber (its species) also has an impact on its hygroscopicity limit. However, the hygroscopicity limit of various timber species at room temperature is recorded in a narrower range of values (from 22 to 35 %).

Average values of bone-dry timber density, basic density, and density of timber with normalized moisture for the most common timber species growing in Russia are given in Table 2.1 (Ugolev 2001; Poluboyarinov 1976).

Various timber species are subdivided by normalized density into low-density species ($\rho_{12} < 540$ kg/m^3), medium-density ($550 < \rho_{12} < 740$ kg/m^3), and high-density ($\rho_{12} > 750$ kg/m^3). The lowest and highest densities are observed

Table 2.1 Average density values for various timber species

Species	ρ_0, kg/m^3	ρ_{12}, kg/m^3	ρ_p, kg/m^3	Growing region
Dahurian larch	611	643	502	Far East
	583	613	472	Yakutia
Siberian larch	640	673	525	North, Urals
	621	653	509	Western Siberia
	603	634	494	Eastern Siberia
Common pine	476	505	405	Kola Peninsula
	495	525	421	Urals
	448	475	381	Western Siberia
	439	465	373	Eastern Siberia
Common fir	457	484	388	North European part
	429	455	365	Central part
Siberian fir	411	436	350	Eastern Siberia
	364	386	310	Western Siberia
	429	455	365	Far East
Cedar	402	426	342	Urals
	429	455	365	Altai
	420	445	357	Eastern Siberia
Siberian fir	383	406	326	Altai
	336	356	286	Western Siberia
	329	346	279	Eastern Siberia
Schmidt's birch	923	970	757	Primorye Territory
White birch	584	614	479	Central European part
Beech	607	643	516	Krasnodar Territory
White elm	513	544	436	European part
Hornbeam	753	792	618	Caucasus
Oak	679	720	577	Central European part
White willow	393	416	334	European part
Maple	650	690	570	European part
Lime	461	485	378	European part
Alder	427	452	363	Leningrad Region
Aspen	455	485	389	Central European part
Persian walnut	560	594	476	Caucasus
White poplar	393	413	334	European part
Black poplar	439	465	373	European part
Common ash	626	663	532	Central European part
Manchurian ash	616	653	524	Far East

in the foreign deciduous species balsa ($\rho_{12} = 120$ kg/m^3) and lignum vitae ($\rho_{12} = 1{,}300$ kg/m^3), respectively (Ugolev 2001). Among Russian species, as is seen from Table 2.1, Siberian Spruce from Eastern Siberia has very low density, whereas Schmidt's Birch from Primorye Territory has the highest density.

Density within the same species may vary depending on the ratio of earlywood and latewood layer dimensions in the growth layer, pith, and sapwood, which in turn depends on the conditions, soil, and climatic factors of tree growth (Shirnin et al. 2004).

The notion of specific gravity of timber is often used in the USA and other countries. This value, G_x, is considered as the relative density of timber, i.e., the ratio of timber density with specific moisture (x %) to water density at a temperature of 4 °C, where $\rho_w = 1.000$ g/cm^3 (Glass and Felinka 2010). In this case, the value G_x is linked to the value ρ_x by the ratio:

$$G_x = \rho_x / \rho_{\mathrm{w}} \, (1 + x/100) \, .$$

The question of the true density of wood matter usually identified with the material that forms the cell membranes is of special interest. It is assumed that true density of wood matter is equal for all species, because the components that form the cell walls do not differ much from each other in their density. Furthermore, cell membranes of woody plants of various species are nearly identical in structure and chemical composition.

The main difficulty in assessing the true density of wood matter:

$$\rho_{\mathrm{wm}} = \frac{m_{\mathrm{wm}}}{V_{\mathrm{wm}}}$$

is in accurate determination of the volume occupied by wood matter in the test specimen. Experimental techniques based on measuring the volume of liquid or gas forced out by the wood specimen give various results depending on the capacity of the liquid or gas to penetrate the pores of the cell wall. The density of wood matter measured in water is the average value for all species amounting to 1.53 g/cm^3, whereas when measured with helium and in nonpolar fluids (benzene, toluene, and mineral oil), it equals 1.46 and 1.44 g/cm^3, respectively. The higher value of wood matter density obtained with water is believed (Ugolev 2001) to be due to apparent volume (V_{wm}) reduction due to penetration of molecules into cellulose microfibers.

Based on data on the wood matter density in redwood and northern white cedar before and after withdrawal of extractive components (average values for these species are 1.505 and 1.530 g/cm^3, respectively), the opinion was expressed that the chemical composition of wood affects ρ_{wm} value. The impact of extractive substances on wood matter density was also discovered in other species (Chudinov 1984). In earlier electron microscopy studies of cell wall density in different timber species, it was found that density values of cell walls were about 10 % lower compared to wood matter density. Despite rightful criticism of these results, the authors' conclusion that cell membrane density depends on timber variety and species and plant age, and may even change within the growth layer, is important (Chudinov 1984).

The assertion that the chemical components in the cell walls of woody plants differ little in density does not seem altogether proper to us. In fact, even cellulose that forms the wood frame and has an amorphocrystalline structure also typically has amorphous macromolecule sections with different densities arranged in crystallites. The true density of crystallites of known polymorphic modifications of native

cellulose 1α and 1β is 1.55 and 1.59 g/cm^3. Disordered cellulose macromolecules usually localized in the space between microfibers have noticeably lower density (Aleshina et al. 2001). The true density of lignin is about 1.25–1.36 g/cm^3 (Ugolev 2001; Siau 1984). Unfortunately, we have not found the data on the true density of hemicelluloses. However, if we take as the upper limit the density of crystal modifications of monosaccharides, mannite, xylose, glucose, arabinose (1.489; 1.53; 1.544; 1.585 g/cm^3), or disaccharides, saccharose, maltose (1.588; 1.540 g/cm^3) (Perelman 1955), we should then expect the hemicelluloses, as oligo-carbohydrates with less ordered amorphous structure, to have true density of about 1.32–1.41 г/cm^3.

The ratio between the bone-dry timber and true density of wood matter in this sample makes it possible to estimate the value of timber porosity, P:

$$P = \{1 - (\rho_0/\rho_{wm})\}\, 100, \%$$

Timber porosity ranges from 40 to 77 % depending on the species.

Features of the morphological structure of timber significantly affect permeability – the capacity to conduct liquids or gases under pressure.

Timber permeability is experimentally determined by the velocity of water or air (nitrogen) transfer through a specimen's unit of area (GOST 16483.34 – 77). Determining gas permeability requires less time compared to water permeability. Due to the close correlation between these properties, the gas permeability parameters are used to assess the capacity of timber to soak up solutions of antiseptics, fire retardants, and other substances.

In order to compare various types of timber, it is recommended (GOST 16483.34 – 77) to use the gas permeability coefficient:

$$K_G = \upsilon h/P, \mathrm{m}^2/\mathrm{s\ MPa}$$

where υ is the gas permeability, m^3/(m^{2}s); h is the specimen height, m; and P is the gage pressure, MPa.

A study of gas permeability of coniferous timber species in Siberia showed that pine specimens had the highest values of K_G (up to 2.2×10^{-3} m^2/s MPa). Cedar and larch have lower K_G. Spruce has the lowest factor. All species show higher gas permeability in sapwood compared to heartwood (Ugolev 2001).

Table 2.2 shows an example of air permeability coefficients in the radial and tangential directions in a sapwood specimen of Siberian larch (Greb and Dzyga 2004).

The conclusion is that the air permeability coefficient of larch sapwood in the tangential direction is on average 22.5 times higher compared to the radial direction. In contrast to the radial direction, there is an end-to-end capillary system in the tangential direction. It consists of vertical tracheids connected by means of open bordered pores.

Table 2.2 Impact of gage pressure on air permeability coefficient in sapwood of Siberian larch

	Air permeability coefficient K_G, $\times 10^{-6}$ m^2/s MPa	
Pressure, MPa	Tangential direction	Radial direction
0.2	19.64	0.75
0.4	49.78	2.11
0.6	78.21	4.36

2.4 Thermophysical Properties of Timber Species

Many parameters of flammability and fire behavior of timber, like other organic materials, depend to a great extent on its thermophysical properties. This is only natural, because heating of a material exposed to an external source depends on the response of the material to the energy applied to its surface and on the way heat is transferred to the underlying layers.

Experimental and theoretical studies of flammability and fire behavior usually refer to such thermophysical characteristics as specific heat, thermal conductivity, thermal diffusivity, and thermal inertia. The last two parameters are inclusive, taking material density into account.

Specific heat of any system is defined as the ratio of amount of heat imparted to the system in a process to its temperature change. The general definition may be valid for systems consisting both of one and several components or several phases. Specific heat is the amount of heat needed to heat a unit of material (substance) mass by 1°. It is usually expressed in kJ/kg · K or J/g · K.

According to the Debye theory of solids, specific heat of a solid body is determined by the vibration frequency of its structure elements and by thermal-motion energy of these elements. The vibration spectrum of macromolecules of wood matter components includes torsional and pendulum vibrations of atoms and atom groups, deformation, skeletal vibrations of separate bonds and sections of the macromolecule chain, valence vibrations of various chemical bonds, and, finally, cooperative vibrations induced by incipiency of macromolecule segmental mobility and by structural phase transitions from one state to the other.

Dry timber is a typical two-phase system consisting of wood matter and air. Specific heat of timber at constant pressure, c_P, hardly depends at all on its density. Since the mass fraction of air in the material is insignificant, specific heat of dry timber is determined by specific heat of wood matter. On the average for all species at 0 °C, it is assumed to equal $c_{P0} = 1.55$ kJ/kg · deg. (Ugolev 2001). According to other sources, $c_{P0} = 1.20$ (Glass and Felinka 2010) and 1.36 kJ/kg · deg. (Spearpoint and Quintiere 2001).

In timber moistening, when air is replaced with water, specific heat of timber is increased. Below the saturation limit of cell walls, the specific heat of moist timber equals the sum of specific heat of dry timber, specific heat of connected

water, and the increment caused by the additional energy of the water – water bond, A_c. The increment, A_c, depends not only on the water content in timber but also on temperature. In the temperature range 7–147 °C, the value of A_c is determined by the equation (Glass and Felinka 2010):

$$A_c = M\,(b_1 + b_2 T + b_3 M),$$

where M is the connected water content, %; T is the temperature, K; and coefficients $b_1 = -0.\,06191$; $b_2 = 2.36 \times 10^{-4}$; $b_3 = -1.3 \times 10^{-4}$.

When saturation limit of the cell walls is achieved (30 % moisture) at zero temperature, specific heat of timber increases to 2.2 kJ/kg · deg., whereas at 100 % moistening, it increases to 3.0 kJ/kg · deg. (Ugolev 2001).

Naturally, a temperature increase enhances the specific heat of timber, because when timber is heated, vibration motions of various structure elements of macromolecules are unfrozen. Specific heat of dry timber changes with temperature by a linear law, reaching almost 2.0 kJ/kg · deg. at 100 °C. According to (Janssens 1991), the relationship between temperature and specific heat may be expressed in the following way:

$$c_{P0}(T) = c_{pr}\,(T/T_r)\,,$$

where c_{pr} is the specific heat of dry timber at temperature $T_r = 293$ K.

The impact of both temperature and moisture on specific heat of timber has been studied in the temperature interval from −40 °C to the boiling point of water (Ugolev 2001). Timber ignition occurs at a fairly high temperature. This being the case, it was suggested to use the value of specific heat of timber adjusted for the thermal properties of water (Simms and Law 1967):

$$c_{PW} = c_{P0} + (\Delta W + L + 4.19\,\Theta_0)\,0.01\left(M/\Theta_{ign}\right),$$

where c_{PW} and c_{P0} – specific heat of timber of moist and dry timber, respectively; ΔW – heat of timber wetting, equals 66.9 kJ/kg; L – latent heat of water vaporization, equals 2,175 kJ/kg; Θ_0 – temperature change from environmental temperature to 100 °C; $\Theta_{ign} = (T_{ign} – T_0)$ – temperature change from environmental value to timber ignition temperature; and M – moisture content in timber, %. Coefficient 4.19 – latent vaporization heat of water.

The authors of work (Spearpoint and Quintiere 2001), following ignition experiments, have assessed specific heat of timber specimens cut from the trunk in crosswise and longitudinal directions relative to fiber orientation (Table 2.3).

The influence of anisotropy on the obtained characteristics is worth noting. Thermophysical properties are better in the longitudinal direction compared to crosswise. This effect is caused by different conditions of heat transfer, when heat flow is applied perpendicular to the specimen surface or parallel to the wood fiber axis, and by the different response of a material to temperature change.

Table 2.3 Values of thermal conductivity and specific heat for various directions of heat flow

Timber	Heat flow direction	Density, ρ_w, kg/m^3	k_w, W/m · deg.	C_{pw}, J/kg · deg.
Redwood	Across fibers	354	0.19	3,200
	Along fibers	328	0.85	7,400
Douglas fir	Across fibers	502	0.23	2,200
	Along fibers	455	0.80	4,000
Champion oak	Across fibers	753	0.44	3,100
	Along fibers	678	0.86	3,200
Maple	Across fibers	741	0.35	2,500
	Along fibers	742	–	7,100

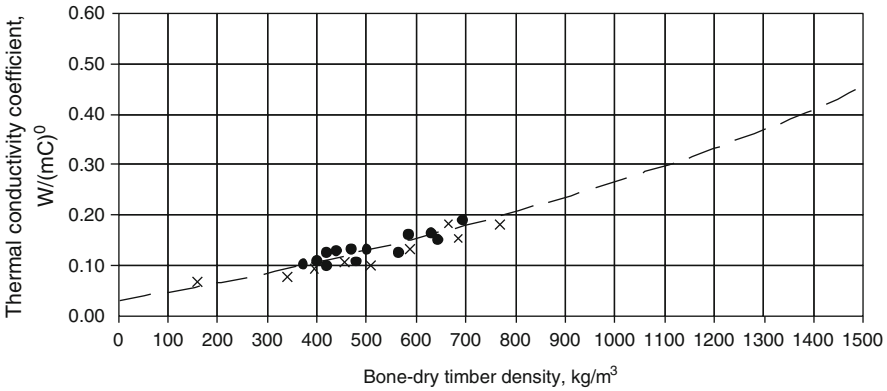

Fig. 2.6 Curve of thermal conductivity coefficient in crosswise direction to the fiber axis vs. timber density in bone-dry state

Thermal conductivity of timber in compliance with Fourier's heat transfer law is described as the rate of heat flow through a unit of material surface area causing temperature drop, ΔT, on the heat flow path, l. Thermal conductivity, k, is numerically equal to the rate of heat flow in J/s through material with 1 m^2 surface area and 1 m thickness providing a temperature difference at the extremities of 1 K. Thermal conductivity of timber depends on various factors: timber density, temperature, water and extractive substance content, heat flow orientation in reference to fiber direction, and structural irregularities.

Figure 2.6 shows the influence of bone-dry timber density on the thermal conductivity coefficient in the crosswise direction to the fiber axis.

Extrapolation of the curve to the density assumed for the wood matter ($\rho_{wm} = 1{,}530$ kg/m^3) gives a value of the wood matter thermal conductivity coefficient across the fibers of about 0.5 W/m · deg. (Ugolev 2001). Experimental data obtained by various scientists for the thermal conductivity coefficient of timber cell walls perpendicular to the fiber axis range from 0.40 to 0.44 W/m · K, whereas in the longitudinal direction, the range is $k_{II} = 0.67$–0.88 W/m · K. According to (Ugolev 2001), $k_{wm\perp} = 0.48$ for birch (in crosswise direction),

whereas $k_{\text{wmII}} = 0.948$ W/m · deg. The thermal conductivity coefficient of timber is much lower compared to that of wood matter (Fig. 2.6). At normal temperature and 12 % moisture, the values of $k_{\perp}$ for many timber species range between 0.10 and 0.20 W/m · deg.

Table 2.3 shows thermal conductivity coefficients of some specimens of coniferous and deciduous species for various fiber orientations in relation to the external heat flow. They were obtained from tests of timber ignition through exposure to radiative heat flow of 25–75 kW/m^2 (Spearpoint and Quintiere 2001). Thermal diffusivity and thermal inertia are physical parameters that characterize thermal inertial properties of material.

The thermal diffusivity is determined from the ratio:

$$a = k/\rho c,\ \text{m}^2/\text{s}$$

and thermal inertia is the product of above parameters: $k\rho c$.

The thermal diffusivity of bone-dry timber decreases in proportion to material density enhancement, as is seen from the ratio above. It was demonstrated that with moisture below the saturation limit of cell walls, the thermal diffusivity of timber does not differ much from the same parameter for dry timber and ranges from 1.6–2.1×10^{-7} m^2/s for various species (Ugolev 2001).

The effect of temperature should be more significant, because a temperature increase causes alteration of both thermal conductivity and specific heat of a material. However, to all appearances, due to the equivalent change of these values with a temperature increase up to 250–290 °C, thermal diffusivity, according to the data from various researchers, hardly depends at all on temperature within this range, yet is constant for every timber species (Spearpoint and Quintiere 2001).

In contrast to the thermal diffusivity, the thermal inertia parameter, $k\rho c$, depends heavily on temperature. This is precisely why the $k\rho c$ parameter derived from ignition tests is an effective value. It corresponds to the average material temperature between ignition and environmental temperatures. The value of the $k\rho c$ parameter obtained in this way is 1.6–2.6 times the value at 293 K (Ugolev 2001; Glass and Felinka 2010).

There is a very limited amount of published data pertaining to direct measurements of thermophysical properties of timber in a wide range of temperatures. Table 2.4 gives the values of thermal diffusivity and thermal inertia for some specimens of coniferous and deciduous species. The influence of external heat flow direction with respect to timber fiber axis is also shown.

High thermal inertia values obtained from ignition experiments with the heat flow applied to a timber specimen surface parallel to the fiber axis orientation are likely the result of enhanced temperature effect on the increase in specific heat and especially on the increase in the thermal conductivity coefficient under these heat transfer condition.

The observed general rule is enhanced thermal inertia of timber in proportion to the increase of its density. Moisture impact is also noticeable. Bone-dry timber from Moscow Region has the lowest $k\rho c$ value. Moisture content in other specimens from Table 2.4 was 4–8 %.

Table 2.4 Values of thermal diffusivity and thermal inertia for various timber species

Timber	Heat flow direction	ρ, kg/m^3	a, m^2/s	$k\rho c$, KJ^2/K^{2}m^{4}s	References
Douglas fir	[a]	465	–	0.158	Janssens (1991)
	⊥	502	1.79×10^{-7}	0.25	Spearpoint and Quintiere (2001)
	II	450	–	1.44	Spearpoint and Quintiere (2001)
Vietnam fir	⊥	400	–	0.148	Bui Din Than (2006)
Pine (Moscow Region)	⊥	450	1.84×10^{-7}	0.070	Sivenkov (2002)
Pine	⊥	460	–	0.156	Janssens (1991)
White pine	⊥	380	6.6×10^{-7}	–	Moghtadery et al. (1997)
Southern pine	⊥	508	–	0.183	Tran and White (1992)
Vietnam pine	⊥	430	–	0.173	Bui Din Than (2006)
Redwood	⊥	430	–	0.141	Janssens (1991)
	⊥	354	1.89×10^{-7}	0.22	Spearpoint and Quintiere (2001)
	II	328	–	2.07	Spearpoint and Quintiere (2001)
	[a]	312	–	0.073	Tran and White (1992)
Thuja	⊥	330	–	0.087	Janssens (1991)
Red oak	[a]	660	–	0.360	Tran and White (1992)
	⊥	753	1.74×10^{-7}	1.01	Spearpoint and Quintiere (2001)
	II	678	–	1.85	Spearpoint and Quintiere (2001)
Maple	[a]	530	1.0×10^{-7}	–	Moghtadery et al. (1997)
	⊥	741	1.75×10^{-7}	0.67	Spearpoint and Quintiere (2001)
	II	742	–	1.09	Spearpoint and Quintiere (2001)
Lime	[a]	420	–	0.141	Tran and White (1992)
Vietnam eucalypt	⊥	595	–	0.139	Bui Din Than (2006)
Eucalypt	[a]	640	–	0.260	Janssens (1991)
Eucalypt	[a]	810	–	0.393	Janssens (1991)
Vietnam acacia	⊥	560	–	0.140	Bui Din Than (2006)

[a]Heat flow direction with respect to timber fiber orientation is not indicated. The data are likely to refer to an external heat flow perpendicular to the fiber axis

2.5 Effects of Heating on Mechanical Properties of Structural Timber and Timber Products

Mechanical properties of timber and its products are of great interest from the point of view of their practical use in building structures. Timber may be regarded as a viscoelastic anisotropic polymer composite. Its behavior under applied forces

and thermal effect is described by various parameters that specify the resulting strains and deformations. The major parameters are elastic modulus, E, and rigidity modulus, G (elastic modulus in shear), Poisson's ratio, and strength properties corresponding to deformations at the material breakdown limit. Since timber is anisotropic, each parameter may be represented by the values defined according to three directions of fibers in the material and to the growth layer: longitudinal, radial, and tangential.

Poisson's ratio expresses the ratio of material deformations in the crosswise and longitudinal directions to the applied load. The value of this ratio for various coniferous and deciduous species is intermediate between 0.5 and 0.9, typical for organic liquids, and 0.02–0.2, typical for reversible deformation of solids with amorphocrystalline structure. Elastic stress occurs in common solids (glass, quartz, metals, and polymers) as a result of the change in intermolecular distances of the material's chemical structure.

This consequently leads to increased volume of the deformed body and alteration of Poisson's ratio. The lower Poisson's ratio, the higher the material strength factor expressed as the ratio of compression strength to tensile strength. Poisson's ratios are affected by moisture content in timber.

At a temperature above the vitrifying point, the transition of solids into the high elastic state occurs. In this state, deformation is not accompanied by a change in volume. Elasticity has a diverse, entropic nature manifested in mobility of separate sections (linkages) of a material's chemical structure.

In everyday practice of timber material science, Poisson's ratio, μ, is not used, in spite of its clear physical content and relation to elasticity and rigidity moduli:

$$E = 2G\,(1 + \mu)\,.$$

On the other hand, some of the frequently used parameters of mechanical properties of timber are considered important but purely technological characteristics. This is the case, for example, with timber static and shock hardness. These parameters are of interest because they may be assessed by nondestructive methods of material testing.

A lot of attention has recently been paid to the analysis and disclosure of the correlation between various mechanical properties of timber and the extent of their variability.

In work (Volynsky 2006), there is a report on statistical processing of the database of mechanical properties of 167 timber species with regard to their growing region in the former USSR. Coniferous and deciduous species have been analyzed as two separate statistical multitudes. In the same way, data on 112 species and their varieties – 47 coniferous and 65 deciduous – growing in the USA and Canada have been analyzed. In addition, certain data of mechanical properties of tropical timbers species have been included.

In fact, this database of mechanical properties covers the prevailing population of timber species growing on the Earth.

Tables 2.5, 2.6, 2.7, and 2.8 sum up the obtained results. It must be emphasized that each variation as such is an arithmetic average describing concrete species and

Table 2.5 Statistical values of mechanical properties of coniferous timber species in the USSR

Parameters	ρ_{basic}, kg/m^3	$E_{bending}$, GPa	H_{later}, N, mm^{-2}	$\sigma_{compres}$, MPa	$\sigma_{bending}$, MPa	$\sigma_{tensile}$, MPa	σ_{shear}, MPa
Average/min–max	485/346–725	11.1/7.42–16.8	22.2/14.1–38	46.8/33.6–69.5	80.6/43.8–117	93.7/50.5–131	7.57/4.05–12.2
Variant number	61	36	28	61	61	31	55
Coefficient of variation, %	18.0	21.4	28.7	16.7	18.7	24.4	21.0

Table 2.6 Statistical values of mechanical properties of deciduous timber species in the USSR

Parameters	ρ_{basic}, kg/m^3	$E_{bending}$, GPa	H_{later}, N, mm^{-2}	$\sigma_{compres}$, MPa	$\sigma_{bending}$, MPa	$\sigma_{tensile}$, MPa	σ_{shear}, MPa
Average/min–max	647/337–973	10.59/4.38–16.7	47.2/15.7–110	52.6/31.4–81.7	97.0/55.7–160.0	113.2/63.2–212.0	10.3/4.67–19.0
Variant number	123	66	64	123	115	39	101
Coefficient of variation, %	20.0	24.7	41.0	18.7	22.7	29.0	30.9

Table 2.7 Statistical values of mechanical properties of coniferous timber species in the USA and Canada

Parameters	ρ_{basic}, kg/m^3	H_{later}, kN	$E_{bending}$, GPa	$\sigma_{compres}$, MPa	$\sigma_{bending}$, MPa	σ_{shear}, MPa
Average/ min–max	398/290–550	2.4/1.4–4.0	10.1/4.3–14.3	41.0/24.8–61.0	72/42–112	7.9/4.9–11.6
Variant number	68	43	68	68	68	66
Coefficient of variation, %	15. 1	26.5	19.2	17.6	19.0	17.9

Table 2.8 Statistical values of mechanical properties of deciduous timber species in the USA and Canada

Parameters	ρ_{basic}, kg/m^3	$E_{bending}$, GPa	H_{later}, kN	$\sigma_{bending}$, MPa	$\sigma_{compres}$, MPa	σ_{shear}, MPa
Average/ min–max	568/340–880	11.1/7–15.7	4.7/1.6–8.1	91.4/47–139	46.1/27.7–70.2	11.6/5.4–18.3
Variant number	65	65	51	65	65	62
Coefficient of variation, %	20.1	19.7	35.3	25.8	21.0	25.2

Table 2.9 Statistical values of mechanical properties of tropical timber species

Parameters	ρ_{basic}, kg/m^3	$E_{bending}$, GPa	H_{later}, kN	$\sigma_{bending}$, MPa	$\sigma_{compres}$, MPa	σ_{shear}, MPa
Average/ min–max	533/170–920	12.4/3.8–25.5	5.1/0.4–16.3	96.0/19.3–181.4	50.8/11.7–92/5	10.7/2.1–17
Variant number	50	49	49	50	50	50
Coefficient of variation, %	29.0	31.1	65.7	33.5	31.2	29.7

growing region of the woody plant. For comparison, the tables show mechanical properties of clean timber species with normalized 12 % moisture and average values of basic density. It is easily determined; the impact of moisture above saturation limit on mechanical strength is insignificant; therefore, conversion into density at normalized moisture is possible. Strength parameters in the tables are given for longitudinal orientation of the load along the fibers. Values of static hardness refer to measurements on the lateral surface (in the radial direction relative to the fibers). Experience shows that there is a slight difference between static hardness values in radial and tangential directions. Timber static hardness on a lateral surface is 30–40 % lower compared to the crosscut end.

Variability of mechanical properties is defined by the coefficient of variation. As follows from the data above, timber density as well as compression and bending strength show the least variability. The greatest variability is observed in static specimen hardness.

Almost the same trend is typical for deciduous and coniferous timber species in the USA and Canada as well as for tropical species. In the latter case, greater variation in hardness may be noted (coefficient of variation 65.7 % – Table 2.9).

All datasets without exception follow Gauss's law. A clear-cut difference in timber density is especially evident between coniferous species from different hemispheres.

It is assumed that the higher density of domestic coniferous species compared to the USA and Canada plants is caused by harsher weather conditions in Russia, especially in Siberia.

Even at the level of two generalized statistical multitudes of timber, the important role of the density parameter may be noted in its impact on a material's mechanical properties.

The closest correlation between timber's mechanical properties and basic density is represented by power equations:

$$Y = aX^n.$$

The equations connecting strength (MPa) and basic density (kg m^{-3}) are given below.

For deciduous timber species of the USA and Canada:

$\sigma_{\text{bending}} = 0.0598\ \rho^{1.172}$, correlation factor $R^2 = 0.807$
$\sigma_{\text{compres.}} = 0.1365\ \rho^{0.932}$, $R^2 = 0.800$
$\sigma_{\text{shear}} = 0.006\ \rho^{1.213}$, $R^2 = 0.832$

For coniferous species:

$\sigma_{\text{bending}} = 0.0716\ \rho^{1.153}$, $R^2 = 0.790$
$\sigma_{\text{compres.}} = 0.0545\ \rho^{1.105}$, $R^2 = 0.862$
$\sigma_{\text{shear}} = 0.03\ \rho^{0.931}$, $R^2 = 0.587$.

Equations of connection for domestic timber species are given separately, because they were established for smaller clean specimens and tested with slightly different standard procedures.

For deciduous timber species from various regions of the USSR:

$\sigma_{\text{bending}} = 0.325\ \rho^{0.879}$, $R^2 = 0.641$
$\sigma_{\text{compres.}} = 0.445\ \rho^{0.737}$, $R^2 = 0.678$
$\sigma_{\text{shear}} = 0.0002\ \rho^{1.022}$, $R^2 = 0.670$

For coniferous species:

$\sigma_{\text{bending}} = 0.271\ \rho^{0.930}$, $R^2 = 0.701$
$\sigma_{\text{compres.}} = 0.309\ \rho^{0.812}$, $R^2 = 0.762$
$\sigma_{\text{shear}} = 0.0131\ \rho^{1.022}$, $R^2 = 0.665$.

It is seen that "n" power in the obtained equations of connection is close to 1.

Therefore, in many studies, the dependence of timber's mechanical properties on density is assumed to be linear (Paul and Koukhta 2011).

A fairly close correlation between other mechanical parameters and density has also been revealed. Thus, an equation of connection was derived for lateral timber hardness (kN) at 12 % moisture and basic density:

$$\rho_{\text{basic}} = 267H^{0.438}, \text{kg/m}^3$$

Analysis of the mechanical properties of small clean specimens of timber showed a strong relationship between strength parameters and elastic moduli. This permits to skip the measurements of all parameters and define only one or two of them. After that, by using the equation of connection, we may predict the other parameters with a margin of error not exceeding 7–8 %.

Thus, analysis of properties of coniferous species from the USA and Canada resulted in the following equation, which ties the bending strength with elastic module E_{bending} and lateral hardness H_{later} of the specimen (Volynsky 2006):

$$\sigma_{\text{bending}} = 6.035 + 4.428E_{\text{bending}} + 8.782H_{\text{later}}, R^2 = 0.891.$$

Bending strength is expressed here in MPa, elastic modulus in GPa, and hardness in kN. In this way, the following equation of relationship of parameters was derived for domestic coniferous timber species:

$$\sigma_{\text{bending}} = 31.8 + 3.16E_{\text{bending}} + 0.707H_{\text{later}}, R^2 = 817; \text{error–}8.55\ \%.$$

The following correlation between strength parameters has been found for small clean timber specimens:

$$\sigma_{\text{bending}} = \sigma_{\text{compres.}} \left(3\sigma_{\text{tensile}} - \sigma_{\text{compres.}}\right) / \left(\sigma_{\text{tensile}} + \sigma_{\text{compres.}}\right).$$

Hence, the axial tensile strength of a timber specimen may be estimated if bending strength and compression strength values are known.

The impact of scale effect on the mechanical properties of timber is worth noting. In larger sawn timber specimens, the strength parameters decrease substantially, some of them nearly twofold due to various flaws. Compression strength is least affected in imperfect large specimens.

Averaging the indices of mechanical properties over two large statistical multitudes of timber species results in an increase of coefficients of variation. But at the same time, it reveals the most crucial characteristics and shows their interrelation.

Variability of mechanical properties of concrete species of coniferous and deciduous timber can be inferred by the data given in Table 2.10 (Tkhan et al. 2006).

Comparison of mechanical properties of pine wood from various growing regions (subtropical climate of Vietnam and the European part of Russia) shows that they are very close and lie within the scatter in corresponding values. The timber of examined coniferous species has lower parameters of mechanical properties compared to those of deciduous species. Therefore, the high significance of the impact of timber density on its mechanical properties is confirmed.

Table 2.10 Mechanical properties of certain timber species

Parameter	Vietnam pine	Vietnam fir	Vietnam eucalypt	Acacia mangium	Vietnam acacia	Pine[a] (RF)	Oak[a] (RF)
ρ_{12}, kg/m^3/min–max	460/410–510	420/370–510	620/570–670	540/470–610	580/480–680	470–520	640–870
$\sigma_{bending}$, MPa/min–max	69.35/54.83–83.9	62.17/43.05–81.3	109.45/88.45–130.0	109.66/86.1–133	118.22/85.3–151	67.4–86.2	114–163.6
$E_{bending}$, GPa	7.15	4.71	12.3	11.68	12.1	6.7–8	10–16.1
$\sigma_{compres}$, MPa/min–max	32.7/25.6–39.8	41.3/30.4–51.1	68.6/46.5–90.7	74.5/60.0–89	75.0/60.5–89.5	33–51	54–61
$\sigma_{compres\ radial}$, MPa/min–max	5.6/4.8–6.4	4.2/3.2–5.2	9.7/7.5–11.9	8.4/6.5–10.3	8.1/5.8–10.4	3.5	6.0
$\sigma_{tensile\ along\ fibers}$, MPa/min–max	78.0/67.0–89	37.2/25.0–49.4	140.7/121.4–160	140.1/121–159	112/92.1–132	78–115	120–144.6
$\sigma_{shear\ along\ fibers}$, MPa/min–max	10.45/9.25–11.6	8.24/7.2–9.2	16.56/15.4–17.7	11.8/8.1–15.5	9.38/7.8–10.9	6.0–7.7	7.8–13
$H_{crosscut\ end}$, MPa/min–max	37.46/32.1–75	43.71/30.4–84	78.81/75.2–82.4	74.83/72.2–85.4	65.52/56.0–75.0	24–32	63–107

[a]Given values are the average values of parameters for pine and oak trees growing in various regions of the RF and tested by procedure (GOST 16483; GSSSD 69–84)

It was found (Tkhan et al. 2006) that environmental moisture and temperature have considerable impact on the mechanical properties of timber. Moisture reduced the values of strength properties only within the range up to the saturation limit of cell walls. It mainly affected the strength of deciduous species. Thus, when moisture increases from 12 to 21 %, the bending strength of Vietnam pine decreased by 21 %, whereas that of eucalypt and acacia mangium decreased by 32.4 and 32.8 %, respectively. A similar trend was observed with moisture impact on static hardness of wood in crosscut view: in coniferous species, this parameter decreased 1.1–1.2 times, whereas in deciduous species it decreased almost 1.5 times.

Lower indices of mechanical properties are caused by plasticization effect of moisture, by reduced intermolecular interaction of wood components, and concentration of strains in places of structural heterogeneity of the material. The changes in the strength of moist specimen at constant room temperature we observed were reversible. After drying the specimen to initial moisture, the strength parameters regained their values (Tkhan et al. 2006).

The effect of moisture on mechanical properties of timber is addressed in a large number of scientific works. According to (Ugolev 2001), if timber moisture is reduced to 12 %, the tensile strength should increase according to the following equation:

$$\sigma_{\text{tensile}12} = \sigma_{\text{tensile}W}\ [1 + 0.01\,(W - 12)]\,.$$

According to the data of (Belyankin 1939), an average moisture increase of 1 % in various timber species results in a 3 % reduction in shear strength at room temperature.

As we see, moisture affects various parameters of mechanical properties of timber differently. The combined impact of moisture and elevated temperature appears to be even stronger. Thus, if compression strength of oak timber went down only three times with moistening at room temperature from 0 to 60 %, the combined increase in both moisture and temperature from 25 to 100 °C resulted in 15–20-fold strength reduction. On the other hand, the relative decrease in strength properties of bone-dry timber for a temperature increase to 40–100 °C was comparable with the impact of moisture alone (Belyankin 1939).

According to (Kollmann 1951), behavior of compression strength of bone-dry timber in the range from −160 to +160 °C is expressed in the equation:

$$\sigma_1 = \sigma_2 - k_T\,(T_2 - T_1) = \sigma_2 - 4.76\rho_0\,(T_2 - T_1)\,,$$

where ρ_0 is the density of bony-dry timber in g/cm^3.

The majority of earlier works on the effect of elevated temperature on timber's mechanical properties were restricted to temperatures from subzero to 40–100 °C. They reported an investigation of timber in the process of its use or natural and forced drying.

In fire conditions, timber structures are more intensely heated. The temperature inside the material under the char layer formed in the process may vary from 250 to

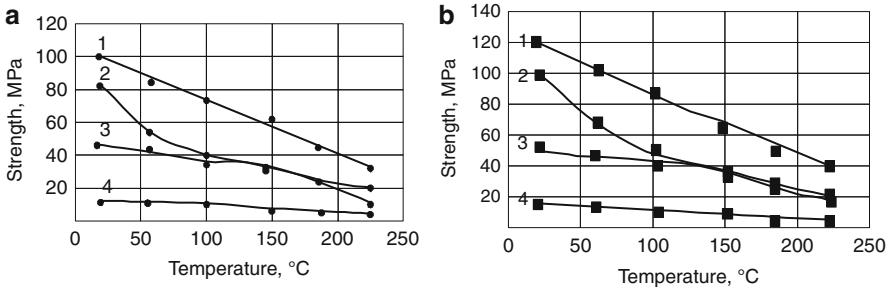

Fig. 2.7 Effect of elevated temperature on: *1* tensile, *2* bending, *3* compression, and *4* shear strength along fibers in pine (**a**) and larch (**b**) wood

Table 2.11 Values of temperature factor of reduction in mechanical properties for pine and larch timber within the range of 20–100 °C

	Factor k_T, MPa/degree (%/degree)			
Timber species	Tension	Compression	Shear	Bending
Pine	0.27 (0.30)	0.11 (0.25)	0.02 (0.22)	0.56 (0.68)
Larch	0.44 (0.36)	0.09 (0.17)	0.08 (0.36)	0.80 (0.72)

300 °C to normal affecting the bearing capacity of a structure. In the range above 240 °C, the physicochemical transformations in the timber structure accompanied by slight losses in mass significantly affect a material's mechanical properties.

In this respect, works (Khmelidze et al. 1986; Rykov 1980), which report the results of determining timber's mechanical properties at temperatures from 20 to 200–230 °C, are of interest.

Figure 2.7a, b show the effect of heating temperature on tensile, compression, shear, and bending strength of timber specimens along the fibers (Khmelidze et al. 1986).

These data were used (Volynsky 2006) to calculate the temperature factor k_T (above equation) up to 100 °C (Table 2.11).

On close examination of the figures, the bilinear character of the curves may be seen, the more evident in the case of bending strength. Up to 100 °C, a temperature change of 1 °C reduces timber bending strength by 0.68–0.72 %. Further on the slope of the curves decreased, due to evaporation of moisture from the specimen. Temperature impact on the changes in mechanical properties in various timber species may be illustrated in relative (%) rather than absolute units (Table 2.12). At temperatures of about 270–300 °C, timber strength is practically lost. Thus, experimental data in Table 2.12 are limited to temperatures of 230–250 °C.

As we see, exposure of various timber species to heat greatly impacts their mechanical properties. The domestic code (SP 64.13330.2011) recommends in design of timber structures excluding the crosscut sections of timber elements at temperatures exceeding 100 °C from consideration of load-bearing capacity.

Table 2.12 Relative change in mechanical properties of timber at elevated temperature

Species	Parameter, % change	50 °C	100 °C	150 °C	200 °C	230/250 °C	References
Pine	$\sigma_{bending}$	85/75	71/51	62/43	53/25	–/22	Khmelidze et al. (1986) and Rykov (1980)
Pine	$E_{bending}$	95	87	79	70	–	Nyman (1980)
Pine	$\sigma_{compression.}$	76/89	58/70	46/51	34/32	–	Rykov (1980) and Nyman (1980)
Pine	$\sigma_{tensile}$	97/93	92/83	88/72	80/61	–	Rykov (1980) and Nyman (1980)
Pine	$E_{tensile}$	98	95	93	90	–	Nyman (1980)
Pine	σ_{shear}	95	85	50	21	4/0	Khmelidze et al. (1986)
Larch	$\sigma_{bending}$	74	41	38	26	21/–	Khmelidze et al. (1986)
Larch	$\sigma_{compression}$	90	81	79	54	34	Khmelidze et al. (1986)
Larch	$\sigma_{tensile}$	87	69	60	42	33	Khmelidze et al. (1986)
Larch	σ_{shear}	80	67	53	40	30	Khmelidze et al. (1986)
Fir	$\sigma_{bending}$	91	76	62	47	–	Nyman (1980)
Fir	$E_{bending}$	96	90	83	77	–	Nyman (1980)
Fir	$\sigma_{compression.}$	91	77	63	49	–	Nyman (1980)
Fir	$E_{compression}$	98	94	90	87	–	Nyman (1980)
Fir	$\sigma_{tensile}$	95/	86	77	68	–	–
Fir	σ_{shear}	92	84	61	–	–	Bobacz (2008)
Fir	G_{shear}	79	71	36	–	0	Bobacz (2008)
Oak	$\sigma_{bending}$	83	67	50	29	16/–	–
Oak	$\sigma_{compression}$	81	63	57	48	28/–	–
Oak	$\sigma_{tensile}$	90	80	65	54	32/–	–
Oak	$\sigma_{compr.across}$	91	75	65	50	30/–	–

References

Afonin AA Palynometric analysis – assessing the level of aneuploidy and possible polyploidy in willow populations. http://www.afonin-59salix.narod.ru/index.html

Aleshina LA, Glazkova SV, Lugovskaya LA, et al (2001) Present-day concepts of cellulose structure. Chem Plant Mater (1):5–36

Antonova GF (1999) Cell growth in coniferous trees. Nauka, Novosibirsk, 232 p

Antonova GF (2000) Comparative analysis of lignification in summer and autumn wood of Siberian larch. In: Materials of the III international symposium "wood structure, properties and quality". Institute of Forest of KNC RAS, Petrozavodsk, pp 27–29

Antonova GF, Stasova VV, Konovalov NT, Konovalova NN (2002) Lignin distribution in structural elements of English oak wood. In: Proceedings of the II international conference for plant anatomy and morphology. SPbGLTA, St. Petersburg, pp 331–332

Belyankin FP (1939) Mechanical characteristics of oak and pine timber. Academy of Sciences, Ukraine, Kiev

Bobacz D (2008) Behavior of wood in case of fire. VDM Verlag Dr. Muller, 307 p

Borodina NA (1982) Polyploidy in introduction of woody plants. Nauka, Moscow, 177 p

Bui Din Than (2006) Impact of chemical components on fire-safety parameters of timber of Vietnam's tropical species. PhD dissertation, ASFS, Moscow, 184 p

Chudinov BS (1984) Water in wood. Nauka, Novosibirsk, 267 p

Gamaley Yu V (2004) Transport system in vascular plants. Publishing House of SPb University, St. Petersburg, 424 p

Glass SV, Felinka SL (2010) Chapter 4: Moisture relations and physical properties of wood. In: Forest Products Laboratory (ed) Wood handbook: wood as an engineering materials. FPL-GTR-190. Forest Products Laboratory, Madison, pp 1–19

Golubovsky AM (2000) Age of genetics: evolution of ideas and notions. Borey Art, St. Petersburg, 263 p

Goodwin T, Mercer E (1986) Introduction to plant biochemistry, 2 vols. Mir, Moscow, 396 p

GOST 16483.34 – 77. Wood. Method of gas permeability determination

GOST 16483. Timber. Methods for determination of mechanical properties

Greb NA, Dzyga NV (2004) Gas permeability of larch sapwood in radial and tangential directions. In: Proceedings of the IV international symposium on "wood structure, properties and quality-2004", vol 1. SFTA, St. Petersburg, pp 212–213

Grif VG (2007) Plant mutagenesis and phylogenesis. Cytology 49(6):433–441

GSSSD 69–84. Timber. Parameters of mechanical properties of small clean specimens. Gosstandart of the USSR, 1984

Janssens MA (1991) Thermal model for piloted ignition of wood including variable thermophysical properties. In: Proceedings of the third international symposium on fire safety science, pp 167–176

Khmelidze TP, et al (1986) Change of elastic modulus of pine and larch wood at heat exposure. Wood-Work Ind (Russ) (7):8–9

Kollmann F (1951) Technologie des Holzes und der Holzwerkstoffe. Berlin, Bd.1, 1050s

Krutovsky KV (2006) From population genetics to population genomics of forest woody species: integrated population-genome approach. Genetics 42(10):1304–1318

Moghtadery B, Novozhilov V, Fletcher D, Kent JH (1997) An integral model for the transient pyrolysis of solid materials. Fire Mater 21:7–16

Nyman C (1980) The effect of temperature and moisture on the strength of wood and gluelines VTT. Technical Research Centre of Finland, Espoo

Paul EE, Koukhta VN (2011) Dependence of timber mechanical properties on its density. For Hunt Econ (Russ) (10):20–23

Perelman VI (1955) Chemist's quick reference book. Scientific Technical Publishing House of Chemical Literature, Moscow, p 119

Poluboyarinov OI (1976) Wood density. Lesnaya Promyshlennost, Moscow, 160 p

Romanovsky MG (1994) Polymorphism of woody plants by quantitative features. Nauka, Moscow, 96 p

Rykov RI (1980) Strength characteristics of timber at high temperatures (Irkutsk). In: Proceedings of symposium on fire resistance of wood structures. VTT. Technical Research Centre of Finland, Espoo

Shirnin VK, Maksimenko AP, Kostrikin VA (2004) Peculiarities of xylogenesis and quality of forest tree wood in Eastern Priazovye. In: Proceedings of the IV international symposium on "wood structure, properties and quality-2004", vol 1. SFTA, St. Petersburg, pp 149–152

Siau JF (1984) Transport processes in wood. Springer, Berlin/Tokyo, 301 p

Simms DL, Law M (1967) The ignition of wet and dry wood by radiation. Combust Flame 11:377–388

Sivenkov AB (2002) Reducing fire safety of cellulose-based materials. PhD dissertation, ASFS, Moscow, 193p

SP 64.13330.2011. Timber structures. Updated edition of SNiP II-25-80. Moscow 2011

Spearpoint MJ, Quintiere JG (2001) Prediction the piloted ignition of wood in the cone calorimeters using an integral model. Fire Saf J 36:391–415

Tkhan BD, Serkov BB, Sivenkov AB, Aseeva RM (2006) Study of mechanical properties of some tropical timber species. Constructional materials of the 21st century (Russia), No. 6(89), pp 42–43

Tran HC, White RH (1992) Burning rate of solid wood measured in a heat release rate calorimeter. Fire Mater 16:197–206

Tsarev AP, Pogiba SP, Trenin VV (2000) Genetics of forest tress species. Publishing House of PGU, Petrozavodsk, 338 p

Tuskan GA et al (2006) The genome of black cottonwood, Populus trichocarpa. Science 313(5793):1596–1604

Ugolev BN (2001) Wood science with fundamentals of forest merchandizing. Publishing House of MGUL, Moscow, 340 p

Volynsky VN (2006) Interrelation and variability of timber mechanical properties. AGTU Publishers, Arkhangelsk, 196 p

Zhdanov VM (1990) Evolution of viruses, 2 vols. Meditsina, Moscow, 376 p

Chapter 3
Pyrolysis and Thermal Oxidative Decomposition of Timber

Abstract This chapter summarizes the data on pyrolysis and thermal oxidative decomposition of solid timber as well as its main components at various thermal and fire loads. The effects of speed and intensity of heating and oxygen content are discussed. The chapter presents comprehensive data for understanding thermal and fire resistance of natural timber, including kinetic parameters of thermal decomposition of timber and its components, effects of various specious and thermal loads on volatile products, charring formation, thickness of char, effective heat of gasification for various species, etc. Some numerical models for thermal decomposition and calculation and charring of timber are discussed.

Thermal decomposition of timber in an oxidative environment on heat exposure is a very important phase in combustion onset and propagation. The combustion process of timber materials prone to charring may take two different forms: flaming and smoldering.

These processes are based on different mechanisms of timber decomposition. In flaming combustion, rapid transport of gaseous products of timber decomposition into the flame reaction zone and flame presence over the decomposing material surface prevent oxygen diffusion from the environment into the near-surface layer. Therefore, what occurs under conditions of stable flaming combustion is pure thermal decomposition (i.e., pyrolysis). It is only after the accumulation of a char layer on the surface of the burning wood and consequent flame combustion extinction then a reaction between the porous char layer with air oxygen and its smoldering combustion may occur.

Timber smoldering initiated by a weaker heat source compared to flaming combustion is a complex heterogeneous exothermic oxidation reaction accompanied by timber charring. Released heat is also capable of inducing purely thermal wood decomposition with the formation of nonvolatile char product that is essentially the main potential of smoldering combustion.

R. Aseeva et al., *Fire Behavior and Fire Protection in Timber Buildings*,
Springer Series in Wood Science, DOI 10.1007/978-94-007-7460-5_3,

It is reasonable that in order to understand the nature of timber material combustion and be able to model it in various fire situations, it is very important to study the kinetics and mechanism of both thermal and thermo-oxidative processes of various types of timber decomposition in a wide range of temperatures.

The process of timber pyrolysis may proceed in two different regimes as a result of the relationship between the rate of heat transfer through a decomposing medium and the chemical reaction rate.

In kinetic regime, the pyrolysis process is controlled by the chemical reaction rate, because the heat transfer rate greatly exceeds the general chemical reaction rate. The second regime is controlled by heat transfer, because its rate is far slower than general chemical reaction rates. In this case, a large temperature gradient is set up, and a narrow pyrolysis reaction front is developed. This regime occurs in larger specimens on exposure to intensive high-rate heat flows (characteristic of ablation regime and heat shock), in flaming combustion of timber materials.

Modern methods of thermal analysis are especially useful for determining the characteristics of the kinetic regime of timber decomposition, particularly thermogravimetric (TG) analysis and differential scanning calorimetry (DSC), which allow quantitative evaluation of effective kinetic parameters and reaction heat in substance decomposition at different phases while minimizing the impact of factors of mass and heat transfer.

3.1 Mechanism and Macrokinetics of Pyrolysis of Timber and Its Main Components

Timber decomposition are addressed in many works, where this process is examined from different points of view (mechanism and chemical kinetics, formation of various products and their distribution, energy of pyrolytic reactions, modeling of the general process, etc.). Early analytical reviews of these studies already noted the complexity of the wood pyrolysis process and analyzed a series of factors that affect timber thermal decomposition, kinetic parameters of the process, and interpretation of the obtained data. In particular, one of the crucial factors is timber species and variety, its chemical composition and physical structure, the autocatalytic effect of inorganic inclusions, specimen dimensions and pyrolysis process conditions (Roberts 1970).

Timber is a typical representative of polymer materials carbonizing on heat and fire exposure. It is their fundamental difference from other polymer materials, which become fully decomposed in similar conditions.

Chemical processes in timber pyrolysis are usually analyzed as two phases involving primary reactions of base wood pyrolysis and secondary reactions of resulting decomposition products.

It is believed that primary wood pyrolysis for a small specimen, moderate temperature (up to 500 °C), and relatively low heating rate (kinetic regime) can

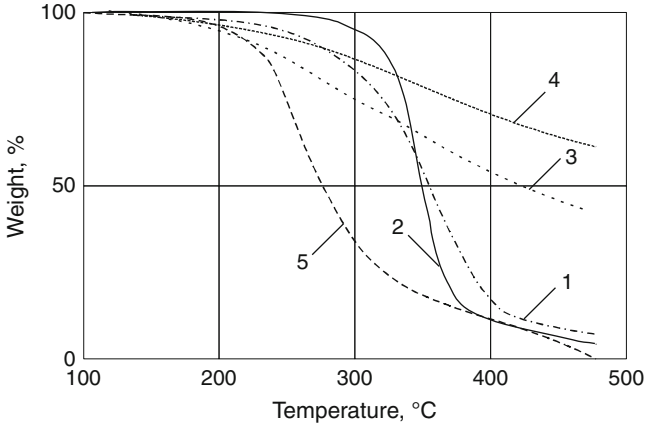

Fig. 3.1 TG pyrolysis curves of poplar wood and its main components: *1* wood, *2* cellulose, *3* lignin of disintegrating wood, *4* Klason lignin, and *5* xylan

be modeled by factoring in the behavior of the main components and their relative contribution to the chemical composition of timber (Di Blasi 1993, 2008).

On TG curves of wood decomposition, zones related to decomposition progress of separate components may be singled out. It has been found that hemicelluloses are actively decomposed within a temperature range of 225–325 °C, celluloses – within a temperature range of 325–375 °C. Lignin loses weight gradually. After slight softening at a temperature below 200 °C, the weight losses are no more than several percent. However, starting from 250 up to 500 °C, significant emission of volatile products is recorded (Fig. 3.1) (Shafizadeh and McGinnis 1971).

On differential TG curves, it is clearly seen that temperature zones pertaining to separate components and used to calculate kinetic parameters overlap to a certain extent (Fig. 3.2) (Branca et al. 2005).

Since this circumstance cannot be excluded from the analysis of TG curves of timber decomposition, the notion of "pseudo-component" was introduced (Di Blasi 2008). Hence, every zone attributed to a pseudo-component reflects the contribution of the main component to the total weight loss of the specimen, which nevertheless does not exclude some participation of other timber constituents.

The authors of works (Gronli et al. 2002; Varhegyi et al. 2004) tried to take low-temperature (below 280 °C) pyrolytic reactions of the substances extracted from wood into account in the mechanism of wood thermal decomposition. By analyzing TG and DTG curves of coniferous and deciduous species with high extractives content, for example, chestnut from Italy (16 %) or Redwood growing in America (11 %), they introduced two additional components belonging to extractives. For a lower extractives content in wood, they are believed to reflect the pseudo-component of hemicellulose. According to our data (Serkov et al. 2005a), it can indeed be noticed that the balance between extractives and hemicellulose in coniferous and deciduous species affects the maximum weight loss rate and relevant temperature.

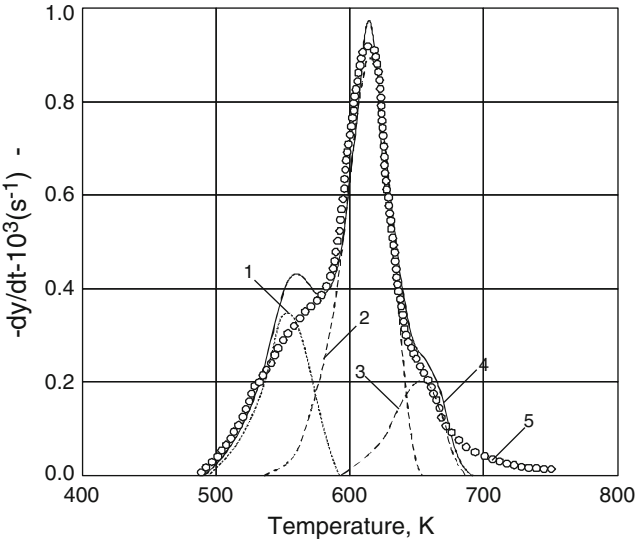

Fig. 3.2 DTG curve of beech wood pyrolysis and singled out temperature zones of its separate components at a constant heating rate of 5 deg./min: *1* hemicellulose (calculated curve), *2* cellulose (calculated curve), *3* lignin (calculated curve), *4* wood (calculated curve), *5* wood (experimental curve)

The higher the extractives content compared to hemicellulose, the higher the maximum wood mass loss is in this low-temperature zone, and the greater the initial decomposition temperature drops. The position of the first "concealed" peak hump (more often in the form of an arm on the DSC curve) also changes toward lower temperatures. This confirms the concept of the extractive substances being the least heat stable compared to other main wood components. Devolatilization by extracting wood specimens with organic solvents or hot-water washing reduced the total yield of char residue (Varhegyi et al. 2004).

The substances extracted from wood are a mixture of organic compounds of different classes. Their thermal decomposition rate is much lower compared to wood decomposition as a whole. Figure 3.3 shows TG and DTG curves of thermal decomposition of substances extracted from chestnuts growing in various regions of Italy and Russia (Varhegyi et al. 2004).

Depending on the growing region, the extractives content in the wood of the same variety changed within a wide range from 5.8 to 16 %.

On DTG curves of weight loss, three peaks may be singled out in temperature ranges of about 200–220, 290–300, and 390–410 °C. Kinetic parameters of pyrolysis were calculated for two fractions of extractives (Gronli et al. 2002). Effective activation energy values of extractives pyrolysis equaled 105 and 127 J/mol, respectively, for all 9 studied wood varieties. Only pre-exponential factors changed: at the first decomposition step, they changed within $8.75 \leq \log A_{e1}/c^{-1} \geq 9.53$, whereas at the second step – $10.05 \leq \log A_{e2}/c^{-1} \geq 10.85$.

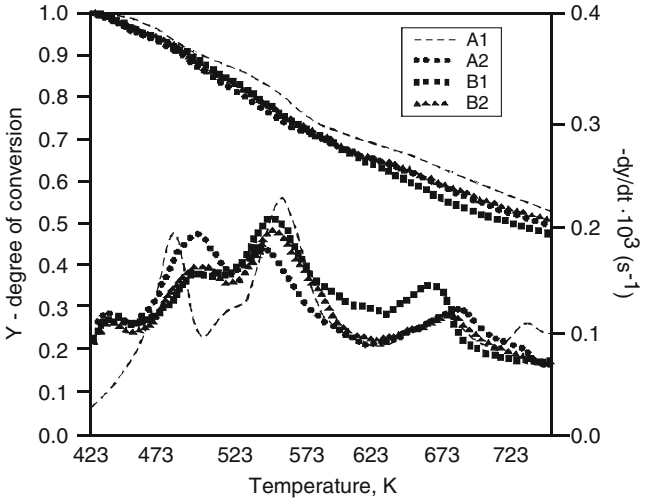

Fig. 3.3 TG and DTG curves of thermal decomposition of extractives removed from various specimens of chestnut wood: *A1* (16 %) and *A2* (8.5 %) – specimens from Italy and *B1* (5.8 %) and *B2* (8.1 %) – specimens from Russia. Heating rate: 5 deg./min

The data on kinetic parameters of wood pyrolysis (reaction order, effective activation energy, and pre-exponential factors) cited in scientific literature show wide scatter, and it is hard to compare them. The reason is not only different wood specimens, often undercharacterized, different test facilities, methods, and conditions but also the methodology of determining kinetic parameters.

Calculation of kinetic parameters for decomposition of wood and its components according to the data of dynamic TG analysis is based on the use of the equation:

$$\frac{\mathrm{d}\alpha}{\mathrm{d}T} = \frac{k}{\beta} f\,(\alpha)$$

where α – degree of conversion; β – heating rate; k – decomposition rate constant: $k = A\,\exp(-E/RT)$, A and E – pre-exponential factor and activation energy, $f(\alpha)$ – function reflecting the individual law of decomposition rate as a function of degree of substance conversion, and reaction order. This function describes the physical mechanism of the process that controls the rate of pyrolytic reactions of the analyzed substance (Shestak Ya 1987).

TG curves plotted for different heating rates (ASTM E 1641-2004; ISO 11358-2005) were used to determine the kinetic parameters and the $f(\alpha)$ function. The approach described in (Rogers and Ohlemiller 1981) is also useful.

Despite the large discrepancy in experimental values of wood pyrolysis kinetic parameters, many researchers have come to the conclusion that all other conditions being equal, it is not so much wood species or variety as its chemical composition that has a significant impact on the kinetics of primary thermal decomposition

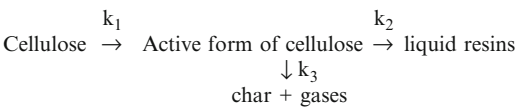

Fig. 3.4 Scheme of reactions in primary cellulose pyrolysis

reactions. It was even proposed to assess the content of the main components (cellulose, lignin, hemicellulose mixed with volatiles) in an unknown wood specimen by TG data proceeding from the assumption that pyrolysis features of the main wood components are not interdependent, and their decomposition rate is only governed by the amount of each component in the timber (Ward and Braslaw 1985).

Primary pyrolysis of timber and its main constituents results in the formation of products, which in process modeling are usually combined into three major groups: (1) low-molecular gaseous substances; (2) liquid, tar-like (resinous) substances in vaporized state at pyrolysis temperature, but condensing at room temperature; (3) solid char residues.

At higher temperatures, the substances generated from primary wood pyrolysis may undergo secondary reactions of molecule fragmentation, as well as condensation or polymerization with the formation of new volatiles and secondary carbonized product. This phase of secondary pyrolysis mainly includes the reactions of vapors of resinous substances and may proceed in the pores of solids, both homogeneously in the gaseous phase and heterogeneously on the carbonized wood surface.

The best studied at present is cellulose pyrolysis. Information on the kinetics and chemistry of thermal conversions of hemicellulose and lignin is scanty. Still less is known of pyrolysis of the substances extracted from wood.

The mechanism and kinetics of primary cellulose pyrolysis may be represented by the following simple scheme (Fig. 3.4) (Bradbury et al. 1979).

The controlling step in this low-temperature cellulose pyrolysis reaction is the formation of the so-called active form of cellulose with reduced macromolecule chain length as a result of breaking glycosidic linkage by the law of randomness. Initial decomposition starts at the boundary of crystalline and amorphous areas of cellulose microfibers or from the equatorial surface of microfibers at the boundary of crystallites and amorphous hemicelluloses surrounding them (Zickler et al. 2007). Reduction of polymerization degree is accompanied by the appearance of free radicals and release of water and carbon oxides. Thermal decomposition of "active cellulose" into levoglucosan, which is the main product of the liquid resinous fraction, starts from the end of macromolecule chains through a mechanism of stepwise depolymerization (Golova 1975). Along with levoglucosan, the "resin" (tar) was discovered to contain 5-methyl- and 5-hydroxymethyl-furfurol, hydroxyacetaldehyde, formaldehyde, as well as anhydrooligosaccharides (from dimeric – cellobiose to oligomers with 7 pyranose chains). The low-molecular products indicated above are formed as a result of partial fragmentation of both "active cellulose" and levoglucosan (Fig. 3.5). Secondary reactions with their participation lead to char formation.

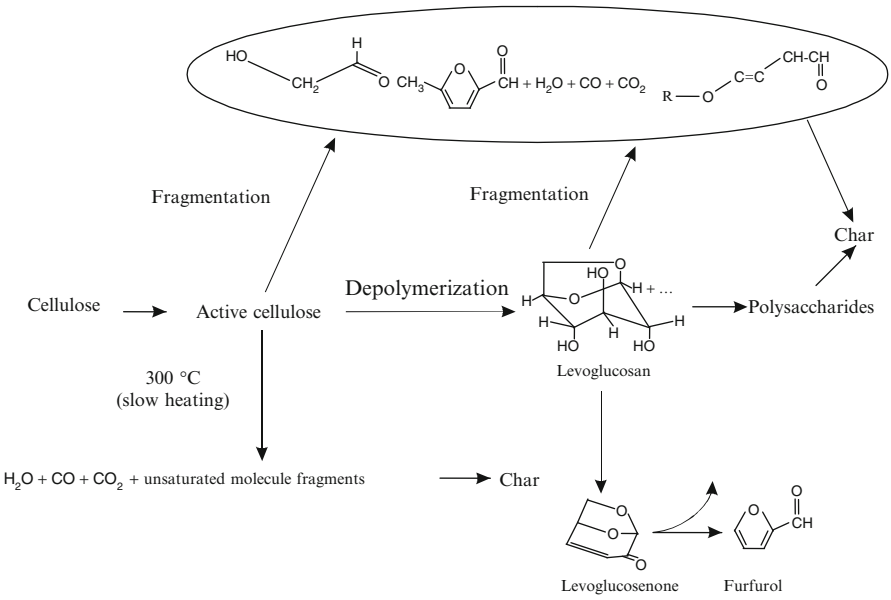

Fig. 3.5 Diagram of thermochemical cellulose conversions

Slow heating of cellulose at a temperature below 300 °C is favorable for the reactions of inter- and intramolecular decomposition, formation of a cross-linked structure and unsaturated fragments, which later take part in the polymer carbonization reactions. This direction of reactions is actively used in the production of various carbon-based materials from cellulose (Konkin 1974).

Hemicelluloses have a more varied structure and have lower thermal stability compared to cellulose, partly due to their amorphous state. They are very sensitive to the presence of inorganic admixtures and easily go through fragmentation of molecular chains and carbohydrate cycles. Among the main products of hemicellulose pyrolysis are furan derivatives, mono- and oligopentosanes, and acetic acid.

Thermal decomposition of lignin is accompanied by the formation of monomeric and dimeric phenol derivatives, coniferyl and sinapic alcohols, divinyl ethers, formaldehyde, methanol, carbon oxides, and water. The methanol source is the reaction of demethoxylation of lignin macromolecules. According to (Nakamura et al. 2008), the formation of coniferyl and vinyl ethers may occur in the following way (Fig. 3.6).

The mechanism of lignin thermal decomposition, which includes competing reactions of depolymerization and condensation (carbonization), is addressed in (Kawamoto et al. 2007a, b).

The gross composition of hemicellulose and lignin pyrolysis products is subdivided into three groups of substances, as in the case of pyrolysis of cellulose

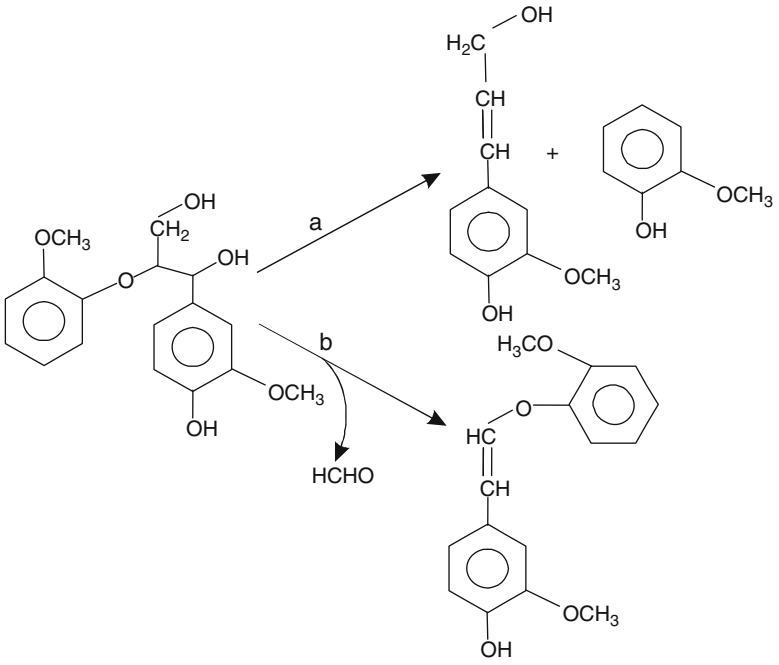

Fig. 3.6 Principal directions of thermal decomposition reactions of lignin with β-O-4 structural fragments

Table 3.1 Kinetic parameters of primary pyrolysis of main wood components (Miller and Bellan 1996)

k, s^{-1}	Cellulose	Hemicellulose	Lignin
k_1	$2.8 \times 10^{19}\exp(-242.4/RT)$	$2.1 \times 10^{16}\exp(-186.7/RT)$	$9.6 \times 10^{8}\exp(-107.6/RT)$
k_2	$3.28 \times 10^{14}\exp(-196.5/RT)$	$8.75 \times 10^{15}\exp(-202.4/RT)$	$1.5 \times 10^{9}\exp(-143.8/RT)$
k_3	$1.3 \times 10^{10}\exp(-150.5/RT)$	$2.6 \times 10^{11}\exp(-145.7/RT)$	$7.7 \times 10^{6}\exp(-111.4/RT)$
υ_c	0.35	0.60	0.75

and wood as a whole (i.e., gases, tar, and char). Analysis of product yield during pyrolysis and product distribution as a function of temperature combined with weight loss measurements makes it possible to assess the kinetic parameters of pyrolysis of main wood components.

Table 3.1 shows kinetic parameters of pyrolysis of cellulose, hemicellulose (mixed with extractives), and lignin.

The values of solid char residue yield, υ_c, in proportions of its initial weight for each component are also indicated. The cellulose decomposition mechanism represented in the scheme Fig. 3.4 is assumed to correspond to the other wood component decomposition mechanism. In Table 3.1, values of activation energy are given in kJ/mol and pre-exponential factors in s^{-1}.

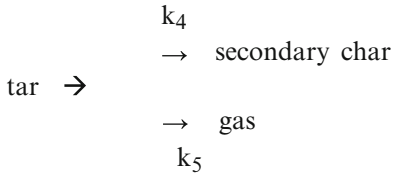

Fig. 3.7 Diagram of secondary pyrolysis reactions of resinous fraction (Di Blasi 1993)

Table 3.2 Kinetic parameters in pyrolysis of model compounds (Di Blasi 2008)

Compound	A_1, s^{-1}	E_1, kJ/mol	A_2, s^{-1}	E_2, kJ/mol
5-hydroxymethyl-furfurol	3.3×10^4	76	1.7×10^7	117
Levoglucosan	3.5×10^{10}	185	7.0×10^{12}	228
Hydroxyacetaldehyde	1.2×10^{12}	218	–	–

It may be noted that the lowest solid char residue yield is predicted for cellulose pyrolysis and the highest for lignin, which has aromatic nuclei and unsaturated groups in its structure that contribute significantly to the carbonization process. Char residue yield should go down in case of a major temperature rise. This conclusion is consistent with experimental observations.

Secondary pyrolitic reactions of timber and its components (above 500 °C) are much less studied compared to the primary reactions. Furthermore, the main emphasis in available studies was the behavior of the resinous fraction formed as a result of primary pyrolysis of various timber species under high-temperature exposure. The kinetics of tar fraction pyrolysis are described by a global first-order reaction with respect to tar concentration as per the Arrhenius law with effective activation energy within 66–123 kJ/mol (Di Blasi 2008). This large spread in values is partly explained by the fact that this fraction contains variously proportioned compounds differing in reaction capacity and thermal stability.

Secondary pyrolysis of the resinous fraction is analyzed in more detail in the form of two competing directions (Fig. 3.7).

The model compounds used for modeling secondary pyrolitic reactions were levoglucosan (the main constituent of resinous product in primary wood pyrolysis) as well as 5-hydroxymethyl-furfurol and hydroxyacetaldehyde.

Pyrolysis products were analyzed by mass spectrometry. Cracking of model compounds into gaseous substances occurs in two successive stages or in one stage with kinetic parameters of first-order reactions presented in Table 3.2.

The mechanism and kinetics of secondary char formation have still not been determined. However, it was found out that the resinous fraction of primary pyrolysis of cellulose contributes significantly to char residue formation.

In fire conditions, timber pyrolysis occurs with strong interaction of chemical and physical processes of mass and heat transfer.

The large distinction in experimental values of wood pyrolysis kinetic parameters, as was noted above, is related to some extent to studying specimens from various species in different heat exposure conditions. The most progressive and fundamental approach to understanding this distinction is the one based on deter-

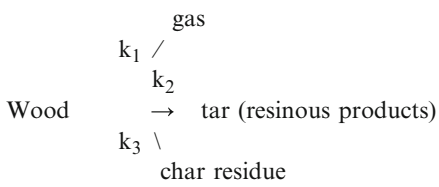

Fig. 3.8 Diagram of primary pyrolysis reactions of wood

mining to what extent pyrolitic reaction rates of the main components contribute to the general mass loss rate in primary wood pyrolysis. It allows one to forecast the mass loss rates for practically any timber species with known chemical composition within wide ranges of heating conditions.

In most cases of pyrolysis modeling, wood is considered a homogeneous material with evenly distributed pores. The primary decomposition process of this homogeneous system leads to the formation of three groups of products (noncondensable gases, condensable vapors of volatile resinous products, and nonvolatile char residue) through three competing reactions (Fig. 3.8). Next, the secondary pyrolitic reactions of volatile resinous products proceed following the diagram in Fig. 3.7.

In the above diagram, the stage of intermediate active product formation, similar to the reaction of active form of cellulose buildup (Fig. 3.4), is disregarded, because it does not limit the general rate of primary wood pyrolysis. Moreover, formation of noncondensable gases is viewed as parallel reaction independent of other wood decomposition reactions. In this case, the yield of each of the three groups of pyrolysis products must be a function of temperature (Di Blasi 1993; Di Blasi and Branca 2001). The composition and distribution of the evolved flammable gases and vapors of resinous products of wood thermal decomposition ultimately determine the characteristics of fire behavior of timber materials.

Figure 3.9 shows the impact of density of external radiant heat flow on the yield of the three groups of pyrolysis products in certain varieties of coniferous and deciduous species with known chemical composition (Di Blasi et al. 2001).

All timber varieties demonstrate the same qualitative tendency to form pyrolysis products. Depending on heating conditions, two distinct areas may be singled out with heat flow up to 40 kW/m^2 (corresponds to specimen temperature below 470 °C) and above 40 kW/m^2. In the first area, the ultimate yield of char residue goes down as heat flow density increases, whereas the yield of volatiles (gases and resinous products) increases as a result of competition between carbonization reactions and volatile product formation in favor of the latter. If external heat flow exceeds 40 kW/m^2, the yield of resinous products reaches its maximum (at 49–69 kW/m^2), whereas gas yield continues to rise due to secondary pyrolitic reactions.

In spite of identical tendency in the changes in yield of the three pyrolysis product groups with a change in heat exposure, large differences are recorded in quantitative proportions and trend of pyrolysis product yield as a function of wood variety. Therefore, it is not so much the timber species (coniferous or deciduous) as its chemical composition and relative content of main chemical constituents which seriously affect the regularities of timber pyrolysis.

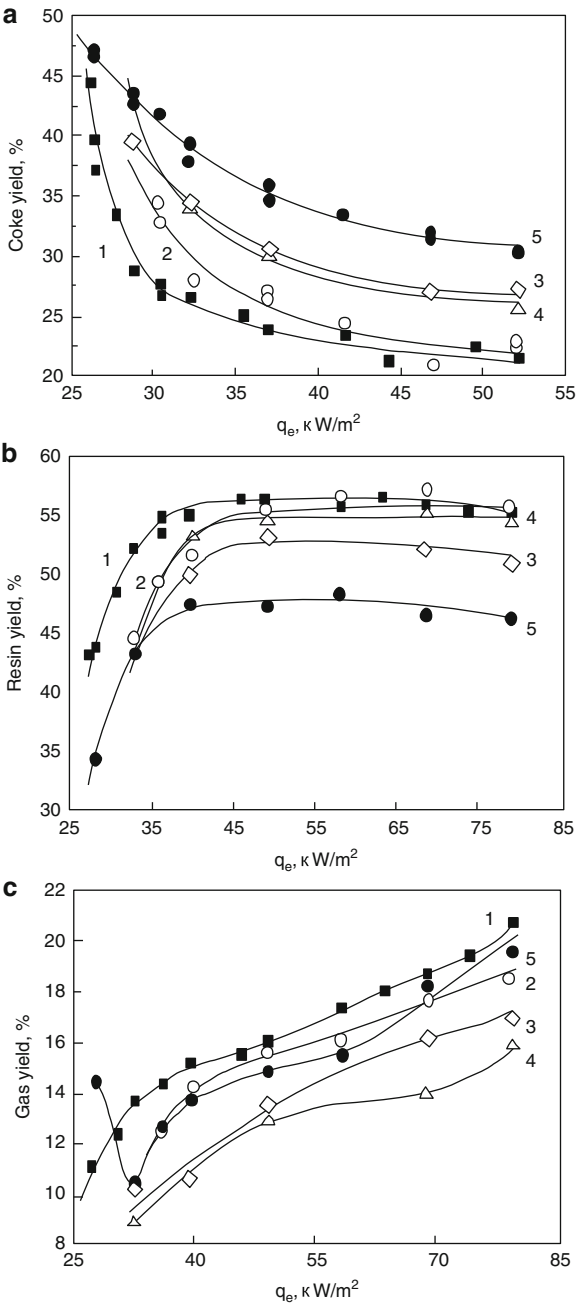

Fig. 3.9 The impact of external radiant heat flow on the yield of char (**a**), tar (**b**), and noncondensable gases (**c**) during pyrolysis of coniferous and deciduous timber species: *1* beech, *2* pine, *3* Douglas fir, *4* redwood, *5* chestnut

3.2 Decomposition of Timber Species at Thermal Oxidation

Timber decomposition in the presence of air oxygen is much more complicated compared to purely thermal decomposition, because the process is already strongly exothermic at the initial stages. The direction of complex chemical reactions and progress of material decomposition depend not only on the chemical composition and structure of the initial timber but also on external heat exposure conditions and access of oxygen to the reacting timber surface.

Figure 3.10 shows an example of environmental impact on the degree and rate of Vietnam Fir timber decomposition when a specimen weighing <8 mg is heated to 500 °C at the rate of 10 deg./min (Serkov et al. 2005b).

Since air oxygen initiates timber decomposition, the loss of specimen mass is recorded at lower temperature compared to heating in an inert medium. The TG curve and position of the DTG peak of wood decomposition in air shift into the low-temperature area relative to the corresponding curves built for a nitrogen environment.

Regardless of the environment type, the initial mass losses when specimens are heated to 120–150 °C are caused by the endothermic process of moisture evaporation. Actual wood decomposition as such starts at a higher temperature. Oxidative decomposition of timber proceeds in two stages. The first stage consists of wood component decomposition and the second of oxidation of resulting char. Both

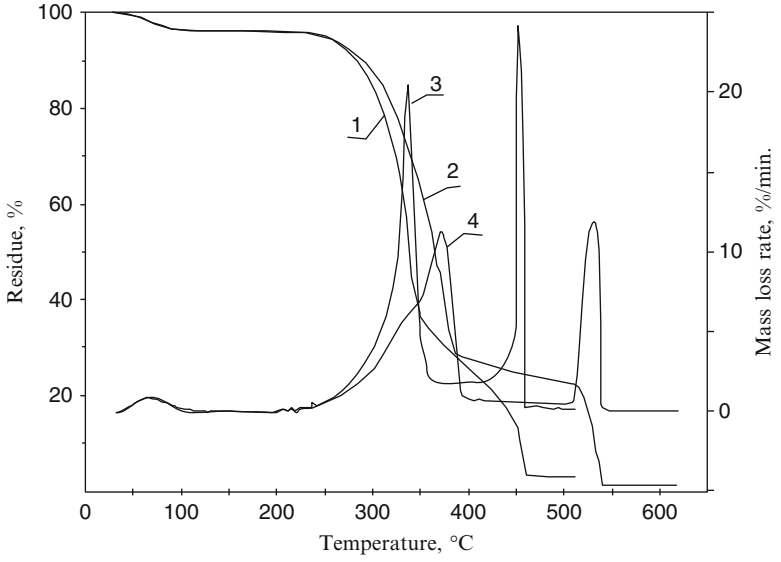

Fig. 3.10 TG and DTG curves of Vietnam Fir timber decomposition on heating in air (1, 3) and in an inert medium

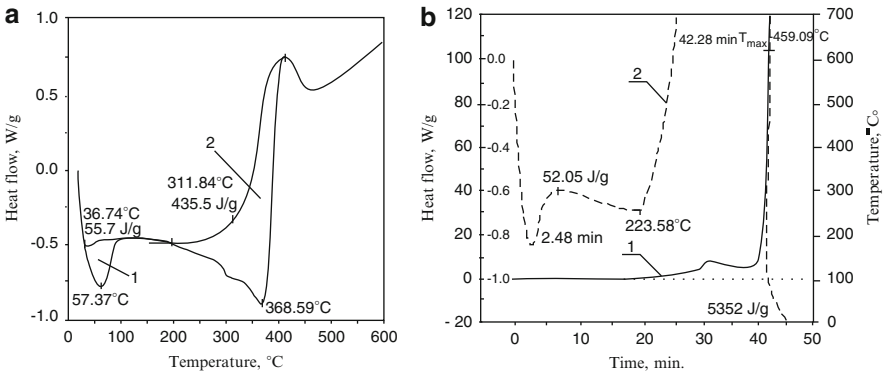

Fig. 3.11 DSC curves of Vietnam fir decomposition at a heating rate of 10 deg./min in an inert medium (**a**) and in air (**b**); (**a**): *1* endopeak of moisture release and *2* epeak of pyrolysis; (**b**): *1* on scale of 1:1 and *2* on a scale of 10:1

decomposition stages are exothermic and proceed with considerable heat release (Fig. 3.11a, b). On heating to 460 °C, nearly full loss of specimen mass occurs with heat release of 5,352 J/g.

TG analysis of various species of timber in air at a heating rate of 5–20 deg./min led us to the conclusion that solid phase oxidative decomposition corresponds to the mechanism of diffusion-controlled process. Pyrolysis in an inert medium mainly proceeds according to a mechanism that controls the formation of nucleation centers by the law of randomness and growth of formed nuclei or a mechanism governed by the reactions at the phase boundary (Serkov et al. 2005b). This conclusion is in full agreement with the new phenomenological model of cellulose (one of the major wood constituents) pyrolysis (Mamleev et al. 2009).

The rate of oxidative decomposition of wood specimens changes with increasing temperature as per the Arrhenius law for a first-order reaction with respect to mass fraction of the reacting solid. According to our data, kinetic parameters of thermo-oxidative decomposition of wood at 20 % decomposition degree were fairly close for various species: effective activation energy was 159.6–166.8 kJ/mol, whereas logarithmic values of pre-exponential factors, lgA, were changing within the range of 13.60–14.73 (min^{-1}) (Serkov et al. 2005b).

When the decomposition degree increased to 60 %, the values of E_{eff} increased, especially significantly in thermo-oxidative decomposition of deciduous species (Fig. 3.12).

Presumably, E_{eff} values reflect the participation of timber components in this process and the contribution of char residue oxidation energy at high wood decomposition degrees. It may be concluded that timber decomposition residues of coniferous species are more prone to oxidation than those of deciduous species (Serkov et al. 2005b).

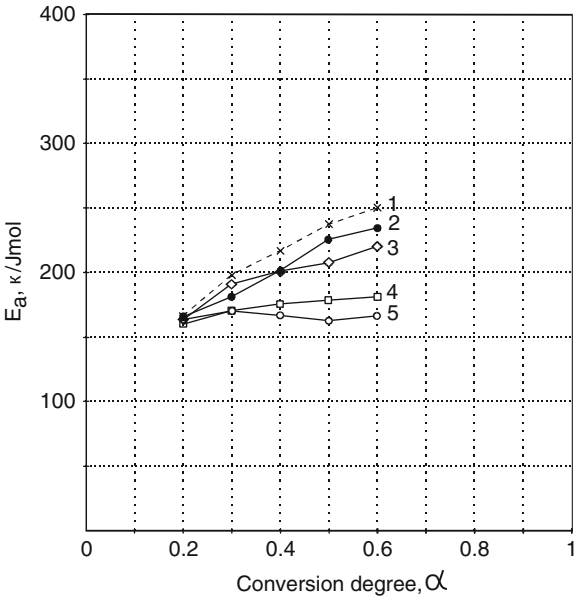

Fig. 3.12 Dependence of effective activation energy of thermo-oxidative decomposition of Vietnam timber specimens on decomposition degree: *1* eucalypt, *2* acacia mangium, *3* acacia auriculiforis, *4* fir, *5* pine

The data on the mechanism and macrokinetic parameters of decomposition of various species of timber, and its main components in an oxidizing atmosphere are rather limited and often inconsistent. A clear-cut subdivision of mass loss into two stages during wood decomposition in air was recorded in TG tests of many researchers (Cordero et al. 1991; Di Blasi et al. 1999).

It was also noted that decomposition degree at each stage depends on timber variety. Weight losses at the second stage were greater in the specimens with higher lignin content.

As was found (Di Blasi et al. 1999), correct determination of kinetic parameters of oxidative decomposition of wood at the second high-temperature stage requires not only very small sample mass but also low heating rates (not exceeding 20 deg./min).

TG and DSC curves of timber decomposition in an oxidizing atmosphere may be interpreted, as was done for pyrolysis, by process modeling with due account of the reaction of separate wood components (Di Blasi et al. 1999; Branca and Di Blasi 2004; Fang et al. 2006). As in the case of pyrolysis, decomposition in air starts with hemicellulose followed by cellulose. Thermo-oxidative decomposition of lignin is recorded in a wide range of temperatures. Each individual timber component also has a two-stage mass loss when heated in an oxidizing atmosphere (Di Blasi et al. 1999). At a heating rate of 5 deg./min in an air medium, the peak temperatures corresponding to the maximum mass loss rate at the first, principal stage of specimen decomposition were 596 K for beech wood, 554 K for xylan, 602 K for cellulose, and 603 K for lignin. E_{eff} values of oxidative decomposition of components equaled

119 kJ/mol for xylan, 245 kJ/mol for cellulose, and 82 kJ/mol for lignin. Beech decomposition at the first stage proceeded with E_{eff} of about 85 and 99 kJ/mol at the second (Di Blasi et al. 1999).

In their later work, the authors of (Branca and Di Blasi 2004) used a 4-stage mechanism for a more accurate description of TG curves for heating of two timber types (beech and Douglas spruce) in an oxidizing atmosphere. At the first, principal stage of wood oxidative decomposition, three reactions which are typical for the above-mentioned wood components were considered, with activation energy values of 106, 226, and 114 kJ/mol. The last stage was assigned to the char burn-off reaction with $E_{\text{eff}} = 183$ kJ/mol. It should be noted that the rates of the first three reactions were described by the first-order Arrhenius equation with respect to mass fraction of the solid substance, whereas the last stage showed power dependence on the mass fraction of a substance with $n = 1.54$. The difference between two timber types showed in the values of pre-exponential factors and stoichiometric coefficients of the reactions in question.

The rate of mass loss in the burn-off of solid substances is usually linked to the oxygen partial pressure and the pore surface area in the reaction volume.

With sufficient air flow in TG tests, the mass fraction of oxygen (partial pressure) remains constant during the wood decomposition process. For this reason, its contribution is introduced into the pre-exponential factor. To describe pore surface area expansion, a simple power law of dependence of decomposition rate on the mass fraction of a solid is used. Thus, the burn-off rate may be expressed as a common equation:

$$\frac{\mathrm{d}\alpha}{\mathrm{d}t} = A_{\mathrm{i}} \exp\left(\frac{-E_{\mathrm{i}}}{RT}\right) Y_{\mathrm{i}}^{n},$$

where n – common reaction order.

A study of timber decomposition and mass loss kinetics depending on the oxygen concentration in gaseous medium that was performed using combined TG-Fourier infrared analysis of the resulting products is of great interest (Kashiwagi and Nambu 1992). On the basis of a thorough analysis of TG and evolved gases, the whole process was subdivided in four stages just as in (Branca and Di Blasi 2004). Values of timber decomposition effective activation energy and burn-off showed linear variation as a function of oxygen concentration.

Both pyrolysis and thermo-oxidative decomposition of the main wood component – cellulose – proceed with fairly high activation energy. Depending on the cellulose source, E_{eff} ranges between 220 and 250 kJ/mol. Sensitivity of mass loss rate to cellulose origin during decomposition is believed to be induced by various cellulose microfiber sizes and the difference in physical crystalline structure of microfibers (Mamleev et al. 2009).

It is believed (Kashiwagi and Nambu 1992) that external heat exposure conditions affect the competition between pyrolysis and cellulose oxidative decomposition reactions. As a result, a study has been performed on the impact of volume

concentration of oxygen mixed with nitrogen (0.28, 1.08, 2.0, 5.2 %) and in air, as well as specimen heating rate within 0.5–5 deg./min, on mass loss and light gaseous product formation rates. As usual, in cellulose decomposition in an oxidizing atmosphere, the first peak on TG curves was seen at a lower temperature than in pyrolysis. This peak represents total mass losses due to oxidative decomposition and pyrolysis of cellulose. Therefore, in order to determine kinetic parameters of thermo-oxidative decomposition, the relevant values pertaining only to pyrolysis in the conditions being studied were deducted from experimental values of mass loss rate recovered from oxidizing atmosphere. Preliminary analysis of cellulose pyrolysis kinetics in nitrogen and an assessment of kinetic parameters of thermal decomposition made it possible to perform this procedure. In particular, the pyrolysis rate constant in the tested cellulose specimen $k_p = A_p \exp(-E_p/RT)$ had parameters: $A_p = 1.2 \times 10^{19}$ ($\min^{-1}$) and $E_p = 220$ kJ/mol. Reaction order in relation to mass fraction of the specimen at this stage, n(f), equaled 1.8. Using this procedure, the authors of (Kashiwagi and Nambu 1992) found that with environmental oxygen concentrations of 0.28 % and 1.08 %, the E_{eff} values of cellulose decomposition were 224 and 182 kJ/mol correspondingly; i.e., they did not differ much from the E_p value. But during decomposition in air and in a medium with 5.2 % oxygen, the activation energy values were close at 157 and 160 kJ/mol, respectively. The latter value was taken as the characteristic of thermo-oxidative decomposition of cellulose to be used to determine pre-exponential factor, $A_{ox}. = 1.5 \times 10^{14}$ ($\min^{-1}$). Therefore, thermo-oxidative decomposition rate of cellulose, r_{ox}, is represented by the bimolecular reaction equation:

$$r_{ox} = A_{ox} \exp\left(-E_{ox}/RT\right) \left(Y_{ox}\right)^{n(ox)} \left(W_s/W_o\right)^{n(f)},$$

where $n(ox) = 0.5$ and $n(f) = 1.3$ – reaction orders found in relation to oxidant and fuel, respectively.

In ignition and combustion conditions, the heating rates are considerably higher than those used in TG studies. This brings up the question of how important the contribution of oxidative decomposition reaction at such high heating rates is to the general process of volatile formation. According to (Kashiwagi and Nambu 1992), although specimen heating rate affects the makeup of cellulose decomposition products, the global kinetic parameters of mass loss in pyrolysis and oxidative decomposition themselves do not depend on it. The effect of heating rate influences the competition of two decomposition directions.

Figure 3.13 shows the variation of the relationship between mass loss rate in cellulose pyrolysis and thermo-oxidative decomposition as a function of specimen heating rate in air.

As is seen from Fig. 3.13, when cellulose is heated at a rate of 5 deg./min, the thermo-oxidative decomposition rate is almost triple the pyrolysis rate. At 50 deg./min, both reactions proceed at almost the same rate. But when heating reaches 500 deg./min, the pyrolysis rate already surpasses the oxidative decomposition rate. Since the increased heating rate shifts the mass loss rate peak toward higher temperatures, the direction of the reaction with higher activation energy

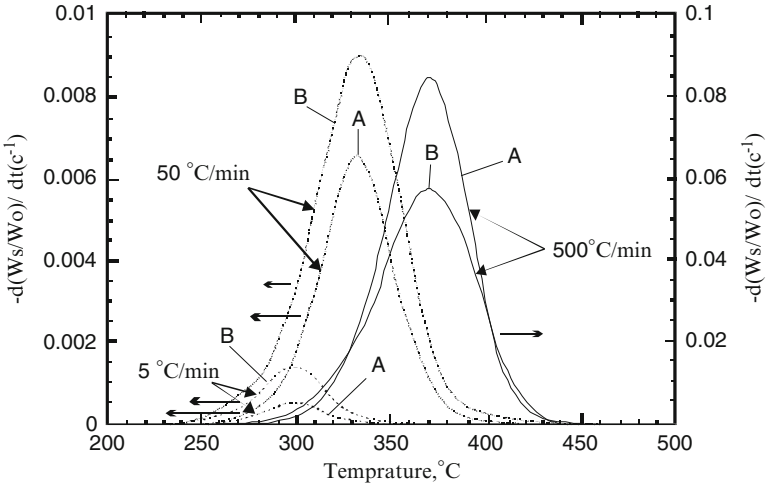

Fig. 3.13 Effect of heating rate on competition between pyrolysis rate and cellulose thermal decomposition rate in air; *A* pyrolysis, *B* oxidative decomposition

(220 kJ/mol) starts to predominate. A similar effect is caused by oxygen deficiency in the environment. For example, with 2 % of oxygen in the environment, even at a low heating rate of 5 deg./min, the calculated cellulose pyrolysis rate surpassed the thermo-oxidative decomposition rate (Kashiwagi and Nambu 1992).

The second stage of cellulose thermo-oxidative decomposition consists of oxidation of carbonized residue. Its oxidation rate is represented by the bimolecular reaction equation:

$$R_c = A_c\,[Y_{ox}]^{n(ox)}[W_c/W_o]^{n(c)}\exp\left(-E_{ox}/RT\right)$$

with experimental values $A_c = 3.4 \times 10^{11}$, min^{-1}; $E_c = 160$ kJ/mol and reaction orders in relation to mass fraction of char $n(c) = 1$, and to mass fraction of oxygen – $n(ox) = 0.78$ (Kashiwagi and Nambu 1992).

During fires in buildings, the density of radiative heat flows onto materials may reach 100 kW/m^2. In these conditions, very high heating rates exceeding 10 deg./s occur. Hence, it is natural to expect the contribution of oxidative direction of timber decomposition will be reduced.

The impact of environmental oxygen concentration on the gasification rate of pine timber, temperature variation, and distribution of decomposition products in the process of flameless radiative heating was studied in (Kashiwagi et al. 1987). A pine timber specimen ($\rho = 380$ kg/m^3) in the shape of a cube with dimensions 3.8 cm received radiative heat flow from above parallel to fiber orientation. Gas flow at a rate of $\approx$1 cm/s was applied from below.

Figure 3.14 shows the impact of environmental oxygen concentration on the mass decomposition rate of the wood specimen registered with a weighing device.

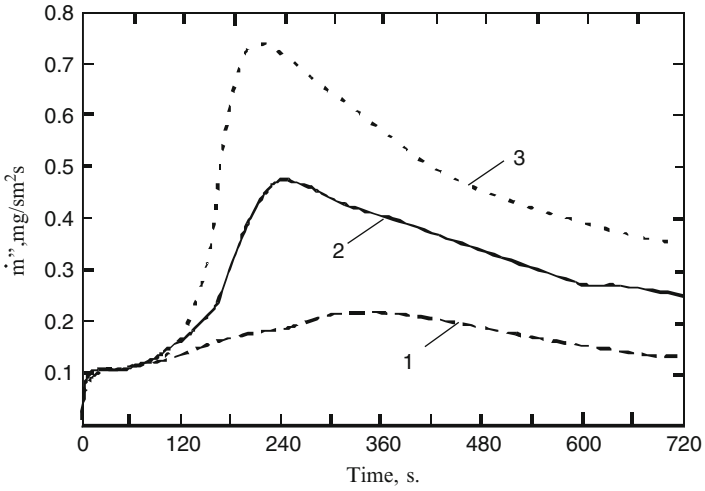

Fig. 3.14 Environmental impact on the mass decomposition rate of a pine specimen on application of an external radiative heat flow of 25 kW/m^2. *1* nitrogen, *2* 10.5 % O_2 + 89.5 % N_2, *3* air

It can be seen that increased oxygen concentration in the gas flow leads to higher mass decomposition rate of wood and to faster achievement of its maximum value. The initial stage of mass loss (up to 90 s) consists in evaporation of hygroscopic moisture and does not depend on the medium type. As the heat flow density increased, the wood gasification rate also increased, and its peak values in air and nitrogen were significantly reduced.

A change in oxygen concentration in the environment affects the thickness of the char layer being formed on the surface, the temperature inside the specimen, and the distribution of gaseous decomposition products. Thus, when a radiative heat flow of 40 kW/m^2 was applied for 15 min, the thickness of the char layer formed as the result of wood decomposition was 4.00 mm in the inert medium, 6.4 mm in the medium with 10.5 % oxygen, and 9.00 mm in air. The specimen surface temperature during decomposition in air was 700 °C and was almost 200 °C higher compared to wood pyrolysis in inert medium. Exothermic reaction of interaction between the char layer and oxygen explains this temperature rise of the specimen surface. According to the authors of study (Kashiwagi et al. 1987), a char layer with a high temperature may easily serve as the source of ignition of inflammable volatiles generated during wood decomposition.

Recently (Lautenberger and Fernandez-Pello 2009), a model of pine timber oxidative pyrolysis under radiative heating in flameless mode was presented. In contrast to other models of timber thermo-oxidative decomposition, which include heterogeneous reactions of oxidation on the surface (or near surface) of initial wood and the charred layer, work (Lautenberger and Fernandez-Pello 2009) examines the reactions only inside the porous wood matrix. It also considers both heterogeneous and homogeneous reactions (gas–gas). In the mathematical model, the pine speci-

men goes through four condensed phases during the process: (1) moist wood, (2) dry wood, (3) char, and (4) ash residue. Volumetric density of each phase is assumed to be constant, but their specific heat capacity and thermal conductivity depend on temperature. The reactions of dry wood and char with oxygen inside the pores are heterogeneous, whereas the reactions of gaseous products of wood pyrolysis and oxidative decomposition with oxygen also inside the pores are classified as homogeneous. Altogether, the mathematical model involves four condensed phases, seven gas-phase products, four heterogeneous reactions, and two homogeneous reactions. Numerical solution of this model requires about 50 input parameters.

According to the authors of (Lautenberger and Fernandez-Pello 2009), the advantage of this model is that it automatically adjusts to variations in environmental conditions, responding to lower oxygen content, for example. Furthermore, the model is potentially suited to simulating the behavior of various carbonizing materials under radiative heating. The only thing required is to account for thermochemical and thermophysical properties of the materials, as well as the mechanism and macrokinetic parameters of the reactions being examined. In order to specify particular experimental conditions, the mathematical model must use the corresponding initial and final settings of temperature, pressure, agent concentration, and other process parameters.

3.3 Numerical Models for Decomposition and Charring

In combustion conditions, timber pyrolysis proceeds in close interaction with chemical and physical processes of mass and heat transfer. Consequently, the general course of wood decomposition reactions depends not only on the kinetic features of the process and its energy performance but also on concurrent complex physical processes characterizing a specific system and its state.

In modeling the processes of ignition, combustion, and its extinction, timber pyrolysis is considered a submodel (submodel).

Modeling of pyrolysis of carbonizing polymer materials under conditions of high-temperature heat exposure and combustion with consideration of various chemical, physical, and transport processes has only been given special attention in recent years (Di Blasi 1993, 2000). Dozens of various models differing in their degree of complexity and elaboration of analyzed physical factors and chemical kinetics have been proposed specifically for the analysis of timber pyrolysis and charring.

The available theoretical models of timber pyrolysis, which give a mathematical description of the processes being studied using various set of differential equations may be subdivided in two large groups: analytical and numerical. Among the numerical models, in turn, two categories are singled out: (1) models that attempt to provide a comprehensive mathematical description for a transient pyrolysis process by means of partial differential equations and (2) integral models.

In the analytical models, pyrolysis of a polymer system is addressed in the most simplified variation without considering many real processes. This makes it possible in certain cases to obtain formulas for calculating mass loss rate or linear rate of wood surface regression in external heat exposure (Wichman and Atreya 1987; Miller and Ramohalli 1986). But, in general, the forecast area of analytical models is limited. The attempt in (Miller and Ramohalli 1986) to factor in the impact of heterogeneous timber structure on the material linear regression rate under external heat exposure is worth noting. The wood in that study was presented as a group of separate holocellulose fibers included in a lignin matrix. However, pyrolysis and wood charring were only described by a common global dependence as per the Arrhenius law, and apart from heat transfer in the decomposed material by thermal conductivity, no other transport process was considered.

Considerable progress was made as a result of developing numerical mathematical models of timber pyrolysis based on a detailed description of chemical and physical processes by means of partial differential equations and specifying the situation of boundary conditions. But even in these models, a number of assumptions are usually made, which simplify problem-solving and reduce the cost of computer-aided calculations. Unfortunately, many necessary input data on the thermophysical and thermochemical properties of wood (variations of these properties as a function of density and temperature) on macrokinetic parameters of pyrolysis and other characteristics of real transport process are largely unknown at present for the majority of specific timber species. The main advantage of numerical mathematical models is the ability to analyze the role and impact degree of certain factors included in the description of both chemical and physical processes in the reacting system by arbitrarily setting the input data on the system within reasonable limits.

Without going into particulars of the employed mathematical tools, we will limit ourselves to noting the elements of the approach to the theoretical study of timber pyrolysis regularities and the most important conclusions of this analysis.

In one of the early numerical mathematical models of wood pyrolysis with one-sided exposure of a timber slab to heat flow (Kung 1972), the chemical process of volatile and char residue formation was represented by one global first-order reaction as per the Arrhenius law. The factors in physical processes were material heating by transient thermal conductivity and internal convective heat transfer by volatile decomposition products. The material's thermophysical properties were assumed to be continuously ramping during initial transformation of wood into char residue. Special attention was paid to the impact of specimen thickness, thermal conductivity of the char layer, and endothermicity of pyrolysis on the total mass loss rate. The calculations showed that for a thermally thick wood specimen this rate depends on the thermal conductivity of the char layer formed on the surface. For a thermally thin specimen, this rate must be greatly influenced by endothermicity of pyrolitic reactions, but not by thermal conductivity of the char layer. Therefore, material dimensions (thickness) are of great importance.

The notion of thermally thick and thermally thin material originated from the general idea of the interrelation between the conditions of heat transfer inside the specimen and its dimensions. If the heat penetration, δ, exceeds the material physical thickness, L (i.e., $\delta/L > 1$) under the external heat exposure conditions being examined, this material proves itself as thermally thin. Otherwise, when $\delta/L < 1$, the material behaves as thermally thick. Intermediate material behavior between thermally thick and thin occurs when the relationship $\delta/L \approx 1$. Strictly speaking, the notion of heat wave size (heating-up) for thermally thin materials loses its meaning.

Among the modern numerical models taking multistage schemes of pyrolysis and physical, transport processes in wood into account, the model from (Di Blasi 1993) deserves attention. It considers a one-dimensional model of thermal decomposition in an inert atmosphere of a dry timber slab exposed to a radiative heat flow of constant density, q_e, on one side. The primary and secondary chemical reactions of timber pyrolysis are taken into account according to the diagrams in Figs. 3.7 and 3.8, respectively. It was assumed in this case that the resinous substances (tar) being formed do not condense, but remain in the vaporized state. All gases and vapors that are products of chemical reactions behave like an ideal gas. Similar to (Kung 1972), it was assumed that as the initial timber turns into char, characteristics of solids such as thermal conductivity, pore diameter, and permeability change linearly. The effects of shrinking, bloating, and surface crack formation were disregarded. Specimen volume change was assumed to proceed in proportion to the mass loss resulting from timber pyrolysis. Heat transfer inside the porous timber specimen by means of radiant energy was factored in as its contribution to the effective thermal conductivity: $k_{\text{eff}} = k_{\text{conv}} + k_{\text{rad}}$.

The mathematical description of the pyrolysis model includes equations based on fundamental physical laws of mass, momentum, and energy conservation, as well as the ideal gas law.

Concentration of wood and the group of products formed during pyrolysis are represented as the apparent mass density of substances M in the volume they occupy V:

$$\rho_{\text{w}} = \frac{M_{\text{w}}}{V}; \rho_{\text{G}} = \frac{M_{\text{G}}}{V_{\text{G}}} = \frac{M_{\text{G}}}{(\varepsilon V)}; \rho_{\text{tar}} = \frac{M_{\text{tar}}}{V_{\text{g}}} = \frac{M_{\text{tar}}}{(\varepsilon V)}; \rho_{\text{c}} = \frac{M_{\text{c}}}{V}.$$

Porosity factor ε here equals the ratio of the gas-phase volume to the total volume of the solid body: $\varepsilon = V_{\text{g}}/V$. Indices w, G, tar, and c specify wood, resulting gases, tar products of pyrolysis, and char residue, respectively.

If we assume that total density of the gas phase $\rho_{\text{g}} = \rho_{\text{G}} + \rho_{\text{tar}}$, then in accordance with the adopted kinetic scheme the mass balance for the initial substance and char may be described by the following equations:

- For wood $\frac{\partial \rho_{\text{w}}}{\partial t} = -(k_1 + k_2 + k_3)\,\rho_{\text{w}}$
- For char $\frac{\partial \rho_{\text{c}}}{\partial t} = k_3 \rho_{\text{w}} + \varepsilon k_5 \rho_{\text{tar}}$

For gas-phase pyrolysis products, the law of mass conservation is represented in the form of continuity equations:

– For tar substances $\frac{\partial(\varepsilon\rho_{\text{tar}})}{\partial t} + \frac{\partial(\rho_{\text{tar}}U)}{\partial x} = k_2\rho_{\text{w}} - \varepsilon\,(k_4 + k_5)\,\rho_{\text{tar}}$;

– For gases and vapors as a whole $\frac{\partial(\varepsilon\rho_{\text{g}})}{\partial t} + \frac{\partial(\rho_{\text{g}}U)}{\partial x} = (k_1 + k_2)\,\rho_{\text{w}} - \varepsilon k_5\rho_{\text{tar}}$,

where U – gas flow velocity in a porous solid body. As per Darcy's law, it is proportional to the pressure change in the system, P, as a result of timber pyrolysis and depends on medium permeability, K, as well as on dynamic viscosity of gas flow, μ:

$$U = \left(\frac{K}{\mu}\right)\left(\frac{\partial P}{\partial x}\right).$$

From the ideal gas law $P = \rho_{\text{g}}\,RT/W_{\text{g}}$, where W_{g} – average-molecular weight of gaseous substances, R – absolute gas constant, and T – temperature.

The energy conservation equation includes the following constituents:

$$\begin{aligned}&(\rho_{\text{w}}C_{\text{w}}+\rho_{\text{c}}C_{\text{c}}+\varepsilon\,(C_{\text{G}}\rho_{\text{G}}+C_{\text{tar}}\rho_{\text{tar}}))\,\partial T/\partial t+(T-T_0)\Big(C_{\text{w}}\partial\rho_{\text{w}}/\partial t+C_{\text{c}}\partial\rho_{\text{c}}/\partial t\\&+\varepsilon C_{\text{G}}\partial\rho_{\text{G}}/\partial t+\varepsilon C_{\text{tar}}\partial\rho_{\text{tar}}/\partial t+(\rho_{\text{G}}C_{\text{G}}+\rho_{\text{tar}}C_{\text{tar}})\,\partial\varepsilon/\partial t\,)+(T-T_0)(\,C_{\text{tar}}\partial\rho_{\text{tar}}U/\partial x\\&+C_{\text{G}}\partial\rho_{\text{G}}U/\partial x\Big)+U\,(\rho_{\text{tar}}C_{\text{tar}}+\rho_{\text{G}}C_{\text{G}})\,\partial T/\partial x = \partial/\partial x\,(k_{\text{eff}}\partial T/\partial x)+\sum r_n\Delta h_n\\&(\text{for } n=1-3)+\sum\varepsilon r_n\Delta h_n\,(\text{for } n=4.5)\,,\end{aligned}$$

where r_n – the rate of primary ($n = 1, 2, 3$) and secondary ($n = 4.5$) wood pyrolysis reactions, Δh_n – heat of the corresponding wood pyrolysis reaction.

The first two members on the left-hand side of the equation represent the energy consumed in heating substances in the condensed and gas-phase states, while the third and fourth members pertain to the energy for convective transport of gaseous products of the reaction. The right-hand side of the equation accounts for heat transfer by thermal conductivity and energy contributions of primary and secondary reactions of wood pyrolysis.

For initial conditions in a stationary environment, it is assumed that $T = T_0$, $\rho_{\text{w}} = \rho_{\text{w0}}$, $P = P_0$, and $U = 0$.

If $t > 0$ on the wood slab side exposed to an external heat flow, the heat loss from its surface through radiation and convection is factored in:

$$k_{\text{eff}}\,\frac{\partial T}{\partial x} = q_{\text{e}} - \sigma\left(T^4 - {T_0}^4\right) - h_{\text{conv}}\,(T - T_0)\,;\, P = P_0$$

where σ – Stefan–Boltzmann constant, h_{conv} – convective heat transfer factor.

For the cold side of wood slab, the following boundary conditions were assumed:

$$k_{\text{eff}} \frac{\partial T}{\partial x} = \sigma \left(T^4 - {T_0}^4\right) + h_{\text{conv}} \left(T - T_0\right); U = 0.$$

Calculation of a transient wood pyrolysis process according to the adopted model was done for a wood specimen 0.025-m thick, exposed to one-sided heating in an inert medium by radiative heat flow with density of 84 kW/m^2. Data from (Lee et al. 1976) on the thermophysical properties of maple and resulting char residue, as well as experimental values of kinetic parameters of the reaction at primary (Thurner and Mann 1981) and secondary stages of wood pyrolysis (Liden et al. 1988), were mainly used for this purpose. According to the data from (Thurner and Mann 1981), the primary pyrolysis reactions are first-order reactions with the following parameters: $A_{\text{G}} = 4.1 \times 10^6$ s^{-1}, $E_{\text{G}} = 112.7$ kJ/mol; $A_{\text{tar}} = 1.43 \times 10^4$ s^{-1}, $E_{\text{tar}} = 88.6$ kJ/mol; and $A_{\text{c}} = 7.4 \times 10^5$ s^{-1}, $E_{\text{c}} = 106.5$ kJ/mol.

Analysis of pyrolitic process development (rates of product formation and distribution, changes in temperature and internal pressure of the gas phase) revealed three main spatial zones in the specimen: initial wood heating, primary pyrolysis, and char layer. The boundary between the area where the decomposition reaction is unobservable and the primary pyrolysis zone features the maximum increase in the internal pressure gradient and very fast buildup of convective gas velocity. The wave of primary pyrolysis of wood $\approx 0.25 \times 10^{-2}$-m thick propagates inside the initial material with decreasing speed. As a matter of fact, a temperature decrease of 30 K drastically slows the pyrolysis rate due to its exponential dependence on temperature. During pyrolysis of the whole specimen, the average speed of pyrolysis front propagation was about 0.02 mm/s.

As the calculations showed, temperature distribution in the primary pyrolysis zone (500–700 K) is determined by the energy of decomposition reactions, by heat transfer through convection and by thermal conductivity.

The yield of tar pyrolysis products is the highest at the maximum wood pyrolysis rate registered at the boundary with char layer zone. Subsequent gradual decrease in tar product yield in the char layer is the result of secondary reactions of wood pyrolysis at temperatures above 700 K.

It is interesting to note that using a model with a multistage kinetic scheme of wood pyrolysis revealed two temperature subranges. In the char zone with temperatures of 700–800 K, the primary pyrolitic reactions are almost fully completed, whereas the secondary reactions are still not very active, and only heat transfer is of great importance. In the high-temperature range of the char layer (800–1,100 K), an important role is played by both secondary pyrolitic reactions, especially in the direction of cracking tar substances with the formation of low-molecular-weight gases, and heat transfer processes with enhanced contribution due to a radiative constituent.

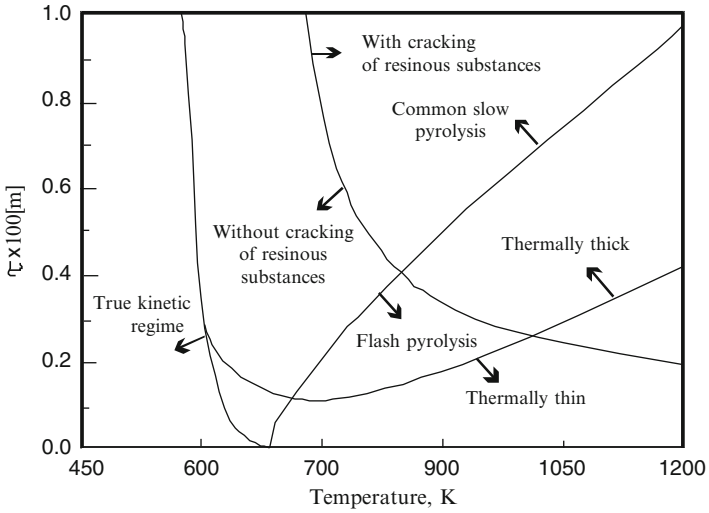

Fig. 3.15 Impact of temperature and cellulose specimen dimension on pyrolysis process regimes and activity of secondary cracking reactions of resinous products (τ – specimen half thickness)

Therefore, wood pyrolysis under external heat exposure actually has four spatial zones with different combinations of chemical and physical processes.

Activity of the secondary reactions of cracking tar products of decomposition depends not only on temperature but also on the dimensions of the heated specimen. A chart of possible process regimes compiled on the basis of calculations of a numerical model incorporating a multistage scheme of cellulose specimen pyrolysis is given in Fig. 3.15 (Di Blasi 2000).

The chart clearly shows the conditions for the occurrence of various pyrolysis regimes (including common slow and rapid, flash pyrolysis of cellulose) controlled by kinetics or heat transfer.

Detailed study of kinetic regularities of thermal decomposition of various wood species and knowledge of the formation and distribution conditions of pyrolysis products are very important for developing effective fire protection methods for timber-based materials, and for understanding the relative rating of their flammability and fire safety in general.

The revealed (Di Blasi 1993) existence of four stages and spatial zones in wood pyrolysis agrees to some extent with the results of simplified model analysis (Wichman and Atreya 1987). Along with the stage of inert heating and primary stage of wood pyrolysis, the authors (Wichman and Atreya 1987) also presented stages of thin and thick surface layers of char formation. At the stage of thin char formation, the mass rate of pyrolysis-induced volatile release reaches its maximum value. At the initial stages, wood decomposes in a kinetically controlled regime, because surface temperature limits the mass loss rate. Release of volatiles at the stage of thick char layer formation depends on temperature gradient. In this case, the pyrolysis regime is considered as a diffusion-controlled process.

It should be noted that the formulas for calculating mass loss rate in wood pyrolysis were obtained in (Wichman and Atreya 1987) by the asymptotic method of analysis (with time $t \to \infty$), making it possible to reduce the mathematic description of pyrolysis by partial differential equations to ordinary differential equations and thus simplify the solution. However, it was found that analytical formulas obtained substantially (12–62 %) underestimated the true values of maximum mass loss rate calculated by exact numerical integration of the partial differential equations. This may be due to idealization of the wood pyrolysis process in the adopted model. Pyrolysis is assumed to be energetically neutral in terms of reaction heat and is modeled by a one-stage first-order reaction with fixed kinetic parameters. But any chemical interrelation between the resulting volatile decomposition products and reacting material is ignored. Accounting for possible heat loss from the surface of charring material through radiation and convection is a step forward in comparison with other analytical model.

Integral models of transient wood pyrolysis (Kunury 1972; Kanury and Holve 1982; Chen et al. 1993; Moghtadery et al. 1997; Spearpoint and Quintiere 2000; Himoto and Tanaka 2004) are particularly interesting for engineering practice and research on fire safety in the building industry.

Integral models are an attempt to develop simple and effective numerical models capable of including many real processes in pyrolysis and combustion of materials. In integral models, the partial differential equations used to describe wood pyrolysis (first of all, transient thermal conductivity equations) are reduced to ordinary differential equations. This procedure is based on a predetermined law of temperature distribution in a solid body in combination with the boundary conditions in the system under consideration. A temperature distribution meeting the boundary conditions is then inserted in the thermal conductivity equation to be integrated over the whole spatial variable (material thickness). The result is an ordinary differential equation of the time variation of the required parameter as an independent variable. The essential thing in this approach is the choice of the assumed temperature profile in the body under heat exposure. Various types of temperature distribution are used in the available integral models of wood pyrolysis. Thus, for example, in earlier studies (Kunury 1972; Kanury and Holve 1982), to simplify the analysis in modeling wood pyrolysis under radiative heat flow of constant density or in heating by convective heat flow with constant heat transfer factor, the linear temperature profile in the initial wood and char layer was selected. In model (Chen et al. 1993), the exponential law of temperature distribution in the heated layers of wood and char was adopted, whereas in (Moghtadery et al. 1997; Himoto and Tanaka 2004) a square-law temperature profile was used. According to the authors of (Moghtadery et al. 1997), it is quite consistent with experimental data on testing of timber structures for fire resistance and meets the corresponding boundary conditions. The integral model used in (Spearpoint and Quintiere 2000) assumes a linear temperature profile in the char layer and a square-law profile in the wood layer still not reacting.

The use of integral models is limited by the basic initial assumption that the temperature variations as a function of material thickness (layer) are monotonic, regardless of whether the material is carbonizing or decomposes integrally like many polymer thermoplasts.

Integral models of pyrolysis of carbonizing polymer materials are in effect thermal models, where the mechanism and kinetics of chemical reactions are disregarded. Thermal models of pyrolysis are viewed as a special type of Stefanov problem, named after the scientist who was the first to draw attention to the important role of physical factors of heat and mass transfer in chemical processes. Along with a transient thermal conductivity equation, a description of thermal models of wood pyrolysis includes nonlinear boundary conditions that take into account the heat losses through radiation from the charred surface (Chen et al. 1993; Jia et al. 1999). Since the pyrolysis rate is mainly limited by the heat transfer process, and the effective activation energy of chemical reactions is sufficiently high, it is assumed that material pyrolysis starts immediately after achieving a certain temperature, T_p. The volatiles resulting from decomposition do not accumulate inside the solid body and are immediately released from its surface.

The problem, therefore, boils down to the definition of temperature distribution over the thickness of a specific material under the given conditions of external heat exposure, and ultimately to the definition of the speed of pyrolysis front propagation or mass burn-off rate.

The square-law temperature profile over the thickness (spatial coordinate x) of a solid slab externally exposed to heat flow on one side may be mathematically described by a polynomial equation:

$$T(x,t) = b_0(t) + b_1(t)x + b_2(t)x^2,$$

where $b_0(t)$, $b_1(t)$, and $b_2(t)$ are coefficients depending on the thermal properties of the material and intensity of absorbed thermal energy. The procedure for determining these coefficients is given in sufficient detail in (Moghtadery et al. 1997; Himoto and Tanaka 2004).

The integral one-dimensional model of carbonizing wood materials in a inert medium considers different phases of the process: (1) preliminary material heating, (2) pyrolysis of a specimen behaving as thermally thick material ($\delta < L$), and (3) pyrolysis of a specimen behaving as a thermally thin material ($\delta \geq L$). Figure 3.16a, b shows the temperature distribution scheme during "inert heating" and pyrolysis of a thermally thick specimen (Moghtadery et al. 1997).

In the "inert heating" phases, the heat flow applied externally and absorbed on the specimen surface transfers heat inside the specimen by thermal conductivity. The density of absorbed flow, q''_{net}, depends on the external heat flow, q''_e, and heat loss from the frontal surface through radiation and convection:

$$q''_{net} = q''_e - \varepsilon\sigma\left(T_s^4 - T_0^4\right) - h_{conv}\left(T_s - T_0\right).$$

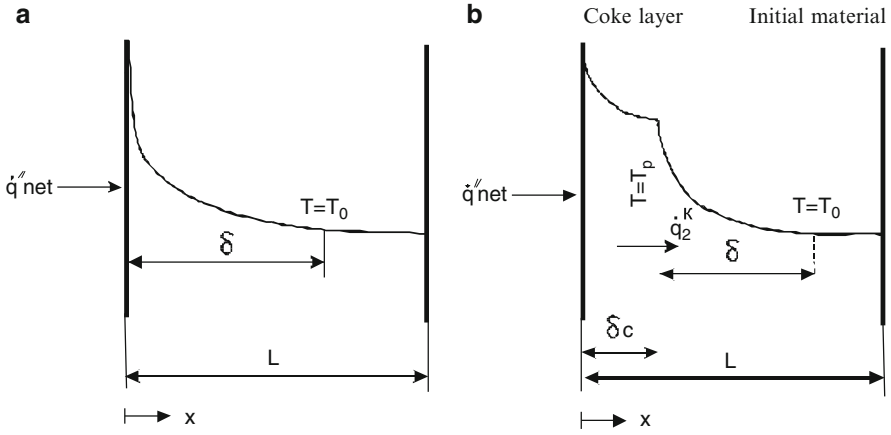

Fig. 3.16 Model of preliminary heating (**a**) and pyrolysis (**b**) of carbonizing material in one-dimensional configuration

The "inert heating" phase of the initial material is usually mathematically represented by a transient thermal conductivity equation:

$$\frac{\partial T_{\mathrm{w}}}{\partial t} = \frac{\alpha_{\mathrm{w}} \partial^2 T_{\mathrm{w}}}{\partial x^2}$$

where α_{w} – thermal conductivity of wood and the corresponding initial and boundary conditions for a thermally thick specimen:

$$T_{\mathrm{w}}|_{x=0,t=0} = T_0; k_{\mathrm{w}} \partial T/\partial x|_{x=0} = q''_{\mathrm{net}}; k_{\mathrm{w}} \partial T/\partial x|_{x=\delta} = 0; T_{\mathrm{w}}|_{x=\delta} = T_0$$

and for a thermally thin specimen on an insulating base for $x = \delta = L$: $\partial T/\partial x = 0$.

Two layers are singled out in the wood pyrolysis phase: the char formation layer and the initial wood layer. Char formation starts when the specimen's surface temperature reaches the onset temperature of thermal decomposition of wood, T_{p}.

The front of the wood pyrolysis (charring) wave propagates inside the specimen. Heat transfer in the char layer is described by a thermal conductivity equation:

$$\frac{\partial T_{\mathrm{c}}}{\partial t} = \frac{\alpha_{\mathrm{c}} \partial^2 T_{\mathrm{c}}}{\partial x^2}$$

with initial and boundary conditions: $T_{\mathrm{c}} \mid_{x=0,t_{\mathrm{p}}} = T_{\mathrm{p}}; k_{\mathrm{c}} \partial T_{\mathrm{c}}/\partial x \mid_{x=0} = q''_{\mathrm{net}}$; $T_{\mathrm{c}} \mid_{x=\delta \mathrm{c}} = T_{\mathrm{p}}; k_{\mathrm{c}} \partial T_{\mathrm{c}}/\partial x \mid_{x=\delta \mathrm{c}} = q_2$.

The square-law temperature profile in the char layer under the indicated boundary conditions corresponds to the equation:

$$T_{\mathrm{c}} = T_{\mathrm{p}} + \left(T_{\mathrm{p}} - T_0\right) \left\{ \frac{(\delta_{\mathrm{c}} - x)}{\delta_{\mathrm{c}}} \right\}^2.$$

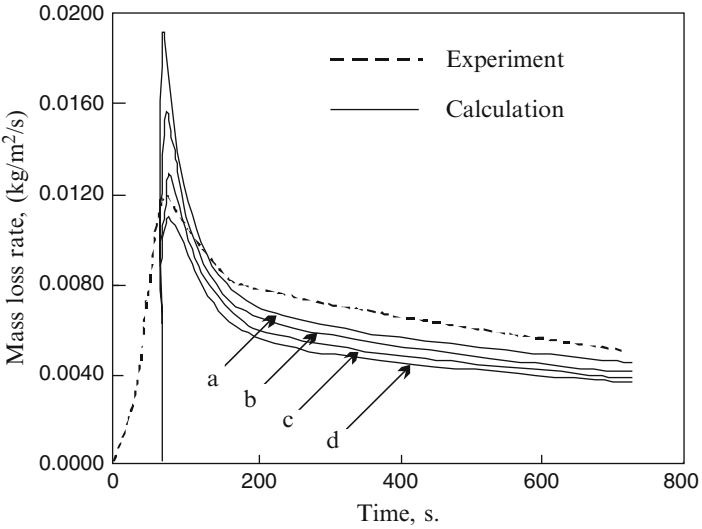

Fig. 3.17 Comparison of calculated (—) and experimentally measured (- - -) rates of mass loss during pyrolysis of white pine in an inert atmosphere. The values of Q_L, kJ/kg: *a* 255, *b* 400, *c* 600, *d* 800

Heat transfer in the layer of initial undecomposed wood is described by the equations of the "inert heating" phase but with initial conditions corresponding to the boundary conditions in the char layer. The temperature distribution in this layer according the square law will be the following:

$$T_w = T_p + (T_p - T_0)\left\{\frac{(x - \delta_c)}{\delta}\right\}^2.$$

The heat balance equation at the char and initial wood phase interface in the pyrolysis front (the so-called Stefan equation) determines the linear regression rate $d\delta_c/dt$, and mass loss rate, m'', during pyrolysis:

$$k_w \partial T_w/\partial x|_{x=\delta c} - k_c \partial T_c/\partial x|_{x=\delta c} = m'' Q_L,$$

where Q_L – timber pyrolysis heat and $m'' = (\rho_w - \rho_c)\, d\delta_c/dt$.

The proposed procedure for estimating temperature distribution in carbonizing material (Moghtadery et al. 1997) makes it possible to calculate the temperature on a wood specimen's surface and in its pyrolysis front for a specific system and conditions. This in turn makes it possible to estimate the heat loss and heat flows on the specimen surface, q_{net} and q_2, from the char layer to the initial wood layer and then the mass flow of pyrolysis volatiles.

The impact of heat from the endothermic pyrolysis reaction, Q, on the mass loss rate during heating of a thermally thick specimen of white pine in an inert atmosphere with heat flow of 40 kW/m^2 is shown in Fig. 3.17.

An experimental curve is also given here for comparison. The following baseline data on wood and char properties were used in calculating the mass loss rate on the basis of the integral model: $\rho_w = 380$ kg/m^2, $\alpha_w = 6.6 \times 10^{-7}$ m^2/s, $k_w = 0.3$ W/m K, $\alpha_c = 2 \times 10^{-6}$ m^2/s, $k_c = 0.15$ W/m K, and $\rho_c/\rho_w = 0.2$. Pyrolysis temperature is assumed to be $T_p = 673$ K; radiation factor $\varepsilon = 0.9$; and convective heat transfer factor $\eta_{conv} = 15$ W/m K. $Q = 255$ kJ/kg was used as the baseline wood pyrolysis heat value.

As is seen from Fig. 3.17, the integral model of timber pyrolysis simulates the complex character of the experimental mass loss rate curve. However, the best agreement with the experimental curve is obtained at $Q = 600$ kJ/kg. In this case, the observed difference between the calculated and experimental maximum values m'' is only 8 % (Moghtadery et al. 1997). The decrease in mass loss rate after the peak is mainly caused by the formation of a char layer, which acts as thermal insulator.

In an oxidative medium, there is a more complicated situation with thermal decomposition of carbonizing timber materials. At relatively low temperatures, the direct interaction of environmental oxygen with porous timber material, as well as oxidizing decomposition, charring, and smoldering reaction, is possible. But if a certain heating threshold is achieved and inflammable volatiles are formed in sufficient concentration, they ignite in the gas phase above the solid body surface. Stable flame prevents access of air oxygen to the wood specimen surface, and its decomposition after ignition practically conforms to purely thermal conditions of pyrolysis.

In integral models of timber pyrolysis under conditions of combustion in an oxidizing atmosphere, it is assumed that the ignition temperature matches the pyrolysis (charring) temperature. The heat flow absorbed by a wood surface equals the sum of flows arriving from the external source and the flame and exhausted due to radiation and convection: $q''_{net} = q''_e + q''_{fl} - q''_L$.

After the inflammable volatile pyrolyis products cease to evolve due to completion of material charring reaction, the flame over its surface dies out ($q''_{fl} = 0$). The reaction of oxidation of the char formed through pyrolysis becomes possible.

In this case we have $q''_{net} = q''_e - q_L + m''_c \Delta H_c$,where m''_c – mass rate of char burn-off per unit surface of the specimen, ΔH_c – combustion heat of char.

Experimental values of total combustion of char formed on the surface of various timber species range between 32 and 35.5 mJ/kg (Spearpoint and Quintiere 2000).

Figure 3.18 shows the curves of mass loss rate variations for combustion of maple wood, both obtained experimentally and calculated according to the integral model and a stricter numerical model with the use of partial differential equations (Moghtadery et al. 1997).

The following characteristics of maple timber and resulting char were used in the calculation. Wood density $\rho_w = 530$ kg/m^3, $\rho_c/\rho_w = 0.2$, $\alpha_w = 1 \times 10^{-7}$ m^2/s, $\alpha_c = 7.5 \times 10^{-7}$ m^2/s, $k_w = 0.16$ W/m K, and $k_c = 0.08$ W/m K. Pyrolysis heat $Q = 255$ kJ/kg. Combustion heat is 20 MJ/kg.

In spite of the omission of the details of chemical kinetics, the integral model of wood decomposition during combustion adequately predicts both peaks on the specimen burn-off rate curve, which are characteristic of the stages of wood flaming

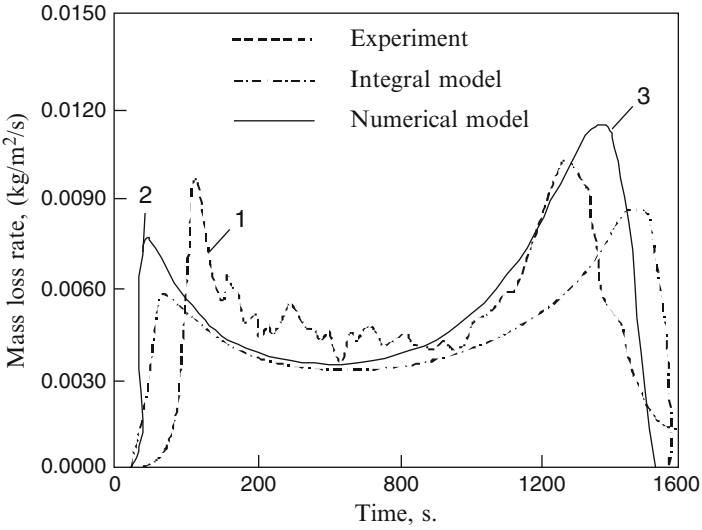

Fig. 3.18 Experimentally measured *1* and estimated mass loss rates for one-sided heating of a 19-mm thick wood slab in air by radiative heat flow of 20 kW/m^2: *2* integral model and *3* numerical model

combustion and char smoldering combustion. The peak pertaining to char oxidation appears when the wood specimen behaves as thermally thin in the specified conditions of heat exposure and chars through its entire thickness in response to the presence of an insulating base.

As follows from the work of Japanese scientists (Himoto and Tanaka 2004), the onset of intensive char oxidation, peak position, and maximum char burn-off rate depend not only on the heat of the endothermic timber pyrolysis reaction but also on the thermal conductivity of the char layer. This effect is apparently the consequence of the latter parameter reflecting the nature of the char layer's porosity and reaction capacity.

The results of experimental and theoretical studies of the burn-off of four deciduous and coniferous species (oak, maple, Douglas fir, and redwood) are of great interest (Spearpoint and Quintiere 2000). The studies examine the impact of radiative heat flow of constant density of 25–75 kW/m^2 perpendicular and parallel to the fiber orientation in the wood structure.

A standard cone calorimeter was used to test the specimen (thickness 50 mm) in the horizontal configuration. Based on the integral model of wood pyrolysis, the authors presented an analytic solution for burn-off rate for short-term heating of the specimen immediately after ignition ($t \approx t_{ign}$) and for long-term heating ($t \gg t_{ign}$) before termination of the flaming combustion stage. The intersection of the resulting curves corresponds to the maximum (peak) wood burn-off rate (Fig. 3.19).

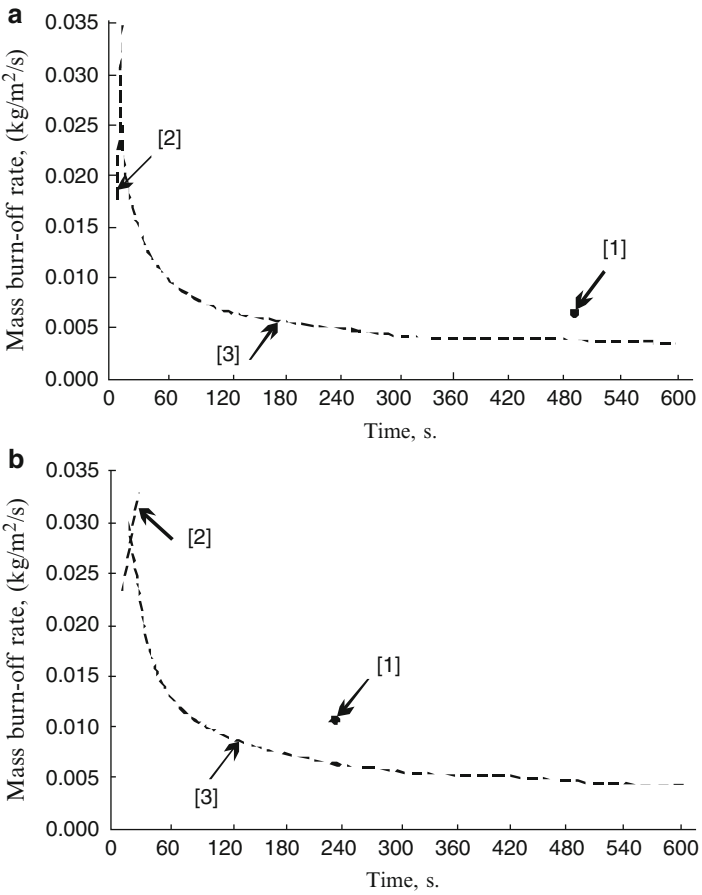

Fig. 3.19 Measured and theoretical values of burn-off rate for specimens of Douglas fir (**a**) and oak (**b**) with heat flow of 75 kW/m^2 perpendicular to the fiber orientation. *1* experiment, *2* and *3* short-term and long-term solutions, respectively

More active growth of char layer thickness after the peak under otherwise equal conditions is reported in coniferous timber species (Fig. 3.20).

This being the case, the total fraction of char residue, ϕ, at the end of the flaming period is inversely proportional to the density ratio of incident and critical heat flows in wood ignition:

$$\phi = 0.74\left(\frac{q_e}{q_{cr}}\right)^{-0.64}$$

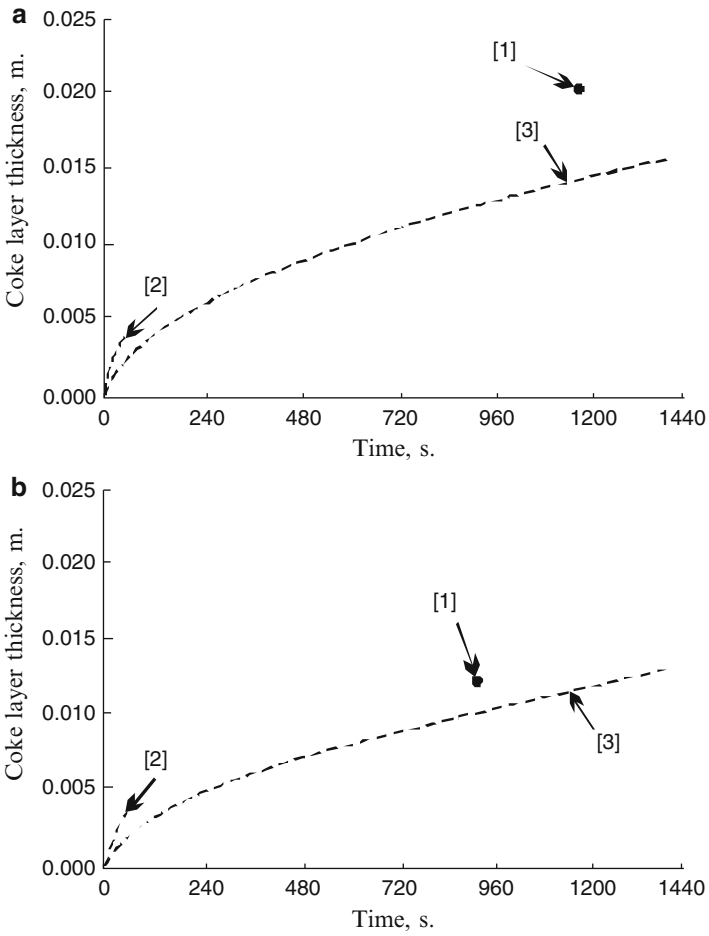

Fig. 3.20 Measured *1* and theoretically calculated *2*, *3* thickness of the char layer formed during exposure of specimens of Douglas fir (**a**) and champion oak (**b**) to 75 kW/m^2 perpendicular to the fiber orientation

Our observations of the growth of char layer thickness on the surface of specimens of tropical, coniferous, and deciduous timber species confirm the conclusion cited above. As is seen from Fig. 3.21, the thickness of the resulting char layer is greatly affected by the external heat flow intensity. A marked difference in charring rate is observed not only between coniferous and deciduous species but also between varieties within the same species (Serkov et al. 2009).

The average charring rate at 50–75 kW/m^2 may reach 1.1–1.8 mm/min for coniferous timber species, and 0.7–0.9 mm/min for deciduous timber species. Moisture slows the timber charring rate, because it affects timber density, thermal capacity, and gasification heat. The effect of moisture content in timber on its

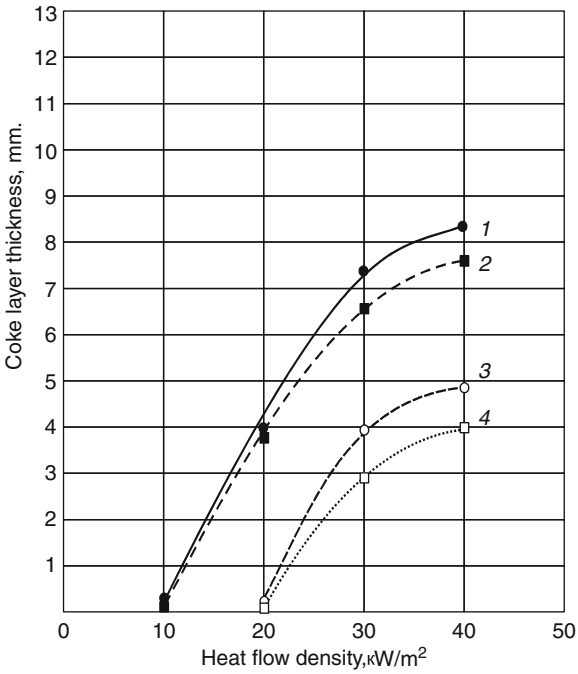

Fig. 3.21 Impact of radiative heat flow density on char layer thickness during flaming combustion for 5 min in timber specimens of *1* fir, *2* pine, *3* birch, *4* oak

charring rate compared to a dry specimen, based on the thermal model of this process, may be roughly estimated by the equation (Mikkola 1991):

$$\beta = \frac{1}{(1 + 2.5w)},$$

where β – charring rate of a moist timber specimen, mm/min; w – relative fraction of moisture in the timber. The equation is plausible at $w < 0.2$ (<20 %).

After termination of timber flaming combustion in an oxidizing medium, heterogeneous oxidation of the resulting char starts.

It was found, for example, that maximum mass loss rate as a result of oxidation of a Douglas spruce char layer for a heat flow of 75 kW/m^2 applied perpendicular to the fiber axis reaches 0.0010 kg/m^2 s (Spearpoint and Quintiere 2000).

In the integral model, it is usually assumed that the heat flow from the burning specimen flame, q_{fl}, remains constant for a specific material and adopted configuration and does not depend on external flow intensity, q_{e}.

Iterative analysis of the obtained results (Spearpoint and Quintiere 2000) made it possible to estimate the values of flame-induced heat flow and gasification heat in different timber species under external heat exposure perpendicular and parallel to the fiber axis, which are crucial for modeling timber pyrolysis in various situations (Table 3.3).

Effective gasification heat is the amount of heat needed to convert a solid into volatile vapors and gases. This value includes the enthalpy increase in the initial

Table 3.3 Impact of specimen orientation relative to heat flow direction on gasification heat and density of flame-induced heat flow during combustion of various timber species (Miller and Ramohalli 1986)

Timber	Heat flow direction with respect to fiber axis	Gasification heat, kJ/g	Flame-induced heat flow, kW/m^2
Douglas spruce	Perpendicular	1.6	17
	Parallel	2.9	46
Redwood	Perpendicular	2.8	35
	Parallel	3.2	33
Oak	Perpendicular	2.3	35
	Parallel	2.3	33
Maple	Perpendicular	1.7	16
	Parallel	3.5	36

Table 3.4 Effective gasification heat of various timber species (Kunury 1972)

Timber specimen	Q_L, kJ/g of volatiles	Timber specimen	Q, kJ/g of volatiles
Douglas fir	5.9	Walnut	5.1
Canadian spruce	1.7	Ash	2.2
Larch	5.2	Podocarpus (Podocarpaceae)	2.8
Pine	–	Abura (*Rubiaceae*)	1.8
Cedar	5.6	Baku (Sapotaceae)	4.7

wood prior to the onset of pyrolysis, heat of the pyrolysis reaction, and any possible heat losses from the pyrolysis zone. It is generally believed that the effective wood gasification heat is

$$Q_L = \Delta H_v + c_{p,w}\left(T_p - T_0\right),$$

where ΔH_v – heat of the endothermic timber pyrolysis reaction.

Table 3.3 gives the values of gasification heat calculated per unit mass of initial. It is seen that when the heat flow is applied perpendicular to the fiber axis, the effective gasification heat equals 1.6–2.8 kJ/g, whereas in the parallel direction it equals 2.3–3.5 kJ/g of timber.

In most published sources, the effective gasification heat value for timber is indicated per unit mass of volatile pyrolysis products. According to these data, the effective heat of timber gasification may range between 1.7 and 7 kJ/g of volatile products (Table 3.4).

Examination of a large quantity of factual data pertaining to the kinetics and mechanism of thermal and thermo-oxidative decomposition of various timber species naturally leaves many questions unanswered. Even in the case of individual timber components, for example, cellulose, it is not clear why the formation of certain product groups proceeds with high apparent activation energies (Mamleev et al. 2009).

References

ASTM E 1641-2004. Standard test method for decomposition kinetics by thermogravimetry
Bradbury AGW, Sakai Y, Shafizadeh F (1979) Kinetic model for pyrolysis of cellulose. J Appl Polym Sci 23:3271–3280
Branca C, Di Blasi C (2004) Global intrinsic kinetics of wood oxidation. Fuel 83(1):81–87
Branca C, Albano A, Di Blasi C (2005) Critical evaluation of wood devolatilization mechanisms. Thermochim Acta 429:133–141
Chen Y, Delichatsios MA, Motevalli MA (1993) Material properties. Part 1: an integral model for one-dimensional transient pyrolysis of charring and non-charring materials. Combust Sci Technol 88:309–328
Cordero T, Rodriguez- Maroto JM, Garcia F, Rodriguez JJ (1991) Thermal decomposition of wood in oxidizing atmosphere. A kinetic study from non-isothermal TGA experiments. Thermochim Acta 191:161–178
Di Blasi C (1993) Modeling and simulation of combustion processes of charring and non-charring solid fuels. Prog Energy Combust Sci 19:71–104
Di Blasi C (2000) The state of the art of transport models for charring solid degradation. Polym Int 49:1133–1146
Di Blasi C (2008) Modeling chemical and physical processes of wood and biomass pyrolysis. Prog Energy Combust Sci 34:47–90
Di Blasi C, Branca C (2001) Kinetics of primary product formation from wood pyrolysis. Ind Eng Chem Res 40:5547–5556
Di Blasi C, Branca C, Fumo E (1999) Non-isothermal kinetics of wood degradation and combustion. In: Proceedings of the 8-th international conference on fire science and engineering, interflam'99, vol 2. Edinburgh, Scotland, pp 873–884
Di Blasi C, Branca C, Santoro A, Gonzales Hernandez E (2001) Pyrolytic behavior and products of some wood varieties. Combust Flame 124:165–177
Fang MX et al (2006) Kinetic study on pyrolysis and combustion of wood under different oxygen concentrations by using TG-FTIR analysis. J Anal Appl Pyrolysis 77(1):22–27
Golova OP (1975) Chemical effects of heat on cellulose. Russ Chem Rev 44(8):1454–1474
Gronli MG, Varhegyi G, Di Blasi C (2002) Thermogravimetric analysis and devolatilization kinetics of wood. Ind Eng Chem Res 41:4201–4208
Himoto K, Tanaka T (2004) A burning model for charring materials and its application to the compartment fire development. Fire Sci Technol 23(3):170–190
ISO 11358-2005. Plastics. Thermogravimetry of polymers, Part 2. Determination of kinetic parameters
Jia F, Galea ER, Patel MK (1999) Numerical simulation of the mass loss process in pyrolizing char materials. Fire Mater 23:71–78
Kanury AM, Holve DJ (1982) Transient conduction with pyrolysis (approximate solutions for charring of wood slabs). J Heat Transf 104:338–343
Kashiwagi T, Nambu H (1992) Global kinetic constants for thermal oxidative degradation of cellulosic paper. Combust Flame 88:345–368
Kashiwagi T, Ohlemiller TJ, Werner K (1987) Effects of external radiative flux and ambient oxygen concentration on nonflaming gasification rates and evolved products of white pine. Combust Flame 69:331–345
Kawamoto H et al (2007a) Pyrolysis behaviour of wood and its constituent polymers at gasification temperature. J Anal Appl Pyrolysis 78:328–336
Kawamoto H et al (2007b) Cellulose-hemicellulose and cellulose-lignin interaction in wood pyrolysis at gasification temperature. J Anal Appl Pyrolysis 80:118–125
Konkin AA (1974) Carbon and other heat-resistant fiber materials, Moscow, Chemistry, 375 p
Kung HC (1972) A mathematical model of wood pyrolysis. Combust Flame 18:185–195
Kunury AM (1972) Rate of burning of wood. Combust Sci Technol 5:135–146

Lautenberger C, Fernandez-Pello C (2009) A model for the oxidative pyrolysis of wood. Combust Flame 156:1503–1513

Lee CK, Chaiken RF, Singer JM (1976) Charring pyrolysis of wood in fires by laser simulation. In: Proceedings of 16-th symposium (international) on combustion. The Combustion Institute, Pittsburgh, pp 1459–1469

Liden A, Berruti F, Scott D (1988) A kinetic model for the production of liquids from the flash pyrolysis of biomass. Chem Eng Commun 65:207–221

Mamleev V, Bourbigot S, Le Bras M, Yvon J (2009) The facts and hypothesis relating to the phenomenological model of cellulose pyrolysis. Independence of the steps. J Anal Appl Pyrolysis 84(1):1–17

Mikkola E (1991) Charring of wood based materials. In: Proceeding of 3rd international symposium on fire safety science. Elsevier, pp 547–556

Miller RS, Bellan J (1996) A generalized biomass pyrolysis model based on superimposed cellulose, hemicellulose and lignin kinetics. Combust Sci Technol 126:97–137

Miller CA, Ramohalli KNR (1986) A theoretical heterogeneous model of wood pyrolysis. Combust Sci Technol 46:249–265

Moghtadery B, Novozhilov V, Fletcher D, Kent JH (1997) An integral model for the transient pyrolysis of solid materials. Fire Mater 21:7–16

Nakamura T, Kawamoto H, Saka S (2008) Pyrolysis behaviour of Japanese cedar wood lignin studied with varies model dimmers. J Anal Appl Pyrolysis 81:173–182

Roberts AF (1970) A review of kinetics data for the pyrolysis of wood and related substances. Combust Flame 14:261–272

Rogers FE, Ohlemiller TJ (1981) Pyrolysis kinetics of a polyurethane foam by thermogravimetry. A general kinetic method. J Macromol Sci Chem A 15(1):169–185

Serkov BB, Sivenkov AB, Tkhan BD, Aseeva RM (2005a) Thermal decomposition of tropical wood species. Lesn Vestn (Russ) 2(38):70–76

Serkov BB, Sivenkov AB, Than BD, Aseeva RM (2005b) Thermal decomposition of tropical wood species, No 2(38). Moscow State Forest University Publishing House, Lesnoy Vestnik, pp 70–76

Serkov BB, Sivenkov AB, Souleikin EV, Degtyaryov RV, Tarasov NI (2009) Fire hazard features of archaeological wood. Fires and emergencies: prevention, response. Moscow, ASFS, No 1, pp 4–28

Shafizadeh F, McGinnis GD (1971) Chemical composition and thermal analysis of cotton wood. Carbohydr Res 16:273–277

Shestak Ya (1987) Theory of thermal analysis. Mir, Moscow, 456p

Spearpoint MJ, Quintiere JG (2000) Predicting the burning of wood using an integral model. Combust Flame 123:308–324

Thurner F, Mann U (1981) Kinetic investigation of wood pyrolysis. Ind Eng Chem Process Des Dev 20:482–488

Varhegyi G, Gronli MG, Di Blasi C (2004) Effects of sample origin, extraction, and hot-water washing on the devolatilization kinetics of chestnut wood. Ind Eng Chem Res 43:2356–2367

Ward SM, Braslaw J (1985) Experimental weight loss kinetics of wood pyrolysis under vacuum. Combust Flame 61:261–269

Wichman IS, Atreya A (1987) A simplified model for the pyrolysis of charring materials. Combust Flame 68:231–247

Zickler GA et al (2007) In situ X-ray diffraction investigation of thermal decomposition of wood cellulose. J Anal Appl Pyrolysis 80:134–140

Chapter 4
The Ignition of Timber

Abstract This chapter formulates the main chemical and physical conditions for initiation and propogation smoldering and flame burning of timber. Data on intensity of external heating to initiate smoldering and self-ignition of solid timber and generation of flame burning in the presence of piloted source of ignition are discussed in detail. Based on the presented data, the critical parameters for initiation of flame burning of various species of timber are determined.

One of the main determinants of timber flammability is its ability to initiate and develop the combustion process when heated in the open air. Under normal conditions, timber products are stable, and experience shows that they may retain their main technical properties over a long period of service (many decades and even centuries). The ignition is only the initial stage of the combustion process, which may develop in both flaming and smoldering modes fundamentally differing from each other in mechanism and kinetics of chemical reactions, as well as in the significance of various physical factors.

Timber is a material with relatively low porosity and gas permeability; however, specific values of the characteristics depend on species of timber. Pores in wood are essentially closed or partially open cell cavities in the form of elongated tubes or capillaries with a certain orientation. Wood porosity, P, is calculated in volume fractions by its density when dry, ρ_0, and cell wall density, ρ_s:

$$P = 1 - \rho_0/\rho_s.$$

Porosity may be presented as the pore volume to cell wall volume ratio. Porosity of widespread wood species varies from 45 to 75 %.

Gas permeability reflects the ability of wood to be permeable to various gases, including air. It depends on grain orientation. Cross grain gas permeability of wood is generally several tenfold lower than along the grain. Sapwood is characterized by a higher gas permeability factor than heartwood (Ugolev 2001). In natural

R. Aseeva et al., *Fire Behavior and Fire Protection in Timber Buildings*,
Springer Series in Wood Science, DOI 10.1007/978-94-007-7460-5_4,

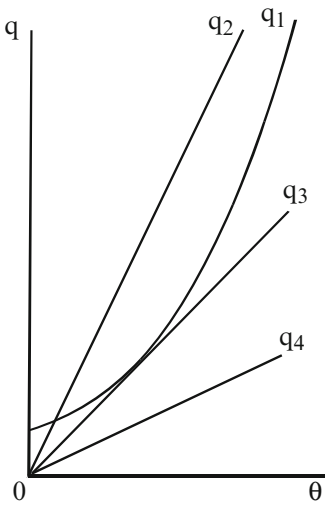

Fig. 4.1 Semenov diagram: q_1 – heat release curve; q_2, q_3, q_4 – different possible positions of curves of heat loss from the chemical reaction area

conditions, penetration of gases takes place through the system of pores and capillaries and apertures in wood cell walls. Gas penetration into the hard wood matrix takes place by means of diffusion and natural convection. Considering that dry wood has predominantly closed porosity, it is understandable that its interaction with atmospheric oxygen occurs as a typical heterogeneous surface process.

In order to initiate not only flaming but also smoldering of timber, an initial heat energy is required.

Occurrence of smoldering or flaming is a critical condition for transition from a slow reaction of timber decomposition to a self-accelerating exothermic reaction, which is able to maintain itself and spread in space due to back draft. This critical condition results from the fundamental law that combustion is only subject to excess heat release rate relative to heat loss rate in the chemical reaction area, which is clearly represented by the diagram of N. N. Semenov (Fig. 4.1 (Frank-Kamentsky 1967)).

The condition for spontaneous heating and ignition of the system is characterized by contact of the heat release curve, q_1, and the straight line of heat loss from the chemical reaction area, q_3. The intersection of the curve q_1 with the straight line q_2 determines the condition for stationary reaction mode, which in case of this ratio between the rates of heat generation and consumption corresponds to moderate heating of the system controlled by the reaction kinetics.

In case of smoldering combustion, heat release is achieved by a heterogeneous oxidation reaction on direct contact of oxygen with the timber surface and a carbonized product formed as a result of timber decomposition. In case of flaming combustion, it is achieved by exothermic gas-phase reactions of oxidation of combustible volatile products of timber decomposition in the flame reaction zone.

A heat sink from zones of smoldering and heat reaction is achieved by different processes, which to a considerable degree depend on combustion conditions, the state of the material, and the environment.

Different criteria for timber ignition may serve as an equivalent of the aforesaid fundamental law of combustion mode initiation. According to D.A. Frank-Kamenetsky (1967), ignition of combustible solid substances and materials is inevitably associated with the transition of the chemical reaction from kinetic to diffuse behavior.

4.1 Smoldering Ignition of Timber

Heterogeneous chemical reactions of interaction of timber and atmospheric oxygen and underlying smoldering combustion of timber are still poorly understood, despite the global importance of the problem of smoldering timber combustion because of the fire hazard it poses. Although the chemistry of this process is very complex, the rate of any heterogeneous reaction must be a function of the local concentration of gaseous reagent (oxygen in this case), the specific area of a solid body surface available for reaction, as well as local temperature.

Multiple studies of the conditions of smoldering combustion, as well as studies aimed at identifying the factors influencing the rate at which the smoldering area spreads and its transition from smoldering to flaming or petering out, were mainly conducted on materials with high open porosity and gas permeability. These materials included polymeric foams; powdery substances, including coal substances; as well as sawdust and timber chippings, cellulose fabrics, and heat-insulating materials (Moussa et al. 1976; Rogers and Ohlemiller 1980; Ohlemiller and Rogers 1980; Ohlemiller 1985; Ohtani et al. 1991). A characteristic feature of these materials is their relatively high ratio of total surface area to volume. There is a very limited number of works studying smoldering of timber as such.

It was not until fairly recently that cases of fires were analyzed, which were recorded as early as the beginning of the twentieth century and which resulted from ignition of wooden structures with hot water or steam heating pipes with a temperature just above 100 °C passing through them (Babrauskas 2001). The lowest recorded temperature at which a fire was caused by prolonged (over a period of several years) contact between wood and heated pipes was 77 °C. The author (Babrauskas 2001) concluded that the observed temperature threshold corresponded to a temperature sufficient to start wood charring in the presence of limited access of oxygen and a subsequent self-accelerating exothermic reaction of carbonized product oxidation and later ignition of combustible gases.

There were recorded facts of a reduced temperature threshold and length of time before the start of thermal heating of wood on low-temperature thermal exposure (<120 °C) depending on the sample size.

This agrees with the results obtained during studies of the conditions for occurrence of smoldering combustion of a high-porosity cellulosic heat-insulating mass ($\rho = 36$ kg/m^3) when it is in contact with a heated plate over a period of 2–7 h (Ohlemiller and Rogers 1980). The experiment was conducted according to the "yes/no" principle as to the occurrence of signs of smoldering. It is clear that the heated plate temperature may not necessarily correspond or be close to the actual temperature at which the cellulosic mass starts smoldering. The minimum plate temperature corresponding to the occurrence of smoldering dropped from 320 to 220 °C when the insulation layer thickness was increased from 3 to 30 cm. This effect is obviously caused by a change in the thermal balance and a reduced rate of heat loss from the reaction zone in the vicinity of the heated plate when the layer thickness is increased (Ohlemiller and Rogers 1980).

The natural question is which reaction is actually associated with initiation of smoldering – oxidation decomposition of cellulose (timber) or carbonized product oxidation? As a rule, the resulting char has higher, more open porosity, and consequently a greater surface area for reaction with oxygen, compared with the initial material. Visible glowing during smoldering is connected to char oxidation. The red color of incandescent smoldering char corresponds to a temperature of approximately 600 °C. This temperature is rather significant and may not be related to the temperature of occurrence of smoldering combustion of wood.

The minimum heating plate temperature required for the occurrence of cellulose smoldering as a function of the heat insulation layer thickness was calculated based on the heat theory of ignition (Frank-Kamentsky 1967; Bowes and Townshend 1962). The kinetic parameters of two stages of cellulosic mass decomposition in air were obtained by thermal analysis (DSC) (Ohlemiller and Rogers 1980).

Figure 4.2 shows experimental data compared with calculation results.

It is clear that experimental values of the initiation temperature of cellulose smoldering are in better agreement with calculations based on thermo-oxidative decomposition of cellulose than oxidation of forming char. It is usually thought that before the ignition point, a substance is heated as an inert body (decomposition degree $\alpha = 0$). If the time required for thermal relaxation of heating and possible cellulose decomposition degree by the ignition point are considered, allowing for combustion agent consumption results in an increased temperature of smoldering initiation (curves 3 and 4). Comparison with experimental data (curve 1) leads to the conclusion that the effect of cellulose consumption in the reaction with oxygen in the period before smoldering occurs should become more apparent for a small heat insulation layer thickness.

Information on the occurrence of wood smoldering subject to the impact of various external sources (contact with a heated surface, flame, hot air) is very limited and contradictory. In this respect, most attention is paid to a study of the action of external thermal radiation flow and oxygen concentration.

Unlike the example of a cellulosic mass with large surface area considered above, the natural timber surface available for thermo-oxidative reaction of decomposition and entry of oxygen to implement it are limited by the outer surface of the material. Before smoldering combustion of wood begins, blackening of the surface layer,

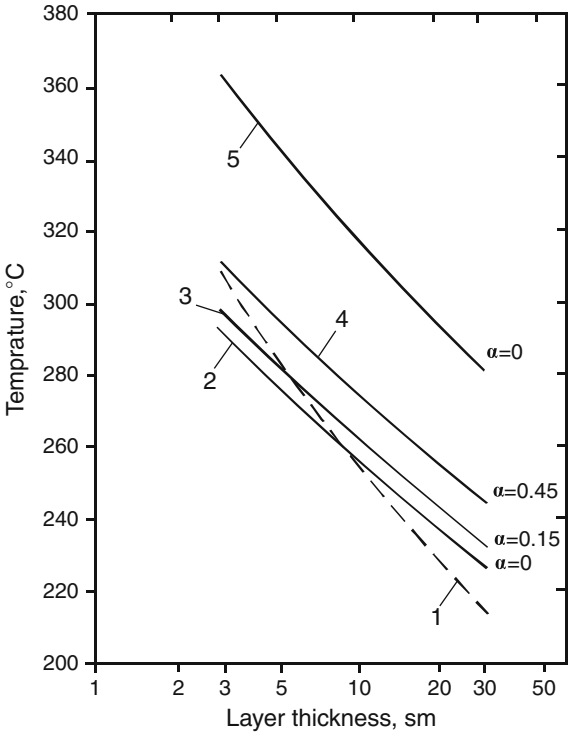

Fig. 4.2 Experimental *1* and calculated values of the temperature at the beginning of cellulose smoldering as a function of the layer thickness: *curves 2*, *3*, and *4* – calculation for kinetic parameters of cellulose decomposition stage (for different decomposition degree, α); *5* – calculation for parameters of the char oxidation stage

i.e., carbonization, and then occurrence of a light fluorescence are recorded. The brightness of fluorescence depends on the air flow rate.

It was observed that spontaneous smoldering of pine timber in a stationary air environment occurs only at low intensity of the thermal radiation flow (below 40 kW/m^2 (Bilbao et al. 2001)). If a local (pilot) ignition source was available, smoldering did not occur at all, even under long-term action of low thermal flows, and ignition and flaming combustion occurred immediately (Bilbao et al. 2001).

In many cases, local (most commonly, on the periphery) occurrence of fluorescence with a flame emerging above it later was observed on a sample surface without a local igniting impulse with one-sided radiative heating of wood. The flame gradually spread over the sample surface, and steady flaming combustion of the whole sample was observed only after that. In contrast with this situation, when a pilot source was present, emerging flame spread over the whole wood sample surface at once. Thus, a small area of smoldering on the surface may be considered as an additional energy impulse and a kind of pilot source for combustion of timber (Spearpoint and Quintiere 2001).

Most researchers believe that heterogeneous oxidation of char on a surface is the main reaction causing it to smolder. The critical temperature on the surface is accepted as one of the criteria for the occurrence of smoldering combustion of timber.

In work (Bilbao et al. 2001), common K-type thermocouples were used to measure temperature on the reacting timber surface. During visual registration of char fluorescence, the temperature of pine smoldering in an air flow of 1 m/s changed as a function of external heat flow (with $q_e < 40$ kW/m^2) according to the equation:

$$T_{\text{smoldering}} = 573 + kq_e,$$

where temperature is given in K and q_e in kW/m^2 and $k = 6$ m^{2}K/kW.

The time before the beginning of smoldering and then flaming combustion of timber was observed visually. Thus, for example, in a stationary air environment for $q_e = 23.8$ kW/m^2, delay time of timber smoldering was 110 s, while the transition to flaming combustion took 737 s. For $q_e = 31.2$ kW/m^2, char fluorescence was observed in 13 s, while spontaneous ignition of timber was observed in only 30 s. For $q_e > 40$ kW/m^2, the critical temperature of pine surface for spontaneous ignition and flaming combustion was equal to 798 K (Bilbao et al. 2001).

It is interesting to note that as the air flow rate over the sample increased from 1 to 5 m/s, the delay before both timber smoldering and combustion also increased. The authors (Bilbao et al. 2001) attributed this mainly to convective cooling of the timber surface.

A simple mathematical model was proposed in the above-mentioned research to describe the main processes leading to smoldering and later ignition of timber subject under radiative thermal action. It was assumed that flaming combustion was enabled by combustible products of timber pyrolysis, while smoldering was enabled by heterogeneous processes of wood and char oxidation. Accordingly, the kinetics of timber pyrolysis at different degrees of decomposition (in different temperature ranges) was taken into consideration, and in the same way, kinetics of timber and char oxidation, as well as thermal effects of the reactions. The authors tried to take into account the effect of moisture content on the processes of occurrence of smoldering and flaming combustion of timber.

A nonstationary system was represented by a partial differential equation:

$$\partial\left(\rho_s C_{ps} T_s\right)/\partial t + \partial\left(\rho_s H\right)/\partial t\ \left(-\Delta H_V\right) = k_s \partial^2 T/\partial x^2 + \left(-\Delta H_r\right)\left(-r_A\right),$$

where $(-\Delta H_V)$ is moisture evaporation heat, H is moisture content, $(-\Delta H_r)$ is the reaction heat of pyrolysis or oxidation decomposition of wood or char burning, and r_A is the weight loss rate during decomposition of timber. For different degrees of conversion X : $(-r_A) = \rho_0 \mathrm{d}X/\mathrm{d}t$.

For dry wood, the second term on the left-hand side of the equation is ignored. Wood is not destroyed before moisture evaporation is completed, and for this reason, the second term on the right-hand side of the equation is ignored. Thermal balance on wood surface is represented in the model as one of the boundary conditions:

$$q_e - q_r - k_s \partial T/\partial t - h_c\left(T_s - T_0\right) = 0,$$

where q_r is heat losses by radiation from the wood surface, the third term of the equation represents heat transferred by thermal conduction into the inner layers of the material, and the fourth term represents heat losses by convection. Influence of air flow rate was taken into account through the convection heat transfer factor h_c.

The authors (Bilbao et al. 2001) focused on calculating the time before beginning of smoldering and autoignition of pine timber. They showed that the maximum smoldering temperature may be regarded as the critical surface temperature for spontaneous ignition. The surface temperature required for the occurrence of smoldering mainly depends on the density of the external radiative heat flow.

Detailed research on glowing autoignition and transition of this process into flaming combustion subject to the action of a radiant heat flux (10–70 kW/m^2) was conducted on redwood samples $4 \times 4 \times 4$ cm in size (Boonmee and Quintiere 2002, 2005). The heat flow from a vertically positioned radiation panel of a cone calorimeter was delivered to the timber surface along or across the grain axis. The air flow rate was changed from 0 to 5 m/s. The temperature on the timber surface was continuously recorded by a noncontact method using an infrared pyrometer. Since a wave range ten times longer was used in this case compared with the color range, the measured temperature was not affected by alteration of the color on the sample surface. A video camera was used to record the beginning of timber smoldering and its transition to flaming combustion. Simultaneous monitoring of changing mass loss rate was also conducted. This approach allowed the evaluation of different indicators of the critical conditions for smoldering combustion of timber.

It was determined that redwood smoldering is not observed for a heat flow below 10 kW/m^2. The autoignition limit corresponds to a critical heat flow of 20 kW/m^2. As the density of the external heat flow increases, the induction period before the occurrence of smoldering decreases, as well as the time before subsequent autoignition of wood. In these circumstances, the influence of the delivered heat flow direction relative to grain orientation in the sample is very clearly manifested. The time for occurrence of wood smoldering was always greater if the heat was delivered perpendicular to the grain axis. This is explained not only by different conditions of timber heating due to the fact that the thermal conductivity of the wood is greater along the grain than crosswise. As a result, less heat is accumulated on the wood surface, and the surface temperature is lower if smoldering occurs. A greater ability for diffusion of gases and decomposition products along the grain should be taken into account. When timber is heated perpendicular to the grain axis, the cell walls of the grains must first undergo degradation to allow free penetration of gases deep into the matrix and exit of volatile decomposition products. It is interesting that the critical mass flow at the limit of occurrence of smoldering combustion (10 kW/m^2), which was associated with wood surface regression, also depended on grain orientation; however, it amounted to approximately 3–4 g/m^{2}s on average.

In experiments, the time of occurrence of smoldering or flaming combustion of wood is usually recorded by the appearance of fluorescence in the solid phase or flame above the wood surface. Other indicators of the system are compared with this

moment. Accurate quantitative criteria for the critical conditions of these processes are important for theoretical analysis of the occurrence and development of wood combustion.

To describe the mechanism of occurrence of smoldering combustion of wood, the authors (Boonmee and Quintiere 2005) examined a wood decomposition model including char surface oxidation.

The kinetics of thermal decomposition of wood was assessed taking into consideration three parallel reactions of main wood components, but it was understood a priori that each component had an equal share in forming char residue. In particular, the mass fraction of char formed during wood decomposition was considered to be equal to 0.2. The authors (Boonmee and Quintiere 2005) accepted that char oxidation takes place only on a solid surface and does not affect its inner layers. The char oxidation rate depends on oxygen concentration and surface temperature. At the same time, char on the wood surface was regarded as pure carbon oxidizing stoichiometrically to CO_2 completely. The ordinary bimolecular char oxidation reaction rate according to the Arrhenius law is presented in the model as a first order reaction only for consumed oxygen, because the heterogeneous carbon reaction was assumed to be independent of its mass fraction on the surface (reaction order for carbon $n_c = 0$):

$$m''_c = Y_{0,s}\ A_c\ \exp\left(\frac{-E_c}{RT_s}\right).$$

The following values of pre-exponential factors and heterogeneous reaction activation energy were used in the calculations: $A_c = 465$ kg/m^{2}s and $E_c = 68$ kJ/mol.

The criterion for occurrence of smoldering combustion was determined from the positions of thermal explosion theory (Frank-Kamentsky 1967) by analysis of the thermal balance on an oxidizing wood surface. It is introduced in the mathematical model of occurrence of smoldering combustion and spontaneous autoignition of wood as a boundary condition for energy conservation at the phase contact area of char and the environment:

$$q''_e + m''_c \Delta H_c = -k_s \partial T/\partial x + h\,(T_s - T_0) + \varepsilon\sigma\left({T_s}^4 - {T_0}^4\right),$$

where ΔH_c is char combustion heat (taken equal to 32.76 kJ/kg).

The right-hand side of the equation represents heat losses through transfer by thermal conduction into the sample, as well as by convection and radiation from the reacting surface, respectively.

If energy arrives by heat from outside and the energy of the chemical reaction of char oxidation on the surface $G(T_s) = q''_e + q''$ is balanced by heat losses $L(T_s, t)$, the point of contact of heat input and heat removal curves will correspond to an unstable beginning of smoldering combustion of wood.

In mathematical terms, this critical condition corresponds to the equation:

$$\frac{\mathrm{d}G\,(T_s)}{\mathrm{d}T_s} = \frac{\mathrm{d}L\,(T_s, t)}{\mathrm{d}T_s}.$$

A slight change in the thermal regime leads to a spasmodic transition to a stationary process of smoldering combustion of wood. In this case, the char surface temperature reaches approximately 600 °C.

The idea of consecutive joining of kinetic and diffuse resistance in the general chain of a heterogeneous reaction is used in the model describing the chemical and physical processes leading to the occurrence of smoldering combustion of wood. The authors (Boonmee and Quintiere 2005) singled out two regimes of heterogeneous oxidation of wood controlled either by the kinetics of carbonized surface oxidation or by diffusion of the oxidizing agent in the reaction area. Surface char oxidation is kinetically controlled at the early stage of the wood heating process, while the diffusion-controlled regime takes place at a later stage. In a normal atmospheric air environment under the action of a heat flow of 40 kW/m^2, the transition from one regime to another occurs at approximately 400 °C.

A dimensionless indicator of critical temperature rise on the char surface is used as a criterion for the occurrence of smoldering combustion of wood, which is represented by the ratio:

$$\frac{q''_{\text{ok}}}{q''_{\text{e}}} = \frac{m_{\text{c}} \Delta H_{\text{c}}}{q_{\text{e}}}$$

At the early stage of char oxidation, the oxygen concentration on its surface is relatively low. The occurrence of smoldering combustion of wood greatly depends on the temperature determined by heat flow density. Even if the environmental oxygen concentration is changed, the ratio between $q''_{\text{ok}}/q''_{\text{e}}$ remains nearly constant within the limits of 0.25–0.35. The starting point of smoldering combustion corresponds to the contact of the heat input and heat removal curves on the reacting char surface. Calculation of the energy balance on a redwood surface, for example, for heat flow $q_{\text{e}} = 15$ kW/m^2 and environmental oxygen mass fraction $Y_{0,\text{env}} = 0.40$ leads to the following critical indicators of the occurrence of smoldering combustion: char layer surface temperature $T_{\text{s}} = 305$ °C; delay before the occurrence of smoldering combustion is $t_{\text{smoul}} = 224$ s. Increased environmental oxygen concentration leads to a significant decline of temperature on the surface for the chemical reaction of char oxidation.

In the diffusion-controlled regime, the temperature on the oxidizing surface increases rapidly as heat flow density increases, and the chemical reaction of oxidation accelerates. In this regime, the dimensionless indicator $q''_{\text{ok}}/q''_{\text{e}}$ is reduced either by decreased environmental oxygen concentration or by increased q''_{e}. In this regime, the condition for the occurrence of smoldering combustion will correspond to the intersection of the heat loss curve $L(T_{\text{s}}, t)$ with the heat input curve $G(T_{\text{s}})$ at its inflection point. In mathematical terms, the condition corresponds to the maximum value of the first derivative of heat input by temperature or accordingly a zero value of its second derivative: $\text{d}^2 G(T_{\text{s}})/\text{d}T_{\text{s}}^2 = 0$. The calculation shows that if the radiation heat flow is 50 kW/m^2, the critical values of char surface temperatures and delay before smoldering combustion are 357 °C and 22 s, respectively. If $q''_{\text{e}} \gg 50$ kW/m^2, smoldering combustion of wood begins at a nearly constant

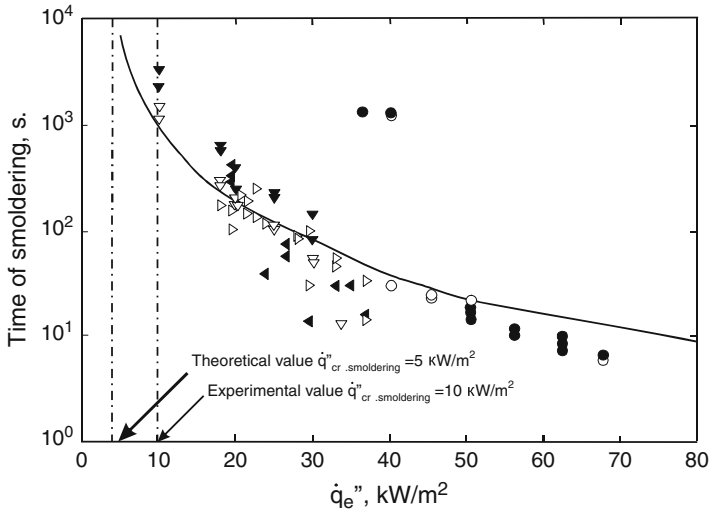

Fig. 4.3 Influence of an external heat flow at the time of occurrence of smoldering combustion of wood: ——— calculation; experimental values $t_{smoldering}$ when wood is heated across ▼,◀ and along the grains ▽, ▷ time of spontaneous ignition of wood when heated across • and along ○ the grain

temperature of approximately 400 °C and does not depend on the environmental oxygen concentration. Autoignition of wood occurs immediately after initiation of smoldering.

Theoretically, the predicted weight loss rate on the occurrence of smoldering combustion of wood (1 g/m^{2}s) gradually increases for a low heat flow (up to 30 kW/m^2), reaching a constant value of 4 g/m^{2}s if the heat flow density is increased from 30 to 70 kW/m^2. Thus, at the limit of occurrence of smoldering combustion, the calculated weight loss rate (1 g/m^{2}s) is lower than the experimentally observed one. It should also be mentioned that the model of smoldering combustion of wood used predicts a lower value of the minimum heat flow (5 kW/m^{2}s) for the occurrence of smoldering combustion over 2 h of heating (Fig. 4.3).

The difference from the experimentally found $q_{cr.\ smoldering} = 10$ kW/m^2 may be caused by uncertainty in the selection of kinetic parameters of the heterogeneous char oxidation reaction, which may affect not only its surface layer but also progress in volumetric dimensions.

4.2 Spontaneous Flaming Ignition of Timber Species

The concept of autoignition usually implies the occurrence of flaming combustion of timber when it is heated in the absence of an additional local impulse of ignition of gaseous decomposition products by an electrical spark, small flame of a gas burner, burning hot spiral, and other so-called pilot heating sources.

Autoignition is a typical process taking place in the gas phase. It may occur when a concentration of combustible volatile products of timber decomposition that appeared in the gas phase in the vicinity of a timber surface exceeds the lower concentration limit for ignition of combustible gases. In this case, the temperature of the formed combustible gases must be sufficiently high to accelerate the oxidation reaction and induce combustion.

As follows from the above-mentioned data, timber materials carbonizing during decomposition have two types of autoignition (Babrauskas 2001; Boonmee and Quintiere 2002; Boonmee 2005).

Type I autoignition is specific to the impact of heat flows with density above 40 kW/m^2. In this case, spontaneous occurrence of flaming combustion occurs almost immediately after the appearance of a sign of local smoldering.

Type II autoignition is observed for an external heat flow below 40 kW/m^2. It is characterized by a greater time interval between the occurrence of smoldering and flaming combustion. This interval increases as the value q''_e decreases. Spontaneous autoignition did not occur when redwood was exposed within a 2-h period if the heat flow was below 20 kW/m^2. The indicated value q''_e is considered as the critical heat flow of autoignition of wood samples in a vertical configuration. Char forming on the surface of sample due to its high temperature and high exothermicity of the oxidation reaction serves as a self-induced pilot source of energy.

The critical heat flow, $q_{e.cr}$, below which flaming combustion cannot occur is one of the important parameters of autoignition of materials.

Early works on autoignition of different timber species provide data showing a large spread of $q''_{e.cr}$ values (from 4.3 to 117 kW/m^2). To a considerable extent, this spread is explained by different exposure times to external heat flows of different intensity (Babrauskas 2002).

Values $q''_{e.cr}$ exceeding 40 kW/m^2 are usually observed for short times of timber exposure (14–90 s) to a high-density flow. For example, exposure of horizontal red oak samples to a radiation flow from CO_2 of a laser heating source for less than 60 s induced autoignition of timber at $q''_{e.cr}$ of approximately 90 kW/m^2 (Kashiwagi 1979).

The lower limit of 4.3 kW/m^2 was obtained by heating vertical wood samples for up to 5.2 h. For heating duration of 9–20 min, the minimum external heat flow for autoignition of wood was within 20–29 kW/m^2 (Babrauskas 2002).

Based on early published results, it is difficult to draw a conclusion on the impact of timber species, sample orientation and size, or other conditions of testing the characteristics of autoignition of timber. There are some examples where the period before autoignition of vertically oriented timber samples was much longer than for horizontally positioned samples with the same density of incident heat flow, and vice versa. According to (Simms and Law 1967), increasing the size of the test samples leads to a marginal reduction of the minimum density of radiation heat flow for autoignition of wood. However, this parameter had almost no dependence on dry timber density. At the same time, the authors (Simms and Law 1967) note the significance of the thermal properties of wood.

When assessing smoke generation during heating of samples of different timber species, we determined that coniferous species generally have higher values of critical heat flow for autoignition (25–26 kW/m^2), compared with deciduous species (20–22 kW/m^2). Autoignition of the volatile timber decomposition products formed causes reduced smoke generation under radiative heating of the samples. The results of work (Asseeva et al. 2004) led to the conclusion that the chemical composition of wood, and, in particular, increased content of extracted substances, has an evident effect on this autoignition indicator. For this reason, samples of chestnut and elm timber were similar to the coniferous species in critical density of autoignition heat flow. It should be mentioned that the standard smoke generation assessment method we used provides for orientating the samples at an angle of 45° relative to the radiative heating panel and 15 min of testing in the heating mode without a pilot energy source.

During an experimental study of autoignition of six timber species, it is also observed the evident impact of the species and chemical composition of timber on key indices of this process (Poespowati 2008). Samples $5 \times 5 \times 2.5$ cm in size were tested in the horizontal orientation under exposure to radiation heat flow of 22 kW/m^2 density. The focus was on determining moisture content in the samples and indices such as time before autoignition, surface temperature before autoignition, charring rate when heated, as well as duration of flaming combustion and surface temperature during extinguishing. As a rule, as the moisture content in the samples increased from 0 to 100 %, the time before autoignition and timber surface temperature at the point of flame appearance increases, while the charring rate becomes slower. It is interesting that dry samples of coniferous species (redwood and pine) had a charring rate several times higher during autoignition, compared with samples of deciduous species (85.7–55.4 mm/h versus 0.3–8.7 mm/h). The observed effects of moisture on the delay before autoignition of timber generally correlate with the research results (Simms and Law 1967).

A study of the wood autoignition process makes it possible to exclude from consideration many parameters taken into account for pilot ignition and influencing the delay before flaming combustion, namely, the type of local ignition source, its size, temperature, and spatial arrangement.

Theoretical analysis of autoignition of timber under external radiative heat action is based on application of the criteria associated with two groups of indices: (1) reflecting the solid phase condition at the point of autoignition and (2) reflecting critical conditions in the gas phase.

Critical conditions of occurrence of flaming combustion of timber reflecting solid phase processes include such indices as critical temperature on the timber surface, critical mass flow of pyrolysis products (critical weight loss rate), and critical (minimum) external heat flow. For materials similar to timber carbonized during pyrolysis, it was suggested to consider additionally critical yield of char residue or char layer thickness on the surface, beyond which autoignition does not occur (Staggs 2001).

The temperature at the beginning of active pyrolysis of timber is taken as the critical temperature on the wood surface. This value is interpreted as a necessary condition for formation of an autoigniting mix of combustible products of timber decomposition. Implementation of the concept of critical temperature on timber surface for the occurrence of flaming combustion of timber under different conditions of thermal action is considered in reasonable detail in (Babrauskas 2002).

Based on published experimental data, the author concludes that, subject to a minimum external radiation heat flow, the timber surface temperature allowing autoignition should be approximately 250 °C.

Some clarification of the terms of critical and minimum heat flow for implementation of autoignition of timber is given in article (Janssens 1991a). In particular, the minimum heat flow for occurrence of flaming combustion of wood, $q_{\min}$, represents the minimum level of intensity of the external heat flow determined under real conditions of material testing. The critical flow, q_{cr}, is a value extrapolated for the test time $t \to \infty$ and is calculated based on respective correlations of experimental data. For this reason, usually $q_{cr} < q_{\min}$.

The critical mass flow of combustible pyrolysis products during autoignition of cellulose fuel may change within the limits of 1–4 g/m^{2}s (Kanury 1977).

Critical conditions for the occurrence of flaming combustion of timber reflecting physical and chemical processes in the gas phase include a number of indices, values of which are accepted conditionally due to the uncertainty of gas-phase reaction kinetics.

In a mathematical radiation model of autoignition of a solid fuel similar to timber in its thermal properties (Kashiwagi 1974), it was assumed that thermal decomposition occurs only on the surface and the pyrolysis rates correspond to a zero order reaction according to the Arrhenius law. In one-dimensional analysis of gas phase, it is assumed that an irreversible chemical reaction of combustible gas oxidation proceeds in one stage as a second-order reaction. When a solid fuel is heated, radiation heat flow is partially absorbed in the depth of a polymer matrix. However, this model did not take into account heat losses by radiation from a solid fuel surface. The influence of six gas-phase criteria on the delay time of autoignition was assessed:

1. Overall rate of gas-phase reaction $\geq 2 \times 10^{-5}$ g/cm^{2}s.
2. Maximum local rate of gas-phase reaction $\geq 10^{-5}$ g/cm^{3}s.
3. Maximum local dimensionless temperature in the gas phase ($\theta = T_{\max}/T_0$) ≥ 2.5.
4. Overall rate of exothermic reaction heat release in the gas phase must be equal to or greater than the radiant energy absorption rate in the solid phase $\geq q_e(1 - r)$.
   Here r is the radiant energy surface reflection factor.
5. Acceleration of the overall rate of gas-phase reaction $\geq 10^{-3}$ g/cm^{2}s^2.
6. Gas-phase temperature gradient at the solid fuel surface becomes equal to zero or takes on a positive value. Reversal of the temperature gradient sign in the gas phase is due to the fact that the reaction in the gas phase becomes significant and gas begins to heat the material surface additionally.

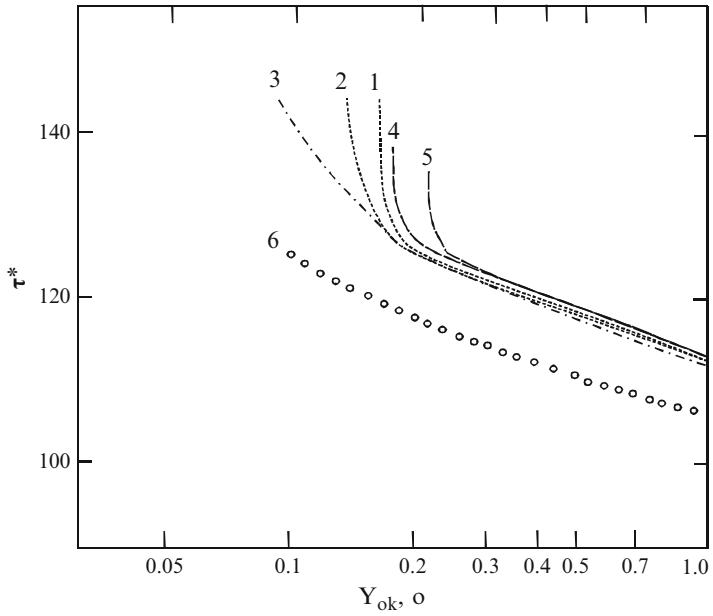

Fig. 4.4 Influence of the initial environmental oxygen mole fraction on the delay before autoignition of solid fuel, if $q''_e = 83.7$ kW/m^2, and various criteria (*1–6*) specified in the text above

According to the author (Kashiwagi 1974), although provisional, the values used for the accepted criteria are quite reasonable.

Numerical analysis of autoignition of solid fuel under the action of an external radiative heat flow conducted in work (Kashiwagi 1974) led to an interesting conclusion. It was determined that for heat flow density below 84 kW/m^2 and oxygen mole fraction above 0.25, nearly all the criteria used have a similar influence on the delay before autoignition, τ^* (dimensionless value) (Fig. 4.4).

Under these conditions, solid matrix heating is the stage at which autoignition is controlled. However, in case of a regime with low initial oxygen content, gas-phase reactions start controlling autoignition.

The critical value of the overall gas-phase reaction rate was used as a main gas-phase criterion for autoignition in the above-mentioned research. It was shown that effective kinetic parameters of solid-phase and gas-phase reactions influence not only the delay before autoignition but also the lower and upper limits of fuel inflammability. For a certain combination of these values, the inflammability limits may be extended or narrowed. Minor influence of exothermic and endothermic pyrolysis reactions on radiative autoignition of solid fuel was observed.

According to (Kashiwagi 1979), the occurrence of flaming combustion under the action of an external radiation heat flow depends on the mechanism and velocity of heating of combustible products of material decomposition in the gas phase. Heating by convection and thermal conduction from a hot material surface is considered as

the main gas-phase mechanism for heating up to the required limit. However, there is a strong possibility that gas-phase heating through direct absorption of the radiant energy plays an important role in the mechanism of autoignition of volatile products of timber decomposition. Implementation of this situation is possible in case of high intensity of the radiative heat flow and high concentration of absorbing agents in the gas phase, i.e., fuel pyrolysis products. Furthermore, there are three radiant energy absorption mechanisms: (1) absorption of energy by gaseous molecules. As a result, combustible gases are heated, and the gas-phase chemical reaction of oxidation is initiated and accelerated. (2) absorption by condensed particles in the gas phase, where the particles then heat the gas phase by thermal conduction and convection and initiate the gas oxidation reaction. (3) absorption of energy by particles and initiation of a heterogeneous oxidation reaction on the surface of these particles. It is not clear which of these gas-phase heating mechanisms may prevail. According to (Kashiwagi 1979), absorbance of radiant energy by volatile products of gas-phase oak pyrolysis may reach 35–70 % by the time of autoignition of red oak wood under a high-density thermal flow from CO_2 of a laser source. This factor is still not taken into consideration when modeling the autoignition process of timber.

Theoretical analysis of autoignition of wood on exposure to an external radiation source of energy is inevitably associated with many assumptions and simplifications in the suggested models. They are related to a description of the actual chemical and physical processes occurring in both the solid and gas phases. This is associated with the absence of information about many specific characteristics of these processes, as well as with the necessity to reduce costs of computer calculations. For example, the latter reason excludes consideration of the actual process of char layer regression induced by cracking during modeling.

However, we note that a certain amount progress is currently observed in the theoretical prediction of different characteristics of autoignition of timber and other cellulose materials with consideration of the growing number of factors reflecting specific features of the phenomenon.

Thus, for example, when autoignition of timber was modeled (Boonmee 2005), a known one-dimensional model of thermal conduction for solid-phase heating was used. However, timber decomposition was analyzed with allowance for pyrolysis of its three main chemical components (cellulose, hemicellulose, and lignin) and surface oxidation of the formed char. A submodel for the gas phase is represented not by a one-dimensional but a two-dimensional boundary layer in the vicinity of a vertical wood surface with nonstationary laminar flow due to natural convection. This extends the predictive capabilities of modeling actual flaming combustion processes. It is assumed that gas oxidation reaction rate in the boundary layer is low until the time of autoignition of volatile combustible products of timber decomposition.

For this reason, partial differential equations describing transport processes in the gas phase according to the laws of mass conservation, momentum conservation, and energy conservation and continuity of chemical components are solved first. These solutions are matched with the timber pyrolysis model through boundary

conditions on the phase contact area of solid matrix and gas, taking into account the components of heat input and heat consumption in the thermal balance on the wood surface:

$$q_e'' + m_c'' \Delta H_c = -k_s \partial T/\partial x|_{c.p.} - k_g \partial T/\partial x|_{g.p.} + \varepsilon\sigma \left(T_s^4 - T_0^4\right).$$

Temperature gradients both on the condensed phase (c.p.) side and gas-phase (g.p.) side are shown here.

Kinetics of gas-phase oxidation are considered in the form of a global one-stage second-order reaction according to the Arrhenius law:

$$\omega_g = A_g \, {\rho_g}^2 Y_F Y_{ok} \, \exp\left(\frac{-E_g}{R T_g}\right),$$

where ρ_g is gas density, Y_F and Y_{ok} are mass fractions of fuel and oxygen in the gas phase, and T_g is gas-phase temperature. The following kinetic parameters were used in calculating the gas-phase reaction rate: pre-exponential factor $A_g = 8.00 \times 10^5$ m^3/kg · s and effective activation energy $E_g = 67$ kJ/mol.

A critical value of the maximum gas-phase reaction rate equal to 0.2 kg/m^3 · s was taken as the autoignition criterion.

The numerical calculation procedure included determination, based on the timber pyrolysis model, of the mass flow of volatile decomposition products and temperature on the solid-phase surface for a specified heat flow intensity. The data obtained served as boundary conditions during analysis of the gas-phase submodel. Taking a reverse heat flow from the gas phase to the solid matrix surface in connection with the gas-phase oxidation reaction into account resulted in new temperature distribution on the surface and new values for the mass flow of combustible gases. This calculation was repeated until the critical condition for autoignition of timber according to the accepted criterion was achieved.

The delay before autoignition of timber depends on the kinetic parameters of the gas-phase oxidation reaction. An increase in the effective activation energy or reduction of the pre-exponential factor leads to an increase in the time before autoignition.

Numerical calculations performed in work (Boonmee 2005) with due allowance for the solid-phase and gas-phase models of autoignition of wood confirmed the general tendencies related to a change in characteristics of this process observed during experiments. Correlation between the delays before smoldering and autoignition of wood as a function of the external heat flow clearly demonstrates the existence of two types (I and II) of autoignition regime (Fig. 4.5).

The anisotropic structure of timber affects not only the delay but other characteristics of the autoignition process as well, which is most noticeable at low density of the external radiation heat flow (<40 kW/m^2).

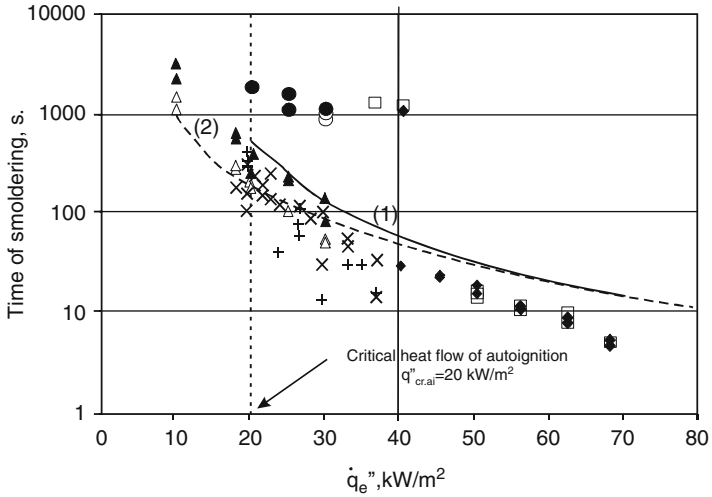

Fig. 4.5 Influence of external heat flow density on the delay before autoignition and smoldering combustion of redwood. *Curve 1* (———) is the autoignition model; *curve 2* (- - -) is the smoldering combustion initiation model. Experimental points: autoignition (⧫, •) – heating along the grains; ∘, □) – across the grains; smoldering (Δ, *x*) – heating along the grains; (▲, +) – across the grains

4.3 Piloted Ignition of Timber from Radiant Heater

Initiation of flaming ignition of timber heated by an external radiative heat flow in the presence of an additional local energy impulse is different from autoignition conditions. After timber decomposition has started, combustible volatile destruction products are released into the environment and mix with the air forming a boundary layer of combustible mix at the timber surface. Autoignition requires not only achievement of the lower concentration limit of inflammability of this mix but also proper warming of it by heat from the surface and an exothermic oxidation reaction of combustible gases. In the presence of an additional pilot energy source, it is actually sufficient to achieve the corresponding combustibility limit of the combustible gases formed. High local temperature in the vicinity of a pilot source in the boundary layer ensures the occurrence of flame. For this reason, the delay before ignition of timber is less than for autoignition under the same external heating conditions. In case of pilot ignition, a lower temperature is implemented on the timber surface, which is especially noticeable with decreasing intensity of the external heat flow (Fig. 4.6) (Kashiwagi 1979).

The dynamics of pilot ignition of timber includes the stage of occurrence of flame from premixed combustible gases and oxidant. This flame spreads from the ignition source over the boundary layer, where almost all fuel from the oxidant and

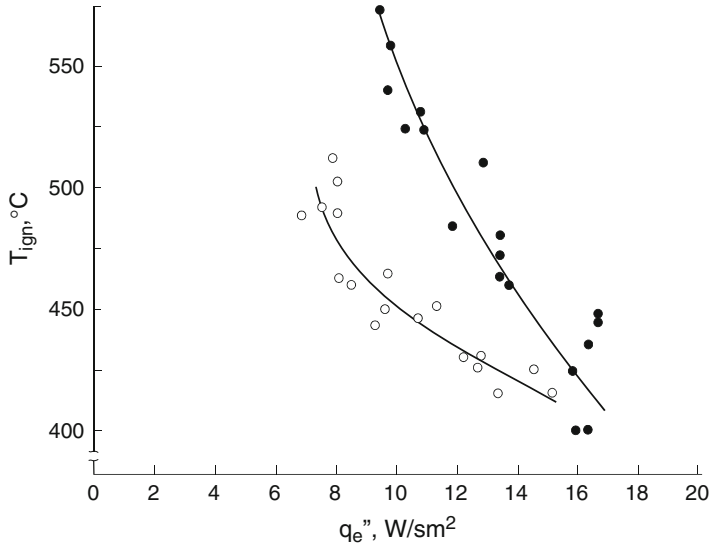

Fig. 4.6 Dependence of temperature on a red oak timber surface on intensity of the external heat flow in case of autoignition (•) and pilot ignition (○)

all oxygen from the fuel are consumed. If there is a shortage of fuel material or cooling, the flame dies out. Thus, before the onset of stable flame, flashes leading to increased temperature on the timber surface may be observed (Fig. 4.7) (Tzeng et al. 1990).

Conditions of transformation of the flame from premixed combustible gases and oxidant into a diffusion flame are the criterion of stable pilot ignition of timber.

It was shown (Simms 1963) that the delay before ignition of timber under radiative heat flow is influenced by the position and size of the pilot flame. It increases with increasing distance of the pilot flame from the wood surface, all other conditions being equal. At the time of ignition, the surface temperature necessary for ensuring the minimum flow rate of the combustible volatile products also increases. Enlarging the pilot flame contributes to faster ignition of the material as well. These facts confirm the concept of the controlling impact of solid phase processes for pilot ignition of timber.

The effects of pilot flame location on the delay before ignition of wood in case of radiative heating were theoretically examined in (Tzeng et al. 1990). It was found that the minimum value of mass rate of combustible gas release should correspond to a certain minimum distance of the ignition source from the material surface. If the distance is shorter, a stable diffusion flame will not be formed due to excessive heat losses from the local energy source to the surface and decreasing flame temperature. Incorrect placement of the local ignition source increases the delay before ignition and temperature on the material surface.

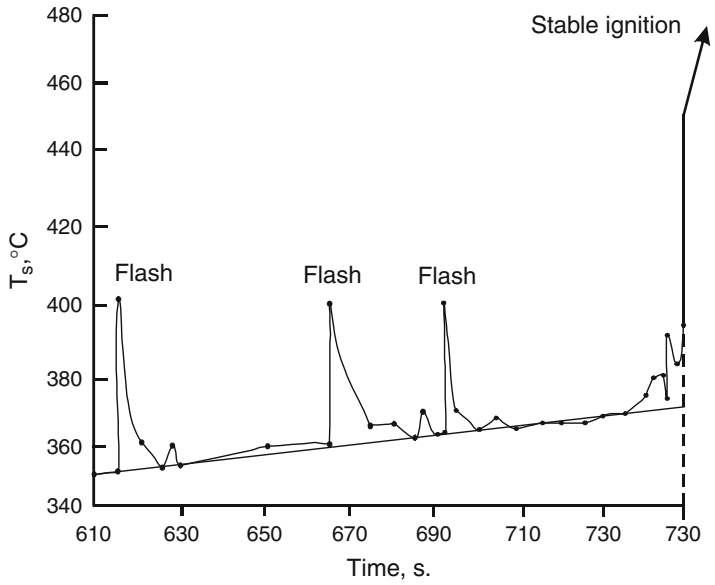

Fig. 4.7 Measurement of temperature on a red oak surface during its pilot ignition on exposure to an external radiative heat flow 18.8 kW/m^2

Many experimental studies of radiative pilot ignition of different timber species as a function of external heat flow intensity demonstrated that density and thermophysical properties of the material have a greater impact on the delay before ignition, all other conditions being equal. However, timber ignition characteristics may be affected by test conditions (orientation of samples and their size, thickness, humidity, type of external radiative heating source, air flow rate, etc.) (Staggs 2001).

Simple thermal models were successfully used in combination with a basic ignition criterion, i.e., achieving the critical surface temperature, to correlate data on pilot ignition of timber.

Functional relationships between the time needed to achieve the timber ignition temperature (delay before ignition) and density of the external radiative heat flow, thermophysical properties, and material thickness were obtained.

Three categories of material according to thickness were considered on identifying the correlations being examined (Mikkola and Wichman 1989).

Samples of materials with a much greater thickness compared with the characteristic size of thermal heating (these timber samples are usually more than 15–20 mm thick) are regarded as thermally thick. The following functional relationship was obtained for them from the solution of a one-dimensional heat conduction equation (on the assumption of constant thermophysical properties):

$$t_{\text{ign}} = \pi\ k\rho c\ \left(T_{\text{ign}} - T_0\right)^2 / 4\ q^2,$$

where k is heat conduction; ρ is density; c is specific heat of the material; T_{ign} and T_0 are surface temperatures at the ignition point and the environment, respectively; and q is radiation thermal heat density.

The abovementioned formula represents an exact analytical solution of the time for achieving ignition temperature on a solid surface during transfer of heat energy in the k-phase by heat conduction and taking into account heat loss from the surface into the environment by convection and radiation in linearized form (i.e., the overall heat transfer coefficient is expressed as the sum of its components). Thus, the q value should be interpreted here as the external heat flow absorbed by the material surface.

Samples of materials with a much lesser thickness compared with the characteristic layer of thermal conduction heating (these wood samples are usually 1–20 mm thick or less) are regarded as thermally thin. The following formula was obtained for them:

$$t_{ign} = \rho c \; L_0 \; \left(T_{ign} - T_0\right)/q,$$

where L_0 is sample thickness.

As it appears from this formula, in contrast to thermally thick samples, the delay before ignition of thermally thin samples depends on their thickness and is inversely proportional to the heat flow density and not to its second-degree value.

These functional relationships between the delay before ignition of materials and heat flow thickness are confirmed during analysis of an integrated thermal model of pilot ignition. In the integrated model (Mikkola and Wichman 1989), the energy balance on the material surface between delivered, q_e, and lost, q_L, heat flows with nonlinear heat losses is considered. In a heating wave, a quadratic temperature profile is taken a priori for thermally thick materials and samples with an intermediate size. In the latter case, the following functional relationship between the time of delay before ignition and heat flow on the surface was determined:

$$t_{ign} \approx \rho c \sqrt{k L_0} \left(\frac{T_{ign} - T_0}{q_e - q_L} \right)^{3/2}$$

Verification of experimental data on pilot ignition of timber of different species, which were obtained earlier using cone calorimeters and other standard apparatus for characterizing the fire safety of materials, confirmed the validity of the theoretically predicted correlations (Mikkola and Wichman 1989).

These correlations have major practical importance. They allow an assessment of the fundamental properties of timber and other materials, where ignitability is determined by the properties required for modeling the occurrence and spread of fires in buildings under different conditions.

Operating with the experimentally determined relationship $t_{ign} = f(q_e)$ or $t_{ign} = f(q_e – q_L)$, it is possible to identify, first, the critical heat flow for ignition, q_{cr}; second, the critical surface temperature at the ignition point, T_{ign}; and third, the

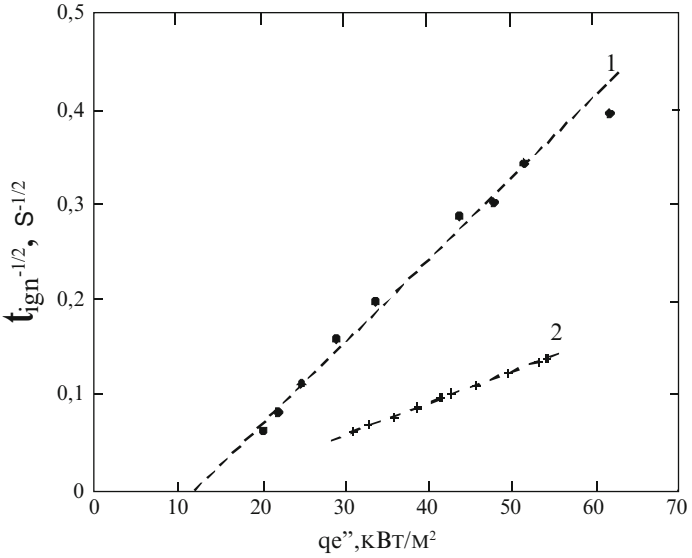

Fig. 4.8 Relationship between time before ignition of timber samples of pine *1* and some deciduous species *2* and density of external radiative heat flow

value of thermal inertia of the material, $k\rho c$. This parameter serves as a measure of temperature increase rate on the surface of a material exposed to an external heat flow.

In order to identify the above-mentioned characteristics, the relationship between the delay before ignition and radiation heat flow density is usually determined using fairly thick samples of materials and large heat flows (20–80 kW/m^2). According to some researchers (Delichatsios et al. 1991), external heat flow during tests should be at least three times higher than the q_{cr} value. In this case, experimental data may be presented in coordinates $\left(t_{ign}^{-1/2} - q_e\right)$, as, for example, in Fig. 4.8 (Mikkola and Wichman 1989).

The value of critical heat flow for ignition of the material is determined by extrapolation to the period $t \to \infty$ using the intersection of the obtained straight line with the abscissa, while thermal inertia of the material, $k\rho c$, is determined using the slope of this straight line.

With a known critical heat flow for ignition, it is possible to evaluate critical temperature on the wood surface at ignition, based on the thermal balance:

$$\alpha q_{cr} \approx \varepsilon q_{cr} = h_c \left(T_{ign} - T_0\right) + \varepsilon\sigma \left({T_{ign}}^4 - {T_0}^4\right) = h_{ign} \left(T_{ign} - T_0\right),$$

where α and ε are the material surface absorption and emissivity factors and h_c and h_{ign} are convective and overall heat transfer factors during ignition, respectively.

Known standard methods, including evaluation of the ignitability of materials, are based on the use of various apparatus, air intake conditions, orientation of samples relative to the heat source, etc. All of these affect the delay before ignition due to differences in convective cooling of the material surface and heat losses by radiation from the surface.

For example, when vertical samples of timber materials were tested according to the standard ASTM E 1321 method (LIFT apparatus), the convective heat transfer factor was estimated as equal to $h_c = 15$ W/m$^2 \cdot$K for $\alpha = \varepsilon = 1$. In the cone calorimeter with smaller vertical samples, it was taken as $h_c = 13.5$ and 10 W/m$^2 \cdot$K for a horizontal sample configuration. According to (Dietenberger 1996), the convective heat transfer factor in a cone calorimeter (ASTM E1354) with horizontal sample placement changed depending on q_e (in kW/m^2) by the following equation:

$$h_c = 0.01433 + 1.33 \times 10^{-4} q_e'', \quad \text{kW/m}^2 \cdot \text{K}.$$

Using the simple thermal model of pilot ignition applied to thermally thick timber samples, Janssens (1991b) proposed the following formula for correlation of experimental results:

$$q_e'' = q_{cr}'' \left[1 + 0.73 \left(\frac{k\rho c}{h_{ign}{}^2 t_{ign}} \right)^{0.547} \right],$$

where h_{ign} is the overall factor of heat transfer from the surface during ignition.

Experimental data plotted in coordinates $t_{ign}^{-0.547} - q_e''$ provides an estimate of values q_{cr}'' and $k\rho c$. In particular, values q_{cr}'' for samples of coniferous wood (pine, fir, thuja, and redwood) were in the range of 12.9–14.0 kW/m^2, while for deciduous species (two types of eucalyptus) they ranged from 9.7 to 10.4 kW/m^2. A cone calorimeter with vertically configured samples was used for determining timber ignitability characteristics. According to the author (Janssens 1991b), effective thermal inertia values obtained by this method correspond to a temperature which is approximately average between the environmental temperature and the timber surface temperature during ignition.

Values of q_{cr}'', which we identified for tropical species of pine and fir wood using the standard method according to GOST 30402-96 and the aforesaid procedure, were equal to 10.8 and 9.7 kW/m^2, while for two types of acacia, these values were 6.5 and 7.0 kW/m^2, respectively. However, deciduous wood samples of tropical eucalyptus were characterized by $q_{cr} = 14.3$ kW/m^2. All other conditions being equal, values q_{cr}'' for vertically configured wood samples are usually approximately 10 % higher compared with the same samples in the horizontal position. Therefore, we may conclude that the species and kind of timber have a significant impact on its ignitability characteristics.

Theoretical analysis of the impact of heat losses on the delay before ignition of materials only by radiation from the surface and only by convective cooling led to

the conclusion that this factor affects the numerical value of q''_{cr} determined by the intersection of the experimental data line $\left(t_{ign}^{-1/2} - q_e\right)$ with the abscissa axis when sufficiently high external heat flows are applied (Delichatsios et al. 1991).

For heat losses due only to radiation from the surface, the following equation was used:

$$t_{ign}^{-1/2} = \frac{2}{\sqrt{\pi} k \rho c} \frac{q''_e - q''_{cr.\,min}}{T_p - T_0}.$$

An extrapolated critical heat flow value should differ from the actually calculated minimum flow by a numerical factor of 0.64:

$$q''_{cr} = 0.64\, q''_{cr.\,min}.$$

When all heat losses are caused only by convective cooling of the surface, the numerical factor reaches the values $\pi/4$ and $q''_{cr} = 0.785 q''_{cr.\,min}$.

With decreasing density of external radiative heat flow and approximation to the actually calculated minimum critical value ($q_e < 1.1 q''_{cr.\,min}$), the contribution of heat losses due to radiant energy becomes predominant (Delichatsios et al. 1991). In this case, the point of intersection of the regression line and the abscissa axis in coordinates $t_{ign}^{-1/2} - q''_e$ should correspond to the value $q''_{cr} = q''_{cr.\,min}$ according to the equation:

$$t_{ign}^{-1/2} = \frac{\pi}{\sqrt{\pi} k \rho c} \frac{q''_e - q''_{cr.\,min}}{T_p - T_0}.$$

In this case, the slope of the experimental point regression line $f\left(t_{ign}^{-1/2} - q''_e\right)$ is different from the slope of the line obtained from high values of q''_e.

According to the authors of (Spearpoint and Quintiere 2001), the mechanism of timber ignition at very low heat flows, even in the presence of an additional local ignition source, is different from the mechanism of ignition under high radiation heat flows. Under these conditions, processes of timber charring and oxidation of char formed on its surface play a major role. Detailed research on pilot ignition of timber was conducted using a standard cone calorimeter by the example of two types of coniferous species (Douglas spruce, redwood) and two types of deciduous species (red oak, maple). The authors studied the impact of density and direction of an external heat flow relative to sample grain orientation on the delay and other indices of ignition of different types of timber. Horizontally oriented samples with surface area 96×96 mm^2 and thickness 50 mm were exposed to an external radiation heat flow of 5–75 kW/m^2. Experimental results were compared with theoretical values calculated based on the one-dimensional integral ignition model applied to carbonizing materials (Spearpoint and Quintiere 2001). According to the developed model, the value q''_{cr} corresponding to the point of intersection of the abscissa axis and regression line in coordinates $t_{ign}^{-1/2} - q''_e$ for $q''_e > 20$ kW/m^2 should

Table 4.1 Measured and predicted parameters of pilot radiative ignition of coniferous and deciduous species

Sample	Grain orientation	ρ_{cp}, kg/m^3	W_{av}, %	t_{ign}, h:min:s	$q''_{cr.\,min}$, kW/m^2 measured/theory	q''_{cr}, kW/m^2 extrapolated	T_{ign}, °C (theory)
Redwood	⊥	354	8.6	0:36:10	13/15.5	11.7	375
	∥	328	7.4	0:23:36	9/5.9	4.5	204
Douglas spruce	⊥	502	7.4	1:33:00	12/16.0	12.2	384
	∥	455	8.5	0:39:55	9/8.4	6.4	258
Oak	⊥	753	5.1	–	–/10.8	8.2	304
	∥	678	5.2	–	–/9.2	7.0	275
Maple	⊥	741	4.8	1:10:00	12/13.9	10.6	354
	∥	742	4.8	0:44:40	8/3.8	2.9	150

be different from the value calculated for $q''_e < 20$ kW/m^2 by a numerical factor $\beta = q_{cr.\,inter\,sec\,t}/q''_{cr.\,min} = 0.76$.

As is seen from Table 4.1, the time before ignition of timber with an external heat flow approaching the critical one is rather considerable. Moreover, for grain orientation parallel to the heat flow direction, the delay before ignition is significantly reduced compared with the time for perpendicular orientation. This factor affects not only the value q''_{cr} but also the surface temperature of timber samples at ignition. The observed effects are caused by anisotropy of the thermophysical properties of timber, in particular, thermal inertia values, $k\rho c$, parallel or perpendicular to the timber grain axis.

Table 4.1 gives some experimental and theoretically predicted parameters of timber ignition.

As we have already noted earlier, pilot radiative ignition of timber becomes possible if the concentration of combustible volatile substances in the gas phase in the vicinity of a local energy source reaches the lower limit of their ignitability in an air atmosphere. A critical mass flow of pyrolysis products as a timber ignition criterion actually reflects the physical nature of this phenomenon.

Not coincidentally, attention to the issue of interrelation between gas-phase and solid-phase criteria for ignition of polymer materials has been growing recently.

Numerical analysis of the pilot radiative ignition model for polymer material in an air flow (Zhou et al. 2002) showed that the chemical process rate in the gas phase is limited by the fuel delivery rate, i.e., its transportation to the location of the ignition source. Predicted values of the delay before ignition and critical heat flow increase with increasing air flow rate. For occurrence of stable flame, a critical stoichiometric ratio of combustible product mass to oxidant must be reached in the vicinity of a pilot ignition source. This stoichiometry is associated with the lower concentration limit of fuel ignitability and does not depend either on external heat flow density or oxidant flow density. If the oxidant flow is increasing, then gas-phase dilution takes place. In this case, fuel delivery to the reaction area must be increased to maintain the critical stoichiometry in the vicinity of the pilot source. As a result, the mass flow of decomposition products at the limit of stable ignition

should increase. With a constant (standardized) oxidant flow rate, the mass flow of decomposition products may serve as a precise criterion for pilot ignition of materials if only condensed phase parameters are considered. The results of analysis (Zhou et al. 2002) indicate the important role played in the ignition process by materials, composition, and concentration of combustible components in a mix of volatile products of material decomposition.

Different methods (Monakhov 1979) are used for calculating concentration limits of ignitability for combustible gases and vapors of low-molecular-weight organic substances, as well as their mixtures. If concentration limits of ignitability for individual components (ϕ_i) and their content in the mix (C_i) are known, then Le Chatelier's empirical rule is used, taking cumulative account of the contributions of each mix component:

$$\varphi_{mix} = 100/\sum (C_i/\phi_i)\,,\ \%\ \text{vol.}$$

If there are no data on concentration limits of ignition for individual substances in an air environment, they may be calculated by the approximation method based on the elemental composition of the substance. Another approach is based on application of a critical adiabatic temperature of combustion for lean borderline mixtures of gases and vapors of organic substances and air (Monakhov 1979). For a broad range of aliphatic and aromatic hydrocarbons, as well as for compounds having in their composition atoms of Cl, Br, and B and other nonorganic elements in addition to C, H, O, and N, the critical flame temperature at the limit of combustion of substances in air is equal to 1,600–1,680 K (Drysdale 1990; Lyon and Quintiere 2007).

If a mix with air contains combustible fuel corresponding to its lower concentration limit of ignition, combustion energy density per unit volume of the gas mixture is nearly constant and amounts to 2050 +/− 150 kJ/m^3, regardless of the chemical nature of a combustible organic substance (Drysdale 1990; Lyon and Quintiere 2007).

From the concept of equality between the heat input rate and heat consumption rate during ignition of combustible fuel, it follows that there exists a relationship between critical values of combustion energy density Q''', flame temperature T_f and lower concentration limit ignition ϕ_L. This relationship may be represented as the following ratios (Lyon and Quintiere 2007):

$$Q''' = \rho\,\phi_L\,(M_f/M_{mix})\,\Delta h_c = \rho_f \phi_L \Delta h_c;$$
$$\phi_L = Q'''/\rho_f \Delta h_c \ \text{ and } Q''' = \rho c_p\,(T_f - T_0)\,/\,(1-\chi)\,,$$

where ρ is density of the gas phase; ρ_f is density of combustible vapors, kg/m^3 of the mix; ϕ_L is the concentration limit of ignition; M_f and M_{mix} are values of molecular weight of the combustible substance and mixture: combustible mixture – products of its decomposition – air; Δh_c is combustion heat of the gaseous fuel; and χ is part of the heat lost from the flame at its limit by radiation and convection.

The M_f/M_{mix} value is used for converting fuel concentration in the gas mixture from mole fraction (or % vol) into weight units.

In case of adiabatic combustion of substances, the resultant heat is spent only on heating of the system and raise of flame temperature up to T_{fad}. In a real situation, heat loss from the flame results in lowering of its temperature to the critical value T_f, below which the flame dies out. Taking $Q''' = 1{,}900$ kJ/m^3 and $\chi = 0.25$, the authors of the article (Lyon and Quintiere 2007) calculated that the critical flame temperature for hydrocarbon fuel at the lower concentration limit must be equal to 1,600 K.

Unlike low-molecular-weight substances, it is more difficult to evaluate concentration limits of combustion for high-molecular substances. For this purpose, it is necessary to know the exact chemical composition and content of combustible volatile pyrolysis products formed during pilot ignition of the material and the kinetic parameters of the gas-phase reaction. As this information is not available for analysis of polymer material ignitability, it was suggested to use the rule of constant critical combustion energy density of any substance at its lower concentration limit of ignition and, accordingly, critical value of flame temperature (Lyon and Quintiere 2007).

This allows expression of the lower concentration limit of pilot ignition of polymer materials through a critical mass flow of decomposition products transferred from the condensed phase to an air environment in the following way:

$$m''_{fcr} = \left(\frac{h_{conv}}{c_p}\right)\left(\frac{M_f}{M_{mix}}\right)\phi_L, \quad \text{g/m}^2\text{s},$$

where h_{conv} is the convective coefficient of heat transfer at the surface of the material and c_p is the specific heat of the mix of combustible gases, air, and combustion products.

Given the stated correlations above, the critical mass flow at the lower concentration limits of ignition of polymer materials may be represented by the following equation:

$$m''_{fcr} = \left(\frac{h_{conv}\ Q'''}{\rho c_p \Delta h_c}\right)\left\{1 - \frac{(T_{ign} - T_{env})}{(T_f - T_{env})}\right\},$$

where Δh_c is the combustion heat of combustible volatile products of material decomposition (it is actually equal to the effective heat of its combustion $\Delta H_{c.eff}$) and T_{ign} and T_{env} are the sample surface temperature at ignition and environmental temperature (K), respectively.

Assuming $Q''' = 1.9$ MJ/m^3, while $T_f = 1{,}600$ K and $h_{conv} = 10$ W/m^2 K, and using experimentally obtained values of $\Delta H_{c.eff}$ and T_{ign} for some timber species (Sivenkov 2002; Tkhan 2006), we estimated the critical mass flow of decomposition products corresponding to the lower concentration limit of ignition of timber (Table 4.2) by analogy with (Lyon and Quintiere 2007).

Table 4.2 Critical parameters of incipient and stable ignition of timber of coniferous and deciduous species

Indices	Pine, Russia	Pine (Pinus massoniana)	Fir (Picea koraiensis)	Eucalyptus camaldulensis	Acacia auriculiformis	Acacia mangium
$q''_{\text{ign. cr}}$, kW/m^2	12	10.8	9.7	14.3	6.5	7.0
T_{ign}, °C	340	387.7	370.1	335.7	319.8	308.9
Q_{eff}, kJ/g	14.0	12.10	12.81	12. 99	13.52	13.04
ρ, kg/m^3	0.775	0.736	0.749	0.778	0.792	0.800
L_{g}, kJ/g	2.82	2.03	1.50	2.3	–	–
m''_{fcr}, g/m^{2}s	1.33	1.54	1.45	1.43	1.37	1.42
$m''_{\text{fcr}}Q_{\text{eff}}$, kW/m^2	18.62	18.63	18.57	18.57	18.55	18.57
m''_{b}, g/m^{2}s	2.5/3.4[a]	3.2/6.3[a]	3.1/4.5[a]	2.9/4.8[a]	–/2.6[a]	–/2.8[a]
$m''_{\text{b}}Q_{\text{eff}}$, kW/m^2	35.0	38.7	39.6	37.6	37.0	37.0

[a]Experimental values obtained with $q''_{\text{e}} = 40$ kW/m^2

Values ρ and c_{p} were accepted for air at the average gas temperature $T_{\text{av}} = (T_{\text{ign}} + T_{\text{env}})/2$. Wood samples were tested in horizontal configuration according to GOST 30402-96 and exposed to an external radiation heat flow perpendicular to the grain axis. The apparatus was equipped with a device for recording sample mass change in the process of heating.

The lower concentration limit of timber ignition is associated with ignition of a premixed blend of air and combustible gas forming at the initial stage of material decomposition. Sometimes it is possible to observe this incipient nonstationary ignition as flashes on the sample surface (e.g., as in Fig. 4.7).

The critical mass flow of combustible products of wood decomposition at the lower concentration limit of ignition we calculated is equal to 1.33–1.54 g/m^{2}s depending on the type of timber material (Table 4.2). However, it is interesting to mention that the heat release rate is nearly constant for all timber species. In its scale it corresponds to the critical heat release rate for nonstationary ignition ($\text{HRR}_{\text{ign}} = 21 \pm 6$ kW/m^2) demonstrated for many carbonizing and non-carbonizing polymers in accordance with the accepted critical density of energy in the gas phase during ignition (Lyon and Quintiere 2007).

Transition from nonstationary to stable ignition means transition to the diffuse mode of combustible gas combustion subject to their stoichiometric concentration with atmospheric oxygen. This stoichiometric fuel concentration is usually 2–3 times higher than in the case of the lower concentration limit of ignition. For this reason, for stable ignition of polymer materials, the mass flow of decomposition products (m''_{b}) should be two to three times greater than in the case of nonstationary ignition (Lyon and Quintiere 2007). Their reciprocal relationship becomes apparent with a change in the thermal balance on the solid fuel surface following the appearance of a stable flame and the additional contribution of the heat flow from flame q''_{fl}:

$$m''_{\text{b}} = m''_{\text{fcr}} + \left(q''_{\text{fl}} + q''_{\text{conv}}\right) / \Delta h_{\text{g}},$$

where Δh_g is the heat of material gasification per unit mass of volatile products and q''_{conv} is the convective heat flow from the hot surface into the gaseous boundary layer for stable ignition.

Heat of material gasification per unit mass of volatile products, Δh_g, is correlated to the heat of material gasification per unit mass of the initial material, L_g:

$$\Delta h_g = \frac{L_g}{(1 - Y_{char})}$$

where Y_{char} is the char residue yield during decomposition.

During timber ignitability testing according to GOST 30402-96 under an external heat flow of 20–50 kW/m^2, it is observed no flash but the occurrence of a stable flame on the surface of timber. It should correspond to the m''_b value and the critical heat release rate, $HRR_b = m''_b Q_{eff}$.

The m''_b values calculated by analogy with (Lyon and Quintiere 2007) and the equation given above are approximately two times higher than the values m''_{fcr}. In this case, the critical heat release rate at the occurrence of stable ignition of wood samples is equal to 37 kW/m^2 on average.

The parameter of critical heat release rate on the occurrence of stable flame is the ignition criterion, which does not depend on the type of material (Lyon and Quintiere 2007).

References

Asseeva RM, Tkhan BD, Serkov BB, Sivenkov AB (2004) Release of smoke during thermal decomposition and combustion of wood. For Bull 2(33):99–103

Babrauskas V (2001) "Pyrophoric carbon" and long-term, low temperature ignition of wood. Fire Arson Investig 52(2):12–14

Babrauskas V (2002) Ignition of wood. A review of the state of the art. J Fire Prot Eng 12(3):163–189

Bilbao R, Mastral JF, Aldea ME, Ceamanos J, Betran M (2001) Experimental and theoretical study of the ignition and smoldering wood including convective effects. Combust Flame 126:1363–1372

Boonmee NA (2005) Theoretical investigation of surface glowing ignition leading to gas flaming autoignition. In: Proceedings of the 8th international symposium on fire safety science, Beijing, pp 139–150

Boonmee N, Quintiere JG (2002) Glowing and flaming autoignition of wood. Proc Combust Inst 29(1):289–296

Boonmee N, Quintiere JG (2005) Glowing ignition of wood: the onset of surface combustion. Proc Combust Inst 30(2):2303–2310

Bowes PC, Townshend SE (1962) Ignition of combustible dusts on hot surfaces. Br J Appl Phys 13:105

Delichatsios MA, Panagiotou T, Kiley F (1991) The use of time to ignition data for characterizing the thermal inertia and the minimum (critical) heat flux for ignition or pyrolysis. Combust Flame 84:323–332

Dietenberger MA (1996) Ignitability analysis using the cone calorimeter and LIFT apparatus. In: Proceedings of the 22nd international conference on fire safety, Columbus, 22–26 July, pp 189–197
Drysdale DD (1990) Koshmarov YA, Makarov VE (eds) Introduction into dynamics of fires. Stroyizdat, Moscow, 424 p
Frank-Kamentsky DA (1967) Diffusion and heat transfer in chemical kinetics. Science, Moscow, 492 p
Janssens M (1991a) Pilot ignition of wood: a review. Fire Mater 15:151–167
Janssens MA (1991b) Thermal model for piloted ignition of wood included variable thermophysical properties. In: Proceedings of the third international symposium on fire safety science, Edinburgh, Scotland, pp 167–176
Kanury AM (1977) Ignition of cellulosic solid: minimum pyrolysate mass flux criterion. Combust Sci Technol 16:89
Kashiwagi T (1974) A radiative ignition model of a solid fuel. Combust Sci Technol 8:225–236
Kashiwagi T (1979) Experimental observation of radiative ignition mechanisms. Combust Flame 34:231–244
Lyon RE, Quintiere JG (2007) Criteria for piloted ignition of combustible solids. Combust Flame 151:551–559
Mikkola E, Wichman IS (1989) On the thermal ignition of combustible materials. Fire Mater 14:87–96
Monakhov VT (1979) Research methods for fire hazard of substances, 2nd edn. Chemistry, Moscow, 424 p
Moussa NA, Toong TY, Garris CA (1976) Mechanism of smoldering of cellulosic materials. In: Proceedings of 16-th symposium (international) on combustion. The Combustion Institute, Pittsburgh, pp 1447–1457
Ohlemiller TJ (1985) Modelling of smoldering combustion propagation. Prog Energy Combust Sci 11(4):277–310
Ohlemiller TJ, Rogers FE (1980) Cellulosic insulation material II. Effect of additives on some smolder characteristics. Combust Sci Technol 24:139–152
Ohtani H, Maejima T, Uehara Y (1991) In-situ heat release measurements of smoldering combustion of wood sawdust. In: Proceedings of 3-rd internal symposium on fire safety sciences. Elsevier, New York, pp 557–564
Poespowati T (2008) An experimental study on autoignition of wood. Proc World Acad Sci Eng Technol 30:672–675
Rogers FE, Ohlemiller TJ (1980) Cellulosic insulation materials. I. Overall degradation kinetics and reaction heats. Combust Sci Technol 24:129–137
Simms DL (1963) On the pilot ignition of wood by radiation. Combust Flame 7:253–261
Simms DL, Law M (1967) The ignition of wet and dry wood by radiation. Combust Flame 11:377–388
Sivenkov AB (2002) Reduction of fire hazard of cellulose-based materials. PhD dissertation thesis, ASFS, Moscow, 171 p
Spearpoint MJ, Quintiere JG (2001) Predicting the piloted ignition of wood in the cone calorimeter using an integral model – effect of species, grain orientation and heat flux. Fire Saf J 36(4):391–415
Staggs JEJ (2001) Ignition of char-forming polymers at a critical mass flux. Polym Degrad Stab 74:433–439
Tkhan BD (2006) Impact of chemical components on fire hazard properties of Vietnamese tropical wood species. PhD dissertation thesis, ASFS, Moscow, 172 p
Tzeng LS, Atreya A, Wichman IS (1990) A one-dimensional model of piloted ignition. Combust Flame 80:94–107
Ugolev BN (2001) Wood science with fundamentals of forest commodity research. Moscow State Forestry University Publishing House, Moscow, 340 p
Zhou YY, Walther DC, Fernandez-Pello AC (2002) Numerical analysis of piloted ignition of polymeric materials. Combust Flame 131:147–158

Chapter 5
Heat Release Characteristics and Combustion Heat of Timber

Abstract This chapter presents original data on measurements of the lower heat of complete combustion of various timber species. It is demonstrated that these values directly correlate with the sum lignin content and extractives of various species. Thus, it is possible to determine the heat of complete combustion of hemicellulose and extractives of timber, which helps to evaluate the fire behavior of timber construction members.

The chapter also summarizes the experimental results on heat release characteristics at flame combustion of deciduous and coniferous timber species at different moisture content and effect of external heat flow.

5.1 Chemical Composition and Lower Heat of Complete Combustion of Timber Species and Its Components

There are many scientific papers dedicated to the study of the chemical composition of timber of live plants at all stages of their growth, as well as to felled timber. That is not surprising, if we take into account the use of timber as a renewable source of raw materials for production of many essential chemical substances, as well as the motivation to create high-quality materials for varied industrial applications. Special consideration is given to the problem of correlating the structure and chemical composition of coniferous and deciduous timber species from various geographic regions with the physical and mechanical and other performance properties of timber materials (Proceedings of the IV International Symposium on "Structure, Properties and Quality of Timber" 2004).

There are usually four main components among timber organic chemical compounds: cellulose, hemicellulose, lignin, and extractive substances. As a rule, the amount of inorganic substances does not exceed 1 %. The presence of minerals is the result of absorption of nutritious and toxic components (particularly, metal compounds) by woody plants from the environment (soil, air, rainfall).

R. Aseeva et al., *Fire Behavior and Fire Protection in Timber Buildings*,
Springer Series in Wood Science, DOI 10.1007/978-94-007-7460-5_5,

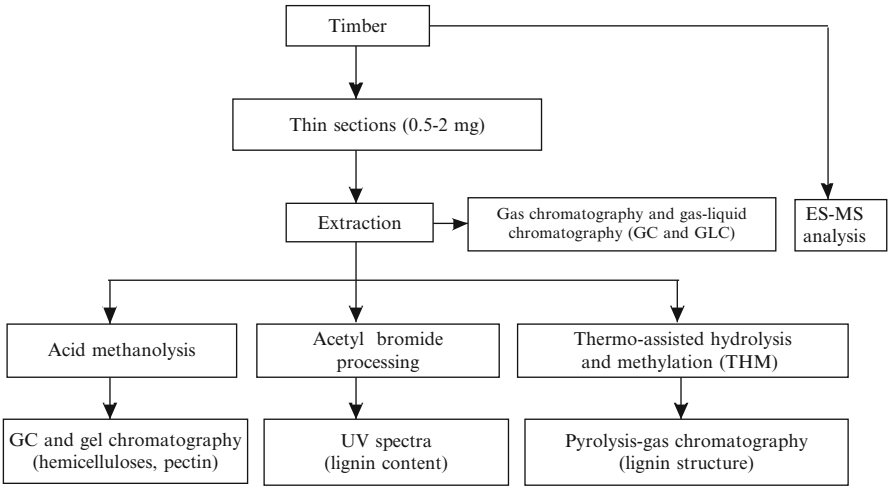

Fig. 5.1 Timber microanalysis scheme

The chemical composition of one botanical species of timber differs markedly from another one, depending on the soil and climatic conditions of woody plants.

Methods of separation and analysis of chemical components of timber are described in monographs (Nikitin 1951; Obolenskaya et al. 1991). Development of new up-to-date research methods not only reduces the time required for analysis of timber chemical composition but also allows microanalysis on timber samples with weights up to 0.5–2 mg.

One of the schemes of this microanalysis included in the program of countries' cooperation on fundamental research on timber for 2003–2007 is shown in Fig. 5.1 (Wood Material Science Year Book 2004).

Thin slices of timber prepared from certain parts of plant stems are freeze-dried and extracted with organic solvents. The extractive solution is tested by gas chromatography. In order to determine the content and composition of hemicellulose and pectin substances in extracted thin sections, acid methanolysis of the samples is carried out, followed by gas–liquid chromatography (GLC) of obtained products. To determine lignin content, the slices are exposed to acetyl bromide and then analyzed according to UV-absorption spectra. This method has similar results to the Klason method; however, the latter requires using samples with a weight up to several grams. Lignin structure can be evaluated using pyrolysis–gas chromatography combined with mass spectrometry (MS). It is generally thought that the thermo-assisted hydrolysis method and methylation (THM) of the samples followed by GLC-MS is more informative when it comes to lignin structure (Hardell and Nilverbrandt 1996).

Traces of many metals that are present in a timber sample are determined in one procedure by mass spectroscopy combined with atomic emission spectrometry (ES) using laser ablation.

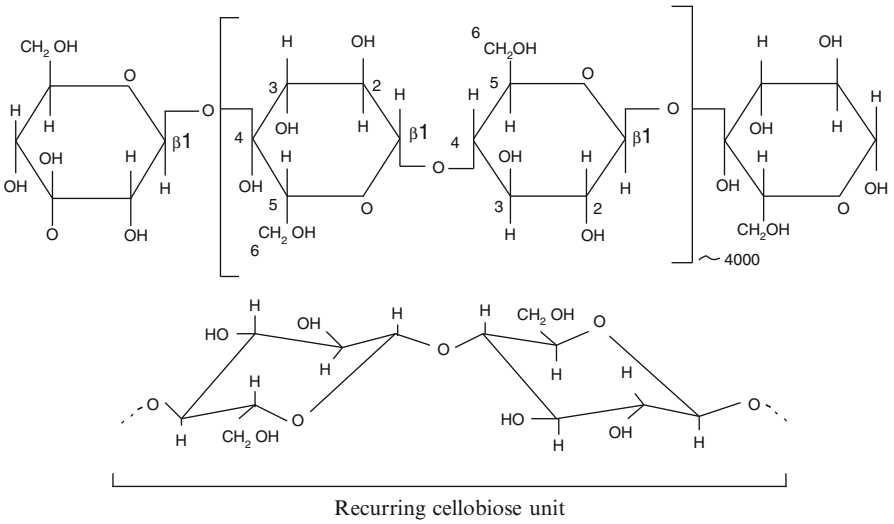

Fig. 5.2 Cellulose structure and molecular conformation

The results of using this microanalysis for analyzing hemicellulose and lignin distribution in early and late zones of annual rings of timber are reported in this paper (Pranovich et al. 2004).

Methods of ion and gel chromatography for separation and analysis of hemicellulose, pectin substances, and water-soluble polysaccharides are widely used today.

A new method including both electrospray ionization (ESI) and mass spectrometry (ESI-MS) (Proceedings of the IV International Symposium on "Structure, Properties and Quality of Timber" 2004, pp. 555, 558) provides a great opportunity for obtaining information about the chemical structure of hemicelluloses and lignin structure (sequence of structural units of lignin and the bonds between them). In this case, fragments of analyzed substances are ionized with generation of both negative and positive ions, which affects retention time during the analysis procedure and thus increases data volume.

The content and ratio of main chemical components vary in different parts of plants (leaves, needles, twigs, bark, bast fiber, various zones of annual rings, etc.), and they depend on the variety and species of trees (Proceedings of the IV International Symposium on "Structure, Properties and Quality of Timber" 2004).

It is believed that cellulose content in coniferous and deciduous timber species is almost always 42 ± 2 % on average, calculated on the basis of the oven-dry weight of a sample (Overend et al. 1985). Analysis of recently published and our own studies leads to the conclusion that cellulose content may vary from 32.6 to 55 % in coniferous timber species and from 33.7 to 49 % in deciduous timber species (Proceedings of the IV International Symposium on "Structure and Properties and Quality of Timber" 2004). Cellulose is a linear rigid-chain polymer built from 1,4-β-D-glucopyranose units with the general formula $[C_6H_7O_3\ (OH)_3]_n$ (Fig. 5.2).

Hemicelluloses are oligosaccharides with polymerization degree $n = 30–200$. This oligosaccharide group includes both pentosans with five carbon atoms in the base cyclic unit with the structural formula $(C_5H_{10}O_5)_n$ and hexosans $(C_6H_{10}O_5)_n$. Pentosans prevail among deciduous hemicelluloses, whereas hexosans are predominant in coniferous timber species. However, hemicelluloses are mainly copolymers of different carbohydrates. In coniferous timber species, for example, there is a set of galactoglucomannans in which molecular chains are constructed from 1,4-β-D-glucopyranose and 1,4-β-D-mannopyranose units, as well as arabinogalactans with an arm-like structure including not only the usual (1 4)-β-D-carbohydrate units but also side (1,3)- and (1,6)-β-D-galactopyranose residues.

Xylans predominate among hemicelluloses in all deciduous timber species, in particular, glucuronoxylans. The main molecule chains of these oligosaccharides consist of 1,4-β-D-xylopyranose residues with acetyl substituents in hydroxyl groups in the 2 (or 3) position of the carbohydrate cycle and rare side groups that are generated during the interaction of xyloglucans with 4-*O*-methyl-α-D-glucuronic acid. The xylan content in some deciduous timber species may reach 30–35 %.

Lignins are three-dimensional polymers that are products of polymerization and condensation reactions of coumaryl, coniferyl, and sinapic alcohols.

Due to the participation of functional groups of these alcohols in polymerization and condensation reactions, the following fragments with the spatial structure of lignins are formed (Fig. 5.3).

Timber of almost all coniferous species contains guaiacyl lignin composed mainly of coniferyl alcohol. Deciduous lignin is a mixed guaiacyl–syringyl type, which is essentially a copolymerization and condensation product of coniferyl and sinapic alcohols in different ratios depending on the species of woody plants. Due to the presence of two methoxy groups in the aromatic nucleus in sinapic alcohol, deciduous lignin has a less dense spatial network structure compared to coniferous lignin. Most coniferous timber species have a fairly high lignin content (30 ± 4 %) compared to deciduous timber species (less than 22–24 %).

The group of extractive components of timber includes complex mixtures of low-molecular-weight organic substances of various classes: terpenes, polyatomic phenols, esters, resin and fatty acids, unsaturated hydrocarbons and alcohols, waxes, etc. The composition and content of these substances, which are extracted from timber with water or organic solvents, depend on the timber species and variety. The total extractive content of coniferous and deciduous timber species may reach 16–20 %.

The above-mentioned main components are characterized by varying heat of complete combustion; therefore, we can expect different heat of complete combustion of timber species. According to existing data (Baldvin 1987), typical average high heat values for complete combustion of deciduous timber species are 19.734 ± 0.981 MJ/kg and 20.817 ± 1.479 MJ/kg for coniferous timber species.

The question concerning the influence of the content of main components on the heat of complete combustion of timber was considered for the first time in work (White 1987). The author determined lignin and extractive content in four coniferous timber species (spruce, pine, red cedar, and redwood) and in four

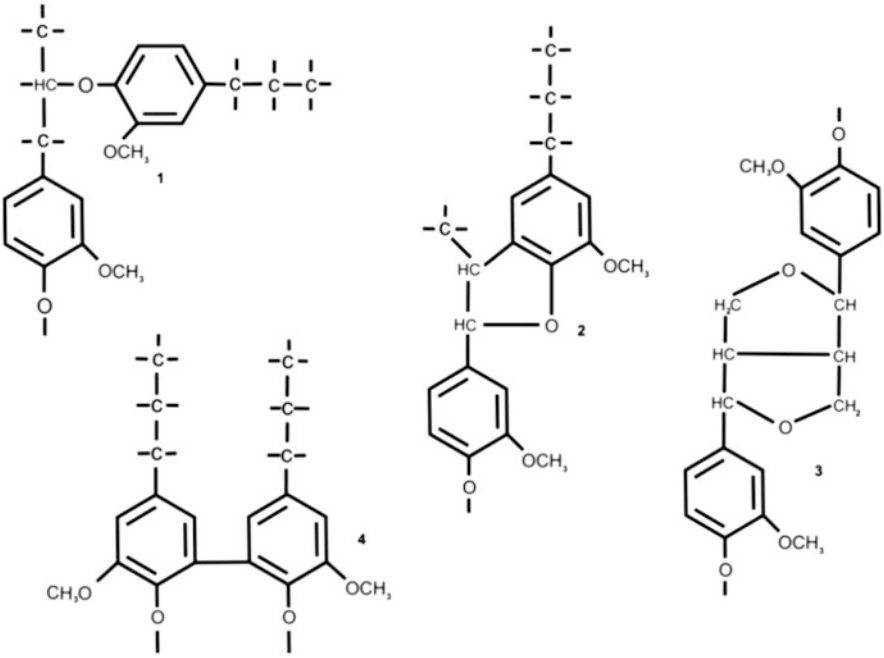

Fig. 5.3 Four main types of chemical bonds and structure fragments of coniferous lignin: *1* arylglycerol-β-aryl ether, *2* phenylcoumarin, *3* pinoresinol, *4* diphenyl

deciduous timber species (maple, poplar, red oak, and basswood). It was shown that there is a close relationship between the high heat value of complete combustion of timber and lignin content. Correlation index $R^2 = 0.70$ increased to 0.97 when dry samples devoid of extractable substances were tested. In this case, the empirical correlation fit the regression equation:

$$Q_{\mathrm{H}} = 17,612,472 + 85,364\, X_{\mathrm{L}},\ \mathrm{kJ/kg}$$

where X_{L} is the lignin content in the timber sample, %.

In this study, Q_{H} values were obtained using an adiabatic oxygen bomb calorimeter without regard for heat of water condensation as a resultant combustion product. According to the author White (1987), the high heat value of complete combustion of timber species should be significantly affected by extractive substance content, in particular, resins and terpenes, in the latter. Q_{H} values of resins of certain coniferous timber species can reach 34.9–37.2 MJ/kg (White 1987).

Since heat of complete combustion is a thermodynamic characteristic of substances and materials, there is great practical interest in determining it. In addition to direct experimental approaches to evaluating heat of complete combustion of substances and materials using calorimeters of various kinds, engineering calculation methods (Monakhov 1979; Marlair et al. 1999) are also used. They are based on

Hess's law of thermochemistry, which states that the total heat effect of a reaction depends only on source reacting substances and end products but does not depend on the intermediate phases of reactions.

Engineering calculation methods can be divided into two groups. The first group includes the use of empirical equations connecting heat of complete combustion of organic substances with their ultimate composition, first of all, with such elements as carbon, hydrogen, oxygen, sulfur, and nitrogen. The Dulong equation (Marlair et al. 1999) is popular abroad, while in our country it is more common to use the Mendeleev equation.

The second group involves calculation of heat of complete combustion of substances with a known chemical structure using structural group contributions (Monakhov 1979; Marlair et al. 1999).

During research on flammability of materials, modeling of the onset and propagation of fire, and solving many practical problems connected with fire safety in facilities, the so-called lower heat of complete combustion is used, which has absolute value less than Q_H (standard higher heat of combustion) for condensation water heat produced during combustion.

In this case, the Mendeleev equation with allowance for moisture level in a substance can be represented as

$$Q_L = 339.4C + 1257H–108.9\,(O + N–S) –25.1\,(9H + W), \text{kJ/kg}$$

where C, H, O, N, S, and W are the contents of the relevant elements and moisture level, %.

As lignin and extractive substances are the most highly energetic components of timber, in examining the influence of chemical composition on lower heat of its complete combustion, we decided to take the sum content of these components into account.

Experimental data on the chemical composition and lower heat values of complete combustion were obtained for 18 species of timber from moderate climate zones of Russia and the subequatorial region of Vietnam. Among them, apart from coniferous timber samples, we studied six deciduous timber samples with diffuse-porous structure (oak, maple, birch, hornbeam, aspen, and Vietnam eucalyptus) and six samples with a ring-porous structure (oak, ash, two species acacia, chestnut, and elm). Table 5.1 shows the results of analysis of the chemical composition and lower heat of complete combustion of these timber samples (Serkov et al. 2003).

Tropical coniferous timber species are represented by Vietnam pine (Pinus massoniana) and fir (Picea koraiensis Nakai) and deciduous timber species by Vietnam eucalypt (Eucalyptus camaldulensis) and two samples of acacia: Acacia mangium and Acacia auriculiformis. They all are characterized by rapid growth (2–2.5 m per year). Due to almost year-round growth, early- and latewood of annual rings can barely be distinguished.

Lower heat of complete combustion of timber samples was determined by the standard method of GOST 147–74, as well as by their element composition.

Table 5.1 Lower heat of complete combustion and chemical composition of different timber species

№	Sample	ρ, kg/m^3	W, %	Q_L, kJ/g	Holocellulose/ hemicellulose, %	Lignin, %	Extractive substances, %
1	Fir	430	9.5	18.90	62.7/—	27.3	10
2	Pine	450	10.0	19.62	62.9/—	28.0	9.1
3	Larch	660	—	18.61	—/—	—	—
4	Cedar	400	10	18.84	61.4/—	30.8	7.8
5	Beech	600	9.2	18.26	74.1/—	21.0	4.9
6	Ash	740	—	18.40	—/—	—	—
7	Maple	610	8.0	18.04	71.9/—	23.2	4.9
8	Oak	570	7.0	18.66	68.7/—	23.6	7.7
9	Birch	540	6.5	18.08	73.3/—	20.6	6.1
10	Hornbeam	595	—	18.42	—/—	—	—
11	Aspen	480	6.8	18.14	74.6/—	21.5	3.9
12	Vietnam pine	430	4	18.62	65.5/10.5	27.0	7.93
13	Vietnam fir	400	4	18.84	82.2/27.5	11.24	5.06
14	Vietnam eucalypt	595	5	18.85	67.3/19.16	25.4	6.40
15	Acacia mangium	420	4	18.11	70.0/21.03	24.75	5.09
16	Acacia auriculi-formis	560	4	18.53	69.1/20.10	25.16	5.56
17	Chestnut	490	4.0	17.86	—/—	18.3	5.6
18	Elm	620	4.0	18.06	—/—	—	—

For the analysis of element composition of oven-dry samples, we used a Carlo Erba 1106 automatic device (Italy).

Contents of main chemical compounds of timber samples were determined by the usual methods (Nikitin 1951; Obolenskaya et al. 1991).

Figure 5.4 shows the dependence of lower heat of complete combustion of the analyzed samples on sum lignin content and extractive substances in the chemical composition of timber.

There is a linear relationship between the analyzed parameters that can be described by the following equation with a correlation coefficient $R = 0.86$:

$$Q_L = 15.45 + 0.1\,(X_L + X_e)\,,\ \text{kJ/g}$$

where X_L and X_e are Klason lignin and extractive contents in oven-dry timber, %.

The greatest spread in Q_L values is characteristic of coniferous timber samples with a high content of extractives. As shown in Fig. 5.4, samples with diffuse-porous structure occupy the central position at the correlation line between coniferous and deciduous timber samples with a ring-porous vessel structure.

The equation derived above makes it possible to estimate the contribution of various chemical components of timber in heat of complete combustion of timber material and calculate Q_L values not only for a mixture of extractable substances from individual timber species but also for hemicelluloses.

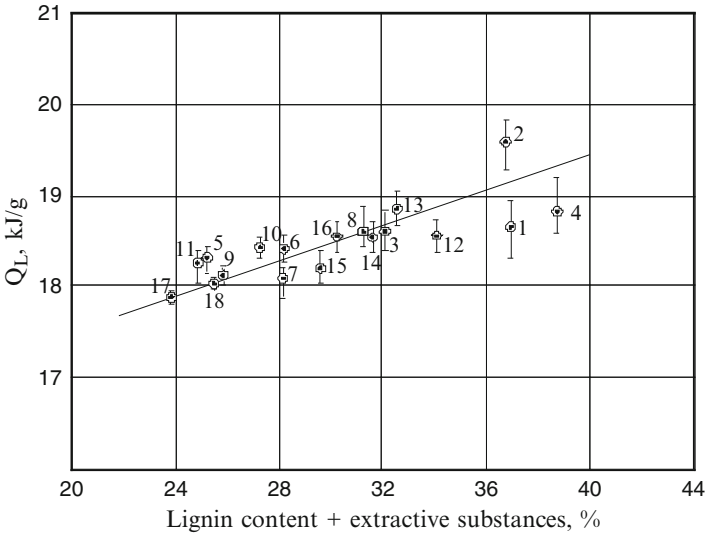

Fig. 5.4 Dependence of lower heat of complete combustion of analyzed timber samples on sum lignin content and extractive substances: *1* fir, *2* pine, *3* larch, *4* cedar, *5* beech, *6* ash, *7* maple, *8* oak, *9* birch, *10* hornbeam, *11* aspen, *12* Vietnam pine, *13* Vietnam fir, *14* Vietnam eucalyptus, *15* Acacia mangium, *16* Acacia auriculiformis, *17* chestnut, *18* elm

If the sum content of lignin and extractives is equal to zero, the lower heat of complete combustion of the remaining amount of timber composition, i.e., holocellulose consisting of cellulose and hemicellulose, must be equal to 15.45 kJ/g. In the other limiting case, when contents $X_L + X_e = 100$ %, the value of ${Q_L}^{L+e} = 24.45$ kJ/g.

Then the corresponding equations for estimating the heat value of complete combustion of extractives, ${Q_L}^{e}$, and hemicellulose, ${Q_L}^{hc}$, for each type of timber can be represented by the following equations:

$$ {Q_L}^{l+e} = 24.45 = X_L {Q_L}^{L} + X_e {Q_L}^{e}, \text{kJ/g} $$

$$ {Q_L}^{c+hc} = 15.45 = X_c {Q_L}^{c} + X_{hc} {Q_L}^{hc}, \text{kJ/g} $$

where X_L and X_e are the relative fractions of lignin and extractives in a mixture; X_c and X_{hc} are the relative fractions of cellulose and hemicellulose in holocellulose; and ${Q_L}^{c+hc}$ is the lower heat of complete combustion of holocellulose.

Thus, relative energy contributions of the main components of timber to lower heat of complete combustion are proportional to their content in timber.

Element composition of Klason lignin from various timber species is nearly the same and includes 63.54 % carbon, 5.54 % hydrogen, and 30.92 % oxygen (Nikitin 1951; Baker 1982). The ${Q_L}^{L}$ value calculated by the Mendeleev equation

Table 5.2 Lower heat of complete combustion of extractives and hemicelluloses of coniferous and deciduous timber species

Timber species	$Q_L{}^e$, kJ/g	Timber species	$Q_L{}^e$, kJ/g	$Q_L{}^{hc}$, kJ/g
Fir	29.66	Fir (Ugolev 2001)	39.1	14.11
Pine	30.20	Pine (Ugolev 2001)	30.97	14.14
Cedar	31.85	Larch (Ugolev 2001)	28.39	14.69
Western red cedar (White 1987)	31.53	Fir (Ugolev 2001)	36.64	13.88
Southern pine (White 1987)	33.07	Vietnam fir	33.78	12.40
Canadian spruce (White 1987)	42.68	Vietnam pine	30.69	12.19
Redwood (White 1987)	31.80	Vietnam eucalyptus	31.56	13.87
Maple	32.76	Aspen	33.91	–
Maple (White 1987)	31.75	Yellow poplar (White 1987)	33.75	–
Red oak (White 1987)	30.86	Acacia auriculiformis	32.93	14.0
White oak	30.17	Acacia mangium	32.41	13.92
Birch	30.67	Beech	32.06	–
Basswood (White 1987)	29.59	Aspen (Ugolev 2001)	34.72	14.13

is 23.91 kJ/g, and $Q_H{}^L = 25.16$ kJ/g. This result is in full agreement with the experimental value of higher heat of complete combustion of lignin $Q_H{}^L = 25.6$ kJ/g (Baker 1982). Calculation of the lower heat of complete combustion of cellulose gives $Q_L{}^c = 16.078$ kJ/g.

Table 5.2 shows the results of estimates of lower heat of complete combustion of substances extracted from various timber species, as well as hemicelluloses from tropical timber species. In addition, Table 5.2 includes $Q_L{}^e$ and $Q_L{}^{hc}$ values calculated using data on the chemical composition of the deciduous and coniferous timber species presented in White (1987), Ugolev (2001).

The contribution of every individual constituent of extractives to complete combustion heat cannot be precisely determined due to lack of information about the chemical composition of the substances extracted from timber. However, as shown in Table 5.2, the values of lower heat of complete combustion of extractives from different timber samples are generally dissimilar. This may be caused not only by the presence of different substances in the chemical composition of extractives but also by their different proportions.

The values of lower heat of complete combustion of substances extracted from coniferous timber species range from 28.39 to 42.68 kJ/g. Moreover, based on the example of spruce timber, we can see that these values depend on the region of plant growth. Heat of complete combustion of hemicelluloses of different timber species differ insignificantly from each other and have a $Q_L{}^{hc}$ value of about 14 kJ/g, which is typical of pentosans. The exceptions are samples of coniferous timber species from subequatorial Vietnam. The results obtained lead us to propose the presence of fragments with high concentration of oxygen, for example, residues of galacturonic acid, in the chemical structure of hexosan hemicelluloses.

5.2 Effect of Fire Conditions on Heat Release Characteristics

The energy source in fire conditions is heat release due to chemical oxidation of fuel, main characteristic of which is an exponential dependence of heat release rate on temperature in accordance with the Arrhenius law. Heat release rate (i.e., the heat amount per unit time) is the most important characteristic of the combustion process. Many fire safety indices depend directly or mutually on the heat release rate during combustion of matter, materials, structural members, and other substances (e.g., flame spread rate, generation of smoke and toxic carbon monoxide).

Fire propagation in different rooms is determined by the behavior of heat release intensity. Greater attention to determining various characteristics of heat release is vital in our country (Molchadsky and Borodkin 1992) and abroad (Babrauskas and Peacock 1992).

However, heat release rate during burning of combustible material is not its fundamental property and depends on the conditions of this process. The fundamental thermodynamic parameter of any combustible substance is complete combustion heat which is determined by calculation or experiment. Heat release rate per unit of material surface area Q'' may be calculated according to the following equation:

$$Q'' = \eta\, m'' Q_{\mathrm{L}},\ \mathrm{kW/m^2}$$

where η is combustion efficiency, m'' is the rate of fuel mass loss per unit of its surface area during combustion (g/m^2 c), and Q_{L} is the lower heat of complete fuel combustion (kJ/g).

The scenario of combustion process affects both the mass (weight) loss rate and effective heat of combustion ($Q_{\mathrm{eff}} = \eta Q_{\mathrm{L}}$).

Numerous devices and techniques, from small-scale (Walter and Lyon 1997) to large-scale and full-scale tests approximating real fire situations (ISO 1991), have been developed for estimating heat release rate during combustion of various products and materials. There are two basic approaches to recording a material's response according to intensity of heat release after thermal exposure: (1) according to temperature increase and (2) by analyzing the decrease in oxygen concentration and dynamics of release of combustion products. Progress in developing methods for estimating heat release characteristics was achieved due to the discovery (Hugget 1980) that during combustion of a large number of organic compounds and polymeric materials, a near constant amount of heat equal to 13.1 kJ/g of absorbed oxygen is released. The advantage of the principle of determining heat release characteristics based on oxygen consumption is that it can be applied to closed and open systems.

The principle of measuring oxygen consumption during combustion of materials on external heat exposure is based on the well-known and presently most commonly used cone calorimeter, which was developed in the USA in the 1980s (ASTM E1354, ISO 5660). The same principle is used in developing the new SBI (Single Burning Item) method recently included in the EN 13823 standard in order

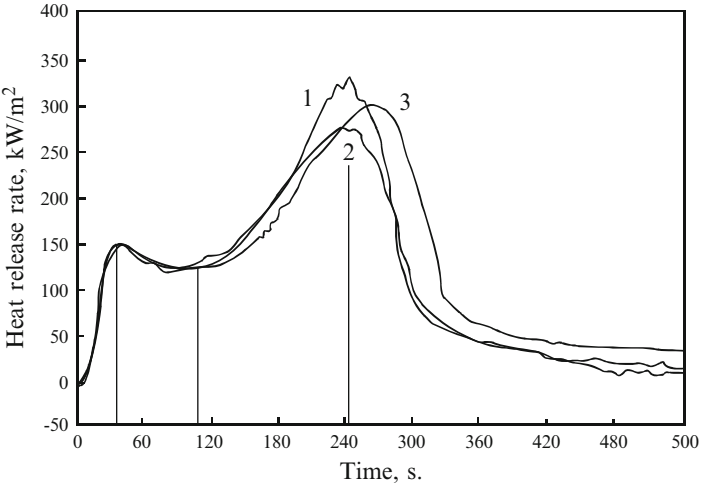

Fig. 5.5 Change of heat release rate during combustion of an oak timber sample under a constant external heat flow $q''_e = 52$ kW/m^2

to harmonize the procedures for determining fire safety indices and classifying construction materials in the European Union (Sundstrom 1999). In the scale of tested samples of construction materials (two vertical panels placed at an angle of 90°, with dimensions 1.5 × 1.0 m and 1.5 × 0.5 m), the SBI method is intermediate between cone calorimeters (ISO 5660) or OSU (ASTM E −906) and the ISO 9705 method.

It should be noted that the principle of temperature measurement in a closed system was used to design the OSU flow calorimeter, where OSU is the abbreviation of the developer's name – Ohio State University in the USA.

Each method of determining heat release characteristics has its own advantages and disadvantages. All devices used in the above-mentioned standard methods are quite expensive and therefore complex. They allow the evaluation of heat release characteristics at combustion, as well as other fire safety indices of materials depending on external heat flow density in one experiment: smoke generation capacity, yield of toxic combustion products, and mass loss rate. It makes it possible to compare the behavior of different fire safety indices of materials under the same conditions and to identify the factors influencing the development of specific physical and chemical processes during combustion.

A typical curve of heat release rate under the influence of an external radiative heat flow with constant density on the surface of a timber sample 19–20 mm thick is shown in Fig. 5.5.

As we can see from Fig. 5.5, the curve of heat release rate has two peaks, each of which reflects different stages of combustion.

Based on this experimental curve, we can directly determine the following most important characteristics:

1. Starting time of intense heat release from the moment of heat exposure, corresponding to ignition delay time, τ_I, s
2. Maximum (peak) value of heat release rate, HRR_{max}, kW/m^2
3. Time to maximum heat release rate, τ_{max}, s, from the beginning of the peak
4. Average rate of increase of the heat release rate to the maximum value, $\Delta HRR_{max}/\tau_{max}$, kW/m^{2}s or vice versa – the ratio of time from the start of ignition to reaching the first peak to the maximum heat release rate, s · m^2/kW
5. Average heat release rate in a definite time (e.g., 1, 2, 3, and 5 min or the overall time period of the test), $HRR_{\tau\ av}$, kW/m^2
6. Total heat release in a definite time or in the overall time period of the test, THR_{τ}, kJ/m^2 or kW · min/m^2

The results obtained for heat release allow to calculate the effective heat of combustion of the studied materials, if data on mass losses of the sample in the same conditions are known.

In particular, there are three methods of calculating effective combustion heat of the samples: (1) by the ratio of maximum heat release rate at the first peak to mass loss rate in the same period; (2) by the ratio of average heat release rate over the combustion period at the stage of the first peak to the mass loss rate during this period; in this case, we believe that averaging of the period of the first peak should not be less than 80 % of the maximum heat release rate; and (3) by the ratio of total heat release to total mass loss in the overall burning time.

The two peaks in the characteristic curve of heat release rate as a function of experimental time period that are often observed for timber samples and carbonizing polymer materials mean a transition from flame combustion mode to heterogeneous burn-off mode of the char layer that forms. Its appearance and increasing thickness after reaching the maximum of the first peak insulates the underlying layers of initial material and decreases the decomposition rate.

The short period of stable heat release between the two peaks or in other words a stable combustion period is apparently caused by a specific balance between endothermic decomposition of the initial material and exothermic oxidation of char residue. Therefore, during the spread of the charred layer through the whole material thickness, the last process starts to dominate up to the total suppression of heterogeneous combustion resulting from exhaustion of the combustible mass.

In fact, a calorimetric study of heat release rate during combustion of very thick (about 60 mm) timber samples in an air environment revealed the absence of a second peak on characteristic curves of heat release within 5 min.

Times to maximum heat release rate during the first stage of flame combustion or speed of increase in the heat release rate are very significant characteristics of the heat release intensity.

This index is used in the SBI method included in the EN-13823 standard and was called FIGRA or Fire Growth Rate.

Full-scale testing of different construction materials according to ISO 9705 revealed a clear correlation between FIGRA values and the occurrence of flashover during an indoor fire. In accordance with ISO 9705, limit values of FIGRA were

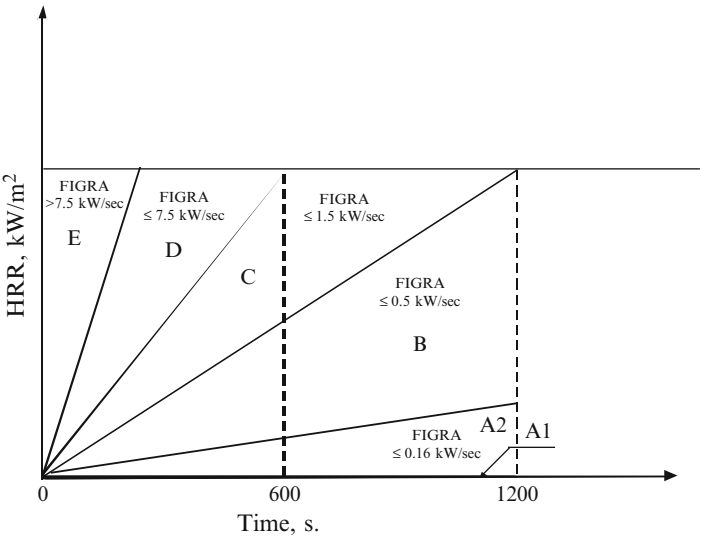

Fig. 5.6 Relationship between FIGRA values and the occurrence of flashover during an indoor fire during tests of construction materials under ISO 9705. Characteristics of classes as a function of contribution of heat release during material combustion to fire propagation are classified as follows: *Class A1* contribution of heat release is absent, *Class A2* flashover is absent, very limited contribution, *Class B* flashover is absent, *Class C* flashover is absent at ignition source $q_e = 300$ kW, *Class D* flashover of more than 2 min at $q_e = 100$ kW, *Class E* flashover of less than 2 min at $q_e = 100$ kW

Table 5.3 Limits of FIGRA (SBI) indices for construction materials of various Euroclasses

Euroclass	FIGRA, W/s	Euroclass	FIGRA, W/s
A1	<120	C	<250
A2	<120	D	<750
B	<120	E	>750

proposed for classifying construction materials and dividing them into groups – Euroclasses from A1 and A2 to class E (Fig. 5.6) (Sundstrom 1999).

Studies of heat release characteristics during round tests of several dozen construction materials in accordance with the SBI method showed complete coincidence of the distribution of the materials in rating order with the results of full-scale tests under ISO 9705. Correlation between FIGRA (SBI) and FIGRA (ISO 9705) reached 95 % (Sundstrom 1999). This was used as the basis for choosing the FIGRA (SBI) values as the main parameter for classifying construction materials by fire safety ratings and standardizing the method of determining it in the European Union.

The FIGRA value in the SBI method is the maximum value of average heat release rate in 30 s of material combustion divided by this time. Table 5.3 shows FIGRA (SBI) classification indices for construction materials.

Table 5.4 Average heat release rate and ignition delay time during testing of Canadian spruce samples by different calorimetric techniques

Method, configuration	OSU, vertical	STFI, vertical	Cone calorimeter, vertical	Cone calorimeter, horizontal
HRR_{300s}, kW/m^2	140	130	122	172
τ_{ign}, s	10	15	15	10

Timber materials such as plywood, chipboard, fiberboard, and pine timber with typical lacquer coating belong to class E and at best to class D according to this classification.

The authors of Messerschmidt et al. (1999) tried to predict the values of FIGRA (SBI) indices based on results of a cone calorimeter studies with constant density heat flow. For this purpose, they proposed an empirical model of flame spread based on the concept that the process rate is a function of ignition time of the material and is controlled by the heat release rate. In investigations of material by the cone calorimeter and SBI methods, the heat release rate is identical as a function of time. It has achieved satisfactory correspondence between predicted and experimental FIGRA (SBI) values during combustion of timber materials.

Laboratory methods of assessing heat release characteristics are attractive not only due to cost savings (especially in new product development). These allow to use the characteristics obtained as input data for modeling and to predict material response in real fire conditions.

Laboratory calorimeter tests on the basis of oxygen consumption or temperature measurements differ by system type (open or closed chamber) and also in the size and orientation of test samples, air flow rate, procedure for measuring oxygen content, type and position of the local ignition source, etc. Such experimental differences have an impact on the results of measuring heat release rate. Therefore, the comparative tests of heat release rate in an OSU calorimeter with routine temperature determination and OSU modified by oxygen consumption (Krause and Gann 1980) for the same samples were conducted. The recorded heat release rate under the second method was about 15–30 % higher than in the standard one.

Heat release rates by oxygen consumption with vertically and horizontally arranged samples are measured using three types of calorimeters (Ostman and Svenson 1985). Along with the mentioned cone and OSU calorimeters, the researchers (Ostman and Svenson 1985) used a STFI device designed by the Swedish Forest Products Research Laboratory. An STFI calorimeter is characterized by vertical arrangement of samples with dimensions of 150×150 mm in an open chamber. Oxygen concentration is measured in the flow of combustion products in the exhaust duct. Samples with dimensions of 100×100 mm were tested in a cone calorimeter in horizontal and vertical configurations.

Table 5.4 represents the results of tests of Canadian spruce at external heat flux $q_e = 50$ kW/m^2 for 5 min exposure. Canadian spruce samples have 11 mm thick and density 450 kg/m^3.

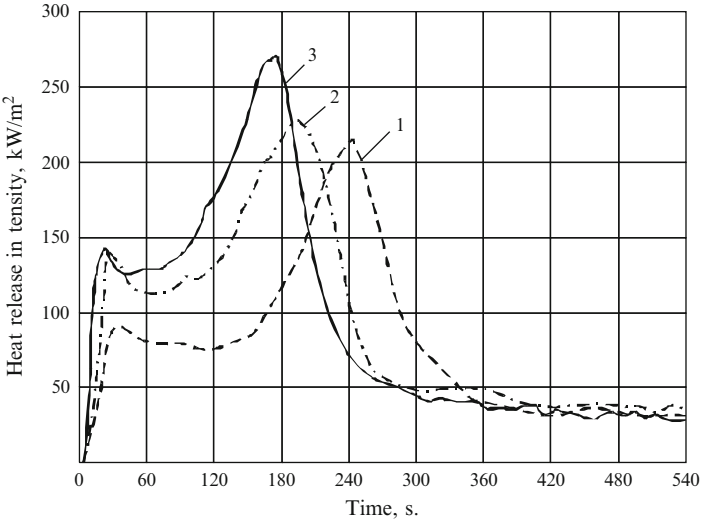

Fig. 5.7 Effect of external heat flow density (*1* 20 kW/m^2, *2* 35 kW/m^2, *3* 52 kW/m^2) on heat release rate during fir timber combustion

Values of average heat release rate are higher for horizontally oriented samples compared to vertically oriented ones. According to the authors of Ostman and Svenson (1985), the results are generally similar in spite of differences in the equipment used and sample sizes. It is obvious that in order to determine the impact of structural features and physical and chemical properties of timber on heat release intensity during combustion, the tests must be carried out under identical conditions.

We have examined the effect of species of timber and its moisture content on heat release characteristics using four of the most common species of deciduous and coniferous plants in Moscow Region: oak, birch, pine, and fir. An HRR-3, OSU calorimeter manufactured by Atlas, USA, was used to determine heat release characteristics. Measurements were made with external radiative flow density equal to 20, 35, and 52 kW/m^2. Samples with dimension of $150 \times 150 \times 10$ mm after drying had a moisture content of 4.3–7 %. Two samples (birch and fir) maintained moisture content at the level of 12 %. An increase in moisture content leads to some increase in timber density (Aseeva et al. 2009).

The general trend of heat release rate of the investigated timber species during combustion in an external heat flow with constant density is similar to the behavior shown at Fig. 5.5. All timber samples have two peaks in the curve with higher heat release intensity in the second stage. However, detailed investigations of different timber species, for example, fir and birch (Figs. 5.7 and 5.8), reveal significant differences in heat release dynamics.

Coniferous timber samples are characterized by shorter ignition time, lower maximum heat release rate at the first stage of the process, and its accelerated achievement in comparison with deciduous species. Coniferous species show a

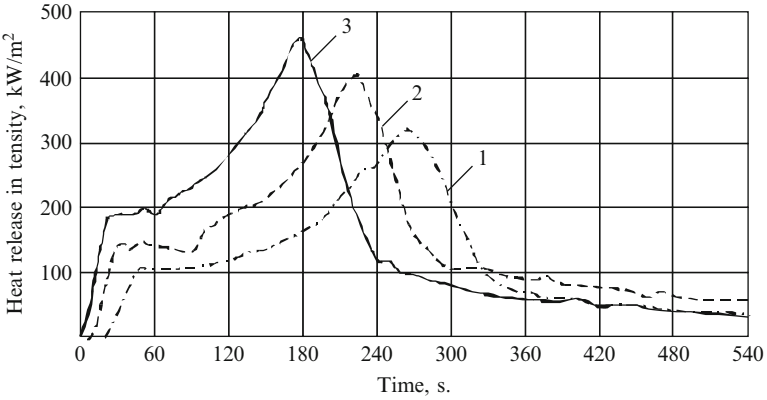

Fig. 5.8 Effect of heat flow density (*1* 20 kW/m^2, *2* 35 kW/m^2, *3* 52 kW/m^2) on heat release rate during birch combustion

Table 5.5 The effect of l heat flow density on heat release characteristics for different timber species

Sample	ρ, kg/m^3	W, %	q_e, kW/m^2	τ_B, s	τ_{1max}, s	$HRR_{1\,max}$, kW/m^2	τ_{2max}, s	HRR_{2max}, kW/m^2	THR_{2min}, kW min/m^2
Fir	422	6.4	20	10	40	94.8	279	202.1	142.5
			35	<10	23	131.2	195	233.2	218.2
			52	<10	<20	141.8	159	256.1	270.2
Pine	448	6.0	20	10	43	98.2	354	159.3	128.8
			35	<10	20	129.0	276	203.5	180.6
			52	<10	<20	137	247	247.3	202.0
Birch	567	5.5	20	23.3	63	104.9	284	321.9	149.3
			35	10	53	157.7	215	400.5	279.9
			52	<10	33	190.8	184	459.6	377.2
Oak	638	4.3	20	20	67	100.9	362	227.7	127.1
			35	10	33	131.3	281	245.1	198.0
			52	<10	27	161.6	246	312.0	261.6

less prolonged section of stable heat release between the two peaks, which is most noticeable at low heat flow density of 20 kW/m^2. The duration of this stable section decreases and peak intensity increases as external heat flow density increases from 20 to 52 kW/m^2 (Aseeva et al. 2009).

The results of evaluating heat release characteristics for the investigated samples are shown in Table 5.5.

Table 5.5 shows that total heat release within the first 2 min of combustion after ignition is higher for fir samples than for pine and is higher for birch timber than for oak.

Furthermore, total heat release for 2-min combustion time of pine timber shows the lowest values, and birch has the highest ones. This appears to be due to different

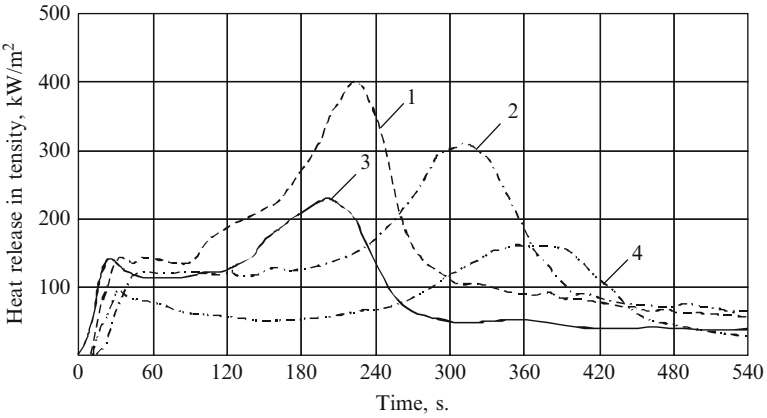

Fig. 5.9 Effect of moisture content (W) in birch timber samples (*1* $W = 7$ %, *2* $W = 14$ %) and fir timber samples (*3* $W = 7$ %, *4* $W = 14$ %) on heat release rate at $q''_e = 35$ kW/m^2

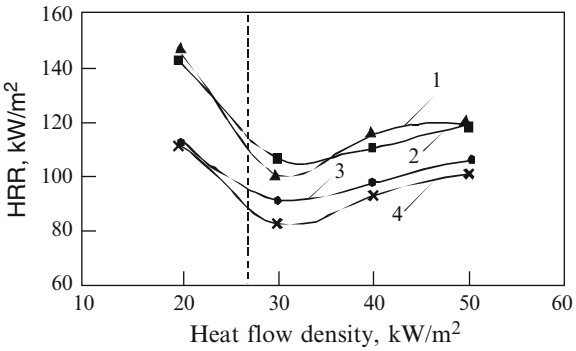

Fig. 5.10 Average heat release rate during timber combustion for different timber species as a function of heat flow density: *1* cherry, *2* kempas, *3* oak, *4* beech

charring behavior of the timber species, structural features of the char layers formed on timber surface, and its oxidation ability.

Moisture has a great effect on heat release characteristics during timber combustion (Fig. 5.9).

It is clear that increased moisture content slows down ignition and decreases maximum heat release rate in the first and second stages. Time to peak heat release rate becomes significantly higher.

There are discrepancies in assessments of the influence of external heat flow density on average heat release rate during timber combustion (Babrauskas and Grayson 1996; Yang et al. 2003). Authors of work Yang et al. (2003) concluded that the dependence of HRR on q''_e is parabolic law rather than linear (Babrauskas and Grayson 1996). Figure 5.10 shows that at low heat flow density of 20 kW/m^2, all investigated wood samples have a significantly higher average heat release rate during combustion than at $q''_e = 30$–50 kW/m^2 (Yang et al. 2003).

An investigation of heat release rate during combustion of ten deciduous and four coniferous species showed lower heat release intensity in the latter case. One of the reasons for this difference has to do with the structural features of deciduous and coniferous species that affect on their thermal decomposition and properties of char surface layer formed (Pofit-Szczepanska 1994).

Electron microscopy was used to investigate the structure of timber and the charred layers formed under heat flow of 50 kW/m^2. After heat exposure, a lot of cracks formed in the structure of softwood species (poplar and spruce); these cracks penetrated across the fiber to the charred area. No cracks were discovered in the structure of oak and larch char. Surface layers were dense and hard with high mechanical properties. In the opinion of the author Pofit-Szczepanska (1994), this fact has the most significant effect on time to peak heat release rate for different timber species. In particular, the FIGRA value is 0.68 kW/m^{2}s for poplar, 0.50 kW/m^{2}s for spruce, and 0.36 and 0.38 kW/m^{2}s for oak and larch, respectively. The average heat release rate in the entire 5 min of the test period was twice as high for timber species that formed a dense, hard char surface layer. Therefore, we may conclude that the structural features of timber, its chemical composition, should have a more significant impact on heat release characteristics during combustion than simple division on deciduous or coniferous species.

References

Aseeva RM, Barbotko SL, Serkov BB, Sivenkov AB, Suleikin EV, Tarasov NI (2009) The influence of service life of timber on its fire hazard properties. Proceedings of X international conference on oligomer chemistry and physicochemistry “Oligomers – 2009”, Volgograd State Technological University (VSTU), pp 270–295

Babrauskas V, Grayson SJ (eds) (1996) Heat release in fire. Elsevier Applied Science, London

Babrauskas V, Peacock RD (1992) Heat release: the single most important variable in fire hazard. Fire Saf J 18:72

Baker AJ (1982) Wood fuel properties and fuel products from woods. In: Proceedings of fuel managements and utilization seminar, November, Michigan State University, East Lansing, MI, pp 14–25

Baldvin SF (1987) Biomass stoves: engineering design, development and dissemination. Volunteers in Technical Assistance (VITA), Arlington, p 178

Bjarne H, Geofrey D (2004) In: Paavilainen L (ed) Chemical microanalysis of wood and fibers (chapter 7). Wood material science year book. Tekes, Helsinki, pp 45–48

Hardell NL, Nilverbrandt NO (1996) Analytical pyrolysis of spruce milled wood lignins in the tetramethylammonium hydroxide. Nord Pulp Pap Res J 11(2):121–126

Hugget C (1980) Estimate of rate of heat release by means of oxygen consumption measurements. Fire Mater 4(2):61–65

International Standards Organization (1991) ISO 9705 fire tests – reaction to fire – full scale room fire test for surface products. International Standards Organization, Geneva

Krause RF, Gann RG (1980) Rate of heat release measurements using oxygen consumption. J Fire Flammabl 12, № 2:117–130

Marlair G, Cwiklinski C, Tewarson A (1999) An analysis of some practical methods for estimating heat of combustion in fire safety studies. In: Proceedings of 8th internal conference on fire science and engineering, Interflame'99, vol 1. Interscience Communication, London, pp 201–212

Messerschmidt B, Van Hees P, Wickstrom U (1999) Prediction of SBI (single burning item) test results by means of cone calorimeter test results. In: Proceedings of 8th international fire science and engineering conference, Interflam '99, Edinburgh, Scotland, vol 1, Interscience Communication, London, pp 11–22

Molchadsky IS, Borodkin AN (1992) Heat release during fires in rooms. Fire Explos Saf 1:45–50

Monakhov VT (1979) Methods of testing the fire hazard of substances. Khimia, Moscow, 424 p

Nikitin VM (1951) Chemistry of timber and cellulose. Goslesbumizdat, Leningrad, 495 p

Obolenskaya AV, Elnitskaya ZP, Leonovich AA (1991) Laboratories studies on the chemistry of timber and cellulose. Ekologia, Moscow, 320 p

Ostman BA-L, Svenson IG (1985) Comparison of three test methods for measuring rate of heat release. Fire Mater 9(4):176–184

Overend RP, Milne TA, Mudge LK (eds) (1985) Fundamentals of biomass thermochemical conversion. Elsevier, London, p 1

Pofit-Szczepanska M (1994) The influence of the natural structure of wood on the heat release rate during its combustion. In: Abstracts of 25th international symposium on combustion, Irvine, CA, Poster Session 4, p 324

Pranovich AB, Konn I, Holmbom B (2004) The distribution of organic compounds in the annual rings of Norway spruce. In: Proceedings of the IV international symposium on "Structure, properties and quality of timber – 2004", vol 1. SPbFT Academy, St. Petersburg, pp 572–575

Proceedings of the IV international symposium on "Structure, properties and quality of timber – 2004", vol 2. SPbFT Academy, St. Petersburg, 2004, 569 p

Serkov BB, Sivenkov AB, Thanh BD, Aseeva RM (2003) Heat release during timber combustion. Lesnoy Vestnik (Russ) 5:74–79

Sundstrom B (1999) European classification of building products. In: Proceedings of 8th international fire science and engineering conference, Interflam'99, Edinburgh, Scotland, vol 2. Interscience Communication, London, pp 769–780

Ugolev BN (2001) Wood science with the fundamentals of commodity forestry. MSFU, Moscow, 340p

Walter RN, Lyon E (1997) Microscale combustion calorimeter for determining flammability parameters of materials. In: Proceedings of 8th annual BCC conference on recent advances in flame retardancy of polymeric materials, Stamford, CT, USA

White RH (1987) Effect of lignin content and extractives on the higher heating value of wood. Wood Fiber Sci 19(4):446–452

Yang L, Chen X, Zhou X, Fan W (2003) The pyrolysis and ignition of charring materials under an external heat flux. Combust Flame 133:407–413

Chapter 6
Flame Propagation on Timber Surface

Abstract This chapter describes the effect of flame propagation on the timber surface. It is shown that flame propagation rate depends on timber species, their physical properties and thickness of timber specimen, direction of flame propagation and incoming air, and also intensity of external heat flow. The minimal meanings for intensity of external heat flow to prevent the flame propagation for various timber species are formulated.

Conditions for initiation of a stable combustion timber process determine the nature of its initial development stage. With respect to fire safety, the ignition and flame spread are responsible for fire initiation and its growth in timber buildings, heat release rate, and the formation of smoke and toxic combustion products.

The ability to support itself by means of heat flow feedback from the reaction zone to the neighboring initial substrate layer, even if there is no initial external heat source, is the main feature of combustion spread process in timber (as well as other combustible materials).

An understanding of such aspects as global heat flow rate from flame (out of the reaction zone) depending on its scale, effect of material's properties and environmental characteristics, the mechanism of heat transfer from flame to heated substrate, the role of kinetic factors, and limiting conditions of combustion are the key points.

These aspects are considered in multiple experimental and theoretical studies dealing with flame spread, beginning with the pioneering works of N. Semenov, Ya. Zeldovich, D. Frank-Kamenetsky, and followers of their school.

Knowledge of combustion spread regularity makes it possible to define and predict fire development dynamics in buildings (Aleksashenko et al. 1982, 1988; Abduragimov et al. 1984).

R. Aseeva et al., *Fire Behavior and Fire Protection in Timber Buildings*,
Springer Series in Wood Science, DOI 10.1007/978-94-007-7460-5_6,

6.1 Model Approach for Flame Propagation on Carbonizing Timber Materials

The main quantitative characteristic of flame propagation (or flameless spread) on timber surface is the process rate. It is defined as the path taken by the flame (smoldering) front per unit time.

The concept of a continuously repeated ignition process, where its own flame serves simultaneously as a solid material heating source and local ignition source for produced inflammable decomposition products, is used in analysis of flame spread over a solid material surface.

Materials producing nonvolatile char during thermal decomposition differ from non-carbonizing materials in their ability to spread the flame over the surface. Apart from timber, the former material's group includes a fair number of natural and synthetic polymeric materials (Aseeva and Zaikov 1981). Following ignition, carbonizing materials sometimes show a quick run of flame over the surface, which is followed by instantaneous carbonization of the near-surface layer and damping. By this moment, a significant amount ($\sim$10 %) of the material weight has been consumed, but carbonization changes heat and mass transfer conditions and improves the material's resistance to flame spread (Astapenko et al. 1988; Newman and Tewarson 1991). Charring of the material introduces great difficulties into flame spread analysis. The process becomes transient, and the properties of the material change with time and depend on temperature. Compared to ignition, the flame spread simulation problem is a more complicated one. Its solution requires at least two-dimensional analysis: lengthwise and crosswise direction of flame movement on the material surface. Moreover, we have to consider the processes for charring material in two condensed phases: parent matrix and char layer.

During exposure to external heat, combustible volatile products are generated in the pyrolysis area under the char layer. It is important to assess the effect of this char layer, its accumulation rate and change in structural characteristics, on physical and chemical processes during timber combustion and, finally, on flame spread rate.

Flame spread at fire in timber buildings occurs in different configurations, which are organized by orientation of solid material and direction of main flows of gases (fuel and air) relative to direction of flame spread.

Flame can propagate on timber surface both around origin fireplace and in a linear direction. The complexities and the importance of the flame spread processes make to model different flame spread tests, changing scale of fire equipment, specimen's orientation and sizes, and the conditions of heat and fire effects.

Experimental studies of flame spread over the surface of timber materials with using different tests have showed that not only external thermal action conditions but also timber species affect flame spread characteristics.

The influence of timber species has been observed to some extent by examination of the values of the so-called flame spread index (FSI). This indicator is used for rating construction materials by ability to spread flame over the surface under controlled conditions. According to laboratory method of GOST 12.1.044-89, the

material sample is heated using a radiant panel and ignited by a pilot burner on the top. As the sample is placed at a 30° angle to the vertical radiant panel, flame is propagated downward over the lower surface of the sample. This sample position ensures heat flow distribution close to linear along the sample's length and precise fixation of the flame front. FSI is a complex index, because when it is calculated, the data on maximum temperature of exhaust gases and time to reach this temperature are used in addition to the rate of flame spread along separate sections of the sample surface and spread distance limit. These data give an idea of the maximum heat generation rate. Materials with FSI values of $\leq$20 are classified as materials with slow flame spread. For FSI >20, materials are classified as materials that spread flame quickly. According to this standard, all timber species are assigned to the latter group. Their FSI values are all over 55. Thus, pine samples from various areas of Moscow Region had FSI in the range of 55–67.

Construction materials are traditionally classified abroad by their ability to spread flame along the ceiling on direct exposure to fire using the large-scale ASTM E84 method developed in the middle of twentieth century, which is often called the tunnel test. The fire hazard rating of construction materials according to this method is statutorily included in various American codes. It is assumed that large-scale tests for flammability of materials reflect their behavior in real fires better. According to the ASTM E84 test, a sample 7.32 m long and 51 cm wide is mounted on the test chamber ceiling and burned from one end using a propane burner flame covering almost 1.37 m of the sample length. As soon as stable ignition occurs, the distance and speed of flame spread over the bottom surface of the material for same-direction air motion are determined. The induced air current is generated by means of chimney ventilation action (1.2 m/s). The FSI value for this method is calculated from the flame front position as a function of time or maximum flame front movement over the surface of the test sample in 10 min. Red oak with FSI = 100 serves as a benchmark. Construction materials are divided according to FSI values into three classes: class I (or A) – with a value of 0–25; class II (or B) with 26–75; and class III (or C) with 76–200 and higher.

Table 6.1 presents FSI values according to the ASTM E84 test for original timber samples 19–25 mm thick (White and Dietenberger 2002). FSI values for asbestos cement board and gypsum board are given for comparison.

Although most types of timber are attributed to class III, which is the most dangerous class by ability to flame spread over the surface of ceiling structures, some samples of coniferous species, as follows from Table 6.1, have lower FSI values and are attributed to class II. It may be assumed that this is due to the absence or low content of energy-consuming extractive substances in the chemical composition of the timber samples. For example, it is well known that Canadian red cedar wood with density of 350 kg/m^2 has almost no resinous extractive substances.

Analysis of the factors influencing the ability of timber materials to spread flame over the surface under the ASTM E84 test has revealed that the FSI value has a complex link with the rate of heat generation at timber combustion. For a heat generation rate of <70 kW/m^2, FSI is small and almost independent of it. At >70 kW/m^2, the FSI value is very sensitive to heat generation rate. In addition,

Table 6.1 Influence of coniferous and deciduous timber species on FSI

Timber species	FSI	FS class	Timber species	FSI	FS class
Red cedar	69	II	Birch	80–110	III
Yellow cedar	78	III	Red oak	100	III
Cypress	145–150	III	White oak	100	III
Douglas fir	70–100	II–III	Maple	104	III
Sitka spruce	69	II	Lime	130–140	III
White spruce	65	II	Cottonwood	170–185	III
White pine	75–82	III	Alder	104	III
Lodgepole pine	98	III	European walnut	130–140	III
Ponderosa pine	105–230	III	Gum	140–155	III
Larch	55–74	II	Asbestos cement	0	I
Redwood	70	II	Gypsum board	10–15	I

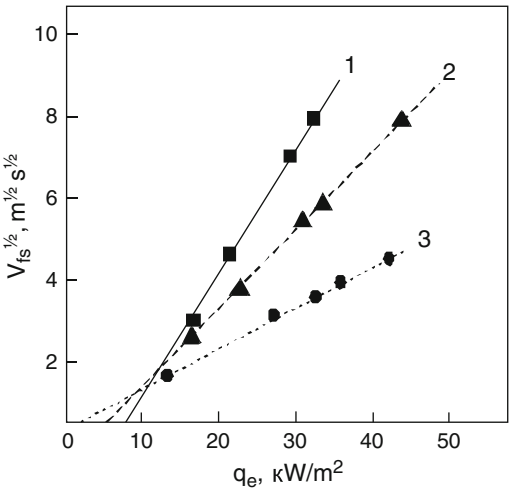

Fig. 6.1 Dependence of the rate of flame spread over the surface of timber samples on density of external radiative heat flow: *1* pine, *2* fiberboard, *3* larch

it has been noted that heat flow from flame is affected by the ratio of gasification heat to effective combustion heat of the material, and flame length is affected by the assisting oxidizer rate and oxygen concentration therein (Quintiere 1985).

Experimental study of flame spread rate over a horizontal timber surface as a function of the density of external radiative heat flow (Fig. 6.1) shows the influence of timber type on this parameter (Serkov 2001).

Minimum (critical) external heat flow value is one of the main characteristics of a material's ability to spread flame over the surface. If this value is lower than the minimum, flame spread over the surface is impossible. This value, $q_{e,min,}$ for thermally thick wood samples is determined from the intersection of experimentally obtained straight lines in the coordinates of Fig. 6.1 with the abscissa axis. As follows from Fig. 6.1, pine timber has a higher value of $q_{e,min}$ than larch.

When flame spread rate over the surface for different timber species samples from New Zealand was studied according to the ASTM E1321 method known

as LIFT (Lateral Ignition and Flame Transport), it was established that the value $q_{e,min}$ was lowest (2.2 kW/m^2) for macrocarpa cypress timber (volume density was 514 kg/m^3). In this case, the flame spread process was unstable closer to the limit; the trend of surface spread over resinous structural zones became evident.

Samples of beech and pine (Radiata Pine) 20 mm thick had $q_{e,min} = 4.4$–4.5 kW/m^2. Timber of *Dacrydium cupressinum* (Maori name – Rimu) with high volume density of 660 kg/m^3 had $q_{e,min} = 7.6$ kW/m^2 and showed significant charring prior to reaching flame spread limit. This wood species was widely used as a construction material in various building structures, as well as for making floors and facing boards (Merryweather and Spearpoint 2010).

There are a lot of standard methods for determining the ability of materials to spread flame over their surfaces. They differ in sample size and thickness, their spatial orientation, type, power of ignition source and external thermal action, mutual directions of combustion wave and gaseous oxidizer flow spread, oxygen concentration in the latter, and in other characteristics. A diagram presenting some technical characteristics of laboratory methods with different sample orientation was given earlier (Aseeva and Zaikov 1981).

Experimental studies of the combustion of timber materials carried out using these methods have shown that flame spread rate over the surface depends considerably on sample thickness and spatial orientation and the rate and direction of incident air relative to combustion wave movement. Moreover, the existence of two basic modes depending on sample thickness (thermally thin and thermally thick) and two basic types of flame spread (with opposed flow, natural or induced, of oxidizing gas and concurrent air movement) is observed.

The effect of sample orientation and thickness on the rate of flame spread over the surface of charring materials was actively studied using paper and cardboard as examples.

Figure 6.2 shows the dependence of flame spread rate over a paper surface on the sample's slope angle relative to a horizontal plane. The paper was 0.16 mm thick (Hirano et al. 1974).

If the slope angle is changed from −90° to −30°, downward flame spread opposite to air flow direction resulting from its natural convection is achieved. Under these conditions, flame spread rate is almost constant. But if the slope angle is from −30° to zero, it starts to increase. If a positive slope angle is increased to +90°, upward flame spread with concurrent movement of natural convection air flow is achieved. The rate of upward flame movement over a vertically sample oriented paper sample is almost 30 times greater than rate of downward spread at −90°.

It was shown experimentally that with increasing thickness within thermally thin samples, the flame spread rate decreases. For thermally thick samples, it does not depend on their thickness. Meanwhile, in contrast to non-carbonizing materials, the thickness limit above which downward flame spread becomes impossible has been discovered in paper samples. According to the authors Suzuki and Hirano (1998), the mechanism of heat transfer and heat loss at flame spread changes with increasing paper thickness as a result of the strong influence of produced char.

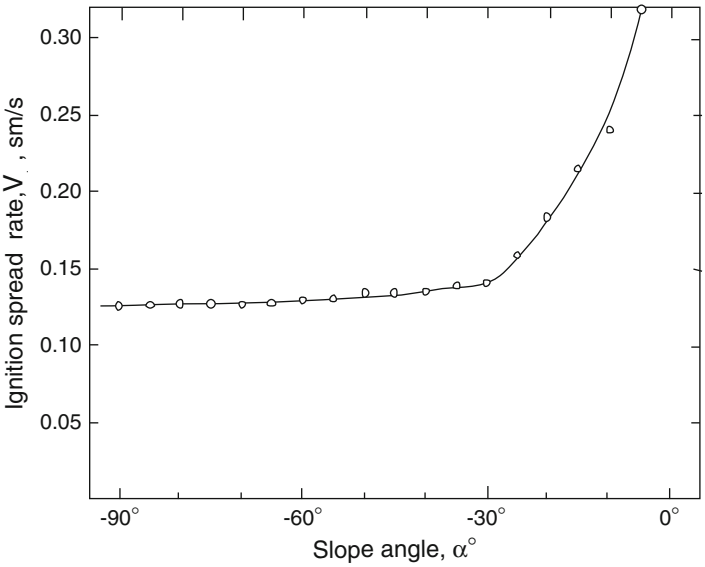

Fig. 6.2 Effect of slope angle of a paper sample on ignition spread rate

Flame spread over the surface of timber materials is a very complex process. Modeling and theoretical examination of different aspects of the process are extremely important for understanding its mechanism and the factors determining the fire growth in timber buildings.

6.2 Flame Propagation on Timber Surface Toward the Direction of Oxidizer Flow

The majority of early theories of flame spread over a solid inflammable material surface dealt with analysis of the diffusion process on the assumption of fast chemical reaction rate in the gas phase. However, the attention should be paid to materials that do not generate carbon residue during pyrolysis, but are completely decomposed into volatile vaporizable substances. Flame spread over the surface of materials was more often considered in configuration with opposed flow of oxidizing gas, as it is experimentally easier to study the process in this case than in the configuration with concurrent air flow. In order to prove the reasonableness and predictive ability of this theoretical model, the calculation results are generally compared to the relevant experimental data.

A critical review of papers on the theory and modeling flame spread over the surface of different materials toward air flow was made in historical chronology in study Wichman (1992).

In principle, approaches to solving this problem may be divided into two categories. (1) Use of models based on a number of assumptions and simplifications of actual physical and chemical processes. This allows to obtain analytical ratios and formulas for calculating flame spread rate depending on properties of the material and external conditions. (2) Use of more advanced models that partially remove some approximations. These models are based on a description of physical and chemical processes by a set of partial differential equations. They allow for the balance of energy, movement and mass of substances, macrokinetics of reactions in gas and solid phases, and relevant boundary conditions. This system of equations is solved numerically, but not analytically. However, this allows one to predict flame spread in approximation to specified actual situations.

Different methods of calculating partial differential equations are summarized in the book Bulgakov et al. (1990).

The first category of analytical determination of flame spread rate over the surface of materials includes the fundamental work of de Ris (1969). The process of laminar diffused flame spread over a horizontal surface of materials toward air flow is presented as a partly idealized situation.

It is assumed that the material is completely decomposed, generating combustible gases and vapors when the specific decomposition temperature on the surface, T_v, constant for this material is reached. Thermal properties of the material and gas phase do not depend on temperature. Released ignitable vapors instantly react with oxygen which inflows from incoming air flux to the flame zone. Meanwhile, the oxidizer flow rate is assumed to be constant for flame height (homogeneous flow profile according to Oseen is assumed). Heat is released due to a global reaction of second-order inflammable gas combustion. But flame rate is controlled by the process of heat transfer from the flame to the primary material section adjacent to the pyrolysis front, the heating of which ensures the required supply of fuel to the combustion reaction zone. A lot of attention was paid to the mechanism of heat transfer from the flame to the surface. All of the chemistry of the process is actually reflected in the adiabatic stoichiometric flame temperature, T_f, and "evaporation" temperature, T_v. Diffused flame lies on the surface of the material. The flame spread process is considered to be stationary due to the use of moving coordinates. The oxidizer rate profile used makes it possible to exclude the equation of motion from analysis of the equation of motion and simplify the solution. Formulas connecting the flame spread rate over the surface with the thermophysical properties of the material and its thickness, rate of incoming air flow, and respective temperatures of flame and condensed fuel decomposition were obtained.

The rate of flame spread over thermally thin materials is determined by the following equation:

$$V_{fs} = \frac{\sqrt{2}k_g\,(T_f - T_v)}{\rho_s c_{ps}\tau\,(T_V - T_0)}$$

where k_g – thermal conductivity of the gas phase and τ – sample thickness.

Rate of flame spread over thermally thick materials:

$$V_{\mathrm{p}\Pi} = \frac{V_{\mathrm{a}}\rho_{\mathrm{g}}c_{\mathrm{pg}}k_{\mathrm{g}}(T_{\mathrm{f}} - T_{\mathrm{V}})^2}{\rho_{\mathrm{s}}c_{\mathrm{ps}}k_{\mathrm{s}}(T_{\mathrm{V}} - T_0)^2}.$$

where V_{a} – rate of incoming air flow and subscripts g and s specify the gas and solid phases, respectively.

As follows from these formulas, flame spread rate depends on thickness in the case of thermally thin samples, and does not depend on thickness, but is directly proportional to the rate of incoming oxidizer flow in the case of thermally thick materials.

The multiplier $\sqrt{2}$ in the formula for the rate of flame spread over thermally thin materials was clarified later. It was shown that it should be equal to $\pi/4$ (Wichman 1992).

During simulation of flame spread over the surface of materials, the simplest homogeneous profile of incoming oxidizer flow in Oseen's approximation is most commonly used in order to simplify solution of the mathematical problem. However, the profile type has an effect on flame spread rate and flame structure (Wichman 1992). According to Di Blasi et al. (1989), the parabolic profile of air flow according to Hagen–Poiseuille reflects the actual conditions and experimental results (De Ris 1969) better.

Equations obtained by de Ris do not reveal conditions when the role of chemical gas-phase reaction kinetics may be significant, i.e., close to ignition and extinguishing of the flaming process. In this case, theoretical analysis of flame spread is conducted with consideration of the so-called Damkohler numbers. A Damkohler number is the ratio of time scales of physical and chemical processes on ignition:

$$D_{\mathrm{a}} = t_{\mathrm{d}}/t_{\mathrm{ch}},$$

where t_{d} – diffusion time (flow transfer) and t_{ch} – chemical reaction time.

According to Zeldovich, diffusion time for generation of a hot boundary gaseous layer is

$$t_{\mathrm{d}} = k_{\mathrm{g}}/c_{\mathrm{pg}}\rho_{\mathrm{g}}{V_{\mathrm{a}}}^2,$$

and chemical reaction time is inversely proportional to its rate in the gas phase according to the Arrhenius equation:

$$t_{\mathrm{ch}} = \rho_{\mathrm{g}}/A_{\mathrm{g}}P^n Y_0 Y_{\mathrm{f}} \exp\left(-E_{\mathrm{g}}/\mathrm{RT_f}\right),$$

where A_{g} – pre-exponential factor, Y_0 and Y_{f} – oxidizer and fuel concentration, and n – general order of gas reaction by pressure, P.

A Damkohler number may vary a lot depending on the conditions (temperature, oxidizer flow rate and oxygen content, rate of component supply to reaction zone, heat loss).

Under specific conditions, the flame spread rate is controlled by the slowest processes. With low oxygen concentration or high oxidizer gas flow rate, the flame spread rate is controlled by the kinetics of chemical gas-phase reactions. The functional connection between flame spread rate and the Damkohler number is shown using the example of flame spread over a paper surface (Khalturinsky and Berlin 1989).

Analysis of a fairly simple model of flame spread over the surface of polymer materials toward oxidizer flow in Oseen's approximation considering the Damkohler number makes it possible to determine the conditions and limits of the combustion process (Aseeva and Zaikov 1981; Rybanin 1988). Similar to De Ris (1969), convective heat transfer from the flame to a neighboring section of original polymer through the gas phase and heat transfer by thermal conductivity in the condensed phase was assumed in this model.

Based on heat balance analysis e in the flame edge, the following equations of flame spread rate for a thermally thin material were obtained:

$$V_{\mathrm{fs}} \approx \left[k_{\mathrm{g}}\left(T_{\mathrm{f}} - T_{\mathrm{p}}\right)/\rho_{\mathrm{s}} c_{\mathrm{s}} \tau \left(T_{\mathrm{p}} - T_0\right)\right]\left(1 + \Omega_{\mathrm{T}} - D_{\mathrm{a}}^{-1/2}\right)$$

and for thermally thick material:

$$V_{\mathrm{fs}} \approx \left[V_{\mathrm{a}} k_{\mathrm{g}} \rho_{\mathrm{g}} c_{\mathrm{g}} \left(\mathrm{T_f}\text{–}\mathrm{T_p}\right)^2 / k_{\mathrm{s}} \rho_{\mathrm{s}} c_{\mathrm{s}} \left(T_{\mathrm{p}} - T_0\right)^2\right]\left(1 + \Omega_{\mathrm{T}}\text{–}{D_{\mathrm{a}}}^{-1/2}\right)^2,$$

where Ω_{T} – dimensionless heat loss.

The ${D_{\mathrm{a}}}^{-1/2}$ value is proportional to the ratio of flow rate in the flame edge to the rate of combustion of a stoichiometric mixture of polymer material decomposition products and environmental oxidizer. For a small value of the Damkohler number ($D_{\mathrm{a}} \approx 1$), the role of chemical reaction kinetics is great. For large D_{a} numbers, flame spread over the surface of a material is controlled by heat and mass transfer. The condition where $(1 + \Omega_{\mathrm{T}}\text{–}{D_{\mathrm{a}}}^{-1/2}) = 0$ roughly corresponds to the flame spread limit. For $\Omega_{\mathrm{T}}\text{–}{D_{\mathrm{a}}}^{-1/2} = 0$, the equations obtained are converted into equations presented by de Ris (Rybanin 1988).

The concept of Damkohler numbers for reflecting the effect of chemical reaction kinetics on flame spread was also used in Fernandez-Pello (2004). Another incoming oxidizer flow profile was taken for process analysis, and consequently this resulted in other formulas. However, they agree with the predictions of Rybanin (1988) on probable limiting conditions of flame spread.

Theoretical analysis of flame spread toward air flow is based on an assessment of a length of flame-heated section of the material surface close to the flame edge and time elapsed for ignition of this section.

The scale of heating in the lengthwise direction from the flame $\delta_H = k_{sx}\alpha_s/k_{sy}V_{fs}$ or $\delta_H = \alpha_s/V_{fs}$ for equal thermal conductivity of the sample in the lengthwise and crosswise directions. The crosswise condensed phase heat wave scale is given by

$$\delta_V = \sqrt{\alpha_s \frac{\delta_g}{V_{fs}}}$$

where δ_g – thickness of the gaseous thermal layer in the flame edge $\delta_g = \alpha_g/V_a$ and α_s and α_g – thermal conductivity of the material and gas phase, respectively. Thermally thin materials are heated through their entire thickness, τ.

The scheme of flame spread over a horizontal surface toward induced air flow used in Fernandez-Pello (2004) assumes that the length of the heated section facing the flame front is proportional to the boundary gaseous layer thickness. As it depends on the rate of incoming oxidizer flow, the equation for induced flow is as follows:

$$\delta_H \approx x\ Re^{-1/2} = C\,(x/V_a)^{1/2},$$

where Re – Reynolds number, C – constant, and x – longitudinal coordinate.

Thus, during the analysis, it is possible to consider oxidizer flow rate as a function of gradient instead of constant length of the heated section facing the flame (as was done in Rybanin 1988).

The total delay in ignition of the material surface section adjacent to the flame front is the sum of the times spent in (1) heating and pyrolysis of the material, t_p; (2) diffusion and mixing of volatile pyrolysis products with the oxidizer in the boundary layer for generation an inflammable mixture, t_{fl}; and (3) induction time before its ignition, t_{in}. Thus, we have $t_{ign} = t_p + t_{fl} + t_{in}$.

Considering that $t_{fl} \ll t_p$, the author obtained analytical expressions for the rate of flame spread over the surface of materials toward an induced air flow for thermally thick and thin materials (Fernandez-Pello 2004). In particular, the rate of flame spread over the surface of thermally thick materials is described by the following equation:

$$V_{fs} = \left[\left\{\pi k \rho_s c_s (T_p - T_0)^2 (V_a/x)^{1/2}/4C_3\left[C_1\left(k_g \rho_g c_{pg} V_a/x\right)^{1/2}(T_f - T_p) - q''_{sr} + q''_{fr} + q''_e\right]^2\right\} - C_4 (x/V_a)^{1/2} \ln\,(1 - D_{a_{cr}}/D_a)\right]^{-1},$$

and for thermally thin materials, the following equation is obtained:

$$V_{fs} = \left[\left\{\rho_s c_s \tau\,(T_p - T_0)\,(V_a/x)^{1/2}/\left[C_1\left(k_g \rho_g c_{pg} V_a/x\right)^{1/2}(T_f - T_p) - q''_{sr} + q''_{fr} + q''_e\right]\right\} - C_4 (x/V_a)^{1/2} \ln\,(1 - D_{a_{cr}}/D_a)\right]^{-1}.$$

Here, $D_{a_{cr}}$ and D_a correspond to critical and characteristic values of Damkohler numbers; $C_{1–4}$ are numeric constants.

The denominator of first member of the equation given in brackets expresses heat flow toward the material surface for laminar-induced oxidizer flow. It is made up of external heat flux, q''_e, heat flux from the flame by radiation, q''_{fr}, and convective heat transfer including the air flow rate gradient, and radiation heat loss from the material surface, q''_{sr}.

The characteristic Damkohler number for the process conditions of interest for laminar-induced oxidizer flow is determined by the ratio:

$$D_a = t_d/t_{ch} = A_g \Delta H_{cg} \rho_g W_0 E Y_0 Y_f \exp(-E/RT_f)/c_{pg} RT_f^2 (V_a/x),$$

where ΔH_{cg} – combustion heat of combustible gases.

For constant length of the section heated by the flame ($\delta_H = \text{const}$), the equation for flame spread rate in the mode controlled by heat transfer from the flame becomes similar to de Ris' formula. In this mode, V_{fs} over the surface of thermally thick materials increases with the increase in V_a, because the reverse air flow presses the flame closer to the material surface and thereby intensifies heat transfer from the flame to solid fuel and its gasification rate.

In the mode controlled by gas reaction kinetics, a decrease in V_{fs} with an increase in reverse air flow rate is observed. Finally, for $D_a \approx D_{a_{cr}}$, the rate of flame spread over the surface of the material decreases, and damping of this process takes place.

The damping limit may result from both significant air flow rate and low reagent content in the flaming reaction zone. At very high values of D_a ($D_a \to \infty$), flame spread over the surface of the material toward the oxidizer flow occurs in the mode controlled by heat transfer from the flame. Experimentally observed limit of diffused combustion for high D_a and oxidizer flow rates is determined by flame disruption by this flow.

In any case, the thermophysical and thermochemical properties of the material have a significant effect on the rate of this process, regardless of material thickness and flame spread conditions.

During a simulation of flame spread over the surface of carbonizing polymer materials, complex chemical processes that usually occur during timber pyrolysis, for example, were barely taken into consideration. These materials were considered as homogeneous systems. Their decomposition was described by a single-stage reaction with generation of gross volatile products, G, and carbon residue, C, according to the scheme:

$$\text{Solid polymer S} \to \nu_g G + \nu_c C,$$

where ν_g and ν_c are stoichiometric factors of the material's decomposition reaction.

The polymer pyrolysis kinetics conform to the first-order Arrhenius equation. Meanwhile, the properties of a nonstationary charring system were rated as effective, changing in proportion to a change in composition from original polymer to full transformation into carbon residue. This approach during simulation of flame

spread over the surface of a material is stipulated by severe simplification of actual processes. As a rule, shrinkage, expansion, regression, or oxidation of the surface were not taken into account. It was assumed that the volume occupied by the sample did not change during its thermal decomposition. In this case, all changes in the material sample may be expressed by the density of this volume until some amount of initial mass remains in the form of carbon residue.

Decomposition products are released to the surface instantly without any obstructions.

Using this simplification of the problem, a model of flame spread over the surface of a carbonizing material downward toward the air flow was developed for assessing the influence of cellulose material thickness on the spread rate (Di Blasi 1994). A closed system (sample burning in channel) was examined. In a two-dimensional setting, nonstationary decomposition of an oxidized sample was presented in conjunction with a quasi-constant submodel of flame processes through boundary conditions on the "gas–k-phase" interphase surface. A moving coordinate system fixed along the solid matrix pyrolysis front, but not along the front flame edge, was used.

Solid-phase processes are described by conservation equations:

- Mass balance of primary polymer: $\partial\rho_s/\partial t = -K_S\rho_s$;
- Mass balance of carbon residue: $\partial\rho_c/\partial t = \nu_c K_S\rho_s$;
- Continuity: $\partial m/\partial y = \nu_g K_S\rho_s$;
- Energy balance:

$$c_s\partial\rho_s\left(T_s{-}T_0\right)/\partial t + c_c\partial\rho_c\left(T_s - T_0\right)/\partial t + c_{pg}\partial m\left(T_s - T_0\right)/\partial y = \partial/\partial x\left(k_s\partial T_s/\partial x\right) + \partial/\partial y\left(k_s\partial T_s/\partial y\right) + K_S\rho_s\Delta h_s.$$

The constant of the polymer pyrolysis reaction rate is given as

$$K_S = A_s\exp\left(-E_s/RT_s\right),$$

where Δh_s – pyrolysis heat and m – mass flow of pyrolysis products:

$$m = \int_0^y \left(\nu_g K_s\rho_s\right)\partial y$$

k_s is the polymer thermal conductivity changing along with composition due to charring according to the equation: $k_s = \eta k_a + (1-\eta)k_c$; conversion degree is determined by the change in system density $\eta = \rho_s/\rho_{so}$; k_c is the char thermal conductivity.

As it is assumed that the flow of volatile decomposition products moves to a heated surface without any resistance, the pressure in the porous matrix is considered to be constant. There is a local balance between char and gaseous polymer decomposition products.

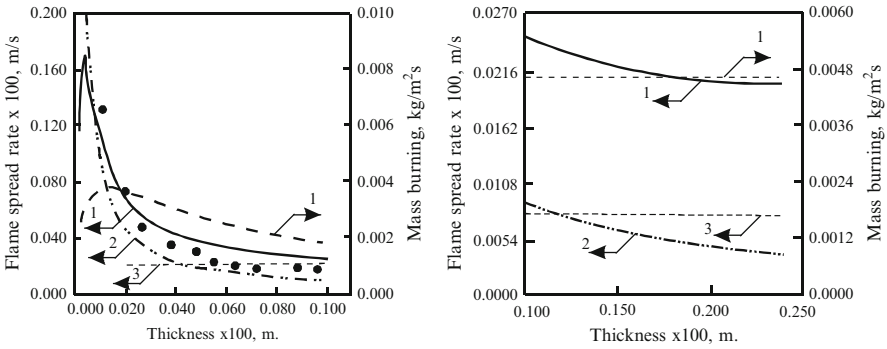

Fig. 6.3 Effect of cellulose half thickness on flame spread rate: *1* numerical simulation, *2* thermally thin sample (according to de Ris' theory), *3* thermally thick sample (according to de Ris theory), • – experimental values

In this flame spread model, gas-phase processes are described as usual by two-dimensional continuity, conservation of substance mass, energy, impulse equations, and state equation. It was assumed that thermophysical properties of the gas phase are constant. Inflammable gases burn according to a single-stage second-order reaction by the Arrhenius equation. The heat generation rate resulting from this reaction is $q = w_i \Delta H_c$. A parabolic profile of incoming air flow with maximum rate $V_a = 0.30$ m/s, which corresponds to the rate induced by natural convection, was assumed.

The following parameters of cellulosic material and produced char were used in calculating flame spread characteristics: $\rho_s = 650$ kg/m^3; $c_s = 1.46$ kJ/kg·K; $c_c = 1.1$ kJ/kg·K; $k_s = 10.5 \times 10^{-2}$ W/m·K; $k_c = 7.1 \times 10^{-1}$ W/m·K; $\nu_g = 0.5$; and $\nu_c = 0.5$. Kinetic parameters of pyrolysis reaction: $A_s = 2.5 \times 10^{10}$ c^{-1}; $E_s = 142.12$ kJ/mol gasification heat $\Delta h_s = -418$ kJ/kg.

Gas-phase properties are equated with air properties: $k = 25.7 \times 10^{-3}$ W/m·K; $\rho D = 4.4 \times 10^{-5}$ kg/ms; and $\mu = 5 \times 10^{-5}$ kg/ms. Kinetic parameters of combustion reaction: $A = 0.313 \times 10^{10}$; $E = 112.86$ kJ/mol; and combustion heat $\Delta H_c = -16{,}720$ kJ/kg.

The role of chemical kinetics in flame spread was tested by increasing the pre-exponential factor A in the Arrhenius equation by 2 orders for the k-phase and by 2 and 6 orders for the flaming reaction. Numerical simulation revealed three basic modes of flame spread over the surface of a charring material with a change in its thickness (Fig. 6.3).

The first regime was predicted for very thin materials ($\tau < 0.004 \times 10^{-2}$ m) for the first time. It is characterized by an increase of flame spread rate with an increase in the sample thickness. The mode is controlled by gas-phase chemical kinetics. In the opinion of the author Di Blasi (1994), it may be proven experimentally only under microgravity conditions. The oxidizer flow rate is low only in this case. Heat loss from the material surface due to radiation may play a significant role.

The second mode for thermally thin materials ($0.005 \times 10^{-2} < \tau < 0.22 \times 10^{-2}$ m) is characterized by reduction of the rate of flame spread over the surface of the material as its thickness increases, which qualitatively conforms to de Ris' thermal theory and has been proven experimentally. The mechanism of flame spread in this mode is controlled by heat transfer from the flame via the gas phase by means of thermal conductivity.

Finally, after some thickness limit is achieved, the third mode is observed – a thermally thick material with constant flame spread rate for a given V_a value. In this mode, heat transfer from the flame to a neighboring section of the original material includes heat transfer through the k-phase. However, its contribution to the total heat transfer does not exceed 50 %. Char layer generation slows down the heat transfer into the depth of the polymer sample. Heat losses from the surface of charring material are significant in the first mode, reduced to a minimum in the second mode and increase again when the thermally thick material mode is established.

The transition from the second to the third mode according to numerical simulation occurs when the sample thickness is five times as great as the calculation according to de Ris' formula predicts ($\tau = 0.0427 \times 10^{-2}$ m).

It has been established that an increase in pre-exponential factor values in the Arrhenius equation for the cellulose pyrolysis reaction results in an increase in mass flow of pyrolysis products, but reduces the temperature of the material surface due to endothermicity of this process. At the same time, the increase in inflammable volatile content in the gas phase increases flame temperature, flame rate, and spread. Within a very high gas flame rate, when the pre-exponential factor value in the flaming reaction kinetics equation is increased by 6 orders of magnitude, the qualitative dependence of spread rate on sample thickness becomes the same as predicted by de Ris' theory.

A change in charring sample thickness affects the flame structure. The flame size during combustion of very thin samples is also small, and the temperature of the sample's adiabatic combustion from $\tau = 0.0025 \times 10^{-2}$ m reaches only 2,020 K. As the sample thickness increases, the flame size becomes noticeably larger. The highest rate of flaming reactions and thus flame temperature (2,700 K) is observed in the second sample thickness mode. After that, due to carbonization of the surface layer in thermally thick samples, the mass flow of inflammable products is reduced, and the gas-phase reaction rate and flame temperature are slightly reduced: at $\tau = 0.5 \times 10^{-2}$, it is equal to $T_f = 2{,}500$ K (Di Blasi 1994).

Theoretical analysis and numerical calculation of the flame spread toward air flow over a horizontal surface of thermally thick material samples charring on combustion, like timber and cellulose, were conducted in studies Atreya and Baum (2002), Baum and Atreya (2005), Park et al. (2007). The proposed model of stationary flame spread is represented by the scheme in Fig. 6.4 (Atreya and Baum 2002).

Here, the beginning of the coordinate system is fixed by the front edge of the flame front, the motion of which is kept constant due to the introduction of solid fuel into the flame with the appropriate spread rate. Actually, the principle of flame

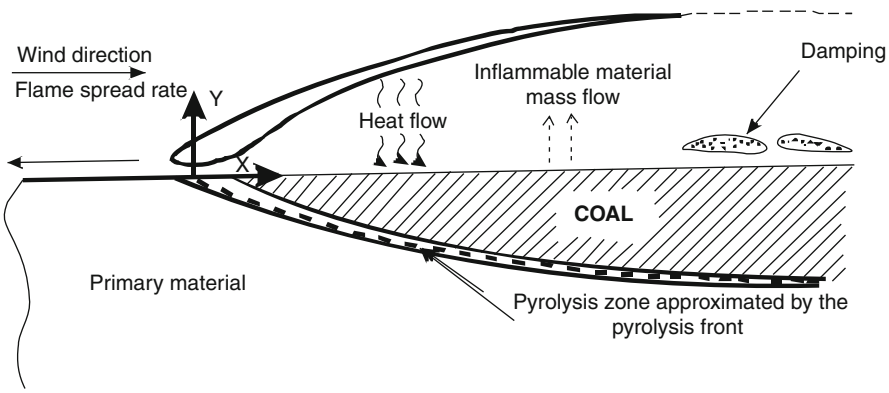

Fig. 6.4 Scheme of flame spread toward air flow over a horizontal surface of carbonizing material. *Dashed lines* indicate chemical reaction zones in flame and k-phases

spread simulation according to de Ris' scheme is used (De Ris 1969), where the initial position of the flame front and the start of material pyrolysis coincide.

The instantaneous decomposition of a solid matrix along with generation of volatile inflammable products and char on reaching temperature T_p is assumed. Originally (Atreya and Baum 2002), it was assumed that the generated char had no effect on transport of inflammable volatile products from the pyrolysis zone to the surface heated by the flame (principle of constant pressure in the k-phase). The temperature of the charred surface was considered constant. A diffused flame that expands from the zero point at $y > 0$ is formed as the result of a rapid inflammable gas oxidation chemical reaction. A parabolic profile of the opposing air flow is assumed. Heat generated in the flaming reaction and required for thermal decomposition of solid fuel after generation of the char layer is transferred via thermal conductivity through this layer and the interphase surface into the original polymer. Its profile is also expressed in a parabolic coordinate system:

$$\tau + \mathrm{i}\omega = \sqrt{\frac{2V_{\mathrm{fs}}}{\alpha_{\mathrm{bI}}}(x + \mathrm{i}y)}$$

where τ and ω are parabolic coordinates the in x and y directions.

The location of the interphase surface is determined by carbonization constant, c:

$$\left(\frac{V_{\mathrm{FS}}y}{\alpha_{\mathrm{S}}}\right)^2 = C^2 + 2C + \left(\frac{V_{\mathrm{FS}}x}{\alpha_{\mathrm{S}}}\right)^2,$$

which in turn depends on solid-phase properties.

According to the model developed in Atreya and Baum (2002), two-dimensional equations describing conservation of fuel mass and its separate components, as well as energy in the gas phase ($y \geq 0$), are examined in conjunction with heat balance

equations for the k-phase ($y \leq 0$) separately for the original material:

$$\frac{\partial T_S \rho_S V_{FS} c_S}{\partial x} - k_S \left(\frac{\partial^2 T_S}{\partial x^2} + \frac{\partial^2 T_S}{\partial y^2} \right) = 0,$$

For $-\infty < x \leq c$ and for char layer:

$$\frac{\partial T_c \rho_c V_{fs} c_c}{\partial x} - k_c \left(\frac{\partial^2 T_c}{\partial x^2} + \frac{\partial^2 T_c}{\partial y^2} \right) = 0, \text{при } c \leq x \geq \infty$$

Thus, the lengthwise areas under and above the char–original polymer interphase surface were analyzed.

Boundary conditions define equality of temperatures at the phase boundary: gas–char and char–original polymer for $x > 0$, absence of heat exchange between the gaseous medium and solid matrix through plane $y = 0$ in front of the flame at $x < 0$.

The energy balance condition in the below flame area on the gas–char surface ($x \geq 0$) is:

$$\frac{q''}{\sqrt{x}} = -\frac{k_g \partial T_g}{\partial y} - \frac{k_c \partial T_c}{\partial y},$$

where q'' – heat flow from the flaming reaction zone (i.e., heat generation rate), considering the above-mentioned equations, allows to determine the rate of flame spread over the surface of timber or cellulosic material.

Analytical solution of the model resulted in the following equation for the rate of flame spread over carbonizing polymer material toward an air flow with a homogeneous profile:

$$V_{fs} = V_a \frac{k_g \rho_g c_g}{k_c \rho_c c_c} \left(\frac{T_f - T_c}{T_c - T_p} \text{erf} \frac{\sqrt{\delta_c}}{2} c \right)^2$$

where $\delta_c = \alpha_s / \alpha_c$ – ratio of original polymer and char thermal diffusivity; T_f, T_c, T_p – temperature of flame, carbonizing surface, and pyrolysis of the material, respectively; and c – constant defining the location of the char–original polymer interphase surface (i.e., char thickness).

In the absence of a char layer $c \to 0$ for a non-carbonizing polymer ($T_c \to T_p$), the equation obtained is transformed into de Ris' formula.

Later on, the authors Baum and Atreya (2005), Park et al. (2007) made the physical model of flame spread over carbonizing materials more complicated. They included transport of inflammable gases through pores in the char layer by onset of a pressure gradient according to Darcy's law, numerically analyzed the effect of the chemical pyrolysis reaction rate on char layer thickness, and temperature distribution in the char layer and original polymer.

The following typical characteristics of timber materials were used in the calculation: density of final char $\rho_c = 140$ kg/m^3 and original polymer $\rho_s = 700$ kg/m^3; thermal conductivity for char $k_c = 0.071$ W/m · K and original material $k_s = 0.209$ W/m · K; and specific heat for char $c_c = 1.1$ kJ/kg · K and $c_s = 1.4$ kJ/kg · K. Temperature of the environment $T_0 = 298.16$ K, pyrolysis $T_p = 598.16$ K and charring surface $T_c = 1{,}298.16$ K. Pyrolysis heat is equal to 497.3 J/g. Char permeability was considered equal to 1×10^{-13} m^2 with porosity of 0.8, but the original solid matrix was assumed to be impermeable (Park et al. 2007).

In order to assess the condition of the fast chemical pyrolysis reaction compared to heat transfer in the k-phase, high values of pre-exponential and activation energy in the Arrhenius equation for mass pyrolysis rate ($A = 1 \times 10^{24}$ s^{-1}; $E_s = 288$ kJ/mol) were assumed for the calculation.

It was established that for $V_{fs} = 0.001$ m/s (typical for the rate of flame spread over a wood surface in air) away from the diffused flame front, the char layer thickness increased and the inflammable gas generation rate decreased. This may result in complete cessation of the flame spread process.

Calculations have revealed that gas pressure increases with char layer and pyrolysis zone thickness. Even for a high material decomposition rate, the width of the pyrolysis zone is considerable. Pressure fluctuation in the char layer is observed. It is especially obvious close to the char–original material interphase surface.

Formation of pressure inside the charring material plays an important role in transport of inflammable decomposition products. It causes damage to building structures due to the formation of cracks in the carbonized layer and further destruction of separate structural elements of timber in a fire.

6.3 Flame Propagation on Timber Surface at Passing Direction of Oxidizer Flow

Concurrent air flows are achieved during flame spread over the surface of building structural elements mounted in vertical (flame spreads over the walls in the upward direction) or horizontal (flame spreads under the ceiling) configurations. In this case, the rate of flame spread over the surface of organic materials may be very significant. Thus, this flame type represents a great fire hazard. The situation is complicated by the fact that even in case of natural convection only, laminar flows easily grow into turbulent flows, which means an increase in fireplace size. Under these conditions, heat transfer by radiant energy plays an important role in the heat exchange process between the flame and the surface of the material.

The first attempt to examine flame spread over the surface of a thermally thick carbonizing material with concurrent induced oxidizer flow theoretically is presented in Carrier et al. (1983). The authors presented a model of flame spread over a horizontal surface of carbonizing material that is structurally the ceiling of any premises (a room or a long corridor).

The description of the complex physical processes is based on a number of assumptions. For example, it was assumed that the profile of induced air flow is homogeneous and pyrolysis of the material with generation of porous char and instantaneous evaporation of volatile products proceeds at a fixed temperature in a thin layer on the char–original material interphase surface. The spatial location of the boundary between char and original polymer material changes with time. Char and polymer have different densities and different thermal properties. Study Carrier et al. (1983) was focused on development of combustion according to thickness of the material. The analysis included potential processes of char surface erosion due to either its sublimation on reaching some temperature or a heterogeneous interaction between char carbon and carbon dioxide – the gaseous product of polymer decomposition or combustion of inflammable products in the gas phase. Processes in the gas phase should ensure heat flow to gas-carbonizing material interphase surface, the conditions of which are important for assessing flame spread rate.

Although study Carrier et al. (1983) includes thorough mathematical analysis of many important aspects of flame spread over the surface of carbonizing material under concurrent air flow, it does not provide enough clarity for understanding the carbonization process and its significance for flame spread over a polymer surface.

Experimental and theoretical studies of flame spread over the surface of non-carbonizing materials in vertical configuration with concurrent oxidizer flow showed that the dependence of flame spread rate was directly proportional to the free oxidizer flow rate. A weak power law dependence of flame spread rate on time and size of the pyrolysis zone was discovered in air without induced flows (under natural convection conditions): $V_{fs} \sim t^{m} \sim {l_p}^{n}$.

It should be noted that due to the complexity of flame spread over a surface with concurrent oxidizer flow, its modeling was limited to conditions controlling only heat transfer and mass transfer of reagents without regard to the effect of chemical kinetics.

Figure 6.5 shows a scheme of flame spread over a vertical surface of a material, including a carbonizing material, with concurrent oxidizer flow (Delichatsios et al. 1991; Delichatsios and Saito 1991).

Total heat flux q_t'' supplied to the surface of the material includes external radiant heat flow, q_e'', and the flow from a flame with radiation, q_r'', and convection, q_c'', components.

It is possible to identify three important areas taken into account during simulation of the flame spread process. (1) flaming reaction area with flame length from lower edge to flame front, i.e., its tip, Z_f; (2) region where the material sample surface is preheated from the flame in area δ_f to the pyrolysis (ignition) front: $\delta_f = Z_f - Z_p$; and (3) material pyrolysis region with length Z_p.

Accordingly, integral one-dimensional models of heating and transient pyrolysis of similar material as well as some empirical correlations for heat flow spread from the flame were used to simulate this type of flame spread over the surface of carbonizing material. It is assumed that beyond its height the flame does not influence material surface heating.

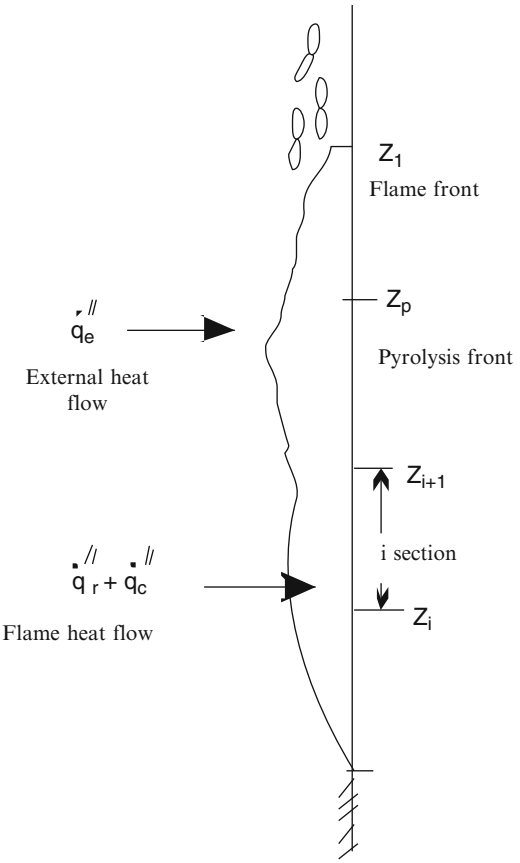

Fig. 6.5 Scheme of flame spread over a vertical surface under concurrent oxidizer flow direction and external heat flow

Flame spread rate may be represented as follows:

$$\mathrm{d}Z_\mathrm{p}/\mathrm{d}t = (Z_\mathrm{f} - Z_\mathrm{p})/t_\mathrm{p} = \delta_\mathrm{f}/t_\mathrm{p},$$

where $t_\mathrm{p} = t_\mathrm{ign}$ – period of time prior to ignition. Its dependence on thermophysical properties of the material and supplied heat flux is known (see the relevant chapter in the book on ignition of timber materials).

Flame length is dependent on heat generation rate per unit of material sample width, Q', through a power law dependency:

$$Z_\mathrm{f} = a\left(Q'\right)^n \quad \text{or} \quad Z_\mathrm{f} = a\left(Q'Z_\mathrm{p}\right)^n.$$

The laminar flame exponent is equal to $n = 2$, and to $n = 2/3$ for turbulent flame (Quintiere 2006). Thus, the study of the upward spread turbulent flame over a vertical surface of large slabs made of timber materials established the correlation between flame height and total rate of heat generation per unit of material sample

width (Delichatsios and Chen 1994):

$$Z_f = 0.052 \left(Q'\right)^{2/3}, (\mathrm{m}),$$

where Q' is expressed in kW/m.

The characteristic length to which the flame spreads upward over a vertical surface of thermally thick material under concurrent air flow and taking into account the effect of its carbonization is calculated according to the equation (Delichatsios and Chen 1994):

$$Z_f = \left(\frac{1}{\rho_\infty} \rho_\infty c_\infty T_\infty \sqrt{g}\right)^2 \left(q''_{net} \chi \frac{\Delta H_c}{\Delta H_v}\right)^2 \frac{(1+\lambda)\, d_c}{\delta_v}$$

The first set of brackets represents environments parameters, and g is gravity. q''_{net} is heat flow to the surface minus heat loss. ΔH_c is complete combustion heat of the material, χ is combustion efficiency. ΔH_v is gasification heat: $\Delta H_v = L + c(T_p – T_\infty)$ and $\lambda = L/c(T_p – T_\infty)$; δ_v is the thickness of the heated layer in the original material: $\delta_v = k_v(T_p – T_\infty)/q''_{net}$; δ_c is the char layer thickness: $\delta_c = k_c\ T^*/4q''_t$. Accordingly, k_v and k_c are thermal conductivity for the original material and char; T^* is the maximum temperature of the surface at which supplied heat flow is equal to heat flow lost due to energy emission from the heated surface:

$$T^* = \left(q''_t/\sigma\right)^{1/4}, \quad \text{if } \varepsilon = 1.$$

The methodology of determining key parameters required for numerical simulation of flame spread over the surface of carbonizing materials is presented in Delichatsios and Saito (1991).

Existing modern methods for testing combustible material characteristics, including large-scale tests, allows to determine heat generation rate, effective combustion heat, surface temperature, pyrolysis front spread, and other parameters. A comparison of test results with the data obtained from numerical models proves the adequacy and reliability of these models.

A new study Weng and Hasemi (2008) in which a numerical model of flame spread over the surface of carbonizing materials under concurrent air flow is presented is of great interest. It examines the problem of flame spread over the surface of construction materials in horizontal and vertical configurations (ceiling, wall). The model includes one-dimensional submodels of flame spread and nonstationary pyrolysis. The calculation predicts different characteristics of this process, including confirmation of its sensitivity to external heat flow exposure that was experimentally discovered earlier (Delichatsios et al. 1994) (Fig. 6.6).

It is evident that an increase in external heat flow intensity results in a considerable increase in flame spread rate. This is due to an increase in initial temperature of the surface, reduction of time before the start of pyrolysis and an increase in mass loss rate.

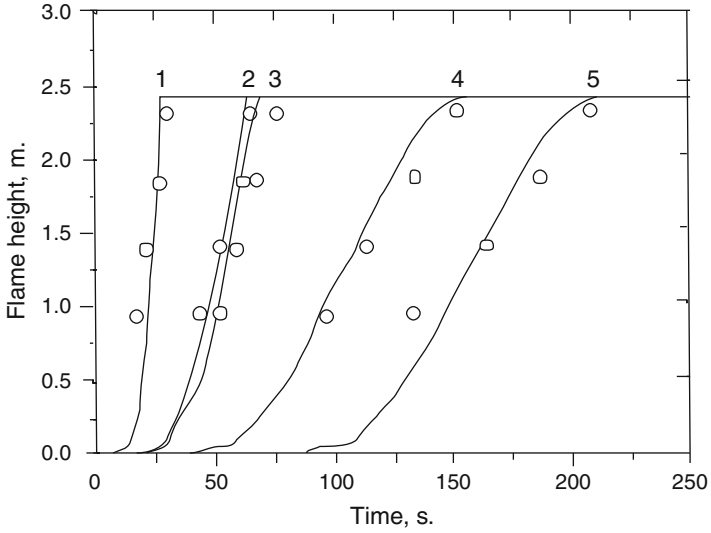

Fig. 6.6 Effect of external radiative heat flow on flame spread over a vertical surface of thick slabs made of fir plywood with concurrent air flow (— calculation, ∘ – experiment); q''_e, kW/m^2: *1* 4.8, *2* 5.2, *3* 7.0, *4* 7.5, *5* 11.0

Cessation of flame spread over the surface of materials in the most rigid conditions presented with concurrent air flow is possible if heat flow from the flame facing the pyrolysis front is less than critical for this material. These conditions are achieved when flame height is reduced and becomes almost equal to pyrolysis length: $Z_f = Z_p$.

Studies of critical issues of diffused combustion of different polymer materials (Rybanin 1988; Krupkin 1993) lead to the conclusion that flame spread limits are first of all determined by ability of the material to provide the flame with a sufficient amount of combustible substance, as well as heat loss from different zones of the burning material.

In contrast to flaming combustion, the factors determining the rate of smoldering combustion spread over the surface of natural wood have not been studied.

The only available information on this issue was Ohlemiller (1991). In this study, wood samples (white pine and red oak) in the form of right-angled U-channels 74 cm long were placed sideways in the horizontal position in a chamber with a controlled air supply of 8–22 cm/s (calculated from the channel's internal cross section). The bottom and walls of the channel were made of two wooden slabs each 3.2 cm thick that were stuck together. The slabs' sidewalls were 11.4 cm thick, and the channel bottom was 20.3 cm wide. Thus, the size of the section between the channel walls was 5.1 × 11.4 cm.

In order to initiate smoldering combustion, an electric heater 12 cm long was used. It was removed as soon as smoldering started. Development of smoldering was monitored visually over several hours. By installing an element initiating smoldering at the beginning of the channel along its bottom on the air supply side,

smoldering mode with concurrent oxidizer flow could be implemented. By installing it at the opposite end, combustion wave spread mode with opposite oxidizer flow could be implemented. Finally, by installing the electrical element in the center of the channel, both types of smoldering wave spread could be observed.

Initiation of smoldering combustion of wood under the given conditions took a long time (∼ up to 1.5 h). As soon as smoldering had been initiated, as confirmed by the appearance of a glow on the surface, the process developed in two directions: lengthwise and through the thickness of the sample. In the latter case, smoldering was accompanied by the formation of cracks in the char layer that, in turn, affected the smoldering wave spread rate and the range of results. The rate of smoldering wave spread along the internal surface of wood in the channel under an air flow of 9–22 cm/s was nearly constant. With concurrent air flow, it increased from 1.8 to 6.2 cm/h. With air flow of about 8 cm/s smoldering petered out, and with air flow greater than 22 cm/s, the transition to flaming combustion mode was observed. The effect of wood species was not discovered due to experimental data scatter.

With concurrent air flow, the rate of smoldering wave movement over the surface of the wood changed from 1.8 to 6.2 cm/h, and maximum smoldering temperature increased from ∼450 to 650 °C as the air flow rate increased, regardless of the wood species. The author Ohlemiller (1991) concluded that heat transfer by radiation from oxidizing char, rather than restrictions of oxidizer supply, dominate in smoldering spread over a wood surface for this type.

When the smoldering wave was directed toward the air flow, the rate of smoldering spread remained almost constant at 12–18 cm/s, as well as the maximum temperature of smoldering in this area (∼480–500 °C). In the opinion of the author Ohlemiller (1991), this situation resulted from synchronous contribution of leading smoldering zone convection cooling to total heat transfer.

In order to clarify the relative effect of different factors on smoldering process dynamics, a model examining the balance of heat generation and sinks in a fairly thin char surface layer was proposed. Thus, a nonvolatile carbonized product of thermal and thermo-oxidative decomposition that is more porous than the original natural timber serves as main source of smoldering combustion of timber.

The model points to the main role of heat transfer by radiation from the char layer in the ability of timber to smolder under the studied conditions.

Meanwhile, it is interesting to note that a constant rate of smoldering wave spread over the surface of timber in the absence of external heating is close to the timber charring rate under the conditions of standard temperature fire regime.

References

Abduragimov IM, Androsov AS, Isaeva LK, Krylov EV (1984) In: IM A (ed) Combustion processes. Higher Engineering Fire-Service Technical School of the USSR, Moscow, 209 p

Aleksashenko AA, Koshmarov YA, Molchadsky IS (1982) Heat and mass transfer during fire. Stroyizdat, Moscow, 175 p

Aseeva RM, Zaikov GE (1981) Combustion of polymeric materials. Science, Moscow, 280 p
Astapenko VM, Koshmarov YA, Molchadsky IS, Shevlyakov AN (1988) Thermogas dynamics of indoor fires. Stroyizdat, Moscow, 448 p
Atreya A, Baum HR (2002) A model for opposed flow flame spread over charring materials. Proc Combust Inst 29:227–236
Baum HR, Atreya A (2005) Transport of gases in charring solids. In: Proceedings of 4th joint meeting of the U.S. Sections of the Combustion Institute, E01
Bulgakov VK, Kodolov VI, Lipanov AV (1990) Polymeric material combustion modeling. Chemistry, Moscow, 240 p
Carrier G, Fendell F, Fink S (1983) Towards wind-aided flame spread along a horizontal charring slab: the steady – flow problem. Combust Sci Technol 32:161–209
De Ris JN (1969) Spread of a laminar diffusion flame. In: Proceedings of 12-th symposium (international) on combustion. The Combustion Institute, Pittsburg, pp 241–252
Delichatsios MA, Chen Y (1994) Flame spread on charring materials: numerical predictions and critical conditions. In: Proceedings of the fourth international symposium on fire safety science, Ottawa, Canada, pp 457–468
Delichatsios MM, Saito K (1991) Upward fire spread: key flammability properties, similarity solution and flammability indices. In: Proceedings of the 3-rd international symposium on fire safety science, Edinburgh, UK, pp 217–226
Delichatsios MM, Mathews MK, Delichatsios MA (1991) An upward fire spread and growth simulation. In: Proceedings of the 3-rd international symposium on fire safety science, Edinburgh, UK, pp 207–216
Delichatsios MM, Wu P, Delichatsios MA, Lougheed GD, Crampton GP, Qiann C, Ishida H, Saito K (1994) Effect of external radiant flux on upward fire spread: measurements on plywood and numerical predictions. In: Proceedings of the 4-th international symposium on fire safety science, Ottawa, Canada, pp 421–432
Di Blasi C (1994) Processes of flame spreading over the surface of charring fuels: effects of the solid thickness. Combust Flame 97:225–239
Di Blasi C, Crescitelli S, Russo G, Fernandez-Pello AC (1989) On the influence of gas velocity profile on the theoretically predicted opposed flow flame spread. Combust Sci Technol 64:289–294
Fernandez-Pello AC (2004) Modelling flame spread as a flame induced solid ignition process. In: Bradley D, Drysdale D, Molkov V (eds) Proceedings of 4th international seminar on fire and explosion hazards. Ulster, Northern Ireland, UK, pp 13–26
Hirano T, Noreikis SE, Waterman TE (1974) Postulation of flame spread mechanisms. Combust Flame 22:353–363
Khalturinsky NA, Berlin AlAl (1989) Polymer combustion. In: Jellinek HHG (ed) Degradation and stabilization of polymers, vol 2. Elsevier, New York, chapter 3, pp 145–294
Krupkin VG (1993) Critical phenomena during diffuse combustion. Abstract of doctoral dissertation. The Institute of Chemical Physics, RAS, Moscow
Merryweather G, Spearpoint MJ (2010) Flame spread measurements on wood products using the ASTM E 1321 LIFT apparatus and a reduced scale adaptation of the cone calorimeter. Flame Mater 34(3):109–136
Newman JS, Tewarson A (1991) Flame spread behavior of char-forming wall/ceiling insulating materials. In: Proceedings of 3-rd international symposium on fire safety sciences, Edinburgh, Scotland, pp 679–688
Ohlemiller TJ (1991) Smoldering combustion propagation on solid wood. In: Proceedings of the third international symposium on fire safety science. Elsevier Applied Science, London, pp 565–574
Park WC, Atreya A, Baum HR (2007) Numeric study of opposed –flow flame spread over charring solids. Proc Combust Inst 31:2643–2652
Quintiere J (1985) Some factors influencing fire spread over room lining and in the ASTM E84 tunnel test. Fire Mater 9(2):65–74
Quintiere JG (2006) A theoretical basis for flammability properties. Fire Mater 30:175–214

Rybanin SS (1988) Non-one-dimensional theory of the combustion of macroheterogeneous systems. Thesis for doctoral dissertation, Institute of Chemical Physics, USSR Academy of Sciences, Chernogolovka, 36 p

Serkov BB (2001) Fire safety of polymeric materials, combustibility reduction and standardization of their fire-safe use in construction. Thesis of doctoral dissertation, SFS Academy, Moscow, 49 p

Suzuki M, Hirano T (1998) A study of flame spread over charring materials. In: Molkov V (ed) Proceedings of the 2-nd international seminar on fire and explosion hazard and venting of deflagrations. All-Russian Research Institute for Fire Protection, Moscow, pp 249–254

Weng WG, Hasemi Y (2008) A numerical model for flame spread along combustible flat solid with charring material with experimental validation of ceiling flame spread and upward flame spread. Fire Mater 32:87–102

White RH, Dietenberger MA (2002) Fire safety. In: Wood handbook – wood as an engineering material. US Department of Agriculture, Forest Products Laboratory, Ch. 17

Wichman IS (1992) Theory of opposed-flow flame spread. Prog Energy Combust Sci 18:553–593

Chapter 7
Generation of Smoke and Toxic Products at Fire of Timber

Abstract This chapter outlines the main chemical and physical characteristics of fire behavior of solid timber such as generation of smoke and toxic products at smoldering and flame burning and selection of timber for safety application based on these characteristics.

The predominant hazard during a fire is posed by the release of heat, smoke, and toxic gases. The hazard of combustion gas release is due to the toxic and irritant action of combustion products as well as reduced visibility in a smoke-filled environment. Reduced visibility complicates evacuation of people from a danger area, which, in turn, increases their risk of poisoning by combustion products. During a fire, the situation is aggravated by the fact that combustion gases spread rapidly and penetrate into rooms remote from fireplace.

7.1 Characteristics of Smoking Ability of Timber Species

Smoke is usually understood to mean a suspension (aerosol) of condensed particles in a mixture of gaseous combustion products with ambient air. Depending on the type of combustible material and combustion conditions, the suspension may consist of condensed liquid drops of combustion products and/or solid particles on which additional condensation of products of material decomposition and flame reactions is possible. The concentration and nature of released smoke depend on the structural features and chemical composition of the combustible material.

Smoke generation is based on both chemical and purely physical processes dependent on conditions of their progress. Combustion of timber in smoldering or flaming mode affects the nature of smoke and toxic product generation. Processes involving generation of condensed carbon particles (soot) in the gas phase are the most important ones for smoke generation in case of timber combustion.

R. Aseeva et al., *Fire Behavior and Fire Protection in Timber Buildings*,
Springer Series in Wood Science, DOI 10.1007/978-94-007-7460-5_7,

Possible chemical reactions leading to generation of soot in the flame are examined in the book (Aseeva and Zaikov 1981). The appearance of soot is a sign of incomplete combustion in the flame of combustible volatile products formed as a result of pyrolysis and thermo-oxidative breakdown of timber.

About 1×10^{11} kg of carbon are released annually during fires involving plant biomass, particularly timber (Simoneit et al. 1993). Carbonaceous smoke and toxic combustion products pollute the environment, increasing the ecological hazard of fires and the possibility of a postponed impact of combustible gases on human health (Isaeva 2001).

The correlation between intensity of heat energy radiation from flames and soot generation capacity of different fuel types has now been determined. For this reason, considerable attention is paid to the mechanism and rate of soot generation during flaming combustion of different substances and materials.

Generation of soot (smoke) in flames is caused by the simultaneous progress of different processes: fragmentation of carbon-bearing fuel decomposition products; generation of active centers and particle nucleation centers; particle growth by deposition of gaseous components on their surface as well by particle collision and coagulation; and heterogeneous oxidation of soot particles.

The phenomenological picture of soot generation in a flame may be presented in the following way. Soot generation begins in the lower, "colder" part of the flame and is transferred by an ascending flow of combustible gases to the upper part of the flame. The most active synthesis process and surface growth of soot particles take place in the high-temperature flame area. A competing mechanism of generation and oxidation of soot particles is balanced at the flame top called the smoke point (De Ris and Cheng 1994). Its location in the flame and local soot concentration are inversely proportional to the heat release rate in this area. The fuel volume fraction transformed into soot increases over time when decomposition products remain in the lower part of the flame. As the time they remain in this part increases with increasing fuel delivery (flame volume), soot concentration and heat losses through energy radiation from a greater flame increase as well. Local flame cooling results in the release of other products of incomplete combustion from the flame top along with inactive soot particles.

Over 200 compounds that were products of incomplete timber combustion were found in smoke gases (Simoneit et al. 1993; Isaeva 2001). It is interesting to note the discovery in smoke of some compounds developed from timber chemical components. They retain in unchanged form as the result of evaporation and subsequent condensation on soot particles or changed only partially. Most compounds undergo significant fragmentation and oxidation in flame after pyrolysis of the original timber.

Some compounds released during combustion of different timber species serve as biomarkers for identifying the particular type to which the initial combusting plant biomass belongs by means of smoke (Simoneit et al. 1993). Thus, for example, using up-to-date analysis methods, diterpenic acids (abietic, dehydroabietic, and pimaric)

and their derivatives were discovered in the atmosphere from combustion of resinous types of coniferous timber (pine and fir). At the same time, these diterpenes were not found in smoke gases during combustion of some types of deciduous timber of tropical plants that have traditionally been a source of resins and rubber. Combustion gases of oak and alder timber do not contain these substances either. On the one hand, it confirms the concept that extractive substances of different timber types and species differ in their chemical composition and content of individual components. On the other hand, it demonstrates their different contribution to the timber combustion process.

Products of incomplete combustion of other important timber components, such as lignin and lignans, which are present in smoke gases, provide additional information on the type of initial combusting biomass. Smoke gases of lignins of coniferous timber species are enriched with derivatives of phenol compounds with a basic structure of coniferyl alcohol. Substances formed from sinapic alcohol were found in traces. Smoke gases of lignins of deciduous wood species are enriched with compounds that preserve two methoxyl groups in the phenol cycles of sinapic alcohol.

Most woody plants contain lignans that are dimers of coniferyl and sinapic alcohols. Like lignins, lignans function as a matrix supporting and enhancing the cellulose molecule skeleton structure of the plant. Lignans were found in substantial amount and unchanged form in smoke gases of pine timber. During combustion of oak timber, smoke contains oxidized derivatives of the sinapic alcohol dimers. All of these compounds are useful biomarkers of woody plant and timber materials origin.

Evaporation of molecules with carbon atom number C_8–C_{31} under conditions of flaming combustion of timber is more akin to steam distillation of hard-volatile compounds. In this case, soot particles act as this carrier.

For identification of the initial biomass using biomarkers in smoke gases during combustion of timber, the availability of certain compounds is not as important as their ratio (Simoneit et al. 1993).

During combustion of timber, the main smoke characteristics are soot particle concentration and their volume fraction in aerosol, shape, and distribution of particles by size. They determine the optical properties of smoke, scattering, and absorption of light by smoke, and visibility in smoke. Visibility is determined by distance, l, at which an object is clearly seen by an observer under room light conditions. Visibility depends not only on the smoke-generating ability of the material during combustion but also on illumination in the room and whether the object radiates or reflects the light.

Smoke-generating ability of materials is usually estimated by the value of maximum optical smoke density in a test chamber based on light ray length (L) and chamber volume (V) during smoke measurement under static conditions or rate of volumetric smoke and gas flow (V_f) (when smoke is measured under dynamic conditions).

According to the Lambert-Beer law, optical smoke density per unit length of a light ray passing through a smoke medium is represented by the extinction coefficient, μ:

$$\mu = \left(\frac{1}{L}\right) \ln\left(\frac{T_0}{T_{\min}}\right), \text{Np/m},$$

where T_0 and $T_{\min}$ are values of initial and final light transmission, %; and $\ln(T_0/T_{\min})$ is optical smoke density, Np (niper).

In effect, the niper unit is arbitrary and dimensionless and is omitted in most works. The connection between visibility (in meters) and extinction coefficient can be expressed by a simple ratio $l = B/\mu$, where B is a dimensionless proportionality constant.

For common objects, B value is taken equal to 2; for light-reflecting objects, B is from 2 to 4; and for luminous objects, $B = 6$–8. GOST 12.1.004-91 recommends using the constant $B = 2.38$ when determining the critical value of the light attenuation coefficient during fires in buildings. At the same time, visibility in smoke is regulated to ensure fire safety of occupants. For example, the condition $l_{\text{limit}} = 20$ m for ensuring visibility of the object in case of fire is often used. The critical value of smoke extinction limit must not exceed 0.119 Np/m.

The extinction (attenuation) coefficient for light in smoke is directly related to the mass soot concentration, C_s, g (soot)/m^3 (smoke), by the ratio:

$$\mu = \mu_m C_s,$$

where μ_m is the specific extinction coefficient for particles in the smoke cross section, m^2/g (soot).

The dynamics of deteriorating visibility in smoke indoors will be determined by the timber material burnout rate, ψ, kg/s, with the respective smoke-generating ability:

$$V\left(\frac{d\mu}{d\tau}\right) = {D_m}^{\max}\psi, \text{Np}\cdot\text{m}^2/\text{s}.$$

In practice, smoke-generating ability of materials is determined from the maximum value of optical smoke density per unit sample area, ${D_s}^{\max}$, or per unit sample mass, ${D_m}^{\max}$, or calculated based on sample mass loss during the testing period – ${D_{\Delta m}}^{\max}$. Unlike the latter two values, ${D_s}^{\max}$ is dimensionless and is used in the ASTM E-662 method.

The domestic standard GOST 12.1.044-89 (GOST 12.1.044-89(4.18)) recommends using the index ${D_m}^{\max}$; the same index and ${D_{\Delta m}}^{\max}$ are used in cone-calorimetric material tests (ISO 5660–1 and ISO 5659, respectively).

The new European standard EN 13823 oriented to the SBI method, along with identification of heat release characteristics during combustion of construction materials, provides for a compulsory assessment of their smoke generation ability.

Smoke generation rate and overall smoke release during testing period, OSR_{600s}, are taken into account. Introduction of a new index, called SMOGRA (SMoke index Growth Rate) by analogy with the FIGRA indicator, is essential. Thus, with regard to smoke, not only the smoke generation rate is important but also the growth rate of the latter up to the maximum value. The SMOGRA index allows for additional subdivision of construction materials by their fire hazard class:

Subclass S1 – SMOGRA value $\leq 30\ m^2s^{-2}$, $OSR_{600s} \leq 50\ m^2$.
Subclass S2 – SMOGRA value $\leq 180\ m^2s^{-2}$, $OSR_{600s} \leq 200\ m^2$.
Subclass S3 – exceeds S2 values (Sundstrom 1999).

The advantage of $D_m{}^{max}$ and $D_{\Delta m}{}^{max}$ indices is that they reveal the dependence of smoke generation on the quantity of material and its composition.

Unfortunately, detailed information on the impact of timber type and species on smoke generation indices is not available. However, there is a general trend: During flaming combustion of timber exposed to an external radiative heat flow, the smoke generation ability is much lower compared with smoke release in the decomposition and smoldering mode. According to (Romanenkov and Zigern-Korn 1984), the smoke generation ability indices for pine timber exposed to an external heat flow of 25 kW/m^2 change in the following way: during flaming combustion, $D_s = 54$–68 m^2/m^2, $D_m = 4$–6 m^2/kg, and $D_{\Delta m} = 7$–10 m^2/kg; in smoldering mode, these indices have values of 339–477, 30–39, and 137–150, respectively. During flaming combustion of pine timber, maximum optical smoke density $D_s{}^{max} = 20$ m^2/m^2 is achieved in just 2 min after ignition. In smoldering mode, this process takes up to 20 min.

We have conducted research on smoke-generating ability of eight types of coniferous and deciduous species of timber in the smoldering regime, which is the most hazardous in terms of smoke generation (Aseeva et al. 2004). Tests were conducted according to the standard method (GOST 12.1.044-89(4.18)) for an external radiative heat flow density of 10–35 kW/m^2. Samples of elm and chestnut wood were taken from the southern maritime region of Russia, and five types of timber (fir, pine, eucalyptus, and two types of acacia) were taken from a tropical region of Vietnam. A pine sample was taken from the Moscow area for comparison with southern types of timber. Sample humidity ranged within 4–9 %.

Figure 7.1 shows impact of the external heat flow on the smoke generation ability of different species of timber in the smoldering mode.

The maximum value of optical smoke density during combustion of each timber species depends in a complicated way on the external heat flow density. At first, index $D_m{}^{max}$ increases with increasing heat flow intensity up to $q''_e = 20 - 25$ kW/m^2, and then it declines. The extremum on dependence curves $D_m{}^{max} = f(q''_e)$ is determined by autoignition of the samples. The nature of smoke changes during the transition from the thermal decomposition and smoldering mode to flaming combustion of timber. Carbonaceous soot becomes the main component of the condensed phase. The extremum position corresponds to the value of critical heat flow density below which the flaming process of timber combustion is not implemented without an initiating local ignition source.

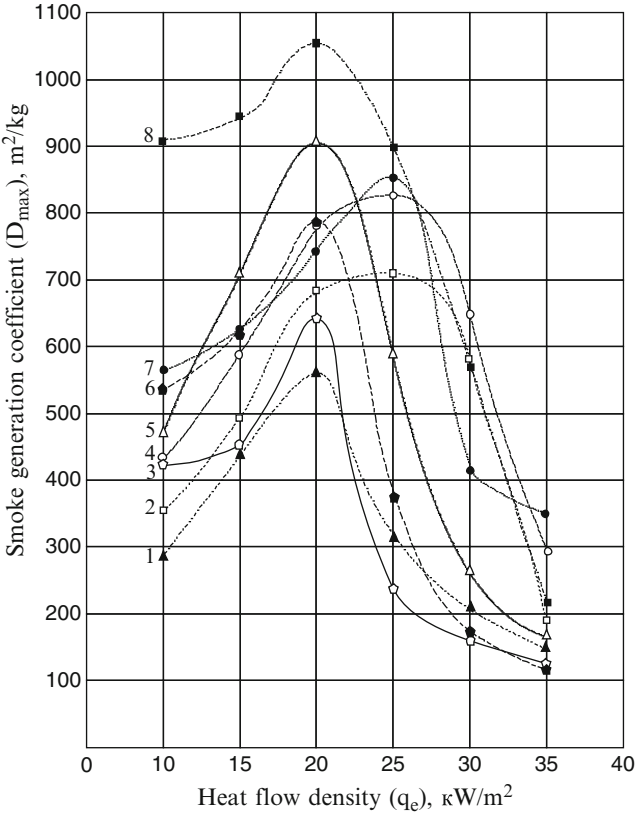

Fig. 7.1 Dependence of the smoke ability $D_m{}^{max}$ during smoldering combustion of different species of wood on external heat flow density: *1* eucalyptus (camaldulensis), *2* chestnut, *3* acacia (mangium), *4* elm, *5* Moscow area pine, *6* acacia (auriculiformis), *7* pine (pinus massoniana), *8* fir (picea koraiensis)

It is evident from Fig. 7.1 that deciduous wood species have lower values of critical autoignition density ($q''_{cr.\,ai} = 20–22$ kW/m^2) compared with the coniferous types (25 kW/m^2).

The exceptions are samples of elm and chestnut wood, which are similar to coniferous species by this indicator, apparently due to a high content of extracted substances (Aseeva et al. 2004).

Samples of coniferous species (pinus massoniana, Moscow area pine, picea koraiensis) have the highest values of smoke generation ability at the limit of smoldering combustion (853–1,066 m^2/kg).

Following autoignition of wood materials, smoke generation decreases quite drastically with increasing thermal heat density. At $q''_e = 35$ kW/m^2, it decreases by several times. However, values obtained for $D_m{}^{max}$ (163–570 m^2/kg) remain higher than those recorded for flaming mode with a local initiating ignition source.

This is apparently associated with a difference in conditions of accumulation of combustible timber decomposition products in a "cold" pre-flame zone before their lower concentration limit and heating of the gas phase to the relevant temperature. This assumption is confirmed by a comparison of autoignition and ignition times (in the presence of a pilot flame as the ignition source) of pine samples exposed to heat flows of the same density equal to 30 kW/m^2:

$$\tau_{\text{autoign}} = 70 \text{ s} > \tau_{\text{ign}} = 23 \text{ s}.$$

When heat flow density increases to 35 kW/m^2, the difference in smoke generation ability of the examined wood species is leveled. However, the general trend in the parameter $q''_{\text{cr. ai}}$ mentioned above still remains: timber of coniferous species, elm, and chestnut has higher values of $D_{\text{m}}^{\text{max}}$, compared with timber of tropical deciduous species.

The conclusion follows that the determining factor for smoke generation during combustion is not timber species (soft or hard) but rather the relative content of main components in its composition.

Thermal decomposition of materials is a determinative stage in the process of their combustion. As was proven in (Di Blasi et al. 2001), parameters such as timber decomposition temperature, average rate of volatile product formation, and yield of char residue, liquid and gas fractions depend on the ratio of timber components. Thus, for example, the temperature at the beginning of decomposition decreases as the summary content of hemicellulose and extracted substances relative to cellulose content increases. Carbonized residue yield increases with increasing lignin content. Liquid resinous fraction yield (tar) depends on the participation of holocellulose in pyrolysis. Apparently, it has a significant impact on smoke generation due to its relatively high content in different types of timber.

7.2 Effect of Timber Combustion Regime on Toxicity of Forming Volatile Products

Smoke gases formed during combustion of timber contain, in addition to soot, a large number of different toxic substances. A combination of high smoke content and combustion product toxicity not only creates a major threat for people in the buildings but also hampers rescue operations and fire fighting. Statistical data show that loss of life during fires in 50 % of cases is caused by smoke in the escape routes and increased toxicity of combustion products (Drysdale 1990). Furthermore, up to 80 % of deaths were recorded as a result of toxic smoke inhalation (Gann et al. 1994).

In case of smoke inhalation, soot particles 7–50 μm in size enter the nasopharynx by inhalation but are filtered and removed by mucoid discharge during coughing. Very small particles 0.5–7 μm in size are the most dangerous. They can get into bronchi, remain there, and cause asphyxia. However, carbonaceous particles are thought to be less carcinogenic than quartz powder.

Toxic substances pose the main hazard in combustion gases released during combustion of timber. It is still very difficult to predict the types and amounts of toxic products released during combustion of timber. For this reason, combustion gas toxicity is determined experimentally.

There are two approaches to assessing combustion gas toxicity: an analytical chemical method and a biological method of animal lethality assessment during a 30-min stay in the test chamber's smoke and gas atmosphere and after 14 days. The combustion product toxicity index, H_{CL50} (g/m^3), is the ratio of material quantity per unit of closed space resulting in death of 50 % of the test animals. Along with the toxicity index, an index H_{EL50} characterizing toxic gas concentration required for loss of mobility of 50 % of test animals is sometimes used. The lower the values of indices H_{CL50} and H_{EL50}, the more toxic the material combustion products.

Although a large number of compounds have been found in smoke gases during combustion of wood, methods of assessing fire hazard by product toxicity, which are based on the analytical approach, focus mainly on the presence of CO, CO_2, and a decrease in oxygen concentration.

The N-gas model based on the concept that a small amount (N) of gases in smoke caused the largest percentage of observed toxicity was developed in the 1980s. A lethal dose of each gas was identified biologically by testing on rats. Similar measurements of a gas combination helped to determine whether the toxic effect is additive, synergetic, or antagonistic. Based on these results, an algebraic equation was obtained which took into consideration the contribution made by each individual compound into the overall lethal dose.

It was ascertained that the greatest contribution in toxicity of timber combustion products was made by carbon monoxide. In the smoldering combustion mode of Douglas spruce wood, the CO yield was 70–240 times higher than the CO yield in flaming combustion (Babrauskas et al. 1991).

We have studied the impact of species of timber on combustion product toxicity on exposure to an external radiative thermal heat with density of 10–65 kW/m^2 and estimated the yield of carbon monoxide and dioxide in the timber flaming and smoldering combustion mode. Samples of pine and fir, as well as stone birch and aspen from a northern region of Russia (Vologda), were used as the subject. Samples of elm, oak, and linden were taken from a southern region (Sochi).

The combustion product toxicity indicator was determined by the gas analytical method according to GOST 12.1.044-89 (GOST 12.1.044-89(4.18)). A local ignition source was not used during the test.

Figure 7.2 shows the impact of heat flow density (temperature) on the combustion product toxicity index for different species of wood (Serkov et al. 2005).

The extreme dependence of index H_{CL50} observed is due to the fact that autoignition occurs at a certain temperature (heat flow density).

Toxicity of timber combustion products is increased during smoldering combustion. In the smoldering mode, products of timber sample combustion have the highest toxicity in the temperature range 450–550 °C (H_{CL50} is in the range of 20–33 g/m^3). Under these conditions, all types of wood prove to be highly hazardous in terms of combustion product toxicity and according to standard

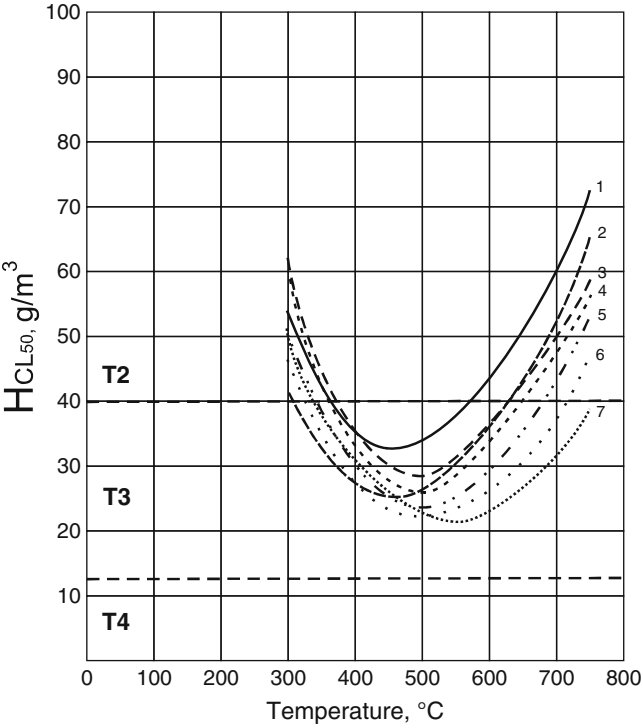

Fig. 7.2 Change in combustion product toxicity index for different species of timber depending on the temperature of thermal exposure: *1* lime, *2* birch, *3* elm, *4* oak, *5* aspen, *6* pine, *7* fir

12.1.044-89 they belong to group T3. As thermal exposure intensity increases to 60–65 kW/m^2 (corresponding to temperatures of 700–750 °C), timber of different species displaces to the group of moderately hazardous materials T2 by combustion product toxicity.

Compared with deciduous species, regardless of their place of growth, pine and fir timber generate combustion products with higher toxicity.

Attention is drawn to the notable difference between indices H_{CL50} of lime and fir timber samples, despite the relatively close values of their density (490 and 430 kg/m^3). At the same time, in terms of this index, an aspen sample ($\rho = 400$ kg/m^3) is closer to pine timber ($\rho = 450$ kg/m^3) in behavior. It is hard to escape the conclusion that processes associated with the development of timber combustion depend not only on structural differences between various species of timber and their density but also mainly on the chemical composition of timber.

The main toxic substance in timber combustion products is carbon monoxide formed during both heterogeneous oxidation of charred surface layers of timber and in the gas phase in case of incomplete combustion of organic substances.

Dynamics of changing CO and CO_2 ratios in combustion products during timber toxicity testing reflects the combustion efficiency factor.

Table 7.1 Change in CO/CO_2 ratio during timber testing at a temperature 500 °C

	Value CO/CO_2 for a fixed test time, s						
Wood species	50	100	150	200	300	400	500
Pine	0.400	0.428	0.583	0.529	0.428	0.326	0.316
Aspen	0.250	0.375	0.433	0.357	0.245	0.236	0.217
Oak	0.230	0.360	0.425	0.446	0.350	0.275	0.239
Elm	0.100	0.333	0.400	0.462	0.394	0.250	0.237

Table 7.1 provides data on the change of CO/CO_2 ratio during timber toxicity testing at a temperature of 550 °C.

It follows from the data given in the table that a change in the CO/CO_2 ratio during tests with different wood species has an extreme character.

During transition to the flaming mode, the yield of carbon monoxide decreases; however, even with high intensity of the external heat flow, its relative content in timber combustion products remains significant. Although moderate, there is still a hazard of human poisoning by combustion gases during a fire involving timber materials.

Based on the data obtained by small-scale methods of testing combustibility characteristics of timber materials, it is possible to assess the dynamics of fire hazard factor growth at the initial stage of fire development indoors and time before reaching a situation critical for human life. A mathematical description of the process of growth of indoor fire hazard factors, such as average volume values of temperature, concentrations of toxic combustion products, optical smoke density, and decrease in oxygen concentration, is presented in monograph (Koshmarov and Rubtsov 1999). According to the proposed methodology (Koshmarov and Rubtsov 1999), the time before reaching a situation critical for humans was calculated for each of the above-mentioned fire hazard factors during combustion of pine wood hypothetically used as a lining material in a public building corridor. Analysis of the obtained results showed that under these conditions, the greatest hazard is posed by reduced visibility during a fire. In this case, a critical situation of visibility loss during a fire appears within about 1 min (Serkov 2001).

References

Aseeva RM, Zaikov GE (1981) Combustion of polymeric materials. Science, Moscow, 280 p

Aseeva RM, Tkhan BD, Serkov BB, Sivenkov AB (2004) Release of smoke during thermal decomposition and combustion of wood. For Bull 2(33):99–103

Babrauskas V, Levin BC, Gann RG, Paabo M, Harris RH, Peacock RD, Yusa Sh (1991) Toxic potency measurement for fire hazard analysis. NIST special publication 827. The Combustion Institute, Gaithersburg, 107 p

De Ris J, Cheng XF (1994) The role of smoke-point in material flammability testing. In: Proceedings of the 4th international symposium on fire safety science, Ottawa, Canada, pp 301–312

Di Blasi C, Branca C, Santoro A, Hernandez EG (2001) Pyrolytic behaviour and products of some wood varieties. Combust Flame 124:165–177

Drysdale D (1990) Introduction into dynamics of fires. Stroyizdat, Moscow, 424 p

Gann RG, Babrauskas V, Peacock RD, Hall JR (1994) Fire conditions for smoke toxicity measurements. Fire Mater 18:193–199

GOST 12.1.004-91. Fire Safety. General requirements

GOST 12.1.044-89(4.18) Fire and explosion hazard of substances and materials. Nomenclature of indices and methods of their determination

Isaeva LK (2001) Ecological consequences of fires. Thesis for doctoral dissertation, SFS Academy, Moscow

Koshmarov YA, Rubtsov VV (1999) Processes of intensification of workroom fire hazard factors and calculation of critical fire duration. Moscow Fire Safety Institute, Moscow, 89 p

Romanenkov IG, Zigern-Korn VN (1984) Fire resistance of building structures of effective materials. Stroyizdat, Moscow, 240 p

Serkov BB (2001) Fire safety of polymeric materials, combustibility, reduction and standardization of their fire-safe use in construction. Thesis of doctoral dissertation, SFS Academy, Moscow, 48 p

Serkov BB, Sivenkov AB, Tkhan BD, Aseeva RM (2005) Study of toxicity of products of combustion of different wood species. For Bull Mosc State For Univ Publ House. Lesnoy Vestnik 3:145–150

Simoneit BRT, Rogge WF, Mazurek MA, Standley LJ, Hildemann LM, Gass GR (1993) Lignin pyrolysis products, lignans and resin acids as specific tracers of plant classes in emissions from biomass combustion. Environ Sci Technol 27:2533–2541

Sundstrom B (1999) European classification of building products. In: Proceedings of 8th international fire science and engineering conference "Interflam'99", vol 2, Edinburgh, Scotland, pp 769–780

Part II
Fire Safety and Fire Protection of Building Structures and Timber Constructions

Chapter 8
Fire Safety and Fire Resistance of Building Structures and Timber Constructions

Abstract This chapter presents general approaches to the system of fire safety in buildings and thermal fire regime's assessment. Dynamics of change of fire hazard factors during fire growth is considered. Charring rate of timber species and glued laminated timber at nominal fire exposure is discussed. Fire resistance of timber building members and charring depth are presented.

Timber is widely used in Russian construction industry practice as a construction material for buildings and structures for various purposes. In the house-building industry, it is used as a construction material for residential, public, industrial, agricultural, livestock, warehouse, and other buildings and structures. In transport infrastructure, it is used as a railroad construction material (used as rail ties) and suspension bridge interchanges; in structures of water facilities, it is used to build small wooden bridges.

In cold northern and northeastern regions of the country with abundant forest resources, log buildings and structures (mainly in small towns and in the countryside) are still popular. Round timber log or machined flat ones are used. Development of the modern timber house-building industry is moving toward creating new progressive industrial technologies for manufacturing various structural materials made of natural timber (Romanenkov and Zigern-Korn 1984; Kovalchuk 2005). In particular, they include massive large-sized glued laminated timber (glulam), laminated veneer lumber (LVL), or cross-laminated timber (CLT).

In Russia, production of the above-mentioned glulam constructions began in the second half of the twentieth century.

Twenty-five plants using imported equipment with total capacity of about $100 \cdot 10^3$ m^3 of constructions per year had been operating since 1973. By 1997, during perestroika (economic restructuring of the former USSR), this sub-sector almost ceased to exist. It was not until later that glulam production was revived. Today glulam is manufactured by 50 companies, but only two of them are large-scale manufacturers with overall production capacity of $(40–60) \cdot 10^3$ m^3 of constructions

R. Aseeva et al., *Fire Behavior and Fire Protection in Timber Buildings*, Springer Series in Wood Science, DOI 10.1007/978-94-007-7460-5_8,

per year. By 2008, more than 600 various buildings and structures with long-span glulam load-bearing constructions had been designed and built (Vatin 2008).

It should be noted that commercial production of new structural glued timber composites with an aligned structure had been launched abroad earlier, for example, oriented strand board (OSB) or parallel strand lumber (PSL) and laminated strand lumber (LSL).

Glued timber constructions (GTC) production is developing very successfully in Europe, North America, and Japan. World output of load-bearing and load-separating GTC was about $4.5 \cdot 10^6\,m^3$ in 2003 and $\sim 5 \cdot 10^6\,m^3$ in 2004. During the next 5 years, annual GTC output increased by 31 %. A further 25 % increase was expected from 2009 to 2013 (Competitive environment 2011).

Up to 2005, Russia manufactured just 2 % of the world's GTC. However, the GTC manufacturing sector is growing rapidly. For example, from 1998 to 2003, GTC output increased ten times, from $7.4 \cdot 10^3\,m^3$ to $76 \cdot 10^3\,m^3$. In 2005, glulam output alone was $67.7 \cdot 10^3\,m^3$. Approximately half of this output was used on the domestic market. Total contracted capacity of Russian GTC manufacturers is currently $456 \cdot 10^3\,m^3$/year. In the medium term outlook GTC will still be mainly used for low-rise structures, including houses made of glulam (70 %), light frame constructions (6 %), and new roofing assemblies (12 %) (Competitive environment; Development prospects of the glued laminated wood market 2009).

Massive large-sized glulam constructions (columns, beams, arcs, frames, trusses) are essential structural members of timber buildings and structures, and they can bear large operation loads. Other types of GTC (partition timbers, slabs, wall panels, etc.) include constructions performing enclosing function. All of these GTC provide stability and fire safety of construction facilities. These GT load-bearing and load-separating constructions are the subject of special attention, which is reflected in scientific, technical, regulatory, and guidance literature. The attractiveness of using GT constructions is due to their resistance to aggressive media, low bulk weight compared to metal and reinforced concrete, and considerable strength at low weight.

For example, glulam constructions were used in building facilities such as an indoor ice rink with a span of 58 m in Tver (Fig. 8.1); a mineral fertilizer warehouse in the port of St. Petersburg with a span of 63 m and a roof arch 45 m high (Fig. 8.2); the Bugry Trade Center with a span of 53 m in St. Petersburg; the Strogino ice rink with a span of 48 m in Moscow; a cable suspension bridge at the 102nd kilometer of the Moscow Ring Road (MKAD); and an aquapark in Mytischi, Moscow Region.

8.1 General Approaches to the Fire Safety System in Buildings and Assessment of Thermal Fire Regime

Timber buildings and structures have a very long service life, but they can be easily destroyed and burn out in a few minutes in case of fire. Fire may occur due to faulty wiring or careless handling of fire. As a result, materials and substances in the compartments initially ignite (temporary fire load) rather than timber constructions or cladding materials (constant fire load).

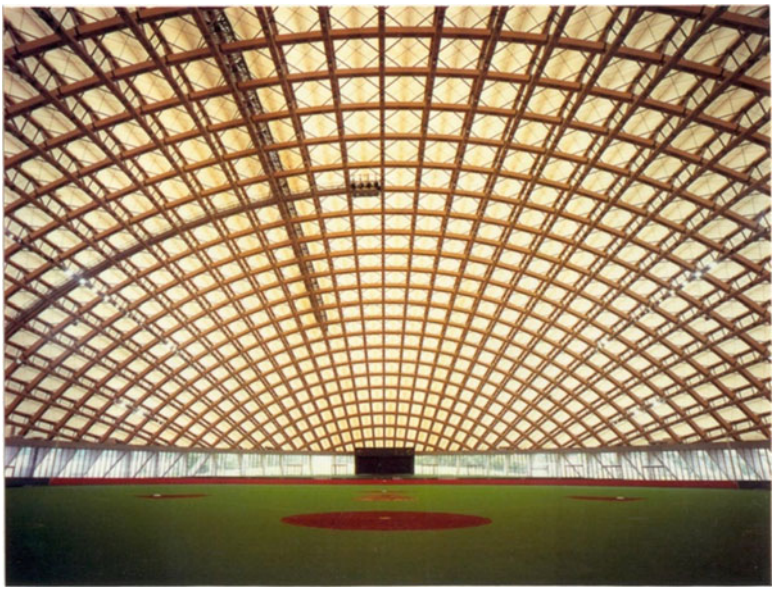

Fig. 8.1 Sports complex in Tver roofed with glulam bearing structures

Fig. 8.2 Structure of a mineral fertilizer warehouse in the port of St. Petersburg

Fire safety system at construction facilities is aimed at preventing the onset and development of fire, as well as preventing the impact of fire hazardous factors on people and preserving the stability of building and structures.

The concept of fire safety is complex and includes all necessary measures during the design, construction, and use of buildings and structures to ensure human life and health and minimize material losses in case of fire.

The concept of fire hazard factors includes all manifestations of fire that affect the state of people in a fire zone: direct effects of flame or sparks, high ambient temperature, reduced oxygen concentration and visibility in smoke, increased concentration of toxic products of combustion and thermal decomposition of materials, mechanical damage of structures, and other factors.

The main provisions of technical regulations on fire safety and general fire safety requirements for buildings and structures are given in Federal Law of the Russian Federation No. 123-FL dated July 22, 2008 (Federal Law of RF No. 123-FL). Some amendments were added later (Federal Law of RF No. 117). In 2011, a set of codes for design and calculation of residential, public, industrial, and other timber structures was enacted especially for buildings and structures made of solid timber and GT constructions (SP 64.13330.2011).

Design and calculation methods for GTC and solid timber structures and regulated and calculated values of the strength of timber constructions under various types of loading are also included in the standard (STO 36554501-002-2006).

Buildings and structures of all types are classified according to their degree of fire resistance and structural and functional fire hazard classes.

Buildings are divided into fire-resistance class I, II, III, IV, or V by their degree of fire resistance. The degree of fire resistance of buildings and structures is set depending on the number of floors (height of a building), floor area (fire compartment), functional purpose of the building (functional fire hazard class), and type of constructions used. One-story timber structures built of massive timber log may be assigned to fire-resistance class IV. Light timber frame buildings and structures with no special fire protection are assigned to class V.

The structural fire hazard class of buildings and structures depends on the same factors as fire resistance. All buildings and structures are divided into four classes according to structural fire hazard: C0, C1, C2, and C3. There are no special requirements for fire resistance and structural fire hazard class for timber housing up to two stories, inclusive. For three-story buildings, structural fire hazard class should not be lower than C2. Four-story residential buildings should have at least class III fire resistance and structural fire hazard class of the buildings no lower than C1.

Functional fire hazard classes of buildings and constructions are set depending on the purpose of buildings, the number of permanent or temporary occupants, and their age and physical state.

Constructions of any type are divided into four fire hazard classes: K0 – non-hazard; K1 – low hazard; K2 – moderate hazard; and K3 – high fire hazard. Timber constructions without fire protection belong to class K3.

A standard method is used to determine the fire hazard class of building constructions (GOST 30403-96 1996). The required structural fire hazard class for constructions is in accordance with the required structural fire hazard class for buildings and structures (Table 8.1) (Federal Law of RF No. 123-FL).

Table 8.1 Correspondence of the structural fire hazard class of buildings and structures to fire hazard classes of building constructions used

	Fire hazard class of constructions				
Structural fire hazard class of buildings	Load-bearing members (columns, girders, trusses)	External walls	Walls, partitions, floors, roofs, ceilings	Stairwell walls and fire barriers	Stair marches, landing (stairwell)
C0	K0	K0	K0	K0	K0
C1	K1	K2	K1	K0	K0
C2	K3	K3	K2	K1	K1
C3	Not regulated	Not regulated	Not regulated	K1	K3

The actual structural fire hazard class of buildings depends on the actual fire hazard classes of main load-bearing and load-separating constructions: columns, beams, trusses, walls, partitions, floors, roofs, walls, stairwells, flights, and stairwell landings. Class C0 buildings and structures have the best fire safety, as all constructions are made of noncombustible materials. The majority of class C3 buildings and structures (except for structural members of stairways, walls, stairwells, and fire barriers) have no fire safety requirements.

The degree of fire resistance of buildings and structures according to fire safety codes is regulated with consideration of the functional purpose of the buildings, number of floors, area, and other factors (Table 8.2) (Federal Law of RF No. 123-FL; SP 2.13130.2009). If the actual fire resistance limit (time to failure) of main building constructions is equal to or greater than the code value required, it is considered that the actual fire resistance of the building meets the requirement.

The behavior of building constructions during a fire depends on the temperature and duration of the fire. In turn, the type and amount of combustible substances and materials (fire load), their location in the room, room dimensions and configuration, sizes of openings in enclosures, and other factors affect fire temperature regime.

This means that with the same fire load, different variants of fire development are possible and each variant will correspond to a certain temperature – time fire regime.

In order to classify constructions according to fire resistance, standard fire regime is used, where the change in average volume temperature of the heating medium at the fire development stage is described by the following equation:

$$t = 345 \lg (8\tau + 1) + T_0, ^\circ\mathrm{C},$$

where τ – fire duration, min, and T_0 – initial temperature, 20 °C.

In actual conditions, fire temperature can be more "rigid" than the standard fire temperature (Fig. 8.3, curve 2). In this case, the fire resistance of a structure will be less than during a standard fire.

In a "softer" mode (Fig. 8.3, curve 3), fire resistance of a construction would exceed the value obtained during a standard test (Roitman et al. 2013).

Table 8.2 Correspondence of the degree of fire resistance of building and structures to fire resistance limits of building constructions

	Building constructions fire resistance limit, min						
				Non-attic roofs		Stairwells	
Degree of fire resistance of the building	Load-bearing wall, column, etc.	External non-bearing walls	Floor/ceiling assemblies (including attic and overbasements)	Decks (including insulation)	Trusses, beams, joists	Inner walls	Stairwell flights and landings
I	R 120	E 30	REI 60	RE 30	R 30	REI 120	R 60
II	R 90	E 15	REI 45	RE 15	R 15	REI 90	R 60
III	R 45	E 15	REI 45	RE 15	R 15	REI 60	R 45
IV	R 15	E 15	REI 15	RE 15	R 15	REI 45	R 15
V	Not regulated						

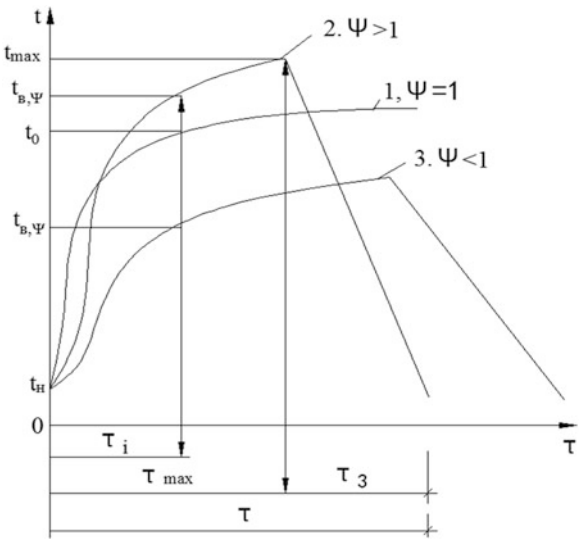

Fig. 8.3 Fire temperature regime: *1* standard regime, *2* more rigid than standard regime, *3* softer than standard regime

Temperature regimes of real fires at the development step are described by the following equation:

$$T = \psi\ 345\ \lg(8\tau + 1) + T_0$$

This equation differs from the previous equation by the presence of fire temperature coefficient ψ. The value of ψ is the ratio of temperatures of actual and standard fires at the same moments of fire development. The value of ψ can be determined by taking into account the opening factor K_{op} in the place of fire:

$$\psi = 1.37 - \left(150\ K_{op} - 0.65\right) / {K_{op}}^2 10^4,$$

where A_{op} – area of vertical openings, m^2; H – average height of openings, m; A – total area of all horizontal and vertical enclosures constructions in the room, m^2; and $K_{op} = A_{op}\sqrt{H/A}$.

For conditions that differ from standard fire conditions (Fig. 8.3), time τ_{max} can be calculated by the following formula:

$$\tau_{max} = \frac{Q_{CY}}{\left(8,318\ K_{op} - 4,021\ {K_{op}}^2\right)},$$

where Q_{CY} – value of reduced fire load (specific fire load, reduced to the total surface area of enclosures), MJ/m^2.

Then the value of the maximum temperature of a gaseous medium during an actual fire will be:

$$T_{max} = \psi\ 345\ \lg(8\tau_{max} + 1) + T_0.$$

The rate of temperature decrease at the fire extinction stage, °C/min, is equal to $V_{ext} = (98{,}000C_0 - 1{,}500)/Q_{CY}$.

A comparable approach that takes into account the area of openings and enclosures and the heat-absorbing capacity of enclosures is recommended when calculating parametric temperature–time fire dependence by European fire standard EN 1991-2-2002, which received the status of National Standard of Russia in 2011 (National Standard of the Russian Federation EN 1991-1-2-2011).

The time to reach the maximum temperature of a gaseous medium in the place of fire depends on the rate of fire development and its nature, i.e., whether it is controlled by the fire load or ventilation. Thus, the temperature regime in the place of fire depends on these factors at the fire extinction stage (National Standard of the Russian Federation EN 1991-1-2-2011).

Other methods for evaluating fire temperature regimes have recently been proposed. They include zoned and/or field modeling of gaseous medium behavior during a fire in a building (Astapenko et al. 1988).

8.2 Dynamics of Change of Fire Hazard Factors During the Fire Growth

Research of the initial stage of fire development inside the buildings and structures is important for organizing and safely evacuating people from these buildings. Determination of the time required to evacuate people from a burning building is based on knowledge of the dynamics of change of fire hazard factors (FHF) in a building with a specific functional purpose and with certain space-planning structure, taking into account the regularities of people's flow movement, human behavior, and the characteristics of the occupants (Holshchevnikov et al. 2009).

According to the valid standard (GOST 12.1.004-91 1992), the time required for safe evacuation is determined in accordance with critical fire duration until at least one fire hazard factor reaches the value that is critical for people:

$$\tau_{cr} = \min\left\{\tau_{cr}^{LV}, \tau_{cr}^{T}, \tau_{cr}^{tg}, \tau_{cr}^{O2}\right\},$$

where τ_{cr}^{LV}, τ_{cr}^{T}, τ_{cr}^{tg}, τ_{cr}^{O2}, $\tau_{cr}^{T\Pi}$ are values of critical fire duration in terms of loss of visibility, gas medium temperature, discharge of toxic combustion products, and oxygen concentration.

In fact, τ_{cr} is a complex index reflecting time up to appearance of critical situation for people in a compartment during a fire.

A rather detailed and comprehensive theory of FHF growth during the initial stage of fire in building is represented in the works (Koshmarov and Rubtsov 1999; Koshmarov 2000). A modified integrated model of pre-flashover fire in a compartment subdivided into zones is considered.

Work zone occupied by people is studied.

A mathematical description of the processes of the growing average volume value of temperature and other fire hazard factors indoors is expressed as a system of ordinary differential equations. These equations reflecting the laws of conservation and thermodynamics, together with boundary and initial conditions, form a closed system for determining fire characteristics in a closed space. Analysis of the full system of equations with some assumptions resulted in formulas for engineering calculation of the dynamics of the increment of FHF indoors.

In case of linear flame spread on the surface of materials, critical fire duration in terms of reaching critical temperature in occupied space is calculated with the following formula:

$$\tau_{\text{cr}}{}^{\text{T}} = \left[\left(\frac{B}{A}\right)\ \ln\ \left(\frac{T_{\text{cr}}}{T_0}\right)\right]^{1/2},$$

where complex $B = c_{\text{p}}\rho_0 T_0 V/(1-\varphi)\eta Q_{\text{L}}$; complex $A = 1/2 b_{\text{g}} v_{\text{fs}} \psi_{\text{sp}}$; T_{cr} – critical temperature for a person in the occupied space, equal to 70 °C; and T_0 – initial temperature in the compartment where the seat of fire is situated.

Dimensional complex B depends on combustion efficiency η and combustion heat of the material Q_{L}; index of heat loss to enclosure φ; free volume of the compartment V, and initial thermal and physical characteristics of the air environment in this compartment.

Complex A makes allowance for specific mass loss rate $\psi_{\text{уд}}$ and area of flame propagation (speed v_{fs}). In case of circular flame spread on the surface of a material, this complex can be represented by the following formula:

$$A = \frac{\pi\ {v_{\text{fs}}}^2\ \psi_{\text{sp}}}{3} = 1.05 {v_{\text{fs}}}^2 \psi_{\text{sp}}$$

In terms of loss of visibility:

$$\tau_{\text{cr}}{}^{\text{LV}} = \left\{\left(\frac{B}{A}\right)\ln\left[\frac{B\ D_{\text{m}}}{(B\ D_{\text{m}} - \mu_{\text{cr}})}\right]\right\}^{1/n},$$

where D_{m} – smoke generating ability of the material, Np m^2/kg^1; μ_{cr} – critical value of smoke optical density connected with the visibility range in a smoke-filled environment, $\mu_{\text{cr}} = 0.119$ Np/m^1; and $n = 3$ for circular flame spread on the surface of the material, and $n = 2$ for linear flame spread.

In terms of oxygen deficiency indoors:

$$\tau_{\text{cr}}{}^{\text{O2}} = \left[\left(\frac{B}{A}\right)\ \ln\left\{\frac{(B\eta L_1 + \rho_{01} V)}{(B\eta L_1 + \rho_{1\text{cr}} V)}\right\}\right]^{1/n},$$

where L_1 – specific oxygen consumption rate; ρ_{01} and $\rho_{1\text{cr}}$ – initial and critical values of average partial density of oxygen; and $\rho_{1\text{кр}}$ depends on the height of the occupied space. It is accepted that $\rho_{01} = 0.27$ kg/m^3 and $\rho_{01} - \rho_{1\text{cr}} = 0.0044$ kg/m^3; $n = 2$ (or 3) depending on the type of flame spread on the surface of the material.

Critical fire duration in terms of hazardous emission of each toxic combustion product:

$$\tau_{cr}{}^{tg} = \left[\left(\frac{B}{A} \right) \ln \left\{ 1 - \left(\frac{V X_{cr}{}^{tg}}{B \eta L_{tg}} \right) \right\}^{-1} \right]^{1/n},$$

where $X_{cr}{}^{tg}$ – maximum allowable amount of toxic agent indoors and L_{tg} – yield of combustion product emitted after burning of one unit of mass of material, kg/kg.

If a number is negative under the natural logarithm, the factor under study is not considered hazardous for this particular fire situation.

During calculation of fire hazardous factors, the following accepted maximum allowable limits for people are used: $T_{cr} = 343$ K; $X_{cr}{}^{CO_2} = 0.11$ kg/m^3; $X_{cr}{}^{CO} = 1.16 \times 10^{-3}$ kg/m^3; $\rho_{1cr} = 0.226$ kg/m^3; and $\mu_{cr} = 2.38/l_{LV} = 0.119$ Np/m^1 with l_{LV} – maximum allowable visibility range in a smoke-filled area, which is equal to 20 m.

Today, due to the development of computing technologies and implementation of powerful computers in engineering, not only integral and zone models of heat and mass transfer during fire but also more complex two- and three-dimensional field models are in demand in the area of fire safety (Puzach 2003). Computational field modeling makes it possible to solve complex problems of evaluating the dynamics of FHF into structures with complex configuration, taking into account the operation of all smoke exhaust and fire-extinguishing systems, to determine fire resistance of structures, etc.

We were interested in a simple problem – how the species of timber influences the dynamics of fire hazardous factors during the initial fire phase. Therefore, using a typical compartment with dimensions of $20 \times 10 \times 3.3$ m with small opening as an example, we evaluated critical fire duration by FHF at circular flame spread on the surface of timber panels as wall lining. During fire simulation, we considered timber panels made of coniferous and deciduous species: fir, pine, birch, and oak. Baseline data for calculating the time of onset of a dangerous situation for people during fire were obtained beforehand through the use of standard fire engineering methods (see Part 1). Circular flame spread is used as the most frequent type of flame propagation on a timber wall surface.

According to the results of our calculations, the most hazardous fire factor during fire simulation is generation of carbon monoxide.

Within a minute after the onset of fire in the compartment, the concentration of this toxic agent becomes critical. Furthermore, due to the lower rate of flame spread on the surface and mass burnout rate, deciduous timber species have a lower rate of increasing FHF. Critical fire duration calculated in terms of reaching dangerous concentrations of carbon monoxide in the compartment has the following sequence:

$$\begin{aligned} &\text{fir} < \text{pine} < \text{birch} < \text{oak} \\ &\tau_{cr}{}^{CO}, \text{s} : 52 < 57 \quad < \quad 61 \quad < 72. \end{aligned}$$

8.3 Charring Rate of Timber Species and Glued Laminated Timber at Standard Fire Exposure

The question of charring rate of timber, glulam, and other types of timber-based products during a fire holds a central position in the studies of fire resistance of timber buildings and structures. This is only logical, because the fire resistance limit of constructions is determined by taking into account total time from the start of fire exposure of a timber structural member to the onset of charring and the time from onset of charring to reaching the limiting critical state.

Charring rate depends on the heat and fire exposure regime. Part 1 describes the effect of constant radiation heat flow density on the thickness of the surface char layer formed during flaming combustion of various timber species.

In this section, we examine the data on the charring rate of timber structural members in standard fire regime.

R. White and E. Nordheim performed a detailed study of charring of eight timber specimens of coniferous and deciduous species in standard fire regime (White and Nordheim 1992).

Using the regression analysis method, the following relationship between heat exposure time in fire conditions and charred layer thickness was found:

$$\tau = m x_c^{1,23},$$

where τ – fire exposure time, min; x_c – the charred layer thickness, mm; and m – the correlation coefficient: the value inversely proportional to the charring rate. This index is a function of the apparent density of dry timber, ρ, kg/m^3; moisture content in the specimen, u, %; and charred layer shrinkage, f_c.

The charring rate index, m, is calculated by the formula:

$$m = 0.000564\rho + 1.21u + 0.532 f_c - 0.147, \quad \text{min}/\text{mm}^{1.23}$$

Here, f_c is a dimensionless parameter of charred layer thinning. It is defined as the ratio of charred layer thickness at the end of fire exposure to the initial thickness of the timber layer that could be charred. The authors (White and Nordheim 1992) believed that the f_c factor depends on the lignin content in the chemical composition of timber.

The value of the charring rate index for dry spruce wood with $\rho = 460$ kg/m^3 is $m = 0.47$ min/mm$^{1.23}$, whereas at 9 % moisture, $m = 0.58$ min/mm$^{1.23}$.

The charring rate for deciduous timber species in standard fire regime is 10–20 % lower compared to coniferous specimens.

The formula given above pertains to the test environment at standard temperature regime of timber constructions in no-load condition. It is known that mechanical stress applied to a specimen "helps" the thermal motion to destroy the material. But how does the loaded condition of a structural member affect the charring rate, if at all? This question remains unanswered.

Experience shows that the average charring rate of various timber species may vary from 0.6 to 1.1 mm/min and depends on many factors, in particular, on timber density (volume weight) and moisture, number of heated sides in the construction, heating duration, cross-section size, surface roughness, and others (Demekhin et al. 2003).

As timber density (volume weight), moisture, and cross-section size of a timber construction member increase, the average charring rate decreases. As the temperature of the heating medium during a fire, air intake, number of heated sides in the construction, and timber surface roughness increase, the charring rate of timber also increases. For example, at temperature–time standard fire exposure on four sides of timber columns in loaded condition, the charring rate increased 1.25–1.3 times compared to one-sided heating. With sufficiently long temperature exposure, the average charring rate of timber decreases.

The charring rate of solid timber is higher compared to glulam. In an experimental study of spruce beams with cross sections of 100×140 mm and 150×250 mm exposed to standard fire regime, the following average rates of charring propagating the from cross-section center were found (Zoufal and Kashpar 1986):

For solid timber beams:

Lateral charring rate was 0.65 mm/min.
Upward charring rate was 0.95 mm/min.

For glulam beams:

Lateral charring rate was 0.55 mm/min.
Upward charring rate was 0.85 mm/min.

It was also noted that the charring rate was not linear, and differed at various stages of timber combustion.

The charring rate of timber depends heavily on the type of load-bearing constructions and their service conditions (Gousev et al. 2008). In some European countries, there are standards establishing the average charring rate for various types of timber constructions at the design stage of building projects.

Thus, for example, circular letter N 91/61 of the Italian Ministry of Internal Affairs states the following average charring rates for various timber load-bearing construction types: external vault-forming beams and side beams – 0.8 mm/min; internal vault-forming beams – 1.1 mm/min; pilasters and columns – 0.7 mm/min; and other horizontal structural members – 1.1 mm/min. The Italian National Standard "Analytical fire resistance assessment of timber structural elements" that was published later specified charring rates of 0.9 mm/min for solid timber and 0.7 mm/min for multilayer glulam.

Tests of various unprotected timber construction members in standard fire regime show that the average charring rate is about 1 mm/min and ranges from a minimum value of 0.6 mm/min for dense and wet timber to 1.2 mm/min for light and dry timber (Gousev et al. 2008).

From the relationship between heat energy balance in the pyrolysis front and on the charred surface layer during timber combustion, the authors of work (Strakhov et al. 2000) obtained the analytic dependence of charred layer thickness buildup, δ_c, on time t adjusted for char shrinkage.

This was made possible through a series of assumptions: quasi-stationarity of the combustion process, relatively small pyrolysis zone thickness, predominantly radiation heat exchange between the flame and flammable material surface, and the use of a pre-specified temperature profile in the material being decomposed according to an exponential law. The shrinkage coefficient of the charred layer, β_{sh}, as well as the yield of carbonized residue, K, as a result of material pyrolysis, are assumed to be constant. The following equation was obtained:

$$\delta_c = \sqrt{2a_c t + b_c^2} - b_c$$

where b_c is a parameter that incorporates the thermal conductivity of the charred layer and radiation heat transfer from the flame at temperature T_f

$$b_c = \frac{\lambda_c}{A_{eff}\sigma T_f^3}$$

where $A_{eff} = 1/[(1/\varepsilon_f)\ (1/\varepsilon_w - 1) + 1/\varepsilon_w]$ is the effective function of radiation parameters of the flame and combustible surface and ε_f and ε_w are radiation capacities of the flame and combustible surface. Parameter $a_c = (1-\beta_{sh})\lambda_c(T_f - T_c)/\rho[(1-K)L_v + c_p(T_c - T_0)]$ incorporates the ratio of the heat transferred from the flame toward the pyrolysis front to the heat consumed for gasification of the combustible material.

For combustion of Douglas fir at $T_f = 1{,}200$ K and assumed timber properties: $\rho = 450$ kg/m^3, $c_p = 2{,}800$ J/kg·K, $k_c = 0.5$ W/m K, $\beta_{sh} = 0.2$, $K = 0.2$, $L_v = 1{,}820$ kJ/kg, and $T_c = 623$ K, the calculation showed that the charred layer thickness in 20 min of combustion reached almost 18.5 mm. The average charring rate was 0.925 mm/min. After the onset of pyrolysis in spruce timber, the mass rate of pyrolysis for this period decreased from 12 to 4 g/m^{2}s (Strakhov et al. 2000).

We have determined the average charring rate for coniferous and deciduous timber in standard fire conditions in a small-scale fire furnace with specimens sized $150 \times 150 \times 30$ mm heated on one side for 20 min. Under these conditions, the onset of active charring in the specimens is observed 4–5 min after the start of the test. Table 8.3 shows the average charring rate values obtained for timber and the characteristics of the surface char layer.

As can be seen from Table 8.3, the deciduous timber specimens charred at a lower rate compared to fir and pine. They form a thinner but denser surface char layer.

The lower thermal inertia value, $\lambda\rho c$, of deciduous species is probably due to the formation of a more homogeneous fine-porous char structure.

The charring rate of unprotected construction members in standard fire regime under one-dimensional heat transfer is usually assumed as the base value in the

Table 8.3 Charring parameters for various timber species and the properties of surface char layer

Specimen	δ_{char}, mm	β_0, mm/min	ρ_{char}, kg/m^3	$T_{s\,char}$, °C	$(\lambda\rho c)_{char}$, kJ^2/m^{4}K^{2}s
Fir	23	1.15	225	780	0.140
Pine	19	0.95	268	732	0.133
Birch	13.5	0.675	285	718	0.115
Oak	9.2	0.46	348	700	0.119

design of timber buildings and structures. For example, Eurocode 5, EN 1995-1-2 recommends a basic charring rate of 0.65 mm/min for coniferous specimens 20-mm thick with density of 450 kg/m^3. If the thickness and density are other, the basic charring rate is multiplied by the specified coefficients (EN 1995-1-2 2004).

If a timber construction is heated on three or four sides with allowance for edge curves, the recommended charring rate for coniferous species is $\beta_0 = 0.8$ mm/min, whereas for glulam and LVL, $\beta_0 = 0.7$ mm/min (EN 1995-1-2 2004). The domestic code (SP 64.13330.2011) recommends assuming a constant charring rate equal to 0.7 mm/min for coniferous timber construction members.

When structural fire protection is utilized, the European standard (EN 1995-1-2 2004) emphasizes the charring onset time in the protected structural member. The fire protection effect of a multilayer construction system in this case is considered additive: it consists of the sum of the fire protection action duration of each layer. The reciprocal influence of adjacent layers on heat transfer variation in complex load-bearing constructions and enclosures of timber structures is covered in the technical guideline of (Fire safety in timber buildings 2010). It was shown that when fire protection is available, the charring rate of a protected timber construction slows down. But after failure of the fire protection, charring proceeds at an accelerated rate that exceeds the charring rate of unprotected timber.

8.4 Fire Resistance of Timber Building Members and Charring Depth

In the construction of timber buildings and structures, two main structural systems with various functions of timber constructions being used can be specified. (1) Frameless structures of massive logs or beams with load-bearing and load-separating constructions for external walls. (These are so-called heavy timber buildings.) Walls take all vertical loads, as well as horizontal loads through the floor/ceiling assemblies of the building. (2) Frame buildings, where the main load is taken by the frame constructions. This type of building can be divided into structures with large-span massive load-bearing constructions and light frame timber buildings.

In a framework structural system, vertical load-bearing constructions are columns, and crossbars, beams, and trusses perform the function of horizontal load-bearing constructions.

Timber frames with massive bearing constructions are used in large-span public buildings (sports halls, exhibition halls), as well as one-story industrial buildings and agricultural enterprises. Frameworks in these buildings may be single-span or multi-span, with or without hanging tap-beams with a capacity of up to 3 tons designed for operating buildings and structures in a normal temperature regime and in corrosive environments.

Timber structures are used to build post-and-beam, frame, and arched frameworks. Post-and-beam frameworks are designed mainly for industrial buildings. Beams or trusses overlap spans with sizes from 6 to 8 m or from 12 to 30 m. Arches with ties are used in construction of large spans. Frames are designed for single-span public and industrial buildings with spans from 12 to 24 m. Bearing frames may be formed of rectilinear elements (crossbars, posts) connected by pegs or fingers. Curved frames can also be used. Arched frameworks are designed for single-span public and industrial buildings (chemical raw material and fertilizer warehouses, etc.) with spans up to 60 m or more. Arch height is usually at least 1/6 of the length of the span L, and the depth of the arch is up to $1/30L$.

Light frame timber buildings are designed for the low- and medium-rise residential sector, offices, small shopping centers, etc.

As the load-bearing timber constructions in frame buildings, glulam and LVL beams with constant and variable depth, metal–timber trusses, brace flatworks (arches, frames), and spatial structures in the form of vaulted and domed covers are used as the load-bearing timber constructions in frame buildings.

Coniferous species – pine and spruce, more rarely larch and cedar – are generally used to manufacture load-bearing timber constructions. Hardwood timber is used to make dowels, timber pads, and other parts.

One of the main requirements for timber constructions s with bearing and separating functions is to provide acceptable fire resistance.

Fire resistance of timber constructions depends not only on the type of material (glued or solid timber), but also on the presence of reinforcement elements, articulator connectors, dimensions and cross-sectional configurations of the structural member, values of mechanical loads, structural fire protection, fire exposure conditions, and many other factors.

The stability of timber constructions at fire and their ability to maintain their bearing and enclosing functions are characterized by a quantitative index – fire resistance limit in standard fire conditions.

Standard methods are used (GOST 30247.0-94 1996; GOST 30247.1-94 1996) to experimentally determine the fire resistance of timber constructions. Russian methods as per GOST 30247.0 and GOST 30247.1 are similar to the ISO 834 and ASTM E-119 standards for parameters of fire furnaces and time–temperature fire regime.

Standard temperature dependence on fire development time is described by the equation:

$$T_f - T_0 = 345 \lg (8\tau + 1),$$

where T_f and T_0 are the current and initial temperatures in the furnace chamber, °C, respectively, and τ is the time, min.

The fire resistance limit of timber constructions may be determined by calculation on the basis of patterns of charring rate and heating of their cross sections at standard fire exposure.

When designing timber structures, it is important to ensure that the fire resistance limit of timber constructions with the connection elements and supporting nodes, including metallic and nonmetallic reinforcement, is no lower than the required fire resistance limit for this assembly in general.

The main signs of the limit state of bearing structures and enclosures are:

1. Loss of load-bearing capacity (sign R) occurs due to the collapse of the structure or the appearance of limit deformations (e.g., abnormal bending).
2. Loss of integrity – through cracks or holes in constructions or joints (sign E), through which combustion products or flame get into an adjacent room.
3. Loss of thermal insulating capacity (sign I) – a temperature rise on the unexposed surface of the structure of more than to 160 °C or higher 180 °C on average at any point of the surface.
4. Achieving limit values of heat flux (3.5 kW/m^2) at a standardized distance (0.5 m) from the unexposed surface of the construction (sign W).

Fire resistance of a building construction is the actual fire resistance limit determined by the time of occurrence (in minutes) of one or more sequential standardized signs (R, E, or I).

The fire resistance limit of timber constructions is usually determined by the time in which cross-section load-bearing capacity decreases due to charring and initial heating to the actual load value.

It has been found experimentally that glulam has higher fire resistance than solid timber. This can be attributed to the better structure of the glued elements, as well as the use of heat-resistant adhesives in the glulam industry. Thus, a glued timber beam with cross section of 100×140 mm has a fire resistance rating of 35 min during tests, which is 10 min more than fire resistance rating of solid timber with a similar section (Zoufal and Kashpar 1986).

The most important factors determining fire resistance of timber structures are cross-section dimensions of the construction and the number of heated sides during fire exposure. The results of determining the fire resistance limit of timber beams as a function of cross-section size and heated sides at standard fire temperature regime are shown in Table 8.4.

The results presented in Table. 8.4 show that decreasing the size of the cross section significantly reduces fire resistance ratings. Therefore, a structure with

Table 8.4 The effect of heating conditions on the fire resistance limit of timber beams with various cross sections

No	Type of construction	Fire resistance limit, min
1.	Timber beams, bending stressed, unprotected (three-sided fire exposure) with dimensions in mm	
	100×140	25
	120×160	30
	140×200	40
	180×260	50
2.	Timber columns, unprotected, buckling stressed, with flexibility $\lambda = 75$ (four-sided fire exposure) with dimensions in mm	
	120×120	10
	160×160	15
	200×200	20

100×140-mm cross section has a fire resistance rating of 25 min, while a structure with 260-mm cross section has a rating of 50 min or twice as long. An increase in the number of heating side reduces the construction's fire resistance rating.

The cross-section configuration of timber structures has a strong influence on their fire resistance and fire safety. For example, in elements with a rectangular cross section, the corners are charred more intensely during "standard fire," and they start rounding 10–15 min after timber charring.

Ribs and similar protruding elements with a large ratio of heated surface area to heated material volume ignite faster than flat or convex elements with a large radius of curvature (Roitman et al. 2013).

In case of fire, the fire resistance of timber construction is determined mainly by the decrease in load-bearing capacity of their timber elements and joints of these elements.

The bearing capacity of timber structural elements is reduced by charring and reducing the size of the effective cross section able to take the actual load and because of the changes in strength of timber in the non-charred part of the section (Roitman et al. 2013). The change in the load-bearing capacity of nodal connections in a fire is affected both by timber charring and reduced strength of steel components used in timber constructions, i.e., steel dowels, reinforcement units – pads, etc. (Fig. 8.4).

The timber charring process is necessarily accompanied by a decrease in the timber structure's effective cross section. Due to its porous structure and low thermal conductivity, the char layer serves as a thermal barrier and restricts oxygen access to the non-charred cross section of a structure. Uneven temperature distribution over the cross section behind the charring front leads to uneven changes in mechanical and thermal properties of the timber at different points of the cross section.

Fig. 8.4 The collapse of wooden structures in a fire due to loss of strength of steel connections

The following formula can be used to calculate the average temperature in the middle section of a timber structure at standard fire temperature regime with allowance for charring rate and heating conditions:

$$T = (1 + kb/h)\ [20 + 180(\beta\tau_f)^{\eta}/(1-\eta)\ (b/h - \beta\tau_f)]\left\{(b/h)^{1-\eta} - (\beta\tau_f)^{1-\eta}\right\},$$

where b and h – the initial width and height of the cross section of a timber structural element; β – the charring rate; τ_f – the duration of the fire; and k – coefficient accounting for the number of heated sides.

The value $k = 0$ is used for 2-sided heating, $k = 0.25$ for 3-sided heating, and $k = 0.4$ for 4-sided heating of construction. η parameter takes into account the duration of the fire: $\eta = 0.398\tau_f{}^{0.62}$.

The temperature is distributed from the charring front with a temperature of 300 °C toward the center section of massive glued timber elements according to a hyperbolic law. Mechanical properties of timber vary linearly with temperature in certain heating intervals.

Mechanical stress applied to a timber sample increases destruction of the material. Thus, the fire resistance limit of 3 m pine beams with a cross section of 120×410 mm decreased from 65 min to about 20 min as the load in the middle of the beam increased from 2,300 to 9,200 kg at standard fire temperature regime (Haritonov and Hmelidze 1989).

It should be noted that under the same mechanical loading conditions, larch beams showed a fire resistance limit nearly 25 % higher than the pine beams. The charring rate of larch timber beams and charred layer thickness were also lower.

According to (Janssens 2004), a similar effect was observed during the testing of Douglas fir glulam with a cross section of 222×419 mm and length of 4.57 m by ASTM E 119 standard. The central part of beams 3.76-m long was exposed to fire in a furnace. Beam loads were evenly distributed at two points at equal distance, such that they were 27, 44, and 91 % of the design value. Permissible stress and stiffness values corresponded to 16.55 MPa and $E = 11$ GPa. Glulam failure under these conditions occurred after 147, 114, and 85 min, respectively. During this period, the charred layer thickness reached 81, 74.5, and 57.3 mm, respectively.

At standard fire temperature regime, the actual fire resistance limit of timber constructions, Π_{ac}, is determined by the sum of time from the start of thermal effect on the timber in a fire before charring, τ_0, and the time from the start of charring before the ultimate limit state in a fire, τ_{cr}:

$$\Pi_{ac} = \tau_0 + \tau_{cr}, \min .$$

The latter value is determined from the timber charring rate:

$$\tau_{cr} = \frac{(\delta_{cr} - \delta)}{\beta},$$

where β – the charring rate, mm/min; δ_{cr} – charred layer thickness at the ultimate limit state, mm; and δ – thickness of the wood behind the charring front, which has zero strength.

In a recent edition of the updated set of codes for timber structures (SP 64.13330.2011), it was recommended to take the thickness of this layer equal to 7 mm, as in Eurocode 5 (EN 1995-1-2 2004). Thus, it is assumed that a timber layer heated from 175 to 300 °C should not be taken into account when calculating the fire resistance limit of timber structures, due to a significant reduction or loss of strength properties. The critical thickness of the charred layer, δ_{cr}, should not exceed 0.25 part of the smallest size (thickness) of the section.

The general principle of calculating fire resistance of building constructions in case of fire is to solve two problems: heat engineering and static (mechanic strength). The goal of the heat engineering task is to evaluate the temperature distribution over the cross section of timber constructions, its heating time, and time to reach the critical value. The purpose of the static task is to calculate the time to reach the ultimate limit state of a structural element by strength loss due to the change in mechanical properties as a function of temperature and the time to reach its critical value.

Exact calculation methods for fire resistance limit of building members, including solid timber and other composite materials, are based on mathematical modeling

and numerical solutions set partial equations of heat transfer and static using modern computers. In this case, input data are required to characterize heat construction materials, in particular, knowledge of the kinetic decomposition parameters and thermal and mechanical properties of timber in a wide temperature range. The presence of fire protection requires the corresponding data on the characteristics of the fire protection material (Strakhov et al. 2000; Koshmarov et al. 1990).

These calculations are very complex. Therefore, simplified methods and techniques for solving specific problems, in particular, finite difference methods and analytical solutions, are used in engineering practice.

Base values of the resistance solid coniferous timber and glued members to various stressed states (bending, compression, stretching, shearing, etc.) are listed in (SP 64.13330.2011; STO 36554501-002-2006).

To take into account operating, loading and dimensional changes, the layer thickness in glued structures, the presence of nodes and connections, and other factors, the appropriate coefficients are used.

The principle of applying the relevant coefficients to take into account the influence of different factors on the onset of charring (fire resistance) of bearing and enclosing elements of constructions is implemented in Eurocode 5 and technical guideline (EN 1995-1-2 2004; Fire safety in timber buildings 2010).

Timber members in light frame structures with no fire protection lose their load-bearing function in a fire within a few minutes. Adequate fire protection for all bearing constructions, correct sequence of flame retardant separating panels and insulating layers in the general assembly, and also fire protection of joints increase the fire resistance limit of light frame assembly to 120 min. The material of the first layer of protective membrane is of great importance. Plasterboard as first protective layer of timber structures contributes the most to increasing the fire resistance limit of the assembly. A positive contribution is also made by mineral insulation between the walls of constructions.

Despite the fact that structurally achievable fire resistance limit may be high, timber constructions remain fire hazardous. The fire hazard class of construction is determined as per GOST 30403-96 (1996). The fire hazard class of timber construction must be determined in order to establish the extent of their participation in the fire development and the occurrence of fire hazards. Fire hazard class depends on the fire safety of the materials from which constructions are made. Unprotected solid timber belongs to materials of class G4 (highly combustible), B3 (easily flammable), and D3 (high smoke generation capacity), and glulam with no fire protection is a material with fire safety indices G4, B2, and D3 (Koshmarov 2000).

In this regard, the use of timber constructions without proper fire protection is limited. It is especially limited in construction of large public and industrial buildings and structures. Modern methods of fire protection of timber structures can significantly reduce the risk of fire.

References

Astapenko VM, Koshmarov YA, Molchadskiy IS, Shevlyakov AN (1988) Thermogas dynamics of fires in room. Stroyizdat, Moscow, 448 p

Competitive environment (2011) http://киск-красноярск.рф

Demekhin VN, Mosalkov IL, Serkov BB et al (2003) Buildings, constructions and their stability in fire conditions. SFS Academy, Moscow, 656 p

Development prospects of the glued laminated wood market (2009) http://www.stroyinform.ru

EN 1995-1-2 (2004) Eurocode 5: design of timber structures, Part 1–2: general – structural fire design

Federal Law of RF No. 117 Amendments to Federal Law of RF No. 123-FL Technical regulations for fire safety requirements, dd. 10.07.2012

Federal Law of RF No. 123-FL Technical regulations for fire safety requirements, dd. 22.06.2008.

Fire safety in timber buildings. Technical guideline for Europe (2010) www.jrc.ec.europa.eu; ISBN 978-91-86319-60-1

GOST 12.1.004-91 Fire safety. General requirements. Moscow, 1992

GOST 30247.0-94 Building structures. Fire resistance test methods. General requirements. Standards Publishing, Moscow, 1996

GOST 30247.1-94. Fire resistance test methods. Bearing and enclosing structures. Standards Publishing, Moscow, 1996

GOST 30403-96 Building structures. Method of determining fire hazard. Moscow, 1996

Gousev AI, Paznikova SN, Kozhevnikova NS (2008) Enhancement of the fire resistance of timber constructions. Fire Explos Saf 15(3):30–35

Haritonov VG, Hmelidze TP (1989) The behavior of glued timber beams at standard fire conditions. Fire resistance of building components and fire safety people and property. Fire Safety Research Institute of Ministry of Internal Affairs of the USSR, Moscow

Holshchevnikov VV, Samoshin DA, Isaevich II (2009) Field studies of traffic. ASFS, Moscow, 191 p

Janssens ML (2004) Modeling of the thermal degradation of structural wood members exposed to fire. Fire Mater 28:199–207

Koshmarov YA (2000) Prognozing fire hazardous factors inside facilities. ASFS, Moscow, 120 p

Koshmarov YA, Rubtsov VV (1999) The process of growth of fire hazardous factors in industrial buildings. IFS, Moscow, 90 p

Koshmarov JA, Geraskov GV, Voinov AN, Molchadsky IS (1990) Mathematical modeling of charring during combustion of thermally thick material burning. FTHS, Moscow, pp 172–175

Kovalchuk LM (2005) Production of glued laminated wood structures, 3rd edn. RIF Stroymaterialy, Moscow, 336 p

National Standard of the Russian Federation EN 1991-1-2-2011, Eurocode 1: effects on structures – Part 1–2: main effects – effects on buildings in fire conditions. Moscow, 2011

Puzach SV (2003) Mathematical modeling of gas dynamics and heat and mass transmission in solving problems of fire-explosion safety. Academy of the State Firefighting Service of the Ministry of Emergency Situations of the Russian Federation, Moscow, 264 p

Roitman VM, Serkov BB, Shevkunenko YG, Sivenkov AB, Barinova EL, Pristupiuk DN (2013) Roitman VM (ed) Bulidings, structures and their fire-resistance, 2nd edn. ASFS, Moscow, 366 p

Romanenkov IG, Zigern-Korn VN (1984) Fire resistance of building structures made of effective materials. Stroyizdat, Moscow, 240 p

SP 2.13130.2009 Systems of fire protection. Providing fire resistance for protection objects. Moscow, 2009

SP 64.13330.2011 Wood constructions. Current edition. SNiP II-25-80. Moscow, 2011
STO 36554501-002-2006 Glued wood and all-wood construction. Moscow, 2006
Strakhov VL, Kroutov AM, Davydkin AM (2000) Koshmarov YA (ed) Fire protection of building constructions. TIMR, Moscow, 433 p
Vatin NI (2008) Long span bearing structures made of glued laminated wood. StroyProfil 1(63):38
White RH, Nordheim EV (1992) Charring rate of wood for ASTM E 119 exposure. Fire Technol 28(1):5–30
Zoufal R, Kashpar Y (1986) Study of timber constructions in terms of fire safety. Bulletin of the Specialized Higher School, Sofia, pp 70–88

Chapter 9
Fire Protection of Timber Building Structures and Constructions

Abstract This chapter presents the industrial approach to improve the fire resistance and fire safety of timber constructions. A comparison analysis of the efficiency of two types of fire protection of timber constructions based on surface and deep impregnation of timber by novel fire-retardant impregnation compositions and based on novel intumescent coatings from plant raw material is presented.

The method of modification of plant raw material and some physicochemical characteristics of product are presented. The effect of fire protection on charring parameters of wood species at standard fire regime is discussed.

The world's developed countries have adopted common principles of fire safety of building structures and constructions aimed first of all at protecting human life and health, as well as minimizing material damage from fire. The fire safety system of building structures involves fire protection measures at their design, construction, and operation stages. Fire protection measures applied in practice are aimed at reducing the risk of fire onset and spread. These measures depend on the fire resistance class and structural fire safety of buildings and their functionality.

Fire safety and fire protection measures for building structures and constructions are conventionally subdivided into active and passive. The first group includes space planning and design solutions developed at the building's design stage with regard for its function (processes taking place in the building) and fire resistance class. Thorough consideration is given to safe evacuation of people and constraining fire spread beyond its seat by fire barriers and smoke control.

Active fire protection measures for building structures and constructions at the operation stage include provisions for early fire detection by various detectors, fire alarm, and notification to alert occupants of fire. Manual and automatic fire-extinguishing devices are to be used to suppress fires in premises at the initial stages.

Passive measures involve the use of various fire protection means and materials. As practice shows, in most cases, the use of fire protection is a cost-effective way to increase the fire safety and fire resistance of constructions. These same measures with reference to timber building structures and constructions are addressed below.

R. Aseeva et al., *Fire Behavior and Fire Protection in Timber Buildings*,
Springer Series in Wood Science, DOI 10.1007/978-94-007-7460-5_9,

9.1 Recent Ways and Means of Fire Protection to Increase Fire Safety and Fire Resistance of Timber Building Constructions

Fire safety and fire resistance of building structures are the basic parameters that determine the stability of building structures and constructions during a fire. Stability is understood as retention of load-bearing capacity of constructions and structural integrity of a building facility and preservation of its functionality. Fire protection of building structures takes into account their design features and properties of constituent materials, as well as operating conditions.

In buildings and structures with constructions of solid timber or glued laminated timber (glulam) materials with load-bearing and enclosing functions, there are different approaches to enhancing stability and protecting the structures from collapsing during a fire.

If massive load-bearing timber frames of logs, beams, or multilayer glulam materials are employed, then increasing their cross section is one way to enhance their fire resistance rating (see Chap. 8). The optimal necessary dimensions of structural members may be calculated at the design stage if taken into account the charring rate and depth, preserved part of the cross section during a specific period of fire, and changes in mechanical properties of timber during heating.

The main lines of passive fire protection include the use of structural fire protection; impregnation of timber with fire-retardant compositions; direct application of fire-resistive coatings on the material surface, including intumescent types; and the use of combined fire protection.

Combined (integrated) fire protection is an optimal combination of structural fire protection with intumescent fire-retardant coatings or a combination of different types of structural fire protection, e.g., a combination of sheeting and thermal insulation.

The structural fire protection enhancing fire safety and fire resistance rating of timber constructions is similar to fire protection of load-bearing structures and enclosures made of metal, concrete, or reinforced concrete.

Slab and coiled materials, fire-resistive coatings, and inorganic thermal insulation, as well as various types of timber-based panels, are used for this purpose. The main purpose of these claddings is to slow down the heating of protected timber constructions to critical temperature when active pyrolysis starts and timber ignites. They are also supposed to decrease the timber charring rate and heating of its remaining unaltered part beyond the charring front to the limiting temperature responsible for the loss of mechanical properties of timber. The efficiency of timber fire protection by these structural methods depends in the first place on the resistance against fire action and the heat insulation capacity of the fire-resistive materials being used.

Combined fire protection is especially promising in terms of enhancing fire safety and fire resistance of light frame timber buildings.

It is assumed that in standard temperature fire conditions, timber starts to char at 270–300 °C. Experience shows that timber heating beyond the charring front under these conditions is close to the hyperbolic law for cross-sectional temperature changes, whereas mechanical properties decrease linearly with temperature.

When the integrity of structural fire protection is broken due to cracks or delamination, its effect on the timber charring rate is minimized. And in case of global failure of fire protection, it could even turn negative.

Specifications and trademarks of currently used fire protection means, cladding, and heat insulation materials for timber structures are given in works (Romanenkov and Leveetes 1991; Strakhov et al. 2000; Korolchenko and Korolchenko 2006; Leonovich and Sheloumov 2002). The cheapest ones are dry gypsum plasterboard types domestically produced on a large scale: gypsum board (GB) and gypsum-fiber board (GFB).

Structural methods may notably increase the fire resistance rating of timber constructions. However, the fire-resistive materials must be fairly thick, usually more than 10–15 mm.

It was found by experiment, for example, that in a standard fire temperature regime, the time before charring onset, τ_0, for solid timber constructions fire protected by with semirigid slab of glass mineral cotton wool (GOST 9573-89) 50-mm thick was 30 min (Strakhov et al. 2000). The fire resistance rating of timber partitions with double-sided GFB cladding was 28 min (Strakhov et al. 2000). Increasing the number of layers or thickness of fire-protective material raises the fire resistance rating of a timber construction.

Typical modern slab materials employed for fire protection of timber constructions include slabs based on cement–silicate binders (Promatect-L), liquid–glass-based vermiculite slabs (PVTN, Ecoplast), noncombustible basalt fiber slabs (PNTB), and rock wool slabs (CONLIT-150).

Thermal calculations of fire resistance of glulam with the indicated structural fire protection means show the effect of fire-resistant material thickness on the increase in time before charring onset, τ_0, and reduction of average timber charring rate for a specified period of heat exposure (Table 9.1) (Roytman et al. 2013).

For example, the use of 40-mm-thick vermiculite slabs PVTN increases the τ_0 value to 106.7 min, reducing the average charring rate of glulam from 0.73 for unprotected items to 0.3 mm/min. Light plaster SOTERM-1M, a material based on a light porous filler and mineral binder, is quite effective.

Calculations of the required thickness of structural fire protection for various load-bearing structures and enclosures made of solid timber or timber-based materials are based on the use of mathematical models that take into account the features of heat and mass transfer during a fire within a "fire protection – construction being protected" system (Strakhov et al. 2000; Roytman et al. 2013). In the process a concept is applied, which states that charring reduces the effective cross section of a timber construction and its strength properties at elevated temperatures and a layer with zero strength is formed in close proximity to the charring front. It was assumed that the timber layer with zero strength was 5-mm thick. Calculations of

Table 9.1 Time before charring onset and average charring rate of glulam with various means of fire protection

No	Means of fire protection	Thickness, mm	τ_0, min	ν_{av}, mm/min in time span of, min	
				30	45
1	Without fire protection	–	4	0.73	0.65
2	Cement–silicate slab Promatect-L	10	15.5	0.67	0.61
		20	35.5	0.58	0.54
		30	60.8	0.52	0.49
3	Vermiculite slab PVTN	10	16.0	0.52	0.49
		20	38.5	0.4	0.38
		30	68.9	0.32	0.31
		40	106.7	0.3	0.29
4	Basalt fiber slab PNTB	20	33.0	0.4	0.38
		30	53.1	0.33	0.31
		40	73.2	0.3	0.29
5	Rockwool slab CONLIT-150	20	35.2	0.43	0.39
		30	54.5	0.36	0.32
		40	74.3	0.32	0.3
6	Coating SOTERM-1M	10	21.5	0.53	0.5
		20	54.5	0.41	0.39
		30	99.8	0.32	0.31
7	Intumescent coating PROTERM WOOD	0.6	26.9	0.87	0.78
		1.0	35.1	0.84	0.73
		1.5	41.8	0.8	0.69
		2.0	47.3	0.78	0.67
		1.0	38.5	0.91	0.78
		1.5	44.5	0.89	0.76
		2.0	49.9	0.87	0.74
8	Intumescent coating OGRAKS-V-SK	0.6	22.5	0.66	0.65
		1.0	34.2	0.73	0.71
		1.5	45.0	0.8	0.73
		2.0	53.8	0.87	0.74
9	Intumescent coating OSP-1	1.0	11.3	0.67	0.6
		3.0	40.5	0.55	0.51
		5.0	78.0	0.46	0.44

temperature fields in glulam in a standard fire regime made in work (Garashchenko et al. 2006) showed not only excessive thickness of the layer $\delta = 5$ mm confined between isotherms 175 and 300 °C and unable to resist the acting load. A tendency was also revealed toward an increase in this layer, when the structural fire protection thickness grows and heat exposure time is prolonged.

European Standard EN 1995-1-2, Eurocode 5 recommends assuming a zero-strength layer thickness under the charred timber layer equal to 7 mm. The question of the effect of structural fire protection on zero-strength layer thickness is addressed in the work (Schmid et al. 2010) with cross-laminated timber (CLT) as a case study.

Thickness of zero-strength layer below char layer for timber members in load-bearing structures depends on fire exposure conditions, configuration of the construction, and strain type in timber member. Technical guideline on fire safety in timber buildings (Ostman 2010) introduces the improved design methods of load-bearing and load-separating timber structures and presents the effect of different factors on sizes of charring layer and zero-strength layer resulting in standard fire regime.

Fire resistance of timber member is increased with using fire-resistive structural panels or fire-protective intumescent coatings. The efficiency of timber protection depends on the thickness and durability of the coatings. Therefore, fire protection means for timber can be devised on two groups: (1) fire retardant means reducing the spread of flame over a surface and (2) fire resistive means reducing the rate of charring.

Fire protection of timber constructions by surface and deep impregnation with special compositions containing fire retardants, as well as application of fire-retardant coatings, is popular today (Romanenkov and Leveetes 1991; Strakhov et al. 2000; Korolchenko and Korolchenko 2006; Leonovich and Sheloumov 2002; Ostman 2010; Leonovich 2003; Bazhenov et al. 1999; Deyeva 1999; Tychino 1999, 2003). The use of thin-layer intumescent fire-retardant coatings is especially attractive. Even when relatively thin, they demonstrate high fire protection efficiency, and allow the use of modern mechanized methods of application on the item being protected, while retaining the basic texture of the timber and its esthetic appearance.

As a rule, fire-retardant impregnation compositions and coatings for timber are multicomponent systems. Each component of the system has its function in providing the total fire-protective effect and required performance properties.

In most cases, impregnation compositions are salt solutions in water medium or in organic solvents. Surface impregnation is done by multiple manual or mechanized applications of the composition on the timber surface and materials being protected.

Surface impregnation is cheap and versatile but is less effective than deep impregnation. It is attractive because it may be used to protect already installed timber structures directly at a construction site. However, it is very difficult to obtain reliable timber protection by this method. This is mainly due to poor penetration of salts into timber, requiring high salt consumption. Deeper penetration in the surface timber layers is provided by such impregnation methods as hot-and-cold bath and treatment in industrial apparatus – autoclaves with incremental pressure buildup or alternation of vacuum and increased pressure.

The hot-and-cold bath method is used as the principal method of construction timber impregnation in a number of woodworking plants (Novitsky and Stogov 1959). Deep impregnation with fire-retardant salt solutions is based on the characteristics of the capillary-vascular structure of timber. A series of bottlenecks in technology, the high consumption of fire retardants, and the need for specialized equipment for deep impregnation constrain the practical use of this timber fire protection approach.

Today, many impregnation compositions for timber have been developed, which have different sets and proportions of low-molecular inorganic substances and derivatives of organic compounds demonstrating fire-retardant properties. Academic and practical research in this field continues with the objective of finding still more effective fire-retardant compositions for timber and improving the performance properties of the end product.

The substances frequently used in formulas of fire-retardant impregnation compositions include various derivatives of phosphoric and phosphonic acids: mono- and diammonium phosphates and mixtures thereof (ammophos) urea-, melamine-, and amidophosphates and amidomethylphosphonates. Boric acid, ammonium and sodium tetraborates, ammonium salts of sulfuric and hydrochloric acids, chlorides of alkaline-earth metals and polyvalent transition metals, sodium and potassium carbonates – this is by no means a complete list of inorganic substances used as components of fire-retardant impregnation compositions for timber.

Many of the indicated substances have a polyfunctional effect on the chemical constituents of timber. For example, they have the properties of catalysts for etherification of both hydroxyl-containing macromolecules of timber components by phosphorus acids and of agents of cellulose dehydration. In this way, they promote directional change of timber thermal decomposition reactions toward reduction of flammable volatiles through increased yield of char residue. Ammonia and hydrogen chloride generated in thermal decomposition of the employed salts may function as inert flame diluents and inhibitors of radical oxidation reactions in the gas phase. As the temperature rises, the product of thermal decomposition of phosphoric and phosphonic acids derivatives – orthophosphoric acid – turns into pyro-, tri-, and polymetaphosphoric acids, which have low volatility. Upon melting they may form a glassy protective layer on the charred surface. It works as a physical barrier against oxygen diffusion into the carbonized product. An important feature of phosphorus compounds is their unique ability to suppress smoldering combustion reactions in timber. Boric acid and other boron compounds have a similar effect.

The above-mentioned substances making up part of impregnation compositions are hygroscopic and soluble in water. That is why in an atmospheric environment with moisture above 70 % or in direct contact with water, the fire protection efficiency of timber impregnations may be totally or partially lost. To prevent this, it is recommended to apply additional water-resistant covering varnishes and paints or use fire-protected timber materials only inside the buildings.

In terms of enhancing the resistance of materials against moisture, the double impregnation method consisting in consecutive treatment of a timber surface with interacting salt solutions is worth noting. As a result, insoluble or poorly soluble fire retardants are formed in the near-surface timber layers (Romanenkov and Leveetes 1991; Strakhov et al. 2000; Gorshin and Maximenko 1977). For example, consecutive treatment of a surface with solutions of calcium chloride and diammonium phosphate produced moisture-resistant materials (Gorshin and Maximenko 1977).

Another way to enhance moisture resistance of fire-protected timber is introduction of organic and organoelemental substances with low viscosity and

water-repellent properties into impregnation compositions. Organosilicon fluids (Baratov et al. 1988) are of great interest in this context.

An important line in creating modern fire retardants for timber is the development of a new generation of bio-protective and fire-retardant impregnation compositions with partial or full substitution of salt components (Leonovich and Sheloumov 2002; Leonovich 2003; Tychino 2003). Thus, the new-generation biocide Mipor based on water-soluble ethers of phosphorous acid with broad bio-protective action against mold and wood-destroying fungi has proved quite effective. Timber impregnation with Mipor in conjunction with oligomeric organosiloxanes not only provides bio-fire protection of timber but also increases moisture and water resistance of fire-protected timber with retention of the high mechanical parameters of the initial timber (Pokrovskaya et al. 2009; Pokrovskaya and Naganovsky 2004).

Several certified bio-fire-retardant compositions that are widely used in domestic house-building are also worth mentioning. For example, the inner surfaces of timber and glulam constructions in all types of buildings (attic structures, roof frames, voids between walls and cladding) are treated with Pirilax, Attic, and Latic-KD.

Analysis of the situation with research on new lines in the development of impregnation compositions for timber shows continuous endeavors by developers of timber fire retardants to enhance the fire protection effect and limit flame spread over the material surface. This is achieved by increasing the ability of an impregnation composition to form char and expand at the decomposition stage, regardless of interaction with timber components. Another way is to increase the charring rate in the near-surface impregnated layer of timber with the formation of a dense carbon structure and glassy protective layer.

Examples of this approach are the impregnation compositions OK-GF and OK-DS based on orthophosphoric acid, products of carbohydrate hydrolysis, as well as ammonium salts of phosphoric (or sulfuric) acid and dicyandiamide developed in the Republic of Belarus (Tychino 1999, 2003). Low-molecular products of carbohydrate hydrolysis (starch) in this case serve as an additional source of char formation on heat exposure of fire-protected timber, and its expansion occurs at the thermal decomposition stage of the impregnated timber layer.

To lower the fire hazard of timber and other organic materials, a new generation of water-soluble oligomeric fire retardants, which contain elements of both phosphorus and boron in their macromolecules, has been proposed. Their synthesis is based on the reaction of dimethyl phosphite and boric acid with different mole ratios of reagents and temperatures. Treating pine timber with the water composition of P- and B-containing fire retardant increases the oxygen index of the timber from 20–23 to 53 (Bondarenko et al. 2009).

Another example is the development of the fire-retardant composition KSD-A (grade 1) by Lovin-Ognezashchita in collaboration with the SFS Academy. It was shown that the introduction of dihydroxyaromatic compound in an optimal proportion with diammonium phosphate into the impregnation composition enhances charring of the near-surface layer of timber and effectively protects its lower layers (Bondarenko et al. 2009).

The fire-retardant properties of impregnation composition KSD-A will be given in more detail below. Meanwhile, we note that laboratory small-scale GOST R 53292-2009 is the principal method currently used in Russia for evaluating fire-retardant efficiency of the newly developed impregnation compositions and coatings for timber. In situations when the material is exposed to intensive radiative heat flows, fire protection with impregnation compositions may prove to be inefficient. There are cases where timber specimens treated with impregnation compositions were classified among materials with the highest group 1 of fire protection efficiency. However, they showed rapid flame spread over timber surface during the test as per the standard method of GOST 12.1044-89. Therefore, we think the small-scale method of GOST R 53292-2009 may be considered an express method for evaluating fire protection efficiency at the creation stage of novel fire retardants for timber. Solving the practical problems of fire protection of timber-based constructions, cladding, and finishing materials for timber requires full information on all basic fire safety parameters of the recommended fire-protected timber materials. This conclusion is equally valid for all timber fire protection means with the use of both impregnation compositions and coatings.

Intumescent coatings, whose protective properties are revealed on exposure to high temperatures and fire, have a special place among currently used fire retardants. Development of this line of timber fire protection is being widely pursued both in this country and abroad.

Intumescent coatings must contain the following important components: (1) film binders that are simultaneously sources of the carbon skeleton at decomposition; (2) catalysts of carbon skeleton formation reactions; and (3) expansion (intumescence) agents. Various additives capable of influencing the technological, heat-shielding, and other performance characteristics of coatings are introduced to enhance the overall fire-retardant effect. These include fillers with the properties of fire retardants, thickeners, pigments, stabilizers, etc.

The following thermoplastic polymers are recommended as binders acting as the source of carbon skeleton formation: polyvinyl acetate, polyvinyl alcohol, chlorinated polyvinyl chloride, chlorinated rubber, latexes of copolymers of vinyl chloride with vinylidene chloride, chlorosulfonated polyethylene, and polyurethanes.

Urea-formaldehyde, phenol-formaldehyde, dicyandiamide-formaldehyde, and epoxy resins, which form the greatest number of cross-links during curing, are frequently used as thermoreactive polymers. Intumescence of paint coatings requires the transition of a polymer into a plastic, viscous elastic state. Rapid curing of thermoreactive polymers breaks the synchronism with the processes of formation and emission of incombustible vapors and gases as a result of thermal decomposition of expanding agents. Breaking this synchronism prevents the formation of an intumescent coating during heating.

The additional introduction of low-molecular sugars, polyatomic alcohols (e.g., pentaerythritol), and polyatomic phenols into the organic binder increases the yield of carbonized product.

A combination of organic binders and liquid glass is also used for intumescent fire-retardant coatings. For example, the Ekran coating comprises sodium water glass and urea-formaldehyde oligomers. The OSP-1 coating is based on a combination of polyvinyl acetate and liquid glass.

Catalysis of carbon skeleton formation reactions in thermal decomposition of organic binders occurs when there are substances through which strong acidic dehydration and dehydrochlorination agents, cyclization of the formed fragments with unsaturated cyclic olefinic bonds, and cross-linking reactions appear in the system. These substances include the above-mentioned ammonium salts of phosphoric and polyphosphoric acids, sulfates, and other compounds used in fire-retardant impregnation compositions for timber.

These same derivatives of various acids serve as effective intumescent agents for coatings by emitting a lot of incombustible gases (NH_3, CO_2, HCl, H_2O). High-temperature gas developing agents, such as dicyandiamide, melamine, and melem (e.g., as in the VPM-2 coating (Strakhov et al. 2000)), may be introduced into intumescent coating formulas in an independent state.

These intumescent agents belong to typical gas developing agents, which generate incombustible vapors and gases as a result of chemical decomposition reactions when the substances are heated. Physical agents that generate intumescent fire-retardant coatings include vermiculites and thermally expandable graphites. Vermiculites are laminated mineral compounds that expand and increase in volume when heated. Thermally expandable graphites are intercalation-laminated compounds of natural graphites. Delamination and expansion of graphite particles occurs when they are heated.

Depending on the method of intercalated compound's production and intensity of heating exposure, 300–400-fold intumescence of the substance may be achieved (Fialkov 1997).

The intumescence coefficient of coatings with thermally expandable graphites also depends on their content in the overall coating composition. It was shown, for example, that intumescent coatings based on thermally expandable graphites and organic binders, i.e., urea-formaldehyde oligomers (VPM-2[1]) or chlorosulfonated polyethylene (SGK-1), had intumescence coefficients in standard fire regime providing 7-and 25-fold increases in thickness (Strakhov et al. 2000). The OGRAKS-V-SK coating based on chlorosulfonated polyethylene rubber and thermally expandable graphite has intumescence coefficient 44.

Experimental studies on the effect of fire-retardant coatings on fire resistance rating and fire hazard class are very limited. The results of experimental work on glulam fire protection with the intumescent coatings PROTERM Wood and Phoenix DP (Garashchenko 2006) are of great interest.

Firing tests were performed on glulam panels made of pine Grade II boards with cross section 30×127 mm with above fire protection according to the standard temperature regime as per GOST 30403-96.

The test apparatus included a combustion chamber with standard temperature regime and a heat chamber with the temperature regime set according to the following time dependence:

$$T_f = T_0 + 200 \log (8\tau + 1), ^\circ C$$

Five layers of the transparent intumescent varnish coating PROTERM WOOD based on a water suspension of expansion agents, fire retardants, and other specific additives in polyvinylchloride latex were applied on the surface of glulam panels with total composition consumption of 1.8 kg/m^2. The coating was 1–1.2-mm thick. Covering varnish PROTERM WOOD TOP A1 was applied with the consumption of 0.05 kg/m^2 to increase water resistance. Independent tests of the fire hazard parameters of fire-protected timber specimens showed that they belong to Groups G1, V1, and D1; i.e., they are weaken combustible, hard flammable materials with low smoke generation capacity.

It was found that active intumescence of the PROTERM WOOD coating in the combustion chamber started from the 3rd minute at a temperature of 100–140 °C. Its thickness increased 100-fold in 20 min, when the maximum intumescent layer thickness of 120 mm was achieved. A reduction in the intumescent layer thickness due to burn-off was recorded on from the 25th minute of the test. By this time, timber surface charring had started (a temperature of 300 °C was registered). The specified temperature of 300 °C at a depth of 2 mm was achieved only in 31–32 min. Charring zone propagation on the specimen surface in the heat chamber in this period was less than 50 mm. The conclusion after the firing tests was that the fire-retardant coating PROTERM WOOD provides fire hazard class K0 (30) for glulam.

Intumescent coating PHOENIX DP with covering varnish PHOENIX DP TOP also demonstrated high efficiency of glulam fire protection. It differed from PROTERM WOOD in the proportion of PVC latex components and by the presence of some additives. It was applied on glulam panels in three layers with total average consumption of 1.0 kg/m^2 that provided a coating thickness of 0.6 mm. Glulam specimens with PHOENIX DP coating were assigned to Groups G1, V1, D2, and T2 by fire hazard parameters with consumption of 320 g/m^2.

Visual examination of the behavior of fire-retardant coatings in the combustion chamber showed that intumescence of the PHOENIX DP coating starts from the first minute and proceeds intensively at 110–140 °C. By the 17th minute, the thickness of intumesced layer reached 60 mm as a result of a 100-fold increase in the coating thickness. Its reduction as a result of burn-off was observed after 20 min of fire action. Glulam surface charring was registered at the 27th minute, but a temperature of 300 °C at a 2-mm depth in the glulam was not achieved during the 30 min of the test. A similar result was attained in the heat chamber. Therefore, a 0.6-mm-thick layer of intumescent coating PHOENIX DP secures fire hazard class K0(30) for the glulam load-bearing constructions (Garashchenko 2006).

The obtained experimental confirmations of the high efficiency of glulam fire protection by intumescent coatings based on organic polymers are in agreement with thermal calculations of their fire resistance (Garashchenko et al. 2006).

Intumescent fire-resistant coatings have complex behavior in fire conditions. Mathematical modeling of the performance of intumescent fire-resistant coatings and the calculation procedure are given in monograph (Strakhov et al. 2000). Calculation of the optimal thickness for these coatings for effective protection of building constructions requires information on many fire protection characteristics. Along with the thermophysical and thermochemical properties of the material, it is important to know the temperature parameters of its state and decomposition, properties of the coating components, and the dependence of thermal conductivity and specific heat on temperature. As numeric calculations of the mathematical model show that the fire protection efficiency of intumescent coatings depends on three parameters: intumescence coefficient of the coating, radiative heat transfer parameter, and mass loss parameter, which characterizes the stability of char foam. These parameters are defined experimentally and by calculation, on the basis of detected temperature fields in the protected material (Strakhov et al. 2000).

As we have already noted, with few exceptions, the efficiency of timber fire protection by novel intumescent impregnation compositions and coatings is assessed by mass loss during tests on specimens as per GOST R 53292-2009 (Afanasyev et al. 2007; Balakin et al. 2007; New generation of fire protective compositions for timber 2000). To what extent these fire retardants reduce the main parameters of timber fire hazard is unclear. How closely do the data on Group 1 or 2 fire protection efficiency obtained by this method agree with the fire hazard parameters of materials under more intensive radiative flows? Is there any relationship between efficiency and the fire-retardant mechanism of impregnation compositions and intumescent coatings? These questions are of great practical interest.

In foreign practice, fire protection efficiency of impregnation compositions and coatings for timber is mostly assessed by comprehensive tests using laboratory cone calorimeters (ISO 5660, ASTM E1354). This method makes it possible to determine the mass loss rate, heat release parameters (maximum and average heat release rate, total heat release in a certain period), effective combustion heat and smoke generation capacity, toxic gas output, and other parameters. Fire protection efficiency is also assessed by the medium-scale SBI method (EN 13823). It is used to classify building materials by fire hazard. The basic parameters are heat and smoke release (FIGRA, SMOGRA).

For example, the ISO 5660 method was used to prove the high fire protection efficiency of an intumescent coating based on urea–dicyandiamide–formaldehyde resin in combination with mono- and diammonium phosphate and dextrin. Pine specimens with the coating tested for 30 min under a radiative heat flow of 35 kW/m^2 showed neither ignition nor mass loss, nor heat release. After ignition, the maximum heat release rate was almost twofold lower compared to the original timber. The time to reach peak heat release rate, which marks the onset of intensive charring, increased (Wladyka-Przybylak and Kozlowski 1999).

It was interesting to compare the efficiency of two novel fire protection systems for timber belonging to diverse compound classes by molecular structure and

chemical composition. The test program was aimed at determining the factors affecting timber fire protection efficiency, as well as revealing the possible fire protection mechanism of the two systems.

The first fire protection system involved impregnation compositions based on low-molecular substances, i.e., KSD-A compositions. The second system involved intumescent film binders based on modified plant raw materials not containing additional flame retardants.

9.2 Novel Fire-Retardant Impregnation Compositions for Treatment of Timber Products

The novel impregnation compositions for surface treatment of timber constructions manufactured by Lovin-Ognezashchita Research and Production Company under the common name KSD-A are balanced synergetic mixtures with fire-bio-protective functions. KSD-A compositions of grades 1, 2, and 3 are environmentally safe and designed for surface treatment of interior timber constructions. If they are applied under external atmospheric exposure, it is recommended to use additional moisture-protective Biox-Universal textured coating.

An initial assessment of the fire protection efficiency of impregnation composition KSD-A (grade 1) according to the standard method of GOST R 53292-2009 showed that Group II fire protection efficiency is provided after only one layer was applied on a timber surface with consumption of 100–180 g/m^2. Mass loss during firing tests of timber specimens was 8–5.5 % in this case. Guaranteed service life of fire protection (in enclosed premises) is 10 years. Fire-retardant compositions KSD-A (grades 2, 3) with consumption of 240–300 g/m^2 provide Group II fire protection efficiency with a service life guarantee of 3 years. KSD-A compositions of grades 1 and 2 give the timber a beige color. Grade 3 does not color the timber and is recommended for bio-fire protection treatment of the surface of timber constructions with elevated esthetic requirements.

A further comprehensive study of the fire hazard characteristics of timber specimens with fire protection treatment by KSD-A (grade 1) was carried out by standard methods. Ignition parameters and mass burn-off rate were determined with external heat flow of 18–50 kW/m^2 in the unit as per GOST 30402-96. Flame spread, smoke generation capacity, and toxicity of combustion products were determined as per GOST 12.1.044-89, pp. 4.19, 4.18, and 4.20. Modern physical and physicochemical analysis methods (scanning electron microscopy, dynamic thermogravimetric analysis, IR spectroscopy and others) were employed to identify the leading mechanism of action of the fire-bio-protection impregnation composition.

Table 9.2 shows the results of a study of the effect of impregnation composition KSD-A (grade 1) on ignitability and maximum mass loss rate of pine timber.

Table 9.2 Effect of the fire-retardant impregnation composition KSD-A on ignitability and mass loss rate of timber

Specimen	Consumption, g/m^2	q_e, kW/m^2	τ_i, s	q^i_{cr}, kW/m^2	MLR$_{max}$,[a] g/m^{2}s
Pine	–	30	21	12.5	–
	–	40	9		28
	–	50	4		35.7
Pine with impregnation composition	300	30	195	22.5	–
		40	39		–
KSD-A (g.1)		50	16		21.3
	400	30	600	25.0	–
		40	72	–	
		50	29	14.4	

[a] $q''_e = 50$ kW/m^2

Quantitative flammability parameters that allow to compare timber fire protection effects are ignition delay time, $\tau_{i.}$, at a specified external heat flow density, q_e; critical ignition heat flow, q^i_{cr}; and also maximum mass loss rate, MLR$_{max}$.

Surface treatment of timber with the fire-retardant composition KSD-A increases its resistance to ignition by many times. Not only does the ignition delay time of the specimens lengthen, but the values of critical heat flow needed to ignite them also increase.

With increased consumption of fire-retardant composition, the maximum mass loss rate during specimen combustion is more than halved compared to untreated timber, even under very severe conditions of radiative heat flow exposure ($q''_e = 50$ kW/m^2). Therefore, the fire-retardant compositions affect the timber pyrolysis profile by slowing down and reducing the formation and emission of flammable volatiles. The quantity and quality of the char layer formed on the specimen surface is of considerable importance.

As an analysis of electron microscopy replicas from the specimen surfaces showed, the structure of the surface layer changes noticeably when the timber is treated with impregnation composition KSD-A. The surface of an untreated specimen had typical elements of coniferous timber structure: ribbon-shaped microfibers and fibers bordered by round pores. After impregnation with KSD-A (grade 1), the pores were no longer visible, and transverse formations – chords – were seen in space between the microfibrils. The whole thing looks like a kind of spatially cross-linked structure (Balakin et al. 2007). The dense charred layer formed on a timber surface exposed to fire is more homogeneous in this case and has no deep cracks compared to the charred surface of untreated timber.

The question of the effect of a fire-retardant composition on flame spread (FS) over the timber surface was especially interesting. Table 9.3 shows the data on the variation of basic FS characteristics after surface impregnation of timber with KSD-A composition (grade 1) as a function of its consumption.

Table 9.3 Flame spread parameters on a fire protected timber surface

Specimen	Composition consumption, g/m^2	FS index, I_{FS}	FS rate at 32 kW/m^2, mm/s	q_{cr}^{FS}, kW/m^2
Pine	–	55.0	4.4	5.0
Pine + KSD-A	300	2.5	1.10	19.6
Pine + KSD-A	400	0.5	0.74	22.0

Surface impregnation of timber with KSD-A composition significantly lowers the FS index and FS rate over the timber surface and increases the critical density of radiative heat flow for FS, q_{cr}^{FS}. Fire-protected timber materials are transferred to the category of slow flame spreading materials, FS1. With increased consumption of the composition, all parameters improve, and the appearance of materials with $I_{FS} = 0$, i.e., not spreading flame, may be expected. It should be noted that the flame spread rate at the limit of combustion has a certain value probably due to the minimum critical mass flow rate of flammable pyrolysis product emission needed for FS. All tested specimens, regardless of the registered q_{cr}^{FS} values, had the same FS rate at the limit of combustion extinction: 0.23–0.24 mm/s.

Fire-protective treatment of timber significantly affects smoke generation capacity in timber combustion and toxicity of fuel gases. The optical density of smoke during flaming combustion of timber materials is usually lower compared to smoldering combustion. At the same time, oxygen deficiency in the reaction zone of char smoldering leads to enhanced emission of toxic carbon monoxide. In the most dangerous smoldering timber combustion regime with and without fire protection treatment that was studied, there was a characteristic increase in the smoke generation coefficient as external heat flow density increased from 18 to 35.0 kW/m^2 (Fig. 9.1).

However, in equal test conditions, the fire protected specimens had a lower smoke generation coefficient compared to the initial timber and belong to the category of materials with moderate smoke generation capacity according to the established classification. With impregnation composition consumption of 300 and 400 g/m^2, the smoke generation coefficient of pine at a heat flow of 35 kW/m^2 is successfully reduced from 345.1 to 195 and 150 m^2/kg, respectively.

The toxicity of smoldering combustion products of timber depends on external heat flow density. Within a wide range of densities 10–65 kW/m^2, untreated timber belongs to the group of highly hazardous materials in terms of combustion product toxicity (Fig. 9.2, curve 1).

Curve 1 shows the complex extreme character of the ratio of material combustion product toxicity to external heat flow density. Within the interval of 10–23 kW/m^2, there is a typical, although slight, dependence of combustion product toxicity increase (decrease in HCL_{50} due to enhanced CO concentration). Autoignition of pine occurs at 23–24 kW/m^2 during specimen tests as per GOST 12.1.044-89. As a result, oxidation of carbon monoxide increases, and the toxicity index HCL_{50} rises again with the increase in heat flow intensity.

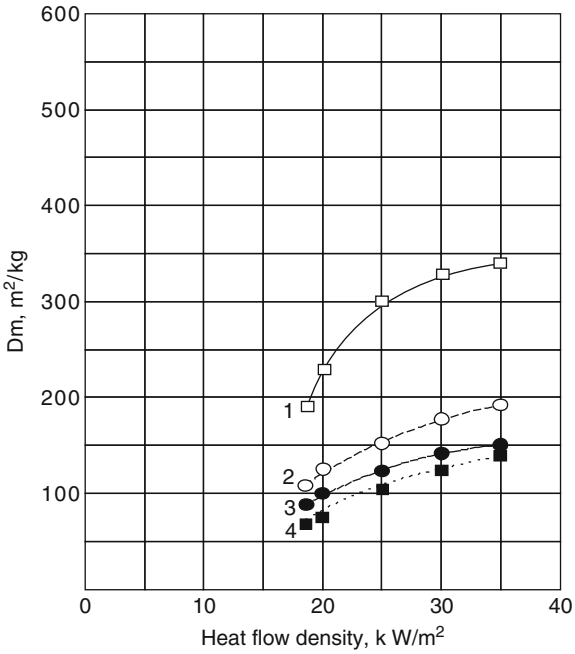

Fig. 9.1 Smoke generation coefficient of timber with applied compositions vs. heat flow density: *1* untreated pine, *2* pine with KSD-A composition (grade 1) (consumption 300 g/m^2), *3* pine with KSD-A composition (grade 1) (consumption 400 g/m^2), *4* pine with starch MP $\alpha = 0.5$ (consumption 300 g/m^2)

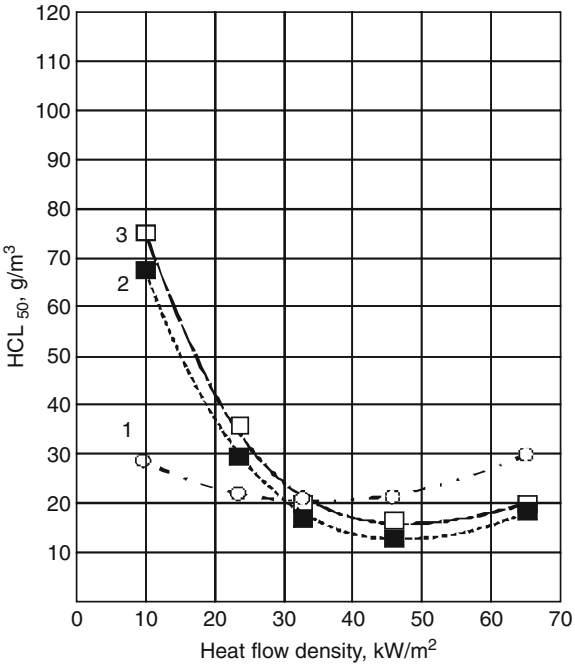

Fig. 9.2 Material combustion product toxicity in smoldering regime vs. external radiative heat flow density: *1* untreated pine, *2* KSD-A composition (grade 1) (consumption 300 g/m^2), *3* pine with starch MP $\alpha = 0.5$ (consumption 300 g/m^2)

Timber treatment with a fire-retardant impregnation composition lowers the toxicity of flue gases at external heat flow exposure of 10–20 kW/m^2. However, it impedes autoignition of timber and expands the range of the smoldering combustion regime. Critical heat flow for autoignition of timber treated with KSD-A impregnation composition with consumption of 300 g/m^2 increases to 44.0 kW/m^2.

Therefore, surface impregnation of timber with a fire-retardant composition moves timber from the highly hazardous group in terms of combustion product toxicity to the moderately hazardous group at low heat flow intensity. This result leads to the conclusion that even a composition that includes phosphorous does not fully suppress smoldering timber combustion. This may be an indication that the timber pyrolysis front penetrates beyond the charred phosphorous-containing surface layer and that the phosphorous concentration is insufficient to suppress char oxidation.

Deep impregnation of timber with KSD-A composition (g.1) under pressure by the hot-and-cold bath method or soaking in cold solution results in obtaining materials with Group 1 fire protection efficiency. The depth of fire-retardant penetration into the timber and its dry pickup per unit volume increase compared to surface impregnation. Fire safety indices of timber constructions significantly improve. In order to select the optimal regime of deep impregnation with the KSD-A composition, the effect of temperature and pressure in the autoclave and impregnation time was studied. It was found that increasing the temperature from 20 to 60 °C and raising the pressure above 8 atm barely improved the impregnation results. Thus, the optimal and most economical regime is impregnation with KSD-A composition (g.1) at room temperature and pressure of 7–8 atm for 1.5 h without preliminary vacuum treatment of the timber. Dry pickup per unit volume of pine timber in this case was 50 kg/m^3.

Deep impregnation with KSD-A (g.1) composition by the hot-and-cold bath method with a temperature change from 50–80 (8 h) to 20 °C (16 h) affected the pickup of dry matter. Pickup of 12 kg/m^3 afforded the material Group II fire protection efficiency, while pickup of 32–43 kg/m^3 afforded Group I, and slightly flammable material was obtained. At dry pickup of 50–60 kg/m^3, there was a stable result of Group I and combustibility characteristics under intensive external radiative heat flow.

Comprehensive testing of timber specimens with deep impregnation with KSD-A composition (g.1) showed that the material became low combustible (Group G1 as per GOST 30244), hard ignitable (Group V 1 as per GOST 30402), flame spread not present (Group FS1 as per GOST 30444-97), with moderate smoke generation capacity (Group D2), and moderately hazardous in terms of combustion product toxicity (Group T2 as per GOST 12.1.044-89, pp. 4.18 and 4.20). These results allow us to define the fire hazard class of fire-protected timber as KM1 – nonflammable material.

In order to assess the structural fire safety class of timber with deep impregnation with KSD-A composition (grade 1), a wall fragment of 200-mm half-logs with dimensions 1,200 × 2,400 mm was constructed.

The half-logs were fastened with 6 × 130-mm bolt screws on the unheated side. The main parameters for assessing the fire safety of building constructions as per GOST 30403-96 are the dimensions of specimen damage in the heat chamber at standard temperature and the occurrence of flaming combustion or other heat effects in the reference area along the specimen's length. Damage is understood to mean charring, melting, and burn-off of the construction material to a depth exceeding 0.2 cm. Tests of timber specimens with deep impregnation with KSD-A composition (g.1) showed neither flaming combustion nor other heat effects in the heat chamber. Minor damage (charring) to the specimen in the reference area was about 2 mm for a length of 270 mm. It was more of the consequence of the fire protection mechanism KSD-A composition than timber construction burn-off. Deep impregnation of timber with KSD-A composition (grade 1) provides effective fire protection for timber and turns it into class K1(30). Based on the results of accelerated tests, it was found that the guaranteed period of preservation of fire protection properties in timber constructions treated with KSD-A composition (grade 1) by deep impregnation method was 30 years.

9.2.1 Charring Parameters of Timber Species with Fire-Retardant Treatment at Standard Fire Regime

The results of thermal analysis and a study of Fourier IR spectra behavior in the surface layers of fire-protected timber specimens during heat exposure have confirmed the important role of char formation in lowering the fire hazard parameters of timber.

The analysis of Fourier IR spectra in the range of 400–4,000/cm focused on areas with a frequency drift of O–H, C–H, and C–O–C bonds in structural units of timber components. These units are especially sensitive to transformations during heat exposure. Increased band intensities caused by the appearance of $C{=}C_{AROM}$ bonds and enhancement of the absorption background indicated active carbonization of the substrate under the effect of the fire retardant. The conclusion was that KSD-A impregnation composition reacts with timber components during heating, speeds up dehydration and molecule cross-linking reactions, and leads to char layer formation with improved heat-shielding properties.

The timber charring rate depends on many factors: intensity and character of external heat flow, oxygen concentration in the environment, timber variety and density, its moisture content, etc. (Mikkola 1991).

A similar approach to that of (Demidov 2005) was used to calculate the charring rate of the near-surface layer in fire-protected specimens. The researchers factored in their own measurements of mass loss rate, temperature in the pyrolysis front and on the char layer surface, thickness and density of the impregnated layer, and average values of gasification enthalpy (Strakhov et al. 2000). For total heat flow (external radiation flow and from flame-generated flow) of 50 kW/m^2, the calculated

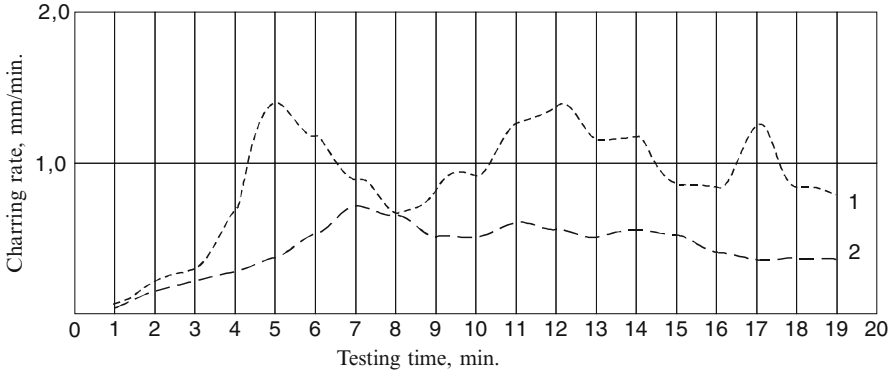

Fig. 9.3 Variation of charring rate of pine specimens during tests at standard fire regime temperature: *1* without fire protection and *2* with surface treatment by KSD-A, grade 1 (400 g/m^2)

Table 9.4 Effect of treating pine timber by fire-retardant composition KSD-A on the density and thermophysical properties of the char layer

Specimen	ρ_c, kg/m^3	d_{av}, nm of pores	T_S, K	λ, W/mK	a, 10^4 m^2/s	$\lambda\rho c$, kJ^2/m^{4}K^{2}s
Pine	268	25.03	1,005	0.32	7.6	0.133
Pine with KSD-A	217	1.98	880	0.093	2.7	0.031

charring rate of the near-surface layer of the timber was 4.67 mm/min. Under these conditions, an untreated pine specimen charred at the rate of 1.39 mm/min. Thus, the fire-retardant composition increases the charring rate of the near-surface layer of the timber by almost 3.5 times. Rapid charring of the surface layer of the timber slows down heating, subsequent pyrolysis, and charring of underlying layers.

A similar effect of fire-retardant composition on the timber charring rate was seen in tests of specimens ($150 \times 150 \times 30$ mm) in a laboratory furnace at standard fire regime temperature (Fig. 9.3).

It can be seen that at the first stage of a standard fire, the maximum fire-protected timber charring rate is higher compared to the original specimen. Then the charring rate of fire protected timber decreases drastically. At the end of 20 min of testing, the charred layer in untreated timber was 19-mm thick. The specimen with fire-retardant impregnation charred to a depth of 8 mm during that period. Therefore, the average charring rate of the original pine specimen was 0.95 mm/min, whereas the rate of the impregnated specimen was 0.4 mm/min.

Surface treatment of timber with fire-retardant composition KSD-A (grade 1) not only results in less charring rate of the timber during combustion, it also affects the characteristics of the porous structure and thermophysical properties of the char layer (Table 9.4).

Fireproofing timber with impregnation composition leads to the formation of char with a fine-porous structure, low thermal conductivity, and thermal inertia. This improves the thermal insulating capacity of the char.

9.3 Fire Protection Properties of Novel Intumescent Coatings for Constructional Timber Based on Plant Raw Material

In recent years, the problem of environmental safety in all spheres of human life and activity has become a fundamental issue. The search for environmentally safe and effective fire protection means for timber turned our attention to intumescent systems that do not contain substances and elements toxic and harmful to human health. We were interested in finding out whether organic systems inherent in natural plant raw materials could serve as effective fire retardants for timber and synthetic polymer materials.

This section addresses the fire protection properties of modified polysaccharides from various plant raw materials for improving the fire safety of timber structures.

Modification of plant raw material polysaccharides holds a prominent place in world materials technology. Modified cellulose-based materials are widely known and have practical importance. Today, researchers' attention is turned to the modification of starch-containing plant raw materials. Similarly to cellulose, starch is modified by producing ethers and esters of polysaccharides by C_6 hydroxyl groups, through the formation of grafted copolymers. The suggested methods are partial decomposition or macromolecule cross-linking under the action of physical means, chemical agents, or enzymes (Cellulose and starch esters 2003).

Many years of fundamental researches on selective catalytic oxidation of organic substances carried out in the Semenov Institute of Chemical Physics of the USSR Academy of Sciences and later in the Emanuel Institute of Biochemical Physics of the Russian Academy of Sciences resulted in the development of a new method. This original, one-of-a-kind modification method is based on catalytic oxidation of various carbohydrates by molecular oxygen in alkaline media (Skibida et al. 1996). It turned out that in the presence of copper and bases, high oxidation rates by oxygen are possible not only for alcohols and ketones with a different structure but also for polysaccharides (starches, dextrans, cellulose). The mechanism of this reaction is addressed in work (Sakharov and Skibida 2001).

A distinctive feature of the method is that in mild oxidation conditions (40–75 °C), the backbone macromolecular chains do not break, and selective modification of macromolecule units and fragments takes place, thus maintaining the high-molecular character of natural polymers, which are the basis of plant raw materials. The method is attractive because it solves the refusing problem for both utilization of reject agricultural products and food and forest industry wastes. It makes it possible to obtain a range of inexpensive, environmentally safe water-soluble reagents for various purposes with almost 100 % yield of end product. The

production process is one stage. The production process is nearly waste-free and is energy-saving, because it does not require high temperatures and elevated pressures.

There are many areas of application for plant raw materials modified in this way. It was shown, for example, that products with various degrees of oxidation of starch-containing raw materials are useful as glues and binders in the production of paper, high-quality chipboard, and fiberboard with low toxicity. Oxidized starch reagents are effective as hardening regulators for gypsum and concrete, corrosion inhibitors of ferrous metals, etc. (Sakharov 2005).

Our work is focused on the use of products of oxidative modification of plant raw materials as intumescent fire-retardant coatings for timber. Although there are numerous versions of various products of plant raw material modification (Skibida et al. 2001), the physicochemical characteristics of only one representative specimen are studied in detail – the product of catalytic oxidation of potato starch.

9.3.1 Method of Oxidative Modification of Plant Raw Material and Some Physicochemical Characteristics of the Product

Common potato starch was with molecular mass $MM = 10^6$; 20 % amylose and 80 % amylopectin were chosen for catalytic oxidative modification of polysaccharides by gaseous oxygen. In its chemical composition, amylose is a linear α-1,4-D polyglucoside, whereas amylopectin is a branched polymer with α-1,4-D- and α-1,6-D-glycoside linkages. Electron microscopy and X-ray diffraction have proved that the structure of a native dry starch granule consists of periodically alternating crystalline and amorphous lamellae formed from fragments of polysaccharide macromolecules. Crystalline regions are formed from side amylopectin chains organized in double helices. Amorphous regions include backbone chains of amylopectin macromolecules with a certain hierarchy of branch points. A significant part of the amylose molecules probably gets into the amorphous region. The specimen used in the test had B-type polymorphic crystalline structure. The degree of crystallinity of potato starch did not exceed 30 %, but the degree of order of polysaccharide macromolecules was higher than the degree of crystallinity of the starch. Catalytic oxidation of starch was performed in the following way.

A reactor with a rapid mixer was sequentially charged with water, starch, and catalyst (salt of bivalent copper) at the content of 5×10^{-3} mol/l and alkali 0.5 mol/l. The system was blown by oxygen to drive out the air, then the reaction mass was heated at 75 °C for 6 h. The resulting starch oxidate gel was dried at room temperature, then in vacuum of 10^{-4} Torr to constant weight. Under the adopted conditions, modified starch was produced with oxidation degree of polysaccharides of 0.5, correspondingly – a product with one carboxyl group per 2 polysaccharide molecular units.

Table 9.5 Effect of temperature on specific heat of oxidated starch polysaccharides

T, °C	C_P, J/g deg	T, °C	C_P, J/g deg
10	1.29	90	1.84
20	1.35 (1.25)	100	1.99 (1.65)
30	1.55	110	2.03
40	1.62 (1.34)	120	2.1 (1.76)
50	1.63	130	2.21
60	1.62	140	2.29
70	1.66	150	2.32
80	1.73 (1.53)	160	2.36

Note: The values of C_P for dry original starch are given in brackets

Various physical and physicochemical methods of analysis were used to determine the chemical composition and structure of the oxidate (Aseeva et al. 2009a). The chemical composition of the oxidated starch polysaccharide can be represented with certainty by the formula:

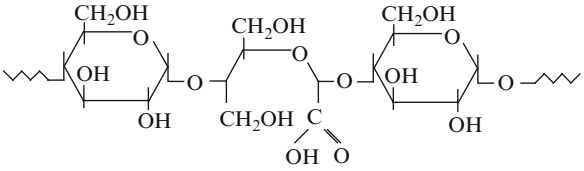

The employed method differs fundamentally from common oxidation of substances by molecular oxygen, which proceeds by the free-radical mechanism. It should be emphasized that it allows salts of polyoxycarboxylic acids to be obtained directly from polysaccharides of plant raw materials. By varying the ratio of catalyst to base and the cation nature, it is possible to change the properties of carbohydrate oxidation products, including fire protection properties (Skibida et al. 2001).

As a result of partial opening of cyclic anhydroglucose units and carboxylation, oxidate macromolecules should have more freedom of movement and molar volume compared to the initial starch. This factor should affect the physical properties of starch oxidate, for example, specific heat and density. Experimental values of specific heat of dry starch oxidate in the amorphous state in the temperature range of 10–160 °C did indeed turn out to be higher (Table 9.5).

The density of dry starch at 25 °C is 1.50 g/cm^3. The density of a dry starch oxidate specimen found picnometrically in acetone at 22–25 °C was 1.479 g/cm^3. The theoretical value of oxidate density at 25 °C in Na-salt form is 1.497 g/cm^3, whereas in acid form it is 1.439 g/cm^3. The calculation was done on the basis of

contributions to the molar volume of van der Waals volumes of groups, atoms, and bond lengths in the structural unit of an oxidate macromolecule (Aseeva et al. 2009a). With consideration of the starch oxidation degree, the difference between the calculated and experimental density values is 1.2 %.

To understand the mechanism of foamed char formation and fire-protective action of oxidated polysaccharides, it is important to know the alteration of their physical state and transition types during heating.

DSC results showed that a low-temperature transition from the amorphocrystalline state of polymer starch oxidate to the amorpho-vitreous state occurs within the range of 49–65 °C.

During thermomechanical testing at constant load, there was only slight deformation of the polymer right up to the glass transition temperature $T_g = 187.7$ °C. Upon reaching the flow temperature $T_f = 209$ °C, the relative deformation increased very rapidly and at 235 °C reached 100 %. Thus, oxidated polysaccharides exhibit the properties of typical rigid-chain thermoplasts. The interval between flow and glass transition temperatures in the case of oxidate is narrower compared to its original starch predecessor (64 °C).

Oxidative modification of starch lowers the degree of crystallinity of polymer almost twofold. However, the structural parameters of crystallites (length of cooperative melting unit and crystallite thickness) remain almost unchanged, though. We believe this is due to the reduction in the length of amylopectin branch fragments capable of becoming ordered in double helices as a result of hydroxycarboxylate clusters.

A comparison of thermodynamic parameters of crystallites in the structures of oxidate and the initial starch sample allows us to estimate crystallite quality after starch modification. Higher values of surface energy, enthalpy, and entropy of crystallites in the amorphocrystalline structure of polysaccharide oxidate indicate an increase in crystallite imperfection compared to starch crystallites (Aseeva et al. 2009a).

Visual examination of starch oxidate behavior during isothermal heating for 5 min showed that at 235 °C the specimen volume grew eightfold. However, Fourier IR spectra did not reveal any break of backbone polymer chains. All polymer transformations below 235 °C are attributable to intramolecular dehydration reactions. The reactions of decarboxylation and intermolecular dehydration occur only above 235 °C. Therefore, water and carbon dioxide serve as intumescent agents of starch oxidate in the viscous-flow state. Macromolecule cross-linking prevents breakage of chemical bonds of polymer backbone chains and promotes the formation of stable foamed char. The free foaming coefficient of the specimen at 250 °C over 5 min was 32.

Analysis of mass spectra of starch oxidate thermal decomposition volatiles at 200–300 °C confirms the observed effects. In mass spectra of decomposition volatiles at 250 °C and especially at 300 °C (Fig. 9.4), mainly the peak with mass number $m/e = 44$ associated with the CO_2^+ ion was recorded. There are no fragments with large mass numbers.

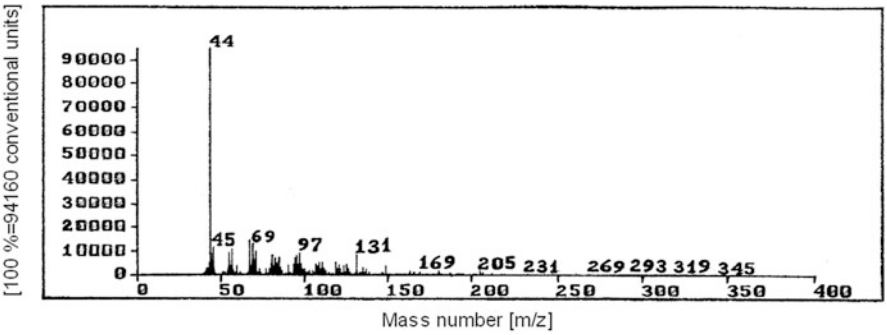

Fig. 9.4 Mass spectrum of starch oxidate decomposition volatiles at 300 °C

After unfreezing of the polymer's segmental mobility, its active thermal decomposition starts, accompanied by the expansion of the specimen during heating to 280–300 °C and the formation of an insoluble carbonized product with mass yield of about 50 %. Thermal decomposition of starch oxidate occurs as a first-order reaction with parameters $E_{\text{eff}} = 116.4$ kJ/mol and $k_0 = 4.3 \times 10^{11}$ min^{-1}. At this stage, it proceeds following a mechanism controlled by the reactions of generation of active centers (nucleus) by the law of randomness and by the growth rate of these nuclei (Aseeva et al. 2009a).

Oxidized polysaccharides produced from plant raw material capable of forming foam during heat exposure may be considered environmentally safe high-molecular reagents with the properties of intumescent fire retardants. In fact, these single-component systems perform several competitive functions inherent in the widely known and most effective P-, N-, and/or halogen-containing multicomponent intumescent fire-retardant compositions. In particular, they simultaneously play the roles of binder, film binder and carbon-forming substrate, gas-forming and foaming agent, polymer dehydration, and carbonization reaction catalyst (Skibida et al. 2001).

The complete combustion heat is an important thermodynamic characteristic of starch oxidate. The values of standard higher and lower total combustion heat of the tested specimen in sodium salt form were calculated by the group contribution method (Aseeva et al. 2009a). They are equal to 15.496 and 14.256 kJ/g. The lower total combustion heat had been also calculated by the Mendeleev equation using the experimental results of element analysis. Its value is 14.409 kJ/g, and it differs from the above-mentioned values by only 1 % (Aseeva et al. 2009a). The lower heat of complete combustion of original potato starch according to experimental data is 16.086 kJ/g.

The study results on the efficiency of timber fire protection by intumescent coatings based on catalytically oxidized polysaccharides of starch-containing plant raw material are presented below.

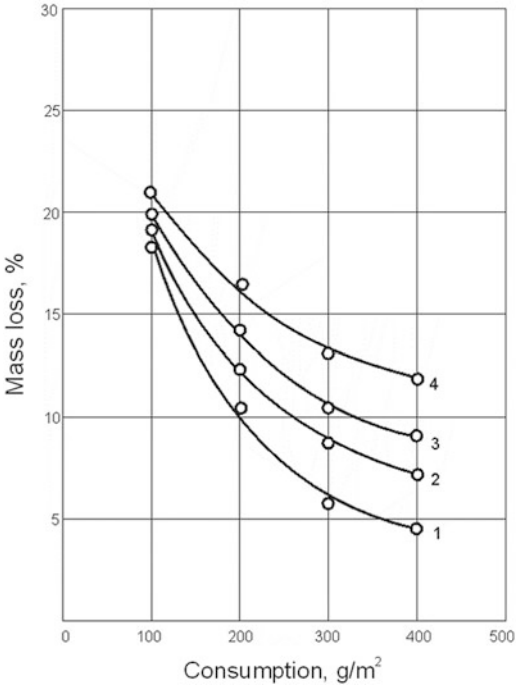

Fig. 9.5 Mass loss during combustion of timber specimens vs. MP composition and oxidation degree, α: *1* starch MP, $\alpha = 0.5$; *2* rice MP, $\alpha = 0.5$; *3* starch MP, $\alpha = 0.3$; *4* rice MP, $\alpha = 0.3$

9.3.2 Effect of Modification and Type of Plant Raw Material on Fire Protection Efficiency of Intumescent Coatings for Timber

The plant raw materials used for modification by catalytic oxidation method not only included potato starch, but also cornstarch and tapioca starch, as well as rice grits – food industry waste (hereinafter referred to as just rice). Products with various degrees of oxidation were produced by changing the proportion of catalyst and base.

When water-based compositions of modified polysaccharides (MP) are applied on a timber surface, transparent homogeneous coatings with good adhesion are formed due to the presence of hydrophilic groups in oxidate macromolecules and their structural affinity to the basic timber components.

Fire protection efficiency of intumescent coatings for timber based on oxidated polysaccharides is affected not only by coating thickness due to fire-retardant composition consumption, but also by such factors as degree of catalytic oxidation of polysaccharides and the source of plant raw material. This is clearly seen if we compare the fire protection effect of modified potato starch and rice according to the GOST R 53292-2009 standard (Fig. 9.5). At the same time, the difference in fire protection efficiency of potato, corn, and tapioca starch oxidates with the same modification degree was insignificant. Rice grits probably contain some other substances besides starch.

Table 9.6 Effect of q_e'' on the characteristics of the char foamed layer formed on a timber surface with MP coatings

Type of MP	q_e'', kW/m^2	Char yield, %	Layer char thickness, mm	ρ_c, kg/m^3
Starch, $\alpha = 0.5$	20	70.4	26.0	231
	30	63.2	28.0	229
	40	59.7	30.0	227
	50	–	31.0	226
Starch, $\alpha = 0.3$	20	50.4	7.0	260
	30	43.9	9.0	255
	40	39.6	11.0	248
Rice, $\alpha = 0.5$	20	68.3	17.0	239
	30	61.3	21.0	236
	40	57.4	24.0	233

All compositions confer Group II of fire protection efficiency to pine timber and the rank of hard flammable material even at consumption of 100 g/m^2. As MP composition consumption increases to 300–400 g/m^2, the mass losses during firing tests decrease considerably. Intumescent MP coatings confer Group I fire protection efficiency. In this respect, MP with $\alpha = 0.5$ is more effective.

The degree of catalytic oxidation of polysaccharides affects the fire protection efficiency of coatings because of its impact on the progress of polymer decomposition and expansion, thickness of the expanded layer, and char yield and properties. For equal MP consumption of 300 g/m^2, the thickness of charring foam increases as the intensity of radiative heat flow increases, whereas char mass yield decreases. At the same time, the density of the intumescent charred layer decreases slightly (Table 9.6).

An MP starch-based intumescent coating with oxidation degree $\alpha = 0.5$ applied on pine timber increased the specimen's ignition time at radiative heat flow exposure $q_e'' = 30$ kW/m^2 to 670 s. Under these conditions, the ignition delay time of the untreated specimen was $\tau_i = 21$ s. The MP coating based on rice grits with the same oxidation degree $\alpha = 0.5$ increased ignition time only to 535 s. Ignition time decreases almost 2.5 times when the oxidation degree decreased to 0.3.

A similar effect of MP oxidation degree and type of initial raw material was seen when the critical density of ignition heat flow, q_{cr}^i, maximum mass loss rate of fire protected timber specimens, MLR_{max}, and other parameters of timber fire safety were being determined (Sivenkov et al. 2002a, b, c).

An intumescent coating based on potato starch with oxidation degree $\alpha = 0.5$ is the most effective. It raises the q_{cr}^i value from 12.5 kW/m^2 for the initial pine specimen to 29.7 kW/m^2. Maximum mass loss rate of timber at constant heat flow of 50 kW/m^2 decreases almost twofold (from 35.7 to 16.1 g/m^2) (Sivenkov et al. 2002a).

In spite of the absence of any additional fire retardants, the organic intumescent MP-based coating efficiently protects timber from the exposure of fire. It lowers the flame spread index for the timber surface from 55 to 0.8.

The critical heat flow value, below which the flame stops spreading over the material surface and extinguishes, increases from 5 kW/m^2 for unprotected timber to 27.8 kW/m^2 for timber with a fire-retardant MP coating. Timber with this fire protection transfers to the category of slow flame spreading materials (FS 1).

As can be seen from Fig. 9.1, the intumescent starch MP-based coating has a significant effect on smoke generation during timber combustion. With equal consumption of KSD-A (g.1) impregnation composition, it further reduces the smoke generation coefficient during pine timber combustion with external heat flows of 18–35 kW/m^2 (Sivenkov et al. 2002b; Aseeva et al. 2007).

The same situation may be seen in examining the effect of a starch MP coating on timber combustion product toxicity (Fig. 9.2).

According to the recognized classification, an intumescent starch MP-based coating moves timber to the group of materials with moderate smoke generation capacity (D2) and in terms of combustion product toxicity, from the rank of highly hazardous materials (T3) to the group of moderately hazardous (T2) at heat flows up to 32 kW/m^2.

When a starch MP-based composition with $\alpha = 0.5$ and consumption of 300 g/m^2 is applied to a timber surface, the resulting coating lowers the maximum and average heat release rate during timber combustion at external heat flow of 50 kW/m^2 almost 3.5-fold compared to an untreated specimen (Sivenkov et al. 2002c).

The mechanism of timber fire protection by MP intumescent coatings consists in the formation on the timber surface of char foam with low-density and low-thermal inertia ($k\rho c = 0.0626$ kJ^2/m^{4}K^{2}s).

A layer of this char foam with high thermal insulating properties is a barrier to heat transfer to the timber surface and lowers the probability of its pyrolysis and charring. The charring rate of timber with an MP coating at an external heat flow of 50 kW/m^2 was only 0.18 mm/min (Sivenkov 2002).

How does fire protection efficiency of the two applied systems depend on the variety of timber being protected? To answer this question, the heat release characteristics during combustion of pine, spruce, birch, and oak specimens were analyzed. An OSU HRR-3 calorimeter was used with external radiative heat flow of 35 kW/m^2 for this purpose. Fire-retardant compositions with total consumption of 400 g/m^2 were applied on the surface of timber specimens with dimensions of $150 \times 150 \times 10$ mm (Aseeva et al. 2009b).

It was found that fire-retardant composition KSD-A (grade 1) and an intumescent coating based on starch MP with $\alpha = 0.5$ increase the time of heat release onset from the moment of external heat exposure, as well as the time to reach the maximum heat release rate. Both fire-protective systems significantly lower the maximum heat release rate and total heat release during the first 2 min of timber combustion.

It was confirmed that in comparison with impregnation composition KSD-A, the composition based on modified polysaccharides demonstrates higher fire protection efficiency due to the formation of a thick expanded coke layer with high thermal insulating properties. In this case, the effect of timber variety is more obvious, especially in terms of total heat release. Thus, an intumescent coating on the surface of pine and fir timber specimens based on modified polysaccharides resulted in a

1.8-fold and 3.2-fold decrease in total heat release THR_{2min}, respectively. When the intumescent coating was applied on the surface of oak and birch specimens, total heat release in this period decreased 3.8 and 9.3 times, respectively, compared to the specimens of untreated timber. This parameter was least affected by timber variety, when KSD-A impregnation composition was used: THR_{2min} value decreased 1.5–2-fold for all timber varieties.

References

Afanasyev SV, Korotkov RV, Kuzmin IV, Tripolitsyn AA (2007) Efficiency study of fire protection compositions based on amidophosphate. Pozharovzryvobezopasnost 18(3):28–31

Aseeva RM, Serkov BB, Sivenkov AB, Kulakov VS, Krasheninnikova NN, Sakharov AM, Sakharov PA (2007) Efficiency and mechanism of action of two fire protection systems for timber. Fire Explos Saf 16(5):23–30

Aseeva RM, Sakharov PA, Sakharov AM (2009a) Physicochemical characteristics of oxidized polysaccharides. Chem Phys 28(9):89–96

Aseeva RM, Serkov BB, Sivenkov AB, Kruglov EYu, Barbotko SL (2009b) Effect of fire protective treatment on heat release characteristics of various timber species. In: "Oligomers-2009", Abstracts of the X international conference on chemistry and physicochemistry of oligomers, Volgograd, VSTU, p 195

Balakin VM, Litvinets YI, Polishchyuk EY, Rukavishnikov AV (2007) Fire efficiency study of nitrogen-phosphorous-containing compositions for timber. Fire Explos Saf 5:30–41

Baratov AN, Andrianov RA, Korolchenko AY et al (1988) Fire hazard of construction materials. Stroyizdat, Moscow, 380 p

Bazhenov SV et al. (1999) Methods and means of timber fire protection: guidelines. Moscow, VNIIPO, 50 p

Bondarenko SN, Kablov VF, Keybal NA, Krekaleva TV (2009) Synthesis and use of phosphorus-boron-containing oligomers. In: "Oligomers-2009", Abstracts of the X international conference on chemistry and physicochemistry of oligomers, Volgograd, VSTU, p 199

Cellulose and starch esters. Bondar VA (ed) Proceedings of science and technology conference with international participation, 2003. ZAO "Polytsell", Vladimir, 195 p

Demidov IA, Kulakov VS, Krasheninnikova NN (2005) Fire retardant composition KSD – a for fire protection of railroad rolling stock. Transport Saf Technol (Rus), No 1, 48–49

Deyeva OA (1999) Formulas of fire protection compositions. NIITEKHIM, Cherkassy, 14 p

Fialkov AS (1997) Carbon, interlaminar bondings and composites based on it. Aspect Press, Moscow, 718 p

Garashchenko NA (2006) Results of firing tests of glulam constructions with intumescent coatings. Fire Explos Saf 15(2):12–16

Garashchenko NA, Garashchenko AN, Roudzinsky VP (2006) Thermal fire resistance calculations for glulam constructions with fire protection. Install Spec Works Civ Eng 10:14–18

Gorshin SN, Maximenko NA (1977) Study on the formation of slightly leachable antipyrenes in timber by the double impregnation method. For J (Rus) 6:113–116

Korolchenko AY, Korolchenko ON (2006) Fire protection means. Reference guide. Pozhnauka, Moscow, 258 p

Leonovich AA (2003) Physicochemical fundamentals of wood board formation. Khimizdat, St. Petersburg, 192 p

Leonovich AA, Sheloumov AV (2002) Lowering the fire hazard for timber materials, products and building constructions. SPb FU, St. Petersburg, 59 p

Mikkola E (1991) Charring of wood based materials. In: Proceedings of 3rd international symposium on fire safety science, Edinburg, pp 547–556

New generation of fire protective compositions for timber: PIRILAX compound. Pozharovzryvobezopasnost, No 1, 2000, 75–76

Novitsky GI, Stogov VV (1959) Wood impregnation plants. Transzheldorizdat, Moscow, 316 p

Ostman BA-L (2010) Fire safety in timber buildings: technical guideline for Europe. SP Technical Research Institute of Sweden, Boras. www.jrc.ec.europa.eu

Pokrovskaya EN, Naganovsky YK (2004) Biological fire protection of ancient wood architecture. Fire Explos Saf 6:33–36

Pokrovskaya EN, Kobelev AA, Naganovsky YK (2009) Mechanism and efficiency of fire protection of organophosphorous and organosilicon systems for timber. Fire Explos Saf 3: 44–48

Romanenkov IG, Leveetes FA (1991) Fire protection of building constructions. Stroyizdat Publ, Moscow, 320 p

Roytman VM, Serkov BB, Shevkunenko YuG, Sivenkov AB, Barinova EL, Pristoupyuk DN (2013) Roytman VM (ed) Buildings, constructions and their stability in fire conditions, 2nd edn. SFS Academy, Moscow, 366 p

Sakharov AM (2005) One-stage method of catalytic oxidation of plant raw material by oxygen: new environmentally clean products and prospects for their practical use. In: Bourlakova EB, Varfolomeyev SD et al (eds) Chemical and biological kinetics: new horizons. Chimiya Publ, Moscow, pp 620–639

Sakharov AM, Skibida IP (2001) Mechanism of catalytic oxidation of polysaccharides by molecular oxygen in alkaline gels. Chem Phys 20(5), 101

Schmid J, Konig J, Kohler J (2010) Fire-exposed cross-laminated timber-modeling and tests. In: Proceedings WCTE, Trentino, Italy

Sivenkov AB (2002) Mitigation of fire hazard of cellulose-based materials. PhD dissertation, SFS Academy, Moscow

Sivenkov AB, Serkov BB, Aseeva RM, Sakharov AM, Sakharov PA, Skibida IP (2002a) Fire retardant coatings based on modified polysaccharides. Part 1. Studies of combustibility and inflammability. Fire Explos Saf 11(1):39–44

Sivenkov AB, Serkov BB, Aseeva RM, Sakharov AM, Sakharov PA, Skibida IP (2002b) Fire retardant coatings based on modified polysaccharides. Part 2. Smoke generation capacity and toxicity of combustion products. Fire Explos Saf 11(2):21–26

Sivenkov AB, Serkov BB, Aseeva RM, Sakharov AM, Sakharov PA, Skibida IP (2002c) Fire retardant coatings based on modified polysaccharides. Part 3. Characteristics of heat release in flaming combustion and thermophysical properties. Fire Explos Saf 11(3):13–19

Skibida IP, Sakharov AnM, Sakharov AlM (1996) Process for the production of oxyacids from carbohydrates. US Patent 5,484,914

Skibida IP, Aseeva RM, Sakharov PA, Sakharov AM (2001) Intumescent carbon-forming flame retardant, method of its production, method of fire protective treatment of flammable substrate and method of combustion source extinguishing. Pat RU 2,204,547

Strakhov VL, Krutov AM, Davydkin NF (2000) Koshmarov YA (ed) Fire protection of building constructions. TIMR, Moscow, 433 p

Tychino NA (1999) Modern fire protection means for timber: research results. Fire Explos Saf 3:13–20

Tychino NA (2003) Means of fire and bio protection of construction timber: quality issues. Pozharovzryvobezopasnost [Fire Explos Saf (Rus)] 6:23–25

Wladyka-Przybylak M, Kozlowski R (1999) The thermal characteristics of different intumescent coatings. Fire Mater 23:33–43

Part III
Effect of Natural and Accelerated Artificial Aging of Timber Building Structures on Fire Behavior

Chapter 10
Effect of Natural Aging of Timber Building Structures on Fire Behavior and Fire Safety

Abstract This chapter presents the authors' original data on the effect of duration of natural (up to 700 years) aging of solid timber of different deciduous and coniferous species on fire safety characteristics and describes transformations in physical structure, chemical composition, and properties of timber species during natural aging of timber buildings and structures. It also presents experimental results of charring parameters and the properties of superficial char layers formed at fire action.

The chapter describes the process of biodegradation of timber species by timber-destroying fungi and the efficiency of complex bio-, moisture, and fire protection of constructional timber materials.

Over the whole period of genetic development of woody plants, transformation has occurred in external appearance, structure, and properties of wood substance as a result of millions of years of evolution. Various biotic and abiotic factors have played the defining role during formation of the feature complex of certain populations.

Historical age-class forms of wood substance may be nominally divided into three groups:

- Genetic age
- Biological age
- Service age

Genetic age, which defines the period of existence of a plant genus and species, has the longest retention of genotype signs, its main structural features and properties. During this age period, transformation of wood substance occurred at the genetic level under the impact of large-scale natural geographical and climatic changes, technical man-made disasters, etc.

Biological age corresponds to the period of sprouting and life of certain plants under certain soil and climatic conditions.

R. Aseeva et al., *Fire Behavior and Fire Protection in Timber Buildings*,
Springer Series in Wood Science, DOI 10.1007/978-94-007-7460-5_10,

For example, Siberian larch trees that reached the age of 500 or more years were found on hillsides of the Altai–Sayan Mountains, in spite of soil moisture deficit and cold weather conditions within the summer plant growth period.

Service age is characterized by the period of using timber of already-cut trees as individual products or members of timber building structures, finishing and lining materials under various usage conditions until they reach a certain marginal capability state. It is fair to expect that the biological age of cut trees and their condition will affect the service life and lifetime of timber building structures, all other usage conditions being equal.

This chapter deals with the problem of durability of timber as a constructional material and effect of its aging during the use under natural climatic conditions on the transformation in structure, chemical composition, and properties, including fire behavior.

The interest in old timber structures in particular is quite understandable, both from the point of view of studying the natural timber aging process and preservation and restoration of historical wooden architectural monuments.

10.1 Transformations in Physical Structure, Chemical Composition, and Properties of Constructional Members in Old and Ancient Timber Buildings

Eight climatic zones are distinguished on our planet, according to the relative importance of climatic parameters and combinations thereof: temperature, humidity, elevation above sea level, proximity of seas, proximity of industrial zones, and other meteorological conditions (solar radiation, atmospheric precipitation, pressure, fog, cloudiness, snow cover, wind). These zones are as follows: equatorial, subtropical, tropical, monsoonal, Mediterranean, oceanic, continental, and polar.

Russian territory has regions with cold and moderate climates. Regions with very cold and cold continental climates (Yakutia, Salekhard), arctic subpolar, eastern and western (Tiksi, Dickson Island), moderately cold (Tyumen), moderate (Moscow, Murmansk), subhumid (Vladivostok), and humid temperate climates (Novorossiysk) are distinguished, respectively. The most representative points of each climatic region are shown in brackets (GOST 16350-80).

A wide combination of various factors affects the durability of timber buildings and structures in a given climatic region. As with synthetic polymers (Emmanuel and Buchachenko 1982; Popov et al. 1987), the most essential physicochemical changes during the use of timber structures result from photochemical, hydrolytic, and thermal oxidative destruction; the effect of mechanical stresses; and other types of destructive processes.

Unfortunately, until now, no clear-cut effect of the conditions and duration of natural aging of timber on the interrelation of transformations in structure and chemical composition with many properties of the material has been established.

There is almost no information on the effect of natural aging of timber building structures on fire behavior and fire safety.

The process of natural aging of timber structures is different for different timber species and usage conditions. It does not lend itself well to a simple description and forecasting. The main reason for difficulties in studying the timber aging process is the complexity of the object itself, the diversity of its usage conditions, and the variability of its mechanical and physicochemical properties.

It becomes clear why the scarce results of studying the timber aging are often largely contradictory.

It is worth emphasizing that the studies of the natural aging of timber are aimed mainly on the analysis of change dynamics in macroscopic characteristics of timber structure and properties during long-term usage. However, the true process of timber aging, the mechanism and kinetics, limiting stages, and also the possibilities of effectively regulating or its slowing have not been examined. Solving this problem requires creating new approaches and methods, considerable collaborative efforts of the scientific community.

The duration and service life of timber buildings and structures, if properly used and promptly repaired, may reach many hundreds of years. Unique examples of long-term preservation of timber buildings and structures are Church of the Transfiguration on Kizhi Island (1714); the Church of the Resurrection (1776) and the eighteenth-century Spaso-Preobrazhensky Church in Suzdal; Voznesenskaya cube church in the village of Kushereka, Onezhsky region (1669); and the eighteenth-century Saviour's Church in the village of Fominskoye, Kostroma, among others (Kisternaya and Kozlov 2007; Varfolomeyev et al. 1990; Isayeva and Bryukhanova 1969; Pischik et al. 1971; Pokrovskaya 2003).

The significant enhancement of the strength characteristics of larch timber during its long-term use from the fifth–ninth centuries to the present as a material for shoring the foundations of various buildings in Venice is truly phenomenal. There are examples of unique preservation of larch timber for 1,800 years (Trajan's bridge piles over the Danube) (Isayeva and Bryukhanova 1969). This shows the very high resistance of larch timber to failure. A law allowing larch to be used for public construction only, i.e., bridges, mills, and dams, but mostly in shipbuilding existed in Russia up to 1858.

The internal constructional members of the Moscow Kremlin Cathedrals, Saint Basil's Cathedral, the Winter Palace in St. Petersburg, and some other historical monuments in Russia were made of larch (Isayeva and Bryukhanova 1969).

In the past, pine and fir were the main material for construction of nearly all timber residential and commercial buildings and structures as well as of the majority of religious buildings in Russia.

The studies carried out to date are the evidence that essential physicochemical changes occur in timber during long-term usage under natural conditions (Kisternaya and Kozlov 2007; Varfolomeyev et al. 1990; Isayeva and Bryukhanova 1969; Pischik et al. 1971).

The research paper (Isayeva and Bryukhanova 1969) established that the mechanical properties of larch from a timber house built in Krasnoyarsk deteriorated

noticeably in 230 years of natural aging under the climatic conditions of Siberia compared to present-day timber. Samples for analysis were taken from the undamaged part of a lower row of logs of the building. Erosion was recorded only in the surface layer of the logs 2–3 cm thick. On average, the density of the larch samples decreased by 8 % (to 585 kg/m^3); compressive strength along the grain, by 15 % (to 45.3 MPa); bending strength in the tangential plane, by 29 % (to 68.1 MPa); and in splitting parallel to the grain in the same plane, by 28 % (to 6.1 MPa). Anatomic analysis of tangential shears of old timber showed degradation of tracheids at their junction points and heartwood ray cells. The authors (Isayeva and Bryukhanova 1969) consider formation of large in-plane tensile stresses in the tangential direction during periodic drying of the logs to air-dry condition to be the reason for this degradation.

The changes in pine timber density, ρ_{12}, static bending strength in the tangential direction and compression along the grain (Varfolomeyev et al. 1990) were identified in timber architectural objects of Arkhangelsk Region that had been standing from 85 to 351 years. Samples were taken from sound clean timber.

Chemical composition analysis was performed for outwardly undamaged external surface layers 2–4 mm thick.

A nonlinear change in pine timber density is observed in the aging process: a reduction from 490 to 420–430 kg/m^3 in 140 and 199 years and a later increase to 565 kg/m^3 (Fig. 10.1). Strength properties are changed almost synchronously. In addition, their variation decreased from 10–12 to 3–4 %, indicating stabilization of timber state over long-term usage of constructional members under load.

Long-term external effects of atmospheric oxygen, solar radiation, wind, precipitation, and increased air temperature on timber result in destructive chemical reactions, primarily in the carbohydrate part of the material. In addition, hemicelluloses, which have a low degree of polymerization compared to cellulose, are especially vulnerable (Table 10.1). The content of main components of pine timber is expressed in % relative to an absolutely dry sample.

The data of Table 10.1 lead to the conclusion that the most significant reduction of carbohydrates in the chemical composition occurs in external constructions under direct influence of the atmospheric environment. It is especially noticeable in the timber of church crosses. Reduction in the content of extractives and an increase in lignin content are observed simultaneously with decomposition of cellulose and hemicelluloses. A rapid change in the extractives content occurs within the first 100 years of aging. This situation is explained by washout and evaporation of extractives (lightly volatile terpenes) from the surface layers of logs at higher summer temperatures. Destructive processes slow down indoors and when logs are protected with a board lining against direct moisturizing and solar radiation.

Changes observed in the chemical composition of pine timber under various usage conditions of building structures point to the important role of photo oxidation and hydrolytic reactions in the general natural aging process of the material.

Data on the behavior of timber construction made of deciduous species under natural aging conditions are very sparse.

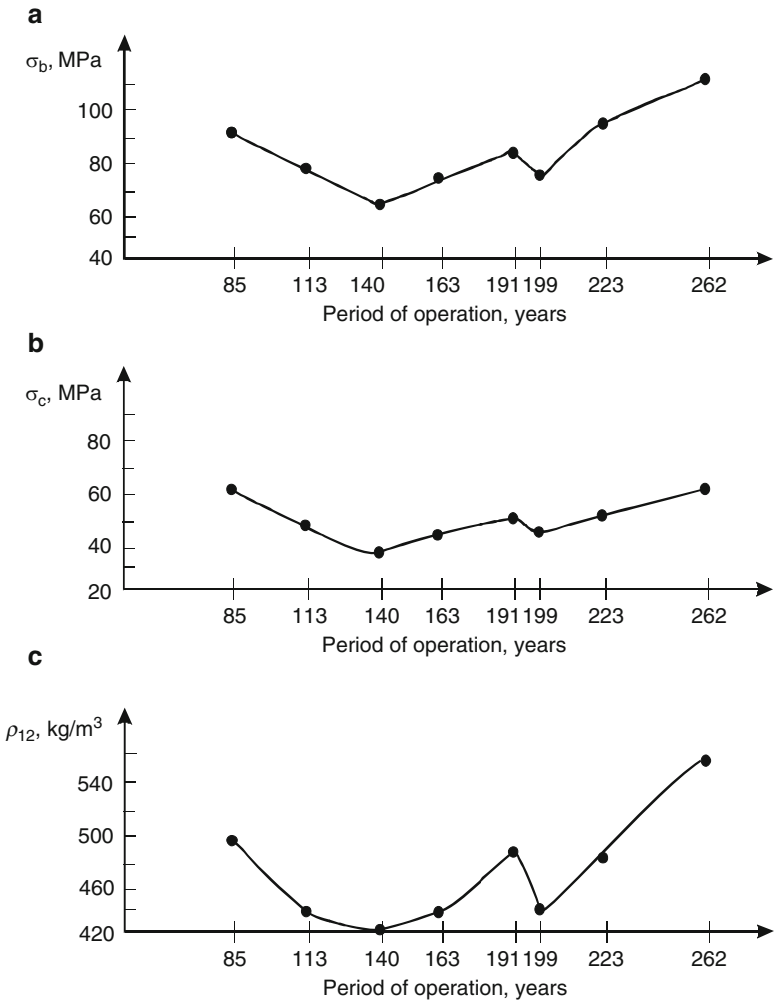

Fig. 10.1 Effect of duration of natural timber aging on bending strength (**a**), compressive strength (**b**), and density ρ_{12} (**c**)

In the 1970s, a group of scientists studied the chemical composition of old and present-day timber of two species: fir and maple (Pischik et al. 1971). The present-day fir samples were obtained from Neysky Timber Mill (Neya, Kostroma Region); fir samples with 50–70 years of usage were taken from demolished buildings in Cherkizovo (Moscow); fir samples with 200 years of usage were from a disassembled ancient monument in Textilshchiki (Moscow); and fir samples with 150–200, 300–400, and 400–700 years of usage were obtained during restoration of various churches in Riga. The present-day maple wood samples were delivered from a timber mill in Apsheronsk, Krasnodar Territory; samples with 60–70 years of

Table 10.1 Effect of the duration of natural aging on the chemical composition of different constructional members of timber structures

Length of usage, years	Constructional member and usage conditions	Lignin, %	Cellulose, %	Easy hydrolysable polysaccharides, %	Extractives, %	Ash content, %
0	–	26.5	54.3	17.8	10.7	–
85	Floor joist in a room	25.3	55.7	16.4	4.9	0.34
113	Cornice detail- external structure	28.2	48.9	14.8	2.2	0.34
124	Upper wall crown under board lining	28.7	49.9	16.7	2.1	0.25
124	Same	26.2	51.6	17.2	3.0	0.74
191	Pole ladder under roof	28.8	50.0	13.7	2.0	1.97
199	Internal structure member	27.9	48.9	16.8	4.6	0.67
223	Upper wall crown under board lining	27.3	50.5	14.4	4.9	0.29
262	Rafter member	26.8	50.9	14.7	3.6	0.18
262	Church cross	29.6	48.5	9.8	0.8	0.89
351	Floor joist in compartment	26.4	51.9	16.7	3.6	0.37

Table 10.2 Change in chemical composition of fir and maple timber in the process of long-term natural aging

	Content in timber, %				
Timber	Ash	Extractives	Cellulose	Lignin	Easily hydrolysable substances
Present-day fir	0.26	3.96	54.47	26.29	17.76
3-year-old fir	0.28	7.5	54.40	25.40	18.50
50–70-year-old fir	0.25	7.28	53.97	25.01	17.80
100–200-year-old fir	0.48	10.63	50.78	24.64	14.16
200-year-old fir	0.24	10.57	51.72	26.12	13.34
200–300-year-old fir	0.48	11.3	52.34	24.90	13.16
300–400-year-old fir	0.47	15.22	50.77	24.26	12.11
400-year-old fir	0.39	13.18	52.78	25.03	12.36
500–700-year-old fir	0.42	21.36	49.45	23.97	10.35
Present-day maple	0.56	8.19	46.53	24.18	22.51
3-year-old maple	0.39	7.59	45.99	24.60	22.79
70-year-old maple	0.51	8.83	46.53	23.97	19.80
100-year-old maple	0.52	7.3	47.71	21.91	18.98

usage were obtained from Sweden. Maple 100 years old was obtained from Moscow Region. The results of chemical analysis of the samples are presented in Table 10.2 (Pischik et al. 1971).

Data analysis leads to the conclusion that easily hydrolysable hemicelluloses suffer the greatest destruction during natural aging. Their content after 700 years of aging of fir timber building constructions is reduced by 8 absolute % or 44 % relative to the initial concentration.

When fir and maple samples with 100 years of usage are compared, the relative reduction of hemicelluloses is 22.5 % in fir timber and 15.7 % in maple. Cellulose and lignin are less changeable. The relative reduction of cellulose concentration in fir is about 9 % in 700 years. The observed tendency of simultaneous reduction in cellulose and lignin content in fir timber during aging suggests minor participation of white rot fungi in the destructive process. Lignin is the most hydrolytically and thermally resistant component of timber.

Figure 10.2 shows the content of main chemical components of coniferous timber in timber architectural monuments as a function of usage time (Pokrovskaya 2003). The nonlinear character of change in cellulose and lignin content can be seen by year built. The minimum lignin content corresponds to the maximum increase in cellulose. In addition, a steady decrease in pentosan concentration with an increase in service age of the timber can be traced.

Data on the properties of ancient archaeological timber of building structures are extremely interesting.

The research paper (Kazanskaya et al. 1975) studies the chemical composition of elements of timber building structures of the tenth–thirteenth centuries found during archaeological digs in Novgorod and Brest (Table 10.3).

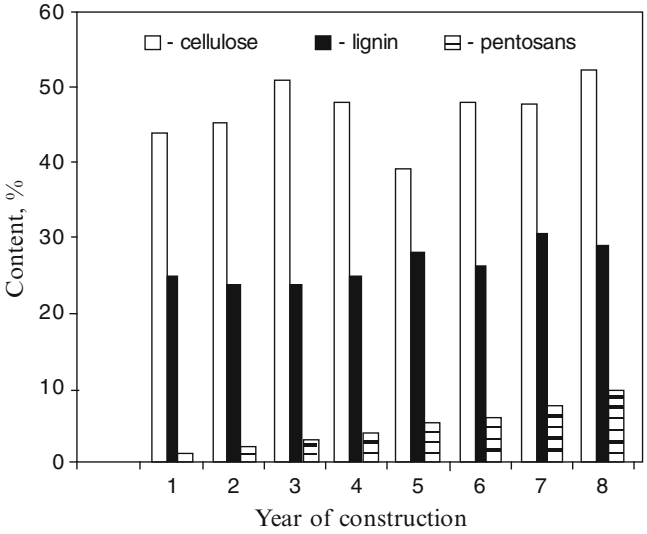

Fig. 10.2 Content of components of coniferous timber in timber architectural monuments: *1* year 1493, *2* year 1600, *3* year 1699, *4* year 1700, *5* year 1750, *6* year 1790, *7* year 1870, *8* year 2000

Table 10.3 Chemical composition of timber of the tenth–thirteenth centuries

Components, % of absolutely dry timber	Timber species		
	Ash tree	Birch	Pine
Ashy substances	6.29	2.71/0.14	7.88/0.17
Substances extractable with cold water	6.20	4.94	3.93
Substances extractable with water at 90 °C	7.60	5.42/1.41	5.14/3.19
Substances extractable with an alcohol–benzene mixture	2.88	3.82	4.88
Lignin	51.69	46.71/19.74	44.97/24.68
Cellulose	14.53	16.49/35.38	31.53/44.10
Pentosans	17.93	15.13/24.57	6.36/7.60
Easily hydrolysable polysaccharides	18.52	16.95/26.54	11.62/17.84
Low-hydrolysable polysaccharides	15.48	18.16/39.40	33.21/47.66

Note: The content of components of present-day timber is given in the denominator

From the foregoing data, it follows that the content of cellulose and other polysaccharides in archaeological timber is significantly reduced compared to present-day samples. The content of pentosans in deciduous wood changes the most. Lignin content almost doubles. The high percentage of ashy substances in archaeological timber may be due to the adsorption of metal-containing substances from the soil over a very long period.

Timber density (volume weight) is the main indicator of the macrostructure of the material. As shown above, many physical and mechanical properties of timber are

closely interconnected with its density (Chap. 2). When timber ages under natural conditions, its density changes nonlinearly with age.

According to (Pischik 2005), a timber density corresponds to each age (biological and service). In the author's opinion, the density and properties of a particular timber species as aging progresses change cyclically according to a single law. The number of annual growth layers in a growing tree and timber destruction during aging are interrelated cyclic processes based on double centennial cycles of solar activity.

These cycles leave their marks on the year-ring analysis scale of woody plants.

The cycle duration is 200 years for coniferous species and 260 years for deciduous species. Graphically, each cycle has the form of an inverted bell and consists of two symmetrical branches: descending and ascending. On a descending branch, density decreases as a result of mass reduction during carryover of destruction products and preservation of specific volume, the timber becomes lighter, and absolute factors of the properties decrease. On an ascending branch, density increases due to shrinkage and irreversible volume contraction, the timber becomes darker, and absolute factors of the majority of properties increase. The author (Pischik 2005) associates the destructive aging processes with hydrolysis and thermal oxidation reactions of timber components. Shrinkage processes are associated with lignin condensation reactions and consolidation of the remaining components. The Fourier equation for harmonic vibrations has been proposed to describe the cyclic dependence of density and other properties of timber on its age (Pischik 2005; Pischik and Vikhrov 1996):

$$y = a_0 + a_1 \cos \tau + b_1 \sin \tau,$$

where y is the observed factor; τ is the year of timber cutting; and a_0, a_1, and b_1 are the constants.

Pine timber density is changed with age according to the equation:

$$\rho = 0.5–0.9 \cos (0.03\tau - 1,339) –0.16 \sin (0.03\tau - 1,339), \text{g/cm}^3.$$

This dependence is suitable for all coniferous species and can serve as a scale for determining the age of the material. A similar approach has been implemented for deciduous species. A way of determining timber age has been proposed based on these scales and the involvement of nondestructive inspection methods for timber product properties. The accuracy of estimating timber age of historical and cultural works (icons, picture frames, parts of musical instruments) is ± 15 years.

However, it should be noted that if two parallel and competing processes – degradation and cross-bonding of macromolecules – occur during material aging, then the dependence of any property on time may be described by an equation of the form of (Emmanuel and Buchachenko 1982):

$$y = a \exp (-k_1 \tau) - b \exp (-k_2 \tau) + y_0,$$

where k_1 and k_2 are the rate constants for degradation and cross-bonding reactions and a, b, y_0 are the constants.

If under aging conditions $k_1 < k_2$, factor $y(\tau)$ will pass through a minimum. However, under operating conditions, it may turn out that $k_1 > k_2$ and then dependence $y(\tau)$ will have a maximum (Emmanuel and Buchachenko 1982).

Within one cycle of global influence of solar activity on timber aging, one might expect the influence of shorter cyclic climatic effects on this process.

A study of the kinetics of various chemical reactions in timber during aging provides ways for clarifying the mechanism of this process.

Natural aging of timber building structures occurs under the effect of mechanical stresses.

The kinetic theory of the durability of polymeric materials is based on thermofluctuation mechanism of their molecular destruction. Mechanical destruction of polymers is regarded as thermal destruction activated by mechanical stress. The activation energy of mechanical destruction U_0 in the famous Zhurkov equation for durability of material τ under load σ:

$$\tau = \tau_0 \exp\left[\left(U_0 - \gamma\sigma\right)/\mathrm{RT}\right]$$

for many polymers coincides with the activation energy of thermal destruction (Regel et al. 1974). In the equation, value γ reflects the probability of accidental statistical disintegration of the main bonds of a macromolecular chain.

Under mechanical loading of solid bodies, the observed deformation primarily affects amorphous regions with the least order of packing of macromolecules, local clustering of structure defects, and strained bonds. Breakdown of these bonds is not accidental (value γ is small); it is the source of consecutive formation of submicrocracks and microcracks and generates the formation of main cracks, growing cracks, and failure of the solid body (Regel et al. 1974).

Later works (Popov et al. 1987) established that tensile load accelerates the process of photooxidation of polymeric materials. In the presence of moisture (in air or in an inert medium), it also accelerates the hydrolysis of heterochain polymers. The double effect of the load on hydrolysis of heterochain polymer PA-6 – linear reduction of activation energy E_0 and reduction of pre-exponential factor k_0 of the reaction of amide bond hydrolysis with increasing load – has been successfully revealed. Reduction of pre-exponential factor k_0 in the equation:

$$k = k_0 \exp\left[-\left(E_0 - \alpha'\sigma/\mathrm{RT}\right)\right]$$

is explained by a decrease in mobility of macromolecules under load as a result of their orientation, which creates entropic difficulties for hydrolysis.

It is reasonable to expect similar effects of stresses on destructive processes of heterochain polysaccharides.

10.2 Effect of Natural Aging Duration on Some Fire Safety Characteristics of Members of Old and Ancient Timber Buildings and Structures

The variety of physical and chemical processes occurring in timber during its service does not allow highly accurate artificial reproduction of all the transformations occurring in it or predicting the pattern of property changes. To assess the impact of aging on the fire safety of timber building construction members, it is preferable to study timber specimens of existing old timber structures and architectural monuments experimentally. This approach requires exact knowledge of the service life of the object and the natural/climatic conditions of its location.

This is why our attention was drawn to timber specimens from existing old residential and other structures in the moderate climate region of Russia (Vologda, Kostroma, and other regions). Timber specimens in the form of saw cuts were taken from buildings situated in the villages of Demyanovo, Levino, Lyabzunka, and Semigory (Vologda Region) as well as in the villages of Nikitino and Shulevo (Kostroma Region).

The service life of the timber structures was 60–150 years according to the registered metrics. The structures were coniferous timber residential and nonresidential buildings, i.e., fir and pine (Figs. 10.3, 10.4, 10.5, and 10.6).

Timber specimens were sawed from the logs of the buildings' northern and southern parts free from decomposition, 1.5 m from the ground surface.

Fig. 10.3 Nonresidential timber structure (Levino vil.), fir, 90 years

Fig. 10.4 Nonresidential timber structure (Lyabzunka vil.), fir, 60 years

Fig. 10.5 Timber house (Semigory vil.), pine, 150 years

Fig. 10.6 Timber house (Nikitino vil.), pine, 130 years

Deciduous and coniferous specimens taken from old religious buildings were partially involved in studying the impact of natural timber aging on decomposition processes, and heat and fire resistance.

To get an idea of the specific specimens being studied, their density, ultimate composition, and content of the basic timber components were determined, and thermal analysis was performed.

We have already mentioned that timber density (volume weight) is an indicator of the macrostructure and influencing its properties. Many characteristics of material fire safety are related to density. Table 10.4 gives the average values of density ρ_{12} of the pine specimens studied.

The characteristic curve plotted according to these data (Fig. 10.7) has a complex nonlinear pattern, maximums and minimums. The maximum density values are observed in timber with a service life of about 100 and 330 years, while the minimum value is reached for pine with a useful life of 190–200 years.

This nonlinear variation of timber density due to long service life agrees with papers (Varfolomeyev et al. 1990; Pischik 2005). Density is nonuniformly distributed in different parts of timber structures oriented in different directions. Density is particularly high on the southern and eastern parts. Apparently, this is not haphazard. This may be a response to sunlight. Unfortunately, exact data on the biological age of the timber used for the timber buildings were lost. Religious buildings were usually made of pine 150–220 years old (Kisternaya and Kozlov 2007), while residential and business structures were 60–100 years old. Fir timber was more often used for business structures.

Table 10.4 Density of timber specimens with different service life

Item no.	Timber specimen, its source, year of construction	Service life, years	Density ρ_{12}, kg/m^3
1	Present-day pine, Vologda Region	–	440
2	Pine, Tolstoy house, 1830	180	410
3	Pine, Volkoostrov, Kizhi, Chapel of Peter and Paul	330	587
4	Pine, Church of Ipatyevsky Monastery, Kostroma, 1628	370	535
5	Pine, Saint George Cathedral, Shulevo vil., Kostroma Reg., 1898	112	North – 488 South – 537 East – 414 West – 426
6	Pine, Nikitino vil., Kostroma Reg., 1876	130	North – 505 East – 591 West – 561

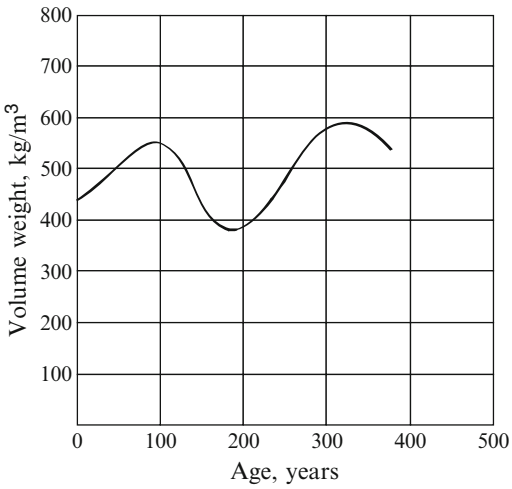

Fig. 10.7 Pine timber density ρ_{12} (volume weight) vs. service life

The dependence of destructive processes in timber on the where the samples were taken in relation direction (sunlight effect) can be judged by the results of chemical analysis (Table 10.5).

We used a simplified scheme of timber chemical analysis (Obolenskaya et al. 1991). The content of cellulose and lignin was assessed. The remaining part was a mixture of hemicelluloses and extractives.

The research results show that cellulose content decreases as service life increases to 150 years, while the lignin content increases (Table 10.5).

It can be seen that the southern part of the timber structure shows more significant changes than its northern part. Under approximately equal conditions, the percentage of cellulose in timber structural elements decreased by 13.9 % on the structure's southern part and by 9.1 % on the northern part over 150 years of service.

Table 10.5 Content of main chemical components of fir timber as a function of its service life

Item no.	Sample, source, service life years	Direction	Main chemical component content, %	
			Cellulose	Lignin
1	Present-day fir (Vologda Region)	–	54.5	25.4
2	Nonresidential timber structure (Lyabzunka vil.), fir, 60 years	North	55.6	25.6
		South	53.4	27.1
3	Nonresidential timber structure (Levino vil.), fir, 90 years	North	50.6	27.1
		South	49.0	28.2
4	Nonresidential timber structure (Demyanovo vil.), fir, 110 years	North	50.8	26.9
		South	48.6	28.1
5	Timber residential structure (Semigory vil.), fir, 150 years	North	49.5	27.6
		South	46.9	28.8

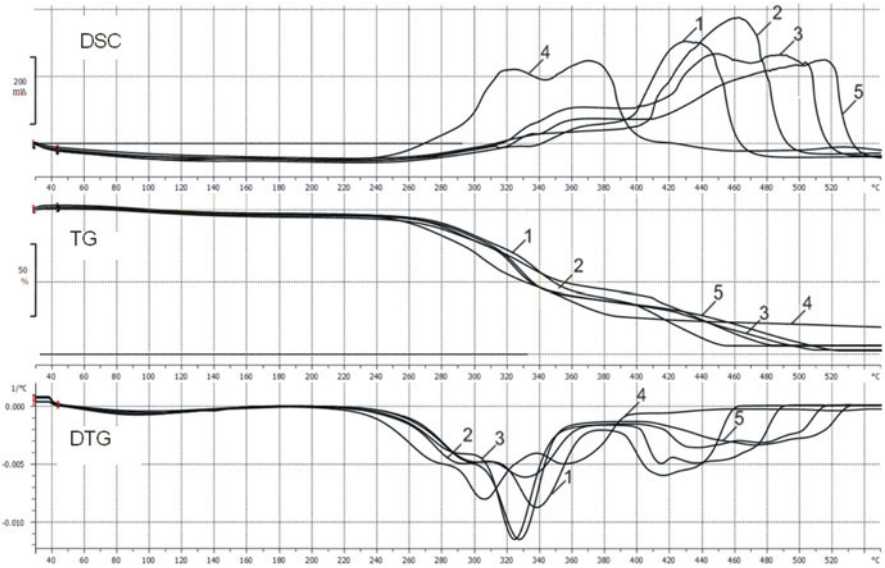

Fig. 10.8 *TG*, *DTG*, and *DSC* curves of oak specimens with different service life: *1* 1650, *2* 1901, *3* aged artificially by 80 years, *4* 1540, *5* present-day timber. Air medium, heating rate 20 °C/min

During aging, a significant role is played by thermo-oxidative timber decomposition reactions.

Therefore, important information on timber decomposition dynamics when it is heated in air can be obtained by thermal analysis methods. A TGA/DSC1 thermoanalytical system manufactured by Mettler Toledo (Switzerland) was used to study the patterns of thermo-oxidative decomposition of different timber species as well as the char residues. The set had a module for programmed calculations of kinetic parameters. Samples were prepared in the form of powder weighing 1.0–8.5 mg. Heating rate was 5–20 °C/min (Fig. 10.8).

All timber varieties are characterized by a low-temperature stage due by moisture and two main stages of specimen weight loss in the region of 240–400 and 400–540 °C. However, the position and maximum values of the characteristic points of TG, DTG, and DSC curves differ considerably for different timber species. An increase in heating rate causes the logical shift of the thermoanalytical curves to the higher-temperature region. Comparative analysis of the curves suggests that coniferous species begin decomposing earlier and faster than deciduous species when heated to 360–400 °C.

Thermo-oxidative decomposition of timber is a process involving significant heat release at all its main stages. This is confirmed by the exopeaks' presence on the DSC curves. Timber decomposition in the air is accompanied by charring. The greatest heat release during thermo-oxidative decomposition is related to the oxidation of the carbonized product at high temperatures.

Natural aging of timber structural elements causes a significant change in their thermal stability (Serkov et al. 2009; Aseeva et al. 2009).

Oak specimens taken from the boards of icons of the Trinity Monastery of St. Sergius (Moscow Region) were used to trace the impact of service life duration on thermo-oxidative timber decomposition (Fig. 10.8). We can actually see significant changes in thermo-oxidative stability of the oak specimens, which are particularly noticeable on the DSC and DTG curves. The longer the timber's service life, the greater the changes will be. All of the temperature indices decrease after natural aging of oak timber during a service life of more than 460 years: the starting temperature of decomposition, temperature of the maximum weight loss rate, etc. (Serkov et al. 2009).

An examination of thermoanalytical timber curves leads to the important conclusion that conditions favorable for timber decomposition, charring reactions, and oxidation of the charred product are created due to natural material aging during long-term service. This is most likely due to the increased lignin content caused by aging (a high-energy aromatic component of timber) and changes in porous timber structure.

The authors of paper (Sandu et al. 2003) observed a similar situation during thermal analysis of specimens of lime timber taken from frames and boards of old icons at Romanian monasteries. As the specimens' service life increased from 6 to 200 years, thermo-oxidative stability decreased, activation decomposition energy decreased, and the pre-exponential factor decreased by three orders compared to the reference lime tree specimen. However, timber with 99 years of service life was more stable than the reference specimen and the product more old. The effective activation energy of decomposition of this lime specimen was estimated in 105.2 kJ/mol and $\ln Z = 20.8$ (the reference sample had values of 85.5 kJ/mol and 16.6, respectively).

Paper (Pokrovskaya et al. 2000) traced a particularly broad range by timber service life and its impact on thermal stability of timber structural elements. The authors had specimens of pine cut in 1990, 1991, 1880, 1790, 1752, 1690, 1612, 1576, and 1511. The specimens in the research conducted in 1990 corresponded to

Table 10.6 Influence of service life of timber structures on timber complete combustion heat

Item no.	Timber specimen, source, service life years	Element composition, %			Qn_e, kJ/g	Qn_r, kJ/g
		C, %	H,%	O, %		
1	Pine	52.14	5.91	41.95	19.6	19.1
2	Fir	52.22	6.04	41.74	18.9	19.25
3	Oak	50.40	5.77	43.43	18.7	18.2
4	Oak, monastery, 1650	47.03	7.25	45.72	18.0	18.3
5	Pine, Tolstoy house, 1830	49.38	3.88	46.74	15.2	15.52
6	Nonresidential timber building (Lyabzunka vil.), fir, 60 years, northern side	50.3	6.44	43.26	18.4	19.21
7	Nonresidential timber building (Levino vil.), fir, 90 years, northern side	48.3	7.11	44.6	18.15	18.6
8	Nonresidential timber building (Demyanovo vil.), fir, 110 years, northern side	46.7	8.2	45.1	19.8	20.3
9	Residential timber building (Semigory vil.), fir, 150 years, northern side	50.5	8.47	41.03	20.1	20.7
10	Timber structures of Saint George Cathedral, Shulevo vil. (year of construction – 1898), pine	45.9	8.15	45.95	18.3	18.9
11	Residential timber building, Nikitino vil. (year of construction 1876), pine	48.8	8.34	42.86	19.9	20.4

a service life up to 525 years. A cyclic nonlinear pattern of variation of weight loss values and kinetic parameters of the timber decomposition process was found. The minimums on the $E_{\text{eff}} = f(\tau)$ curves corresponded to timber structures with service life of about 100, 300, and 500 years; the maximums were in the regions of 200 and 400 years. The values of lg Z are changed almost synchronously. They increased by 2–5 orders at the maximum points. Timber is most vulnerable to destructive processes during the first 50–100 years of service. The cycles are repeated every 200 years.

During these periods, one should expect an increase in timber fire hazard. In the first place, it was necessary to determine the impact of natural aging of timber specimens on enthalpy of complete combustion. For this purpose, dry timber specimens with different service life were used. The lower heat of complete combustion values were determined experimentally using an IKA – calorimeter C 5000 – and were also calculated according to the element composition data by the Mendeleev equation. Table 10.6 presents the results.

As the service life of timber structures increases, the carbon content decreases, while hydrogen and oxygen contents increase proportional to each other. The exception is pine timber dating from 1830, where the hydrogen content decreased to

Table 10.7 Parameters of fir ignitability depending on timber structure service life

Item no.	Timber species, age	q_e, kW/m^2	τ_i, s	q_{cr}^i, kW/m^2	MLR$_{max}$, g/m$^2 \cdot$ s
1	Present-day fir (Vologda Region)	30	20	11.5	–
		40	7		–
		50	3		39.6
2	Nonresidential timber structure (Demyanovo vil.), fir, 110 years, southern side	30	26	13.2	–
		40	12		–
		50	6		31.9
3	Fir (residential building, Vologda Region, Semigory vil.), 150 years, southern side	30	21	12.5	–
		40	9		–
		50	4		35.7

3.88 %. The calculated and experimental assessment of the lower heat of complete combustion of specimens shows that the lower heat of complete combustion tends to increase as the timber's service life increases.

This is caused by a reduction in carbon content and an increase in hydrogen content in the element composition: hydrogen's contribution to complete combustion heat is four times larger than that of carbon. The observed effects fully agree with the results of an analysis of changes in timber chemical composition during aging.

The question of the effect of natural timber aging on such fire hazard properties as ignitability, mass burn-off rate, heat release rate, smoke generation capacity, and toxicity of combustion products is of interest.

Ignitability parameters of timber specimens were determined according to GOST 30402-96. The unit was provided with an additional device for recording mass loss during testing. It is found (Aseeva et al. 2009) that the delay time of ignition and the value of critical heat flux of specimen ignition increase as timber's volume mass (density) increases. These observations are in complete agreement with the thermal theory of ignitability of different materials.

The effect of duration of natural aging of fir timber constructions on the ignitability parameters is given in Table 10.7.

Table 10.7 shows that the ignition delay time of each timber specimen depends on the intensity of external heat flow. In identical testing conditions, fir timber with service life of 110 years shows higher values of τ_i compared to the reference sample and the specimen with service life of 150 years. The same trend is observed for critical ignition heat flow density q_{cr}^i. At the same time, the maximum mass loss rate of timber MLR$_{max}$ decreases accordingly at an external heat flow of 50 kW/m^2.

The impact of natural timber aging on flammability was also checked in severe conditions of exposure to the standard fire temperature regime when the average volume ambient temperature (T) at the process development stage increases according to the following equation:

$$T = 345 \lg (8\tau + 1) + T_0,$$

where τ is the fire exposure duration, min, and T_0 is the initial temperature, °C.

Table 10.8 Impact of natural timber aging on flammability of timber structural members in a standard fire regime

Timber specimen, source	Service life, years	Time τ_{si}, min: s
Present-day fir	–	4 min 17 s
Nonresidential timber structure (Lyabzunka vil.), fir	60	4 min 30 s
Nonresidential timber structure (Levino vil.), fir	90	4 min 52 s
Nonresidential timber structure (Demyanovo vil.), fir, southern side	110	5 min 5 s
Fir, nonresidential structure, Vologda Region	150	5 min 2 s
Pine, present-day structure, Republic of Mariy El	2	3 min 73 s
Pine, nonresidential structure, Republic of Mariy El	12	3 min 59 s
Pine, nonresidential structure, Republic of Mariy El	48	4 min 17 s
Pine, nonresidential structure, Republic of Mariy El	59	4 min 22 s
Pine, nonresidential structure, Republic of Mariy El	88	4 min 31 s
Pine, nonresidential structure, Republic of Mariy El	113 years	4 min 49 s

For this purpose, a small-scale firing furnace was used, where the standard temperature–time conditions were provided by a special gas burner with adjustable propane gas supply. Thermocouple sensors allowed automated recording of the average volume temperature in the furnace as well as the specimen's surface and inner temperature. Vertically oriented timber specimens were $150 \times 150 \times 20$ mm. In this case, the self-ignition delay time of the timber specimens from the time the specimens were placed in the fire furnace was recorded (Table 10.8).

The results obtained for fir timber tests in standard fire regime agree with the above-mentioned nonlinear trend of changes in timber flammability as the service life of timber structures increases. At the same time, this trend was not revealed for pine specimens, although the general upward trend in τ_{si} with an increase of timber structures' service life to 113 has a similar pattern. Pine timber in standard fire regime is a bit more prone to ignition compared to fir.

Combustion is first of all a physicochemical process of oxidation of any substance. Timber chemistry changes during long-term natural aging will affect the materials' fire safety parameters directly related to the chemistry of this process. Smoke generation capacity is also one of these indices.

Figure 10.9 shows the experimental results of assessing the smoke generation capacity of pine timber depending on duration of natural aging of timber structures. Smoke generation capacity was determined by the standard methods according to GOST 12.1.044-89 in decomposition and smoldering conditions at external radiation heat flow of 20 kW/m^2.

The smoke generation capacity of timber structural elements in old constructions changes nonlinearly as service life increases.

Figure 10.9 shows that the minimum smoke generation capacity is for pine timber structures with service life of 100–150 and 300–330 years. This result generally agrees with the above-mentioned pattern of variation of other timber properties during natural aging.

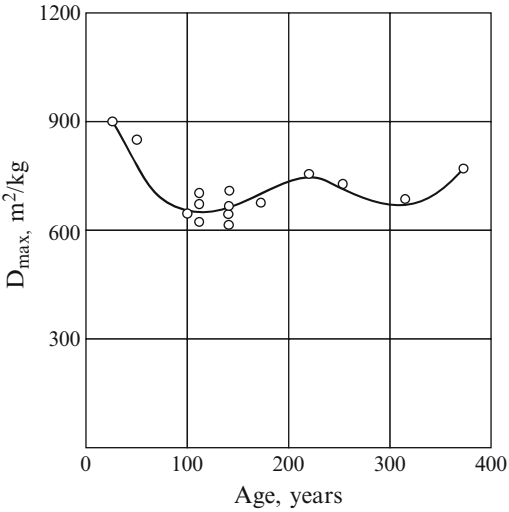

Fig. 10.9 Pine timber smoke generation capacity (D_{max}) vs. service life of timber structures $q_e = 20$ kW/m^2

The research results as a whole lead to the conclusion that the processes occurring during natural timber aging are rather slow. They depend on timber variety and local climatic conditions of timber structure service and are due to a complex combination of thermal, photo-oxidative, and hydrolytic reactions of timber decomposition. As a result of the change in macrostructure and chemical composition of timber materials, all of their properties change, including fire safety characteristics. For a timber building with a very long service life, the observed transformations are nonlinear in time, which affect the materials' fire safety.

10.3 Charring Parameters and Physical Properties of Char Formed During Fire Action on Old Timber Building Elements

Timber charring is one of the important factors determining fire resistance of timber structures and constructions. Timber charring in various fire situations is still a subject of numerous studies. Timber charring parameters during a fire and properties of the charred layer are of great practical interest. This interest is due not only to the need for initial data for engineering estimation and design of building structures with a standardized fire resistance and fire safety level and for predicting the behavior of different timber species in case of fire. By analyzing the charring parameters and properties of the charred layer, experts can determine when the fire started and its duration, seat of fire in a room, and establish the cause and probability of arson.

The process of timber charring under fire exposure is usually characterized by such parameters as charring rate, thickness (depth), and shrinkage of the charred

layer and less often by mass loss rate. Physical properties of the charred layer are studied from various aspects. Its thermophysical, heat-insulating properties, porous structure, permeability, electrical resistance, etc., are of interest.

Charring parameters of timber and materials on its basis depend on conditions of fire exposure. The conditions of external heat exposure and fire determine the conditions of material heating, and its pyrolysis and charring rates. Different standard methods are used to compare the behavior of various timber species and timber-based materials by charring parameters. In particular, these include methods implementing the following regimes: standard temperature–time fire, impact of external radiative heat flow of constant density, and environmental impact at constant temperature.

This section presents the experimental results of studying the effect of natural aging of elements of timber structures in old buildings on charring parameters and properties of the charred surface layer formed in 20 min during a standard fire. For this purpose, we used the above-mentioned small-scale furnace and specimen sizes. Charring rate and thickness (depth) of the charred layer for the whole period of fire exposure were calculated as the mean arithmetic values of three repeated tests of each type of specimen. Timber specimen charring rate in a standard fire after self-ignition increased to the maximum value and then slowed down. The maximum values of charring rate were used for comparison.

Table 10.9 gives the charring parameters and density of charred layers formed on the surface of pine and fir timber specimens with different service life. The char layer surface temperature corresponding to the maximum charring rate is also given here.

A comparison of the values of charring rate as well as the thickness of the charred layer formed in a standard fire and the effect of radiation heat flow of constant density shows that the timber charring process accelerates in more severe conditions of thermal exposure. As the service life of timber structures increases to 150 years, natural aging of structural elements also causes an increase in the charring rate in standard fire conditions (Fig. 10.10).

The observed rise of charring rate and char layer thickness is mainly related to the increased lignin content in the timber due to natural material aging. Density of char layers on the surface of fir timber specimens is virtually identical and does not depend on aging duration. However, it decreases in pine structures with 150 years of service life (from 256 to 212 kg/m^3). This indicates in increase in char structure porosity. The surface of charred layers in a standard fire incandesces to almost 800 °C.

The effect of natural timber aging on some characteristics of its reaction to fire was studied for coniferous species only (fir, pine). It is also important to determine the effect of aging on behavior during fire and fire safety of deciduous timber varieties. Therefore, it seemed reasonable to conduct a comparative study of the change in the main fire safety characteristics of coniferous and deciduous timber species subjected to accelerated artificial aging.

Table 10.9 Effect of natural timber aging on charring parameters and density of charred layers

Specimen, source, service life	δ_C, mm	V, m/min	ρ_C, kg/m^3	T_s, °C	k, W/m K	a, m^2/s	$k\rho c$, kJ^2/m^{4}K^{2}s
Fir, nonresidential timber structure (Lyabzunka vil.), 60 years	22	1.4	223	796	0.37	0.0010	0.128
Fir, nonresidential timber structure (Levino vil.), 90 years	24	1.55	214	805	0.30	0.00089	0.10
Fir, nonresidential timber structure, (Demyanovo vil.), 110 years	26	1.63	213	816	0.26	0.00078	0.086
Fir, nonresidential structure, Vologda Region, 150 years	27	1.72	212	812	0.20	0.0006	0.066
Pine, nonresidential structure, Republic of Mariy El, 2 years	19	1.0	256	731	0.33	0.00082	0.131
Pine, nonresidential structure, Republic of Mariy El, 12 years	24	1.1	254	736	0.31	0.00078	0.122
[a]Pine, 12 years, $q_y = 20$ kW/m^2	19	0.95	278	558	0.10	0.00056	0.043
Pine, 48 years	25	1.25	249	738	0.27	0.00069	0.104
Pine, 59 years	26	1.3	242	744	0.24	0.00063	0.09
Pine, 88 years	25	1.34	237	749	0.23	0.00062	0.085
[a]Pine, 88 years, $q_e = 20$ kW/m^2	20	1.0	256	570	0.07	0.00017	0.027
Pine, 113 years	30	1.5	217	822	0.24	0.0007	0.081
Pine, nonresidential structure, Vologda Region, 150 years	26	1.5	212	812	0.20	0.0006	0.066

[a]Timber specimens were subjected to an external radiation heat flow of constant density $q_e = 20$ kW/m^2 for 20 min as per GOST 30402-96

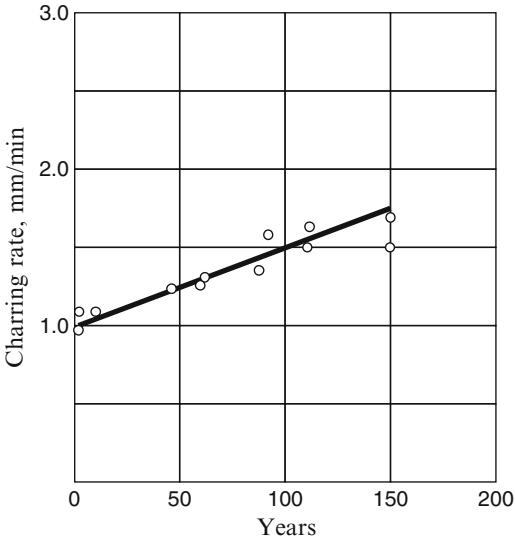

Fig. 10.10 Effect of natural aging of timber structures on timber charring rate (fir, pine) in a standard fire

10.4 Biodegradation of Timber and Complex Bio-, Moisture, and Fire Protection of Constructional Timber Materials

Fungal infections and insects play an important role in damaging timber structures. Timber-destroying fungi are divided into two large groups according to their physiological effect: destructive, destroying cellulose, and corrosive, attacking lignin.

Cellulose-destroying fungi cause brown rot, and those destroying lignin cause white rot. A feature of the enzymatic system of white rot microorganisms is also its activity toward partial or full destruction of polysaccharides.

Destructive brown rots caused by several types of household fungi have been detected in long-used wooden architectural monuments of the Russian North. They include a real household fungus Serpula lacrymans, the membranous fungus Coniophora puteana, white fungi Coriolellus sinuosus and Fibroporia vaillantii (Fr.), and the agaric fungus Paxillus panuoides Fr. (Kisternaya and Kozlov 2007). Timber affected by fungi first acquires a brown color, and deep lengthwise and crosswise cracks appear in it. Then the rot breaks down along the cracks into small prism-like pieces that are easily converted into brown powder.

Under natural conditions, bio-destroyers of timber like white rot mainly affect the wood of living plants. Insects that bring fungi to the conductive tissues of trees serve as fungi agents. The sequence of anatomical and chemical changes in timber of various species under the influence of white rot fungi was studied using light microscopy (Malysheva 2004). It was established that, depending on the timber variety and type of fungi, either selective delignification of timber or simultaneous destruction of lignin and the carbohydrate part of timber (hemicellulose and

cellulose) occurs. Timber damage often started from wood rays, from where white rot hyphae, via bordered pits, penetrated into tracheids and elongated thick-walled cells, and completely destroyed the main components of sheathing tissue.

Furthermore, internal layer S_3 of sheathing tissue with increased hemicelluloses content was the first to be affected. Lignin-enriched middle lamellas were the last to be destroyed, which is why the cells preserved their form for a long time. This type of simultaneous deterioration of the lignin–carbohydrate complex was accompanied by cracking of the timber into small prism-like pieces resembling brown rot.

The process of selective delignification of sheathing tissue of timber under the action of white rot fungi (Phanerochaete sanguinea) was more complicated and diversified. In some cases, delignification started from internal layer S_3 and ended with middle lamella. In other cases, removal of lignin from the same cells occurred simultaneously and in opposite directions: from external layer S_1 to middle lamella and toward it from internal layer S_3. In this case, lignin from layer S_2 was the last to be removed. The cells separated from each other took the form of nearly regular rings.

The varieties of fungi infecting timber are numerous. A detailed mechanism of their destructive action has not been clarified to date.

It has been established that fungal activity depends on ambient temperature, moisture content in the timber, and species and type of the timber itself (Zabel and Morrell 1992). For this reason, the influence of climatic conditions of the region where woody plants grow or wooden structures are used is most pronounced. High destructive activity of fungi is observed at ambient temperatures above 5 °C and moisture content in timber over 20–25 %. Under such conditions, timber infected by fungi decays very quickly, within several years, as temperature and sufficient moisture content promote fast development, growth, and multiplication of fungi. Destruction of timber by fungi slows down considerably or ceases if the ambient temperature falls below 2 °C and below zero.

An increase in the ambient temperature beyond 35–45 °C, in turn, favors the fermentation activity of fungi.

It is assumed (Kisternaya and Kozlov 2007; Zabel and Morrell 1992; Venalainen and Harju 2004) that the mechanism of the destructive effect of fungi is connected with their participation in two processes: (1) free radical formation, initiating oxidative breakdown of polysaccharide molecules, and (2) acid agent formation (like acid of sugar), causing hydrolysis of timber components. In both processes, a large role is played by ferments produced by fungi, which are biocatalysts of destructive reactions.

The importance of the hydrolytic line of timber biodegradation confirms the influence of temperature and moisture conditions on the destructive effect of fungi, and its dependence on species and morphological structure, and timber pore space. Data on the influence of the content of phenol compounds from the stilbene group in extractives from sap and pine trunkwood favor the radical mechanism of timber biodegradation (Venalainen and Harju 2004). A higher concentration of phenols, which are natural inhibitors of radical oxidizing reactions of various substances, explains the higher natural resistance of trunkwood to the destructive effect of fungi.

The destructive effect of fungi is typically judged according to loss of timber weight for a specific period of fungal attack (Kisternaya and Kozlov 2007). The reciprocal value of this weight loss serves as a measure for timber's resistance to destruction by fungi (Venalainen and Harju 2004).

Based on an analysis of the change in the content of main chemical components of timber and ultimate composition of the organic part as a result of biodegradation, the following stoichiometric equations have been proposed for the reactions (Soloviev 2004):

(a) Corrosion (white rot fungi):

$$4C_6H_9O_4 + 25O_2 \rightarrow 24CO_2 + 18H_2O + 11.53 \times 10^3 \text{kJ}.$$

(b) Destruction (brown rot fungi):

$$C_6H_{10}O_5 + 6O_2 \rightarrow 6CO_2 + 5H_2O + 2.83 \times 10^3 \text{kJ}$$
$$C_5H_8O_4 + 5O_2 \rightarrow 5CO_2 + 4H_2O + 2.34 \times 10^3 \text{kJ}$$

In the author's opinion (Soloviev 2004), the foregoing equations show the connection between timber weight loss and the amount of absorbed oxygen; products formed, namely, carbon dioxide and water; and emitted heat.

The kinetic approach to determining the weight loss rate during timber biodegradation via its connection with the rate (intensity) of oxygen absorption or carbon dioxide emission opens wider possibilities for evaluating the functional role and activity of timber-destroying fungi.

Natural resistance of timber to rotting, all other conditions being equal, depends on species and timber variety. The trunkwood of Scotch pine and Siberian larch, oak, and ash is considered most resistant to biodeterioration (GOST 20022.2-80). Fir, silver fir, and beech timber are moderately resistant. Sensitive timber includes elm, maple, and birch. Lime tree, alder, and aspen timber are nonresistant materials. Not only the physical structure of timber and the ratio between sap and trunk parts but also the chemical composition of timber are of importance.

It should be noted that the most intensive destruction of wooden structures by fungi occurs in places where they make contact with the soil.

In research paper (Varfolomeev et al. 2004), the influence of duration of service life of pile foundation timber on its being attacked by wood-destroying fungi in the soil aeration zone was analyzed; strength properties of pile shafts were determined for various extents of fungal attack. Fragments of piles of as-built dimensions (diameter 24 cm) were cut from sites located 0.3 m above and 0.4 m below the ground surface. The service life period of pile foundations of timber houses (Archangelsk) being analyzed was from 10 to 87 years. It was established that the content of timber affected by fungi in cross section of the samples (G, %), depending on the service period (τ, years), can be represented by the equation:

$$G = 1.104\tau - 9.743, \%.$$

The correlation factor R is 0.73.

The healthy part of the trunkwood of piles without defects and not affected by fungi preserved its strength properties after long-term usage.

Dependence of the compressive strength of piles along the grain from the area of fungal attack of the cross section of the samples (G, %) corresponds to the following equation with correlation factor 0.84:

$$\sigma_{\text{compr}} = 11.553–0.106\ \text{G, MPa}.$$

Taking into account the largest stress acting in the shaft of the pile foundations of timber houses (3.65 MPa), the authors (Varfolomeev et al. 2004) distinguished three stages of pile usage: (1) guaranteed safe usage stage, fungal attack up to 13 % (the compressive strength of timber along the grain is higher than the standard value); (2) safe usage stage, fungal attack up to 59 % of the cross section (the actual compressive strength of the samples along the grain is higher or corresponds to the largest value of stresses acting in the pile shaft); and (3) hazardous usage stage when over 59 % of the cross section has deteriorated and pile failure is possible.

The only really effective means for protecting timber structures in contact with ground against biodegradation is careful moisture proofing.

Insects of the wood-fretter family cause a great deal of damage to timber building structures (Kisternaya and Kozlov 2007). The furniture beetle (Hadrobregmus pertinax L.) and northern wood-fretter (Hadrobregmus confuses Kr.) are active in unheated timber structures in the European part of Russia. Their optimal development is observed at a moisture content in coniferous wood above 18–19 % and temperature about 25 °C. At temperatures beyond 48 °C, they die out at all stages of their existence.

The furniture beetle lives mainly in coniferous wood in places exposed to frost action. These are attic floor elements, logs of lower crowns, damp places under window sills, rough timber boarding, etc. The northern wood-fretter damages coniferous wood only. It is detected in crown logs at any height. The grubs cause major damage to timber.

Controlling these pests is a more complicated task compared to wood-destroying fungi, since beetles and their grubs are capable of functioning in timber with low moisture content (10–12 %). External damage and inlet openings in timber made by the beetles are small and invisible.

Various methods were applied historically, most often chemical preservation methods with the use of different antiseptics and disinfectants, in order to protect timber structures against fungal infection and the activity of insect pests. A large number of chemical protection agents were developed and tested (GOST 20022.2-80). The experience accumulated over many years of using various agents showed their benefits and drawbacks.

In Russia, for example, effective antiseptics based on pentachlorophenol or its phenol sodium (PBB-211, PZS) were widely used in order to protect timber architectural monuments against biodegradation. Deep treatment of timber with PBB-211 by the panel method caused additional internal stresses and the appearance and expansion of cracks in log structures. Twenty-four years after treatment of

timber structures of Pokrovsky Church on Kizhi Island, the level of chlorophenol content in air in close proximity to the treated walls exceeded MPC (0.01 mg/m^3) by several times (Kisternaya and Kozlov 2007). From 1984 in Russia (GOST 20022.2-80) and from the beginning of the 1990s in the EU, agents based on pentachlorophenol have been excluded from the List of Authorized Bioprotective Elements for timber residential and public buildings due to the potential formation of highly toxic dioxins.

For reasons of environmental safety, a similar situation has occurred with the use of very effective antiseptics and insecticides based on compounds of chromium, copper, and arsenic (CCA). In these agents, copper played the role of fungicide, arsenic served as a fungicide and insecticide, and chromium was the fixator, contributing to the formation of insoluble compound forms, and, thus solving the problem of environmental emissions of toxic substances from timber.

However in Europe, Directive 2003/2/EC limited sales and use of arsenic compounds, including CCA compounds, for treating the structures of timber residential and public buildings with a high degree of contact between materials and people. A similar practice was subsequently adopted in the USA and Australia.

Many timber preservatives displaying functions of fungicides and insecticides proposed instead of CCA (e.g., complex of copper compounds with quaternary ammonium bases or with cyclic nitrogen-containing substances) cause ferrous metal corrosion.

The preservatives that protect timber against bio-destroyers, enhance fire safety of timber structures, and protect against the harmful effect of moisture are of primary concern. The problem of developing effective protective agents with similar multiple functions is of immediate interest not only from the point of view of preserving historical monuments of timber architecture. Its solution is also important for increasing the durability of timber structures of present-day constructional members.

Work on developing a multipurpose fire-, bio-, and moisture-protective compound for timber, and the detailed study of its effect, was carried out in the SFSA bay leadership of Prof. E.N. Pokrovskaya (Kobelev 2012). The prospects for using "soft" surface modification of timber with organic phosphorus and silicon compounds for this purpose were demonstrated earlier (Pokrovskaya 2003).

It is known that the condition and properties of surface layers of timber are responsible for the decorative and many other important usage parameters of timber products, in particular, hardness, durability, surface heat conductivity, resistance to the effects of atmospheric factors and aggressive media, etc.

The Fokkos compound has been developed from the principle of chemical interaction of surface layers of timber with reactive groups of organic phosphorus and silicon compounds (Kobelev 2012).

The compound's main components are dimethyl phosphite and oligomeric ethylhydrid siloxane. The formation of strong covalent links of these compounds with main timber components was proved by various research methods. Soft surface modification of pine timber as a result of treatment with Fokkos compound considerably increased the biostability of the material, halved the moisture and

water absorption of the samples, and increased the fire-protective characteristics of timber. The properties were assessed for all factors using standard methods accepted for determining biostability, moisture, and water absorption of timber and characteristics of its reaction to fire.

Compared to the known fire- and bio-protective compounds for timber (Latic-B, Attic, BB-11, Texturol-Quattro, etc.) that often require application of additional waterproof protective paint coatings, Fokkos compound is a more efficient, cost-effective compound. Much less of it is needed to achieve the necessary protection level. Tests of modified timber samples under laboratory conditions have shown the high, 100 %, biocidal activity of Fokkos compound against both destructive fungi (Coniophora puteana) and mold fungi causing timber corrosion (Penicillium biforme, Aspergillus niger).

Tests under in tropical conditions of Vietnam confirmed these results and also showed the high efficiency of the developed method for protecting timber against termite attacks (Kobelev 2012).

A detailed study of the fire-protective action of Fokkos compound was carried out not only according to the standard method (GOST R 53292-2009) adopted in Russia for estimating the effectiveness of fire protection means. Important fire safety data, such as flammability, flame spread, smoke generation ability, and toxicity of combustion products, have been determined. It has been established that this compound provides fire rating group I (mass loss on combustion less than 9 %). Timber from the group of materials that quickly spread flame ($I_{RP} = 60$) moves to the slowly spreading group (index $I_{RP} = 1.2$). In practice, due to intensive char formation, flame spreading on the sample surface stops immediately. Surface modification with Fokkos compound increases timber resistance to combustion on exposure to external radiation heat flow. Material from highly ignitability group B3 moves to moderately inflammable group B2. Critical heat flow of combustion increases from 12.5 kW/m^2 for the initial timber up to 20 kW/m^2 after surface modification of the samples. Smoke generation ability and toxicity of combustion products have been determined in the most hazardous regime of smoldering timber samples exposed to external radiation heat flow within the interval of 10–35 kW/m^2. Treating timber with Fokkos compound reduces smoke generation by almost 3.5 times and moves the material from group D3 with high smoke generation ability to group D2 with moderate smoke generation ability. A decreasing rate of toxic carbon monoxide formation is observed.

Unlike the initial timber, the surface-modified samples exposed to fire form uniform fine-pored char (average pore diameter is 2.3 Nm) with greater specific surface.

X-ray fluorescence analysis of the char showed considerable phosphorus and silicon content in the carbonized structure (2.6 and 2.1 %, respectively).

Based on the results of standard accelerated tests of timber samples in a climatic chamber in air with regulated relative humidity and temperature, it was concluded that the bio-moisture- and fire-protective effect of treating timber with Fokkos compound may be preserved for up to 20 years when the material is used under normal conditions.

References

Aseeva RM, Barbotko SL, Serkov BB, Sivenkov AB, Suleykin EV, Tarasov NI (2009) Impact of timber service life on its fire-hazardous properties. In: X international conference on chemistry and physical chemistry of oligomers "Oligomers ─ 2009", VGTU, Volgograd, pp 290–295

Emmanuel NM, Buchachenko AL (1982) Chemical physics of polymer aging and stabilization. Nauka, Moscow, 360 p

GOST 16350-80 (1981) USSR Climate. Regionalizing and statistical parameters of climatic factors for technical purposes, Moscow

GOST 20022.2-80 (1980) Timber protection classification by resistance to rot, Moscow

Isayeva LN, Bryukhanova EB (1969) Physical and mechanical properties and anatomical features of the wood of Siberian larch from a 230 year-old structure. Collected papers of the Institute of Forestry and Timber of Siberian Department of USSR AS, Krasnoyarsk

Kazanskaya SYu, Vikhrov YuV, Golman LP (1975) Some features of the chemistry of archaeological timber. Chimiya drevesiny (2):41–44

Kisternaya MV, Kozlov VA (2007) Wood science aspects of preservation of historical buildings. Karelsky Scientific Centre of RAS, Petrozavodsk, 133 p

Kobelev AA (2012) Development of a complex fire- moisture- and bioprotective formulation based on compounds providing surface modification of timber. PhD thesis, 19 p

Malysheva OI (2004) Change in micromorphologic structure due to lignin-destroying fungi. In: Proceedings of the IV international symposium "Structure, properties and quality of timber – 2004", vol 2. SFTA, St. Petersburg, pp 434–436

Obolenskaya AV, Elnitskaya ZP, Leonovitch AA (1991) Laboratory works on timber and cellulose chemistry. Ekologiya, Moscow, 320 p

Pischik II (2005) Dating long-storage timber by nondestructive methods. Dr dissertation, MSCU, Moscow

Pischik II, Vikhrov YuV (1996) Method for determining the time for cutting timber used for interior items. RF Patent No. 2111487

Pischik II, Fefilov VV, Burkovskaya YuI (1971) On chemistry and physical properties of new and seasoned timber. Izvestiya vuzov, Lesnoy zhurnal (6):89–93

Pokrovskaya EN (2003) Physicochemical basics of increasing timber durability. Preserving wooden monuments using organoelemental compounds. Monograph – M. ASV Publishing House, 104 p

Pokrovskaya EN, Pischik II, Smirnov NV, Naganovsky YuK (2000) Thermal decomposition of timber with different useful life. Constr Mater (8):34–36

Popov AA, Rapoport NY, Zaikov GE (1987) Oxidation of oriented and strained polymers. Chimiya, Moscow, 232 p

Regel VR, Slutsker AI, Tomashevsky EK (1974) Kinetic nature of the strength of solid bodies. Nauka, Moscow, 650 p

Sandu ICA, Brebu M, Luca C, Sandu I, Vasile C (2003) Thermogravimetric study on the aging of lime wood supports of old paintings. Polym Degrad Stab 80:83–91

Serkov BB, Sivenkov AB, Suleykin EV, Degtyarev RV, Tarasov NI (2009) Features of fire hazard of archaeological timber. Fires Emerg Prev Elimin (1):4–28

Soloviev VA (2004) Kinetic method for assessment of timber-destructive ability and activity of fungi. In: Proceedings of the IV international symposium "Structure, properties and quality of timber – 2004", vol 2. SFTA, St. Petersburg, pp 458–460

Varfolomeev YA, Nevzorov AL, Aksenov SE (2004) Experimental studies of physical and mechanical properties of piling timber. In: Proceedings of the IV international symposium "Structure, properties and quality of timber – 2004", vol 1. SFTA, St. Petersburg, pp 194–196

Varfolomeyev YuA, Potutkin GF, Shapovalova LG (1990) Wood property change at long-term service (by the example of wooden monuments in Arkhangelsk Region). Derevoobrabatyvayuschaya promyshlennost (10):28–30

Venalainen M, Harju A (2004) Variation in decay resistance of Scots pine timber. In: Proceedings of the IV international symposium "Structure, properties and quality of timber – 2004", vol 2. SFTA, St. Petersburg, pp 405–408

Zabel RA, Morrell JJ (1992) Wood microbiology. Decay and its prevention. Academic Press, Inc., San Diego, 476 p

Chapter 11
The Change in Fire Behavior of Different Timber Species After Accelerated Artificial Aging

Abstract This chapter describes the method of acceleration of artificial aging of timber equivalent to exploitation duration from 50 to 150 years. It also presents the results of thermal and chemical analyses of timber specimens, the changes in their density, and fire safety ratings and fire resistance.

11.1 Methods of Accelerated Artificial Aging of Timber

Natural aging of living and felled trees is a slow process, if no catastrophic adverse factors (high-level radiation, mechanical wind loads, destructive effect of fungi, insects, hydrologic imbalance, etc.) interfere in it.

Aging of living trees may be described as a gradual loss of reproduction ability in their living cells and tissues resulting from a complex mechanism of biological, physical, and chemical transformations in a woody plant as part of its interaction with the environment.

Aging of felled trees and timber-based materials of various types is caused by a complex of physicochemical changes that occur during storage, processing, and use of timber-based materials and lead to the loss of a series of mechanical properties.

As we see, the decisive role in natural aging of timber is played by competitive chemical processes of decomposition and cross-linkage of macromolecules in this natural polymer composite. The mechanism of chemical processes of timber aging has not been identified. However, it is quite clear that depending on the conditions of external effects, the processes of decomposition and cross-linkage in timber include a wide variety of interrelated (coupled) ionic, radical-chain, and molecular reactions.

The surface layers of timber are most affected by intensive external effects. And it is the surface layers that are responsible for the decorative properties of products and for certain performance characteristics, such as wear resistance, hardness, resistance to aggressive environments, and superficial thermal conductivity.

R. Aseeva et al., *Fire Behavior and Fire Protection in Timber Buildings*,
Springer Series in Wood Science, DOI 10.1007/978-94-007-7460-5_11,

Methods of accelerated artificial aging are commonly used to determine the effect of various factors on the performance characteristics of timber-based materials, on the rate of adverse processes, and on the forecast of service life.

Methods of accelerated artificial aging may be used for a number of purposes and tasks.

One of the trends in artificial aging of timber is to give an ancient look to timber building structures, beams, story posts, building facades, and interior items. There have long been three methods of surface treatment to give timber a period look: chemical, thermal, and mechanical, as well as a combination of these. The objective was to change only the external appearance while maintaining the mechanical properties of the timber. The practice of imitating ancient, aged timber includes such operations as brushing, texturing, and toning.

To emphasize the texture of timber, distribution of knots, and fiber pattern, the surface of timberwork is burned with a brazing torch. After this treatment, excessive scale is mechanically removed. The timber surface may be mechanically treated (brushed) using special brushes and other tools, and then this coarsely treated surface may be toned with alcohol- or water-based paints. To imitate patina, lacquers and paints are often employed, as well as special additives (e.g., fine aluminum powder). Various mechanical methods are used to imitate timber damaged by pruners.

Widely known recipes for chemical imitation of a period look include treatment with aqueous ammonia, vinegar boiled with rusty nails, aniline sulfate and alkali, a mixture of hydrogen peroxide and hydrogen chloride, as well as other chemical agents.

Another trend of really accelerated aging of timber is to carry out the process in climatic chambers with preset conditions. These are usually employed to determine the means effectiveness of protecting timber against various external effects, service life duration of timber structural members, and various materials and products. By way of comparison, reference specimens (e.g., untreated timber) are tested under the same conditions.

The conditions in climatic chambers for accelerated aging of timber materials and timber-based products simulate the conditions of their use to a certain extent. The equipment for accelerated aging may differ in effective volume, automatic control of created conditions, and set of conditions. The following thermostats and chambers are used for accelerated tests of various materials used in various climatic zones and conditions:

- With programmable air temperature and moisture
- With programmable temperature and its rate of change
- With programmable temperature, moisture, UV, or other radiation intensity
- With controllable temperature, medium, and atmosphere: inert and aggressive gases, pure oxygen, salt spray, liquid substances, solvent vapors, etc.

Accelerated aging of materials and products is performed in compliance with the standards valid for each material or product (e.g., GOST 9.057-75; GOST 9.707-81). The new edition of standard (GOST 20850 (draft)) for glued timber constructions

now includes methods of accelerated tests, which make it possible to evaluate the durability of glued joints on cyclic exposure to alternating temperatures and moisture, water resistance, and heat and cold endurance.

Based on the results of accelerated tests, a forecast may be made on the product's service life in storage and operation. The time profile for decrease of the properties to critical values in normal conditions is calculated for this purpose.

Experience shows that aging of fireproofed organic polymer materials increases their fire safety. But the rate of increase in combustibility of materials may be far slower compared to the decreased rate of their mechanical characteristics (Serkov and Aseeva 1996). Thus, assessment of the effect of aging on strength properties of materials must in any case be given great attention.

If we consider artificial aging of timber as a process of accelerated physicochemical transformation of timber substance under the influence of external factors, a new line in timber technologies, namely, thermal modification of timber, may also be ascribed to it.

This line has been developing especially rapidly in the twenty-first century. Industrial development of these technologies started from using new apparatus for high-temperature (150–230 °C) drying of timber in a low-oxygen atmosphere at woodworking plants in Finland.

The best known industrial technologies for thermal treatment of timber today are:

1. The Finnish Thermowood technology. Thermal treatment of timber is performed in a protective atmosphere of water vapor at normal pressure and a temperature of 190–212 °C.
2. The French Retification technology. Its distinctive feature is thermal modification by low-temperature pyrolysis of timber at a temperature of 200–250 °C in an inert medium (nitrogen and/or supersaturated water vapor).
3. The Dutch Plato technology. Thermal modification is performed by cyclic hydrolytic thermolysis of timber at 160–190 °C.
4. The German OHT technology. Thermal treatment of timber is carried out in a medium of plant oils with the use of four thermal regimes.

In this country, we use American West-Wood technology of vapor stabilization of timber patented in Russia at a temperature of 200–240 °C and water vapor gauge pressure of 0.1–0.2 MPa. The process goes in several stages. The first stage consists of heating the material. During the heating process, water vapor is fed into the drying chamber, increasing moisture and temperature to 130–150 °C. At the second stage, timber drying at high temperature occurs, and moisture is removed almost to zero. The temperature in the chamber is increased to 200–240 °C. At the same time, the temperature of the timber itself also increases in the water vapor medium at a low gauge pressure compared to the atmospheric environment. Water vapor as a protective medium prevents timber oxidation and combustion. At this stage, timber acquires new properties. The temperature in the chamber is then lowered, and the moisture of timber is brought to 4–6 %. The duration of the whole cycle of volumetric thermal treatment of timber is 12–15 h.

At the present time, there are more than 20 manufacturers of thermally treated timber in Russia. Potential capacity of Russian companies is 60–65,000 m^3 of thermo timber per year.

The essence of physicochemical transformations in timber during this thermal treatment consists in decomposition and elimination of plant cell wall components, mainly hemicelluloses, and in rearrangement and cross-linkage of lignin molecules (Welzbacher et al. 2007).

Under certain conditions of thermal treatment, the effect of artificially aged timber of any species may be obtained from the color array. In this case, the color of the timber (from ecru and golden to somber brown) turns out homogeneous all across the specimen section. Thermally treated timber acquires a series of positive properties. These include increased water resistance (four to fivefold), lower hygroscopicity, and low equilibrium moisture (4–6 %). Stability of timber dimensions against environmental moisture and temperature drops is significantly improved. This parameter is 10–15 times better compared to untreated timber. Swelling and shrinkage due to environmental moisture variations are reduced.

But the greatest achievement is a 15–25-fold increase in service life longevity of the material due to greater resistance of the timber to biological damage. This is the consequence of extermination of biodeteriorating agents (bacteria, fungi and their endospores, insects and their maggots) during thermal treatment and eliminating the conditions for active generation of fungi at low equilibrium moisture of the timber (Welzbacher et al. 2007; Kortelainen et al. 2011). It is noted, however, that thermo timber is not suitable for use when there is direct contact with soil.

As for physical properties, the first thing to note is a slight (10–15 %) decrease in timber density after thermal treatment. As treatment duration and temperature increase, many strength properties degrade. Elasticity modulus undergoes the least changes; surface hardness and compression strength along fibers increase, whereas the thermal conductivity coefficient of thermo timber decreases compared to the initial specimens (Welzbacher et al. 2007; Kortelainen et al. 2011; Finishes Thermowood Association 2003). However, the use of structural thermo timberwork as load-bearing members of buildings is not recommended until the problem is fully clarified (Finishes Thermowood Association 2003).

The task of our work is to evaluate the effect of very long aging of timber members of ancient timber architecture on fire behavior and fire resistance. Chapter 10 describes the information obtained on physicochemical processes in timber occurring during long-term natural aging of hundreds of years in the constructional members of ancient wooden structures. An assessment of variation profiles of certain fire safety indices is given. But due to an insufficient number of specimens, a number of important fire safety characteristics of timber during its natural aging were not determined.

Thus, it was decided to make use of accelerated artificial aging methods to obtain specimens with such properties as the material in service under natural conditions for hundreds of years.

Method (Pishchik et al. 1980) for accelerated artificial aging suggests complex thermal treatment of timber specimens at a temperature of 110–190 °C for

10–48 h and subsequent exposure to an aqueous solution containing 10–15 % hydrogen peroxide for 12–15 h.

This procedure was used, for example, to obtain artificially aged specimens of fir with an approximate time of service of 250 years (Pishchik et al. 1980). It resulted in changes in properties reported in Table 11.1 compared to the specimens of freshly felled timber and timber with long service life in natural conditions.

A decrease in temperature and duration of accelerated artificial aging operation leads to slowing of physicochemical reactions of timber substance transformation.

Based on the data from (Pishchik et al. 1980), we have selected milder conditions for accelerated artificial aging of coniferous and deciduous timber species.

Timber specimens 55-mm thick were seasoned for 7 days at 45–65 °C to a constant weight. They were then heated in an air thermostat at a temperature of 160 °C for 10 h and held in a 10 % hydrogen peroxide solution for 12–14 h.

After washing and air curing, the specimens were analyzed for all parameters. The adopted procedure of artificial aging allowed us to age deciduous specimens by 50–80 years and coniferous specimens by 100–150 years. Change in service life was assessed by nondestructive methods by the character of internal stresses in the specimens (Pishchik 2000).

11.2 Results of Physicochemical and Thermal Analysis of Aged Timber Specimens

Aging of timber in natural conditions occurs under the influence of various external factors in the presence of air oxygen. Therefore, artificial aging of timber specimens was performed in an air atmosphere and aimed at accelerating thermal oxidation and hydrolysis of the wood substrate. This method of artificial aging causes significant changes in chemical composition, structure, and properties of timber. The progress of these changes depends on timber species and variety.

Table 11.2 shows the data on changes in density and element composition after artificial aging of specimens of four timber varieties.

What stands out is a slight change in density, probably due to very slight shrinkage and moisture of the specimens. Variations in element proportions are more conspicuous. A decrease in carbon content and an increase in hydrogen content are characteristic of all types of timber. Artificially aged fir and pine contain five to eight times more hydrogen than oak and birch. It is interesting to note that coniferous species contain less oxygen after artificial aging, whereas deciduous species on the contrary show an increase of 2.2–2.9 %.

Aging of coniferous species in natural conditions also brings about an increase in hydrogen and decrease in carbon in the element composition of timber (Table 10.6). But hydrogen over-enrichment in artificially aged fir compared to fir naturally aged for 90–150 years is evidence of different directions of physicochemical transformations in timber during aging.

Table 11.1 Changes in physicochemical properties of fir timber after aging in natural and artificial conditions

Fir specimens	Hemicellulose, %	Lignin, %	Swelling ratio			Hygroscopicity limit, %	$\sigma_{bending}$, MPa
			Radial	Tangential	Volumetric		
Freshly cut	18.5–19.5	25.4–26.9	0.170	0.310	0.500	35.00	77.0
Service life, years:							
300	17.2	25.2	0.242	0.535	0.783	25.65	51.5
500–700	10.4	24.0	0.257	0.478	0.769	28.08	20.6
Artificially aged, 250 years	16.8	24.9	0.217	0.408	0.683	26.21	52.0

Table 11.2 Effect of accelerated artificial aging of timber on the density and element proportions of specimens

Specimen	ρ, kg/m^3	*W*, %	*C*, %	*H*, %	*O*, %
Fir	422	6.4	52.22	6.04	41.74
Fir, 150 years	430	7.2	48.81	11.2	40.0
Pine	448	6.0	52.14	5.91	41.95
Pine, 150 years	462	6.4	49.20	10.4	40.4
Oak	638	4.3	50.40	5.77	43.43
Oak, 80 years	626	5.1	48.9	6.43	44.7
Birch	567	5.5	50.58	5.78	43.64
Birch, 80 years	593	6.2	48.7	6.72	44.6

Table 11.3 Chemical composition of various timber species before and after artificial aging

No	Timber species	Lignin, %	Cellulose, %	Lignin[a], %	Cellulose[a], %
1	Fir	28.6	44.2	36.1	29.8
2	Pine	27.5	43.3	36.4	30.3
3	Oak	29.6	41.0	27.0	32.4
4	Birch	21.0	41.0	21.2	29.7

[a]Artificially aged timber

The lower carbon content in the aged timber indicates the occurrence of decomposition reactions, which induce the emission of low-molecular carbon-containing products (e.g., carbon dioxide and monoxide, formaldehyde, methanol, formic, acetic acids). Enrichment of aged coniferous timber with hydrogen with concurrent reduction in oxygen content may be caused to a certain degree by intermolecular reactions of condensation of all timber components, especially with lignin participation.

It is not improbable that in timber substrate (in our adopted conditions of artificial aging), a relative accumulation of hydrocarbon derivatives from the extractives – waxes, resin, and saturated fatty acids C_{18}–C_{22} – will take place. They cannot evaporate from the timber at normal pressure and a temperature of 160 °C. Decarboxylation of these acids should lead to lower relative carbon content and retention of hydrogen.

In contrast to accelerated artificial aging with heating the specimen in air at 160 °C, thermowood production is accompanied by different processes. For example, spruce timber thermally treated in a vapor–gas medium at 200 °C shows hydrogen enrichment by 6–10 %. Lignin content increases by almost 35 %.

When the spruce treatment temperature is increased to 250 °C, lignin content increases by almost 50 %.

Reactions of intra- and intermolecular dehydration of polysaccharides and lignin macromolecule condensation lead to lower hydrogen and oxygen contents, respectively.

We have done a simplified analysis of timber chemical composition after artificial aging, which included determining cellulose and lignin content. The remainder was a mixture of noncellulosic polysaccharides and extractives (Table 11.3).

As follows from Table 11.3, artificial aging results in significantly altered cellulose content. In coniferous species, cellulose content decreases by 30–32 %. In deciduous species, the decrease is only 21–27.5 %. It is known that lignin is the most oxidant-resistant constituent of timber. Therefore, the increase in relative lignin content in coniferous species of 26–32.4 % is quite understandable. In artificial aging of oak and birch, the situation is more complex. In the case of birch, lignin content remains practically at the initial level, and in oak it even goes down by 8 %. The cause of this difference is unclear. Maybe the divergence in approximate aging duration of different species affects the nature of the chemical reactions that occur. In any case, the details of physicochemical processes going on during artificial aging must be thoroughly examined.

Long thermal treatment of timber in air at 160 °C already contributes to the evaporation of light volatile part of extractives (terpenes). Although the mass loss in this period is insignificant, the wood substrate undergoes conspicuous transformations that affect the color of the timber. This is especially true for oak.

Activation of the radical-chain process of thermo-oxidative decomposition of timber by air oxygen occurs by the law of randomness. Oxidation rate depends on the permeability and specific surface area of the porous material structure. This means that surface and amorphous areas of the material's structural organization will be the first to undergo changes.

Oxidative decomposition of the main chains of high-molecular polysaccharides of cellulose by the radical mechanism and the law of randomness is accompanied by the formation of shorter fragments compared to the initial value. However, they are still quite long and are incapable of evaporating at normal atmospheric pressure. For this reason, they are not easily removed from the matrix and make up part of the group of noncellulosic polysaccharides together with hemicelluloses. Oligomeric polysaccharides – hexosanes and pentosanes – partially hydrolyze to sugars under the action of acids that are products of timber component oxidation. The sugars in turn are decomposed in water, and low-boiling point substances are formed (furfurol and hydroxymethyl-furfurol).

The process becomes even more complicated with the impact of a strong oxidant – hydrogen peroxide – on the timber. We assume that oxidation of polysaccharides by hydrogen peroxide in a water medium in the presence of ash salts at low temperatures may cause partial cleavage of glycosidic cycles along C_2–C_3 bonds with the formation of cellulosic polyoxyacids. Their formation and subsequent decarboxylation may explain the reduction of native cellulose in the chemical composition and of carbon in the element proportions of the product of artificial timber aging.

On the other hand, hydrogen peroxide has recently attracted attention in engineering practice as a reagent for delignification and bleaching of cellulose pulp in paper production. Hydrogen peroxide exhibits low reaction capacity toward lignin at normal and moderate temperatures. Conspicuous delignification by means of hydrogen peroxide requires a temperature increase to 60–80 °C or the use of redox-type catalysts. The products of deep lignin oxidation by air oxygen are carbon

dioxide and water. The products of partial oxidation are various oxygen-containing derivatives of hydroxyphenylpropane fragments. Oak timber lignin is a mixed type of syringyl–guaiacyl molecular structure in almost equal proportions. Judging by the alterations in Fourier infrared spectra of aged specimens, syringyl fragments (with two methoxy groups in aromatic ring) are more prone to decomposition than to condensation reactions.

Under the conditions of accelerated artificial aging of timber we have adopted, the transformation processes of wood substrate proceeds in the most thermodynamically favorable directions. Lignin auto-oxidation by air oxygen results in the formation of phenoxy and hydroxy radicals. They attack hemicelluloses and cellulose, as well as macromolecules of lignin itself, and initiate material decomposition reactions. The resulting acids speed up hydrolytic reactions of cellulose decomposition. Therefore, the process of accelerated artificial aging of timber is a truly closed cycle of complex coupled heterogeneous reactions of decomposition and cross-linkage of material components.

As a result of artificial aging of timber and removal of part of its main components, material porosity increases, thus increasing the possibility of contact of the wood matrix with air oxygen.

Cellulose is the basic structural component of timber, which provides its high-strength properties. The reduced relative cellulose content in the wood matrix as a result of accelerated artificial aging should especially affect such mechanical properties of timber as bending strength, elasticity modulus, shear, and splitting strength. The changes in compression strength and modulus of compression across fibers and hardness parameters should be smaller.

Thermal analysis of timber specimens after accelerated artificial aging reveals certain changes in their behavior.

Figures 11.1, 11.2, 11.3, and 11.4 show TG and DTG curves of initial specimens and artificially aged oak and fir timber heated at different rates in air atmosphere.

On examining the TG and DTG curves of decomposition of present-day and artificially aged timber specimens, a common effect of heating rate for all of them may be noted. A characteristic feature is the existence of two decomposition stages: low-temperature (140–400 °C) and high-temperature (above 400 °C). The first stage incorporates the processes of thermo-oxidative decomposition of timber substance and formation of inflammable volatiles. The second includes the processes of carbonization and oxidation of the carbonized product. Slight mass losses when specimens are heated to 140° are attributed to moisture evaporation.

Under equal heating conditions, the aged specimens start to lose mass at a lower temperature compared to the initial material. The effect of aging is especially observable when comparing the temperature maximums on DTG curves of corresponding specimens. Artificially aged timber has a T_{max} value several degrees lower compared to T_{max} of the initial timber specimen.

At the first low-temperature stage, coniferous and deciduous specimens lose more than a half of their weight. This stage has an exothermic nature. After artificial aging, the amount of heat emitted at this stage increases 1.5–1.8 times (Fig. 10.8).

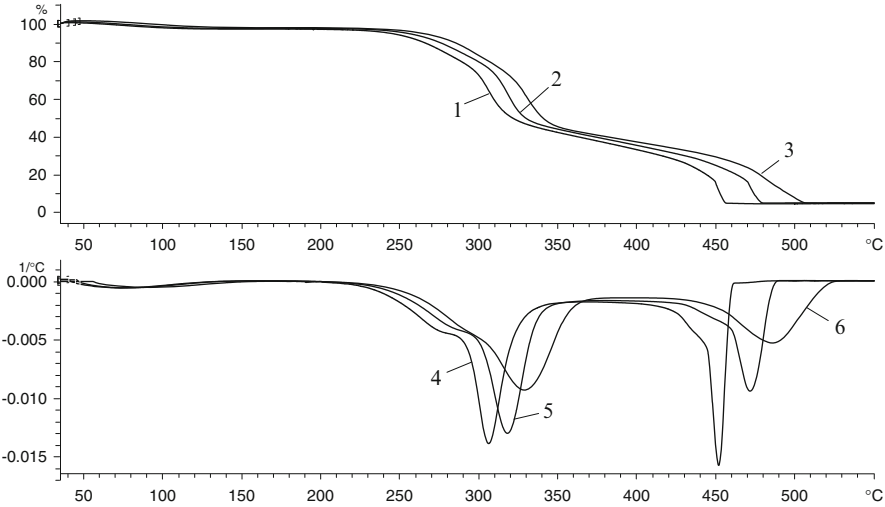

Fig. 11.1 TG (*1*, *2*, *3*) and DTG (*4*, *5*, *6*) curves of oak timber in air atmosphere at a heating rate of 5 °C/min (*1*, *4*), 10 °C/min (*2*, *5*), and 20 °C/min (*3*, *6*)

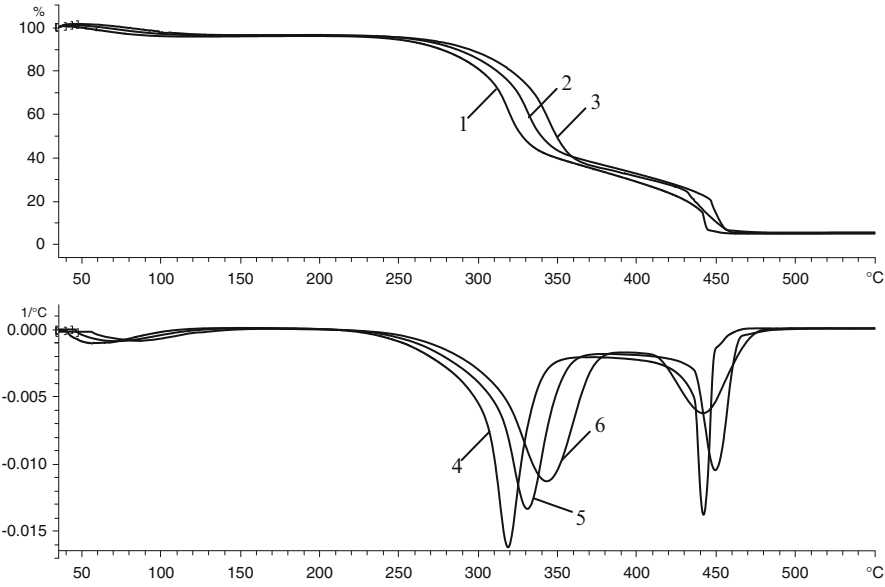

Fig. 11.2 TG (*1*, *2*, *3*) and DTG (*4*, *5*, *6*) curves of fir timber in air atmosphere at a heating rate of 5 °C/min (*1*, *4*), 10 °C/min (*2*, *5*), and 20 °C/min (*3*, *6*)

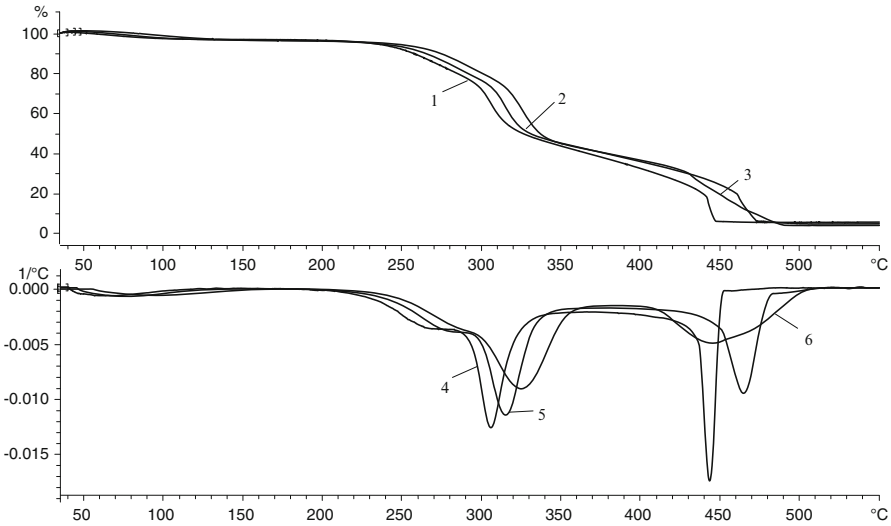

Fig. 11.3 TG (*1*, *2*, *3*) and DTG (*4*, *5*, *6*) curves of artificially aged oak timber in air atmosphere at a heating rate of 5 °C/min (*1*, *4*), 10 °C/min (*2*, *5*), and 20 °C/min (*3*, *6*)

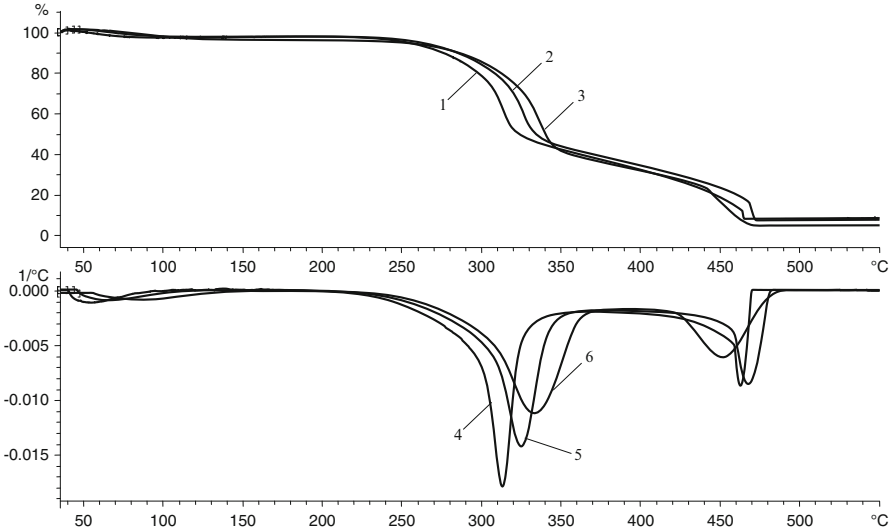

Fig. 11.4 TG (*1*, *2*, *3*) and DTG (*4*, *5*, *6*) curves of artificially aged fir timber in air atmosphere at a heating rate of 5 °C/min (*1*, *4*), 10 °C/min (*2*, *5*), and 20 °C/min (*3*, *6*)

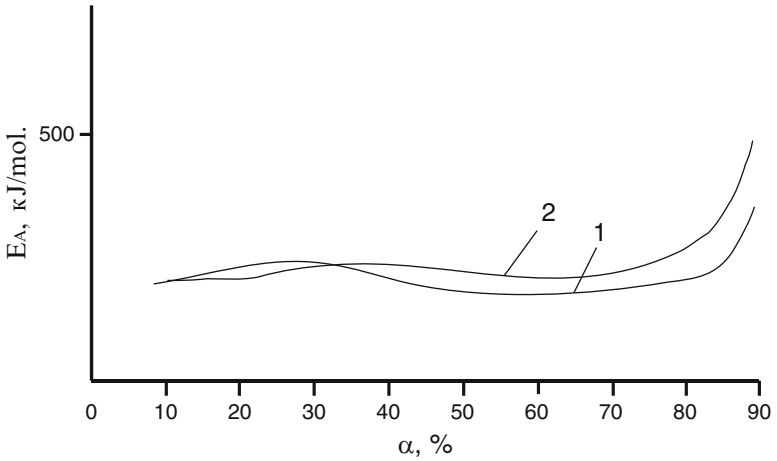

Fig. 11.5 Activation energy (E_{eff}) of thermo-oxidative decomposition of oak timber (*1*) and artificially aged oak (80 years) (*2*) depends on conversion degree (α)

Effective activation energy of the thermo-oxidation process of timber depends on the conversion degree and changes within a certain range $\alpha = 10$–90 %. Thermal analysis showed the following ranges for kinetic parameters of decomposition of the specimens of various species of present-day timber used:

$$\begin{aligned}
&\text{Fir}: E_{\text{eff}} = 180 - 210\ \text{kJ/mol}; \quad \lg\ k_0 = 14.0 - 15.16\\
&\text{Pine}: E_{\text{eff}} = 160 - 215\ \text{kJ/mol}; \quad \lg\ k_0 = 13.8 - 15.7\\
&\text{Birch}: E_{\text{eff}} = 130 - 170\ \text{kJ/mol}; \quad \lg\ k_0 = 10.7 - 11.6\\
&\text{Oak}: E_{\text{eff}} = 190 - 220\ \text{kJ/mol}; \quad \lg\ k_0 = 16.2 - 17.8
\end{aligned}$$

After artificial aging, the values of activation energy do not change drastically at this stage of decomposition.

Figures 11.5 and 11.6 show the effect of artificial aging of oak and fir timber on the effective activation energy of thermo-oxidative decomposition for various conversion degrees.

In thermo-oxidative decomposition of artificially aged oak at the initial phase of the low-temperature stage (α up to 30 %), the activation energy values are slightly lower compared to the present-day timber (Fig. 11.5). Later on, they exceed these values of E_{eff}. In coniferous species, we observe a different situation. As it follows from Fig. 11.6, the E_{eff} values of artificially aged fir timber hardly differ from untreated fir. The difference in mass loss rates of the aged and present-day timber seen on DTG curves is caused by different values of the pre-exponential factor in the Arrhenius equation. In other words, the kinetics of thermo-oxidative decomposition of timber is affected by entropic and structural factors.

The second stage of thermo-oxidative decomposition of timber within the range of 400–550 °C consists in active char formation and oxidation. Under the

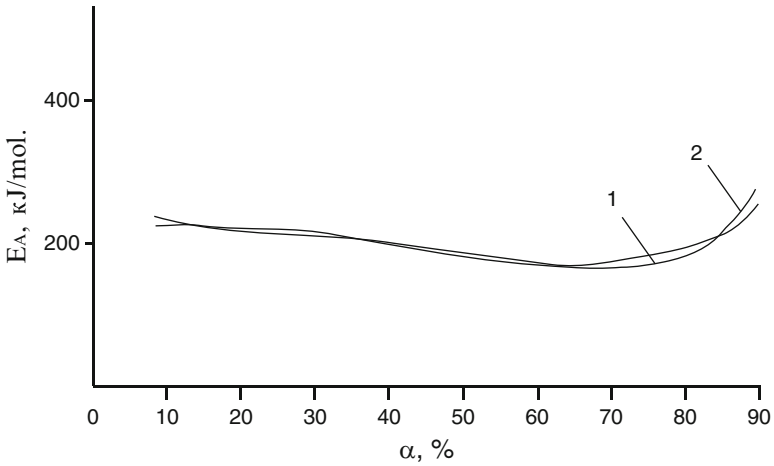

Fig. 11.6 Activation energy (E_{eff}) of thermo-oxidative decomposition of fir timber (*1*) and artificially aged spruce (150 years) (*2*) depends on conversion degree (α)

dynamic conditions of heating to 500–550 °C, the carbonized products of timber decomposition are oxidized completely and lose their mass. Judging by the DTG curves, the oxidation of residual char of artificially aged specimens of fir proceeds at a higher rate compared to the char of present-day timber. Oak aging also leads to such changes in the progress of mass loss at this stage, although they are not as pronounced as in coniferous timber. At the degree of oxidative decomposition of carbonized products of oak α up to 30–35 %, the oxidation reaction of aged timber char proceeds with lower activation energy compared to char oxidation of the initial timber. With a higher degree of char burn-off, the differences in E_{eff} are leveled. The char oxidation process in this period proceeds with an activation energy of 200–215 kJ/mol. The same trend in E_{eff} changes is observed in oxidative decomposition of char residues in artificially aged birch timber (Aseeva et al. 2010).

The porous structure of char in the initial pine timber and pine timber artificially aged to 100–150 years was examined by the method of isothermal sorption of benzene vapors. To perform a comparative analysis, samples were taken of charred layers that had formed on the surface of timber specimens exposed to flame after the test by the method of GOST R 53292-2009 and those resulting from standard temperature conditions of a fire. Total pore volume, average pore diameter, and specific surface area of porous structure of the chars were calculated on the basis of the benzene sorption isotherms obtained (Keltzev 1984).

After accelerated artificial aging of pine timber, the average diameter of pores in the charred layer decreased from 25.03 to 21.56 nm, whereas the specific surface area almost doubled. These results explain the enhanced reaction capability of the charred layer in aged timber toward air oxygen. It should also be noted that formation of the fine-porous structure of char leads to lower thermal conductivity and improvement of its heat-insulating properties.

The quantity and quality of carbonized product formed on the timber surface significantly affect the character of flaming and smoldering combustion of timber-based materials.

11.3 Fire Safety Indices of Artificially Aged Timber Species

As we see, the dynamic of natural and artificial aging of timber depends to a certain extent on the timber species. Aging affects the changes in chemical composition of the material and its properties as a whole. In this case, we are particularly interested in the way accelerated artificial aging affects various characteristics of timber fire safety. In addition, from the practical point of view, it is important to know to what extent timber aging may affect the effectiveness of various flame retardants.

Changes in chemical and element composition of coniferous and deciduous timber after aging affects timber complete combustion heat (Table 11.4).

Accelerated artificial aging of timber, as well as long-term natural aging, leads to enhanced values of lower heat of complete combustion. Experimentally obtained values Q_l^e and calculated values Q_l^c are sufficiently close. Due to enhanced lignin content and hydrogen enrichment, fir timber artificially aged to 150 years has higher Q_l^c values compared to the specimen with 150 years of natural service life.

Thermal treatment of spruce timber in water vapor medium at 200–250 °C also leads to the increase Q_l^c of 6–8 % (up to 19.9–20.26 kJ/g) compared to the untreated specimen. But in this case, the increase in Q_l^c is due to considerable (by 34–54 %) lignin enrichment of the wood substrate.

The effect of artificial aging on mass loss rate of timber at exposure to radiation heat flow was assessed by standard method of GOST 30402-96.

Figure 11.7 shows the curves of mass loss rate for artificially aged specimens of pine as a function of external heat flow density. The behavior of initial specimens of present-day timber is given for comparison. As can be seen in Fig. 11.7, there are certain common patterns: as external heat flow density increases from 30 to 40 kW/m^2, the mass loss rate of the specimen increases, and its maximum value becomes higher and is attained faster.

Table 11.4 Effect of accelerated artificial aging of timber on lower heat of complete combustion

Timber specimen	Density, kg/m^3	W, %	Q_l^e, kJ/g	Q_l^c, kJ/g
Fir, present-day	422	6.4	18.9	19.25
Fir, aged 150 years	430	7.2	22.7	23.6
Pine, present-day	448	6.0	19.6	19.1
Pine, aged 150 years	462	6.4	–	22.87
Oak, present-day	638	4.3	18.7	18.2
Oak, aged 80 years	626	5.1	–	18.2
Birch, present-day	567	5.5	18.1	18.22
Birch, aged 80 years	593	6.2	–	18.45

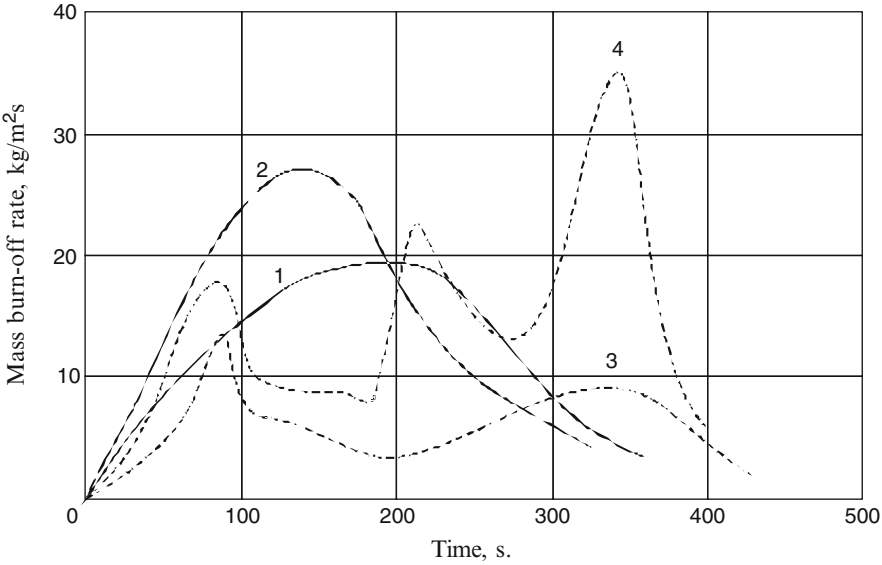

Fig. 11.7 Progress of mass loss rate in present-day (*1*, *2*) and artificially aged pine (*3*, *4*) on exposure to external heat flows of various intensities 1, 3–30 kW/m^2 and 2, 4–40 kW/m^2

The mass loss rate curves for artificially aged timber are more complicated compared to the present-day timber. This situation is partly caused by different thickness of the tested timber specimens (20 mm for present-day pine and 10 mm for artificially aged).

During the testing period of 120–180 s, a thinner specimen evidently manages to char, and in later time spans, mass loss occurs due to char layer oxidation. In the first part, the artificially aged timber decomposes very rapidly. The peak values of mass loss rate corresponding to the onset of active charring of artificially aged timber are significantly lower compared to the present-day timber. This means that artificially aged timber starts to char more rapidly, and the effect of the char layer on specimen burn-off begins to appear earlier compared to the present-day timber.

When the heat flow density increases to 40 kW/m^2 and test duration to 400 s, peaks with high mass loss rate due to char oxidation appear.

The specimens were placed in the horizontal position for determining the mass loss rate of timber as per GOST 30402-96.

It is known that when specimens are in the horizontal position, the mass loss rate and heat release rate of timber are higher compared to the vertical position.

The standard unit for the flammability test did not allow registration of heat release during material burning. For this purpose, an OSU calorimeter of type HRR-3 manufactured by Atlas (USA) was used. A timber specimen with dimensions $150 \times 150 \times 10$ mm was exposed to an external radiant heat flow of 35 kW/m^2 in the vertical position.

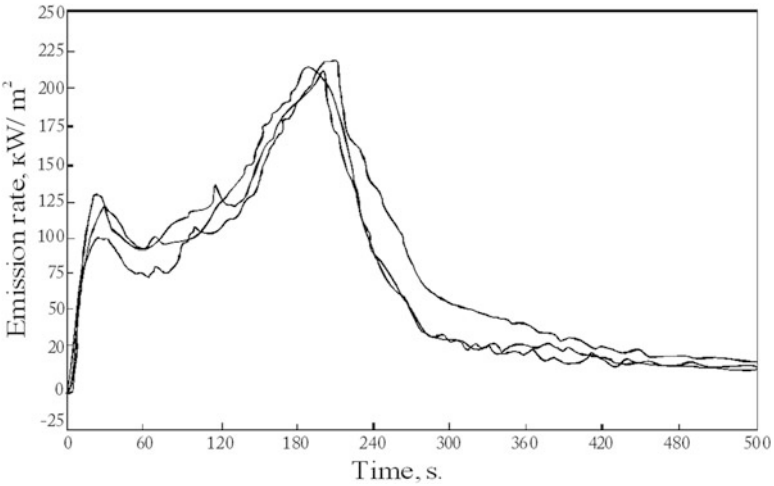

Fig. 11.8 Progress of heat release rate during flaming combustion of present-day fir as a function of time at $q_e = 35$ kW/m^2

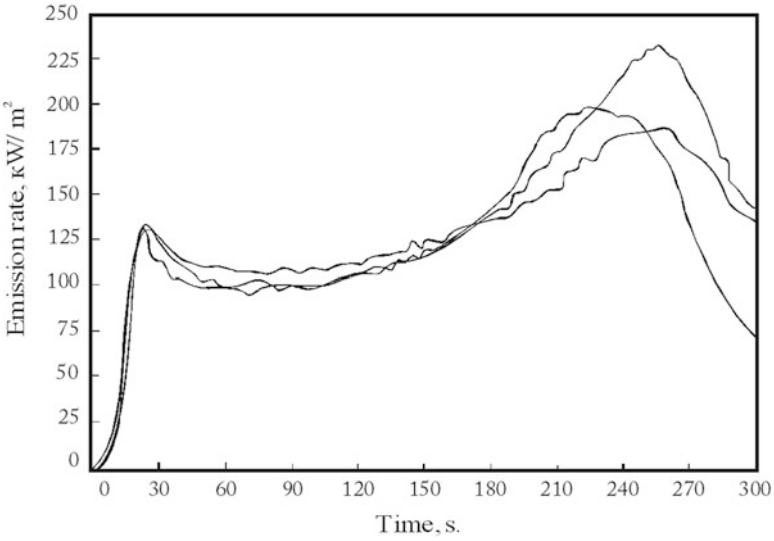

Fig. 11.9 Progress of heat release rate of artificially aged fir timber (100–150 years) at a heat flow of 35 kW/m^2

Figures 11.8 and 11.9 show the results of fire tests for specimens of present-day and artificially aged (100–150 years) fir with moisture of 6.4–7.2 %.

Table 11.5 gives heat release rate characteristics for various species of timber before and after artificial aging at external heat flow $q''_e = 35$ kW/m^2.

Table 11.5 Effect of artificial aging of various timber species on heat release characteristics

Specimen	ρ, kg/m^3	W, %	T_i, s	τ_{1max}, s	HRR_{1max}, kW/m^2	τ_{2max}, s	HRR_{2max}, kW/m^2	THR_{2min}, kW · min/m^2
Fir	422	6.4	<10	23	131.2	195	223.2	218.2
Fir (100–150 year)	430	7.2	15	26	135	245	207.9	190.7
Pine	448	6.0	<10	20	129.0	276	203.5	180.6
Pine (100–150 year)	462	6.4	17	25	130	268	214	179.9
Birch	567	5.5	10	53	157.7	215	400.5	279.9
Birch (50–80 year)	593	6.2	20	–	–	261	375	240
Oak	638	4.3	10	33	131.3	281	245.1	198.0
Oak (50–80 year)	626	5.1	20	40	125	297	260.6	191.8

Each figure shows the curves for three replicated tests. The heat release rate curves are seen to have two clear-cut peaks, which characterize the sequence of timber combustion stages.

The table shows the average values of parameters for three replicated tests. The following parameters were determined specifically: ignition delay time ($\tau_{i.}$); maximum heat release rate value at the first (HRR_{1max}) and second (HRR_{2max}) stages and the time of achieving them from the start of the test; and total heat release in 2 min of the combustion process (THR_{2min}).

It is worth noting that ignition delay time of birch and oak is markedly higher compared to fir and pine. This is in full agreement with the thermal ignition theory, which states the existence of a direct relationship between ignition time and thermal inertia, $k\rho c$, or, correspondingly, density, ρ, of the material. After the onset of pyrolysis and ignition of flammable decomposition products, the heat release rate in timber combustion starts to increase up to the maximum value (HRR_{1max}). This value corresponds to the onset of surface layer carbonization. Given equal external heat flow values, less time is needed in coniferous timber species to attain the first peak of the heat release. They apparently decompose more rapidly and start to char due to higher lignin content. The charred layer on the surface of fir and pine specimens is thicker compared to oak and birch under equal conditions of thermal exposure.

The second peak on $HRR = f(q_e)$ relationship curves reflects the oxidation and burn-off of a nearly fully carbonized layer formed on the timber surface. The structure of this layer and its porosity affect the reaction rate of interaction with air oxygen.

After artificial aging of timber, τ_i values increase as a result of the removal of low-molecular substances, part of the easily hydrolyzed hemicelluloses and extractives, as well as some increase in apparent density of the specimens. However, the period from ignition to the peak value of heat release, τ_{1max}, is later reduced. This is especially evident in artificially aged specimens of pine and fir.

Table 11.6 Effect of artificial aging of timber on the charring parameters and efficiency of flame retardants in standard fire conditions

Timber specimen	δ_C, mm	V, mm/min	ρ_C, kgm^{-3}	τ_i, min:s	T_s, °C
Pine, present-day	20	0.95	268	3: 44	732
Pine, 150 years	26	1.5	221	4:52	758
Pine, present-day + KSD-A (grade 1)	8	0.41	217	6:15	605
Pine, 150 years + KSD-A (grade 1)	15	0.77	220	6:52	670
Pine, present-day + OSR ($\alpha = 0.5$)	7	0.47	242	7:14	–
Pine, 150 years + OSR ($\alpha = 0.5$)	12	0.64	225	7:36	–

Note: OSR – oxidized starch reagent, oxidation degree $\alpha = 0.5$

At heat flow $q''_e = 35$ kW/m^2, the values of maximum heat release rate at the first stage of flaming combustion, HRR_{1max}, of artificially aged coniferous timber remain almost at the same level, whereas in the case of oak specimens, there is a slight reduction of HRR_{1max} from 131.3 to 125 kW/m^2.

It should be noted that the time to attain the second peak maximum, τ_{2max}, from the start of present-day and artificially aged fir tests is 195 and 245 s, respectively. Total heat release in 2 min of tests, THR_{2min}, was 218.2 and 190.7 kW min/m^2, respectively. The tendency to lower total heat release for this period, THR_{2min}, is also recorded in artificially aged oak timber specimens.

Smoke-generating capacity of artificially aged coniferous timber depends on the external heat flow intensity, and in terms of D_{max} values, it is lower than the smoke-generating capacity of present-day timber (Fig. 10.9). The extractives, hemicelluloses, and cellulose partially removed during artificial aging greatly contribute to smoke generation during material combustion.

Enhanced lignin content also plays an important role in smoke generation during combustion of artificially aged timber. By virtue of its aromatic polymer nature, lignin displays a high capacity for carbonization during heating and exposure to fire. That is why smaller amounts of carbon-containing volatile products of lignin decomposition – smoke soot particles – get into the smoke formation area of the flame.

The smoke generation parameter of fir artificially aged to 150 years in flameless combustion with external radiative heat flow of 20 kW/m^2 decreased from $D_{max} = 950$ m^2/kg of the initial specimen to $D_{max} = 790$ m^2/kg.

On the other hand, under these conditions the products of flameless combustion of timber artificially aged to 150 years show lower toxicity. The toxicity index estimated by the yield of carbon oxides, HCL_{50}, changed from 28 g/m^3 in present-day timber to 37 g/m^3 in the aged spruce timber.

Timber charring in a fire is an important factor taken into account both in experimental assessment and in calculation of fire resistance of timber-based structures. The effect of artificial aging on charring parameters in standard temperature–time fire conditions was examined with pine timber as an example (Table 11.6).

Table 11.7 Effect of aging and treatment with bio-fire retardants on the parameters of porous structure of surface char layers

		Char parameters			
№ п/п	Char sample	a_m, %	$V_{\sum}$, cm^3/g	d_{av}, nm	S_{sp}, $м^2/г$
1	Pine, present-day	12.8	0.4726	25.03348	377.5744
2	Pine, 150 year	16.2	0.5332	21.56388	814.7575
3	Pine, present-day, with "KSD-A" (grade 1)	17.95	0.5123	19.76785	935.3324
4	Pine, present-day with Pirilax	18.48	0.6812	18.51378	1038.637
5	Pine, present-day with ASFS composition	21.81	0.6327	12.80586	1554.857
6	Pine, present-day with BB-11	16.96	0.7088	20.17486	882.7961
7	Pine, 150 year, with "KSD-A" (grade 1)	20.65	0.5781	16.11560	1434.879
8	Pine, 150 year, with Pirilax	26.76	0.5234	14.65459	1645.746
9	Pine, 150 years with ASFS composition	17.67	0.4992	19.89676	904.5326
10	Pine, 150 year with BB11	16.53	0.3968	20.56678	823.7534

The test was performed on specimens with dimensions of $150 \times 150 \times 20$ mm for 20 min. The parameters to be determined were ignition delay time, τ_i; charred layer thickness, δ_C; average values of charring rate, V; and char density; as well as maximum temperature of the charred layer surface, Ts.

The same table shows a comparative analysis of the effect of artificial aging of timber on the effectiveness of the developed flame retardants.

Accelerated artificial aging of pine specimens leads to an increase in timber ignition delay time in standard fire conditions and charring rate of almost 1.5 times and a 30 % increase in the charred layer thickness, whereas the density of the formed char layer decreases by 17.5 % and its surface temperature goes up by several degrees.

Use of the developed flame retardants for timber in turn significantly affects the charring parameters of the material. Although fire protection contributes to the increase in material ignition delay time in standard fire conditions, slows its charring rate, and reduces the charred layer thickness, timber aging reduces the effectiveness of flame retardants.

It is interesting to note that treatment of present-day timber surfaces with flame retardant KSD-A (grade 1) results in a notable reduction of char layer surface temperature compared to an untreated surface. This means that fire protection should slow the char layer burn-off rate in fire conditions. However, with the same treatment of artificially aged pine, its char layer surface temperature is higher compared to the fireproofed present-day specimen. Unfortunately, the char layer surface temperature in standard fire conditions of timber treated with fireproof intumescent compound on the basis of oxidized polysaccharides could not be exactly measured.

Table 11.7 shows the study results of porous structure of chars being formed during flaming combustion of pine timber treated with various bio-fire protection means. A comparison was made between commercial products (Pirilax, KSD-A – grade 1, BB11), as well as an in-house novel product (ASFS composition).

Fire protection treatment of present-day and artificially aged timber greatly changes the porous structure of the char layer formed during combustion on the material surface. This is manifested first in the enhancement of their absorption capacity, a_m, reduction of average pore diameter, and a corresponding increase in specific surface area. The extent of variation of the indicated parameters of porous structure depends on the type of fire protection treatment of timber and on its artificial aging.

A comparison of the data of two fire protection systems providing effectiveness group 1 as per GOST R 53292–2009 – Pirilax and ASFS compound – is especially indicative. Combustion of artificially aged timber with bio-fire protection of Pirilax generates char with an absorption capacity that increases from 18.48 to 26.76 %, pore diameter that decreases by 21 %, and specific surface area that increases by 58.5 % in comparison with the present-day timber char.

Fire-protecting impregnation of present-day timber with ASFS compound led to char formation with the smallest pore diameter (12.80 nm) and increased specific surface area. However, in artificially aged timber, the effect of ASFS composition on the characteristics of the porous structure of the formed char was less significant.

The average char pore diameter was 19.9 nm, whereas specific surface area increased only 1.1 times compared to a specimen without fire-protecting impregnation. When BB-11 fire-bio retardant was used for present-day and artificially aged timber treatment, there was almost no difference in parameters of char porous structure.

Formation of chars with fine-porous structure leads to a reduction of their thermal conductivity and improvement of heat-insulating properties.

The presence of flame-retardant phosphorus and/or boron in the char structure contributes to lower oxidative capacity and slows down the burn-off of the char layer on timber surface.

The results we obtained highlight once again that the effectiveness of fire protection action of flame retardants used in various impregnating compositions for timber depends on the direction of chemical reactions and the contribution of physical processes into material combustion.

References

Aseeva RM, Serkov BB, Sivenkov AB (2010) Timber combustion and its fire hazard characteristics. SFS Academy, Moscow, 262 p

Finishes Thermowood Association (2003) Thermowood handbook. Finishes Thermowood Association, Helsinki

GOST 20850 (draft) Wooden laminated structures. General specifications

GOST 9.057-75. Unified system of corrosion and aging protection. Methods of testing for resistance to damage by rodents

GOST 9.707-81. Unified system of corrosion and aging protection Polymeric materials. Methods of accelerated climatic aging tests

GOST R 53292-2009. Flame retardants for wood. Method of determining flame-retardant properties

Keltzev NV (1984) Basics of adsorption technologies. Mir, Moscow, 592 p

Kortelainen SM, Paajanen L, Viitanen H (2011) Durability of thermal modified Norway spruce and Scots pine in above ground conditions. Wood Mater Sci Eng 6(4):163–169

Pishchik II (2000) Non-destructive assessment of internal stresses in timber structures by unconventional methods. In: Third international symposium "Structure, properties and quality of wood", Petrozavodsk, pp 203–206

Pishchik II, Koudrya AA, Yankovsky BA et al (1980) Method of accelerated aging of timber. Patent of USSR No. 719870

Serkov BB, Aseeva RM (1996) The influence of thermal ageing on fire safety of electric and electronic products based on polyolefines. In: Twenty-second international conference on fire safety, 22–26 July, Columbus, OH

Welzbacher CR, Brischke C, Rapp AO (2007) Influence of treatment temperature and duration on selected biological, mechanical, physical and optical properties of thermally modified timber. Wood Mater Sci Eng 2(2):66–76

Conclusion

Centuries of experience have given humanity a fairly reasonable idea of the high fire hazard of timber. Modern fire statistics only confirm this opinion about timber, which is still one of the most popular construction materials. It is no coincidence that the problem of reducing the fire hazard of timber and timber products is a major preoccupation. Successfully solving this problem depends on an understanding of the mechanisms of the onset smoldering and flaming timber combustion, fire propagation in buildings and structures with timber structures, and the conditions for preventing combustion.

Despite the vast amount of experimental work in this area, it is often difficult to compare the results, not only because different research methods were used but also because of the timber specimen used without mentioning their species and variety or any description of their characteristics. Evidently, this experimental setup of many works was due to the still-prevalent outdated approach to timber as some kind of generalized substance with properties that differed very little between them.

Rapid growth of theoretical works on pyrolysis and thermo-oxidative decomposition, flammability, and flame spread over the surface of timber and other synthetic materials with allowance for carbonization of these materials began only in recent decades.

To a certain extent, the monograph summarizes the results of the recent development of this line of timber research. The basis for this work is the concept that many properties of timber, including fire-hazardous properties, are simultaneously a function of both the physical macro- and microstructure and the chemical composition of this complex composite material created by nature itself. Therefore, the specific reaction of timber on exposure to high temperatures and fire is examined in terms of the diversity of its species and types, which should necessarily affect the physical, thermochemical and thermophysical properties, and chemical composition of the specimens.

Timber is a product of the vital activities of a living plant. The genetic basis for the diversity of this biological form of living substance on Earth, its adaptation to the habitat, and resistance to adverse impacts has still not been fully revealed.

R. Aseeva et al., *Fire Behavior and Fire Protection in Timber Buildings*,
Springer Series in Wood Science, DOI 10.1007/978-94-007-7460-5,

In the next few years of the twenty-first century, we should expect revolutionary scientific breakthroughs in knowledge of the compete genome of woody plants, the fine mechanisms of biochemical synthesis of plant tissues and the main chemical components of timber, and discovery of the genes controlling this synthesis.

The concept we have used helps us to understand the fire behavior of various timber species and the change in their fire-hazardous properties during natural and artificial aging.

An analysis of the influence of the content of main components in the chemical composition of various deciduous and coniferous timber species on the lower total combustion heat of timber, which is a thermodynamic characteristic of any specific substance, clearly confirms the correctness of this concept.

The authors have tried to organize and summarize the available results from scientific publications on pivotal experimental and theoretical works that provide insight into the relationship between the structure, composition and properties of timber, and the mechanisms of timber combustion in various conditions of heat exposure.

The authors have attempted to describe the overall status of this problem in Russia and the prospects of solving it by using their own results of long-term research and the experience of colleagues at the Academy of the State Fire Service of EMERCOM of Russia and other organizations involved in fire safety of construction projects.

It should be noted that the design and development of modern technologies for manufacturing new timber- and plant-based materials in our country are ahead of the regulatory foundation for their safe use in the construction industry. A striking example of this is the production of new types of laminated timber structures and the restriction on using them in low-rise housing construction due to the absence of the relevant construction standards and regulations in Russia.

The most economic means of legal use of new materials in the construction of medium-rise frame wooden buildings structures is probably to adapt existing international standards and regulations to this sector.

Trends toward basic study of the fire behavior and fire hazard characteristics of timber with allowance for species diversity are very clearly strengthening in world practice.

Although the combustion and fire-hazardous properties of timber are considered as an important area of timber research, it should be emphasized that many aspects of the problem of timber combustion remain unresolved.

There have been almost no studies of the long-term processes occurring in timber during low-temperature heat exposure. The conditions and factors influencing the occurrence of smoldering timber combustion and its transition to flaming combustion are unclear. An understanding of the extent to which both the content of main components in timber and the constituents of these components and their chemical nature will affect timber combustion and its critical conditions is still ahead.

In this context, an analysis of the changes in some important indicators of the fire hazard of timber when it is naturally and artificially aged is of interest. It is clear that the details of the solid phase processes are very important for the gas-phase processes of flaming combustion.

Timber charring during a fire affects the fire resistance of wooden load-bearing structures and enclosures. Data on the timber charring rate as a function only of timber density (specific weight) obtained during tests under standard fire conditions frequently disagree or are contradictory. However, a general trend emerges: all other conditions being equal, coniferous species char at a faster rate than deciduous species. If we take the significant contribution to timber charring of one component, namely, lignin, into account, the observed contradictions become more comprehensible.

We suggest concentrating on the quality of the charred surface layer that forms during the combustion of timber and timber products and the potential for targeted control of the pore structure and properties of the coke layer. This will affect its thermal properties and the temperature distribution in material in close proximity to the charring front and thus the temperature dependence of the mechanical properties of the structural member as a whole.

The optimum balance of combined fire protection methods and achieving a mutual synergistic effect among them is a way to significantly increase the fire resistance and fire safety level of wooden building structures.

The development of verifiable models of the mechanism of fire protection connecting design parameters with its composition, structure, and characteristics of its main constituents will promote the development of effective fire protection measures for timber.

Index

R. Aseeva et al., *Fire Behavior and Fire Protection in Timber Buildings*, Springer Series in Wood Science, DOI 10.1007/978-94-007-7460-5,